CAROTID PLAQUE STRESS ANALYSIS BY FLUID STRUCTURE INTERACTION BASED ON *IN-VIVO* MRI: IMPLICATIONS TO PLAQUE VULNERABILITY ASSESSMENT

A thesis submitted for the degree of Doctor of Philosophy by

Hao Gao

Brunel Institute for Bioengineering

Brunel University

July 2010

Author's Declaration

I hereby declare that I am the sole author of this thesis.

I authorize the Brunel University to lend this thesis to other institutions or individuals for the purpose of scholarly research.

Signature 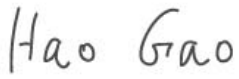

I further authorize the Brunel University to reproduce this thesis by photocopying or by other means, in total or in part, at the request of other institutions or individuals for the purpose of scholarly research.

Signature 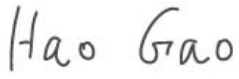

Abstract

Stroke is one of the leading causes of death in the world, resulting mostly from the sudden rupture of atherosclerotic plaques. From a biomechanical view, plaque rupture can be considered as a mechanical failure caused by extremely high plaque stress. In this PhD project, we are aiming to predict 3D plaque stress based on *in-vivo* MRI by using fluid structure interaction (FSI) method, and provide information for plaque rupture risk assessment.

Fluid structure interaction was implemented with ANSYS 11.0, followed by a parameter study on fibrous cap thickness and lipid core size with realistic carotid plaque geometry. Twenty patients with carotid plaques imaged by *in-vivo* MRI were provided in the project. A framework of reconstructing 3D plaque geometry from *in-vivo* multi-spectral MRI was designed. The followed reproducibility study on plaque geometry reconstruction procedure and its effect on plaque stress analysis filled the gap in the literature on imaging based plaque stress modeling. The results demonstrated that current MRI technology can provide sufficient information for plaque structure characterization; however stress analysis result is highly affected by MRI resolution and quality. The application of FSI stress analysis to 4 patients with different plaque burdens has showed that the whole procedure from plaque geometry reconstruction to FSI stress analysis was applicable.

In the study, plaque geometries from three patients with recent transient ischemic attack were reconstructed by repairing ruptured fibrous cap. The well correlated relationship between local stress concentrations and plaque rupture sites indicated that extremely high plaque stress could be a factor responsible for plaque rupture.

Based on the 20 reconstructed carotid plaques from two groups (symptomatic and asymptomatic), fully coupled fluid structure interaction was performed. It was found that there is a significant difference between symptomatic and asymptomatic patients in plaque stress levels, indicating plaque stress could be used as one of the factors for plaque vulnerability assessment. A corresponding plaque morphological feature study showed that plaque stress is significantly affected by fibrous cap thickness, lipid core size and fibrous cap surface irregularities (curvedness). A procedure was proposed for predicting plaque stress by using fibrous cap thickness and curvedness, which requires much less computational time, and has the potential for clinical routine application. The effects of residual stress on plaque stress analysis and arterial wall material property characterization by using *in-vivo* MRI data were also discussed for patient specific modeling.

As the further development, histological study of plaque sample has been combined with conventional plaque stress analysis by assigning material properties to each computational element, based on the data from histological analysis. This method could bridge the gap between biochemistry and biomechanical study of atherosclerosis plaques.

In conclusion, extreme stress distributions in the plaque region can be predicted by modern numerical methods, and used for plaque rupture risk assessment, which will be helpful in clinical practice. The combination of plaque MR imaging analysis, computational modelling, and clinical study/ validation would advance our understandings of plaque rupture, prediction of future rupture, and establish new procedures for patient diagnose, management, and treatment.

Acknowledgements

I would like to express my sincere sense gratitude to Dr Quan Long, my supervisor and friend, for his help, encouragement, guidance, thoughtful advice during my study in Brunel Institute for Bioengineering since December 2006. Without his help and support, this thesis would never have been completed.

I sincerely thank Dr Quan Long's collaborators in the project, who has been actively participated in this research. MRI data and related supported were provided by Professor JH Gillard's group (Jonathan H Gillard, Martin Graves, Zhi-Yong Li) from University of Cambridge. They provided essential help in MRI data processing (tissue characterization from in-vivo MRI and segmentation). My appreciation also goes to my colleagues in my group (Arson Choundary, Warren Hopkins, Saroj Das), for their help in histological data preparation and *ex-vivo* plaque sample data. My grateful thanks also extended to many professors, staff in the Institute for their help and suggestions (Dr Ashraf Khir, Prof Ian Sutherland, Prof Derek Fisher, Prof Hamid Bahai). I also own a big thanks to British Heart Foundation, Brunel Institute for Bioengineering and Brunel Graduate School for the financial support.

My thanks also go to my fellow graduate students in the Institute for their help and friendship (Francesco Clavica, Samantha Fernando, Karnal Patel, Ning Wang, Yan Cai, Yi Li, Ye Li, Xiao Liu, Xiao Yan). I have an unforgettable memory during my PhD, from badminton, squash, football game, beer time (finally managed to improve), Friday evening barbeque to day out trip, Christmas holiday trip, etc.

Finally I would like to give a special thank-you to my parents for their constant love, understanding and support.

For my Parents

Table of Contents

List of Figures

List of Tables

Abbreviations

MRI	Magnetic resonance imaging
FSI	Fluid structure interaction
TIA	transient ischemic attack
SMC	smooth muscle cells
LDL	low density lipids
USPIO	ultrasmall superparamagnetic iron oxide
MMP	matrix metalloproteinase
ECM	extra cellular matrix
FEM	finite element method
CFD	computational fluid dynamics
WSS	wall shear stress
CCA	common carotid artery
ICA	internal carotid artery
ECA	external carotid artery
WSS _tmean	temporal mean WSS
WSS _t max	maximum WSS in the whole cardiac cycle
WTS	wall tensile stress
VWTS	Von Mises stress form
VMStrain	Von Mises Strain
VWTS_tmax	temporal maximum VWTS in a cycle
VWTS_smax	spatial maximum VWTS at a time
rcVWTS	relative cyclic VWTS
FPS	first principle stress
CEA	carotid endarterectomy
ImT2W_FatSat	intermediate T_2 Weighted with fat saturation
T2W	T_2 Weighted
T1W	T_1 Weighted
STIR	short T_1 inversion-recovery

TOF	time-of-flight
mVWTS_fib	local maximum stress on the fibrous cap
mP1	maximum FPS
FCT	fibrous cap thickness
min_FT	minimum fibrous cap thickness
max_SD	maximum degree of stenosis
RB_FEM	region based finite element method
EB_FEM	element based finite element method
ROI	region of interest

Chapter 1 Introduction

Stroke is one of the leading causes of death in the world (Rosamond et al., 2007), mainly caused by atherosclerotic plaque rupture with subsequent thrombus formation (Fuster et al., 1994). In carotid arteries or coronary arteries, atherosclerotic plaques may develop into a high degree of stenosis, which could restrict blood supply to the downstream arteries, and cause reshaping of arterial wall. More often, the rupture of plaques with low grade stenosis degree and subsequent thrombus formation, rather than stenosis, which can block blood flow in the arterial system, causes stroke or myocardial infarction.

However the exact mechanisms of plaque rupture still remain unclear. Plaques that are prone to rupture may often be clinical silent until the time of rupture. Depending on the components and structures, usually two types of plaques can be classified (a) stable plaques: characterized by thick fibrous cap with abundance of smooth muscle cells, small lipid core size, etc. (b) unstable plaques: plaques with very thin fibrous cap, few smooth muscle cells and abundance of inflammatory cells, with a lipid core accounting for more than half of the plaque volume. Research has been devoted to finding features for predicting plaque vulnerability. At present, some plaque features, such as large lipid pool, thin fibrous cap, and high content of inflammatory cells, have been believed to contribute to plaque instability (Naghavi et al., 2003).

It has been accepted that both plaque morphology and biomechanical environment of the plaques influence their vulnerability (Richardson P.D. 2002). The biomechanical factors such as plaque wall tensile stress, wall shear stress are considered to be important factors in plaque rupture process and should be taken into account for plaque vulnerability assessment. Studies by finite element methods have shown that mechanical stress concentrations often occur in the shoulder and thinner fibrous cap regions, where plaques most often rupture (Loree et al., 1992). Recent developments in high resolution multi-spectral Magnetic Resonance imaging (MRI) have allowed plaque components to be visualized *in-vivo*, providing more realistic plaque geometries for stress analysis. Many

studies have been carried out in 2D or 3D structure analysis only, or with limited plaque models (Tang 2004a&b; Li et al., 2006; Kock et al., 2008).

The main objective of the project is to analyze blood flow and wall tensile stress in carotid plaques. Patient specific carotid plaque geometries are generated from multi-spectral MRI data of patients, and imported into ANSYS for computational stress analysis, including one-way fluid structure interaction(FSI), and two-way(fully coupled) FSI. The wall tensile stress distributions in plaque region will be compared among different patients. Specific aims are:

- **Development of fluid structure interaction procedure for carotid plaque stress analysis based on MRI**

  The objective of this aim is to develop a robust procedure for FSI simulation in carotid plaques with multiple components under the framework of ANSYS, including parameter study on plaque components' (fibrous cap thickness and lipid core size) effect to plaque stress distributions. The results will be compared to the existed plaque stress research for the validation of the developed FSI procedure.

- **Reconstruction of 3D carotid plaque stress model based on *in-vivo* MRI**

  The first aim is to reconstruct 3D carotid plaque models from *in-vivo* MRI, in which there are more than 3 MR sequences for plaque reconstruction. Therefore a proper method to accurately segment plaque components according to their characterizations in different MR sequences needs to be developed, including boundary segmentation, imaging registration, and 3D reconstruction from 2D contours. Furthermore the shrinkage in axial and radial direction needs to be applied during 3D reconstruction to account for the stress-free state of plaque in order to start stress analysis. The second aim is to assess the reproducibility of plaque reconstruction from *in-vivo* MRI and their effects to the stress distribution, which will give the confidence in the accuracy and reliability of plaque stress analysis employed in this project.

- **FSI stress analysis on multiple patients with carotid plaques**

  One of the main objectives of this project is to study stress levels in symptomatic and asymptomatic patients in order to assess plaque rupture risk according to plaque stress

levels. 20 carotid plaques (12 symptomatic, 8 asymptomatic) will be reconstructed, and fully coupled FSI simulation will be applied for stress calculation. The stress is going to be compared among the two groups to investigate the potential plaque rupture risk predictors based on plaque stress. The morphological features such as fibrous cap thickness, lipid core size, stenosis degree and fibrous cap surface irregularities will be correlated with plaque stress patterns in order to find the possible links between morphological features and stress patterns.

- **The evidence for plaque rupture caused by extremely high plaque stress**

The hypothesis for plaque rupture in the project is the rupture caused by extremely high plaque stress, however there is no direct evidence for the hypothesis. By studying the stress distribution in patients with ruptured plaques will provide possible evidence on plaque rupture mechanism. Therefore pre-ruptured plaque geometries from patients with recent transient ischemic attack (TIA) will be reconstructed, and FSI is going to be applied to investigate the possible relationship between local high stress concentrations and plaque rupture sites.

- **Combination of histological analysis with plaque stress analysis**

The conventional stress analysis is hard to incorporate information from histological analysis. Therefore the aim is to develop a method for combining histological analysis with plaque stress analysis. It has been accepted that histological analysis is the golden standard for plaque tissue characterization, from macro level to micro level. Therefore how to use the information in conventional stress analysis needs to be resolved.

The organization of the thesis can be found in Figure 1.1, details are:

- **Chapter 2** provides the general background on atherosclerosis plaque from initiation, development, to rupture. Literature review on plaque stress study will be summarized including plaque rupture hypothesis in terms of biomechanical factors, and plaque stress analysis from 2D to 3D, from structure only to fully coupled FSI simulation.

- **Chapter 3** is the development of fluid structure interaction procedure within ANSYS. The developed FSI procedure will be applied for the parameter study (including fibrous cap thickness and lipid core size) on plaque stress distributions.
- **Chapter 4** addresses 3D carotid plaque geometry reconstruction from *in-vivo* MRI. The reproducibility of plaque geometry reconstruction and the effects on plaque stress analysis will be assessed. A group of 4 subjects with carotid plaques is going to be analyzed with the developed FSI procedure in Chapter 3.
- **Chapter 5** will investigate the stress distributions in subjects who suffered TIA recently, in order to find the possible relationship between local high stress locations and plaque rupture sites.
- **Chapter 6** mainly focuses on the FSI plaque stress analysis on symptomatic and asymptomatic patients. The morphological features including fibrous cap thickness, lipid core size, stenosis degree, and fibrous cap surface irregularities will be studied, also the residual stress' effects on plaque stress distributions, and patient specific material model characterization will be discussed.
- **Chapter 7** is the further development of plaque stress analysis in order to incorporate histological analysis for a better understanding of the role of biomechanical factors in atherosclerosis plaques.
- **Chapter 8** is the discussion and conclusion for the thesis

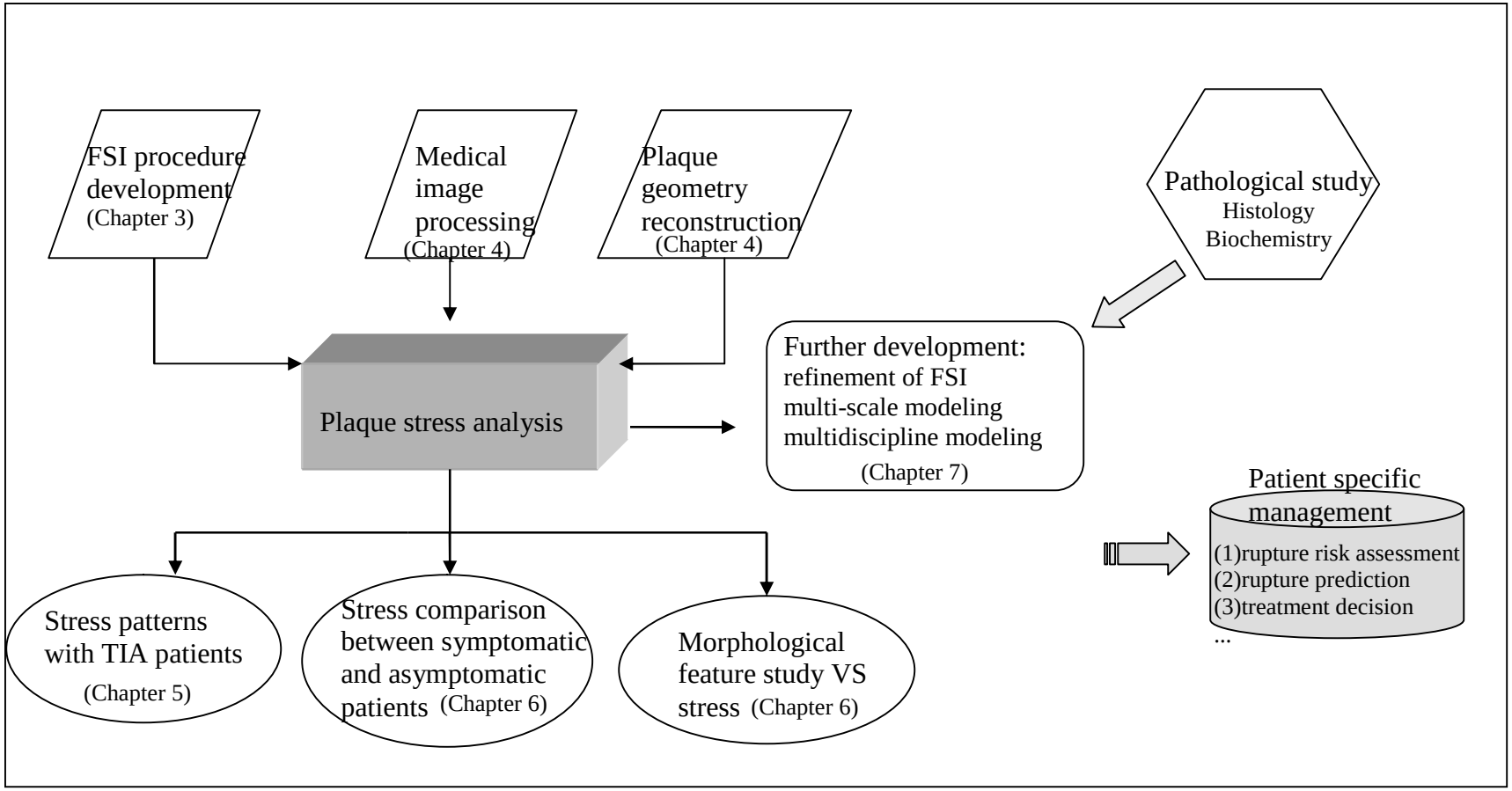

Figure 1.1 Schematic for the organization of the project

Chapter 2

Literature on atherosclerotic plaques and stress analysis

2.1 The Development of Atherosclerotic Plaque

Atherosclerosis is a chronic disease usually occurring in the wall of large- and medium-sized arteries. The healthy arterial wall consists of three layers: the intima, media and adventitia layer (Figure 2.1(a,b)). The intima, the innermost layer, mainly consists of the endothelial cells, and subendothelial layers including some collagenous bundles, elastic fibrils, and smooth muscle cells (SMCs). The media layer, the thickest layer, mainly consists of smooth muscle cells, collagen and elastic fibers, arranged in rings around the lumen. The adventitia principally consists of collagen and elastic fibers. Elastin and collagen fibers greatly determine the structure integrity and stability of arterial wall. Elastin provides elasticity of arterial wall, bearing the force in the beginning of loading. With increased loading, collagen fibers engage to maintain the integrity of the tissue, which is more rigid and less extensible. The exact structure of an artery may vary depending on its type and function (Fung YC, 1993).

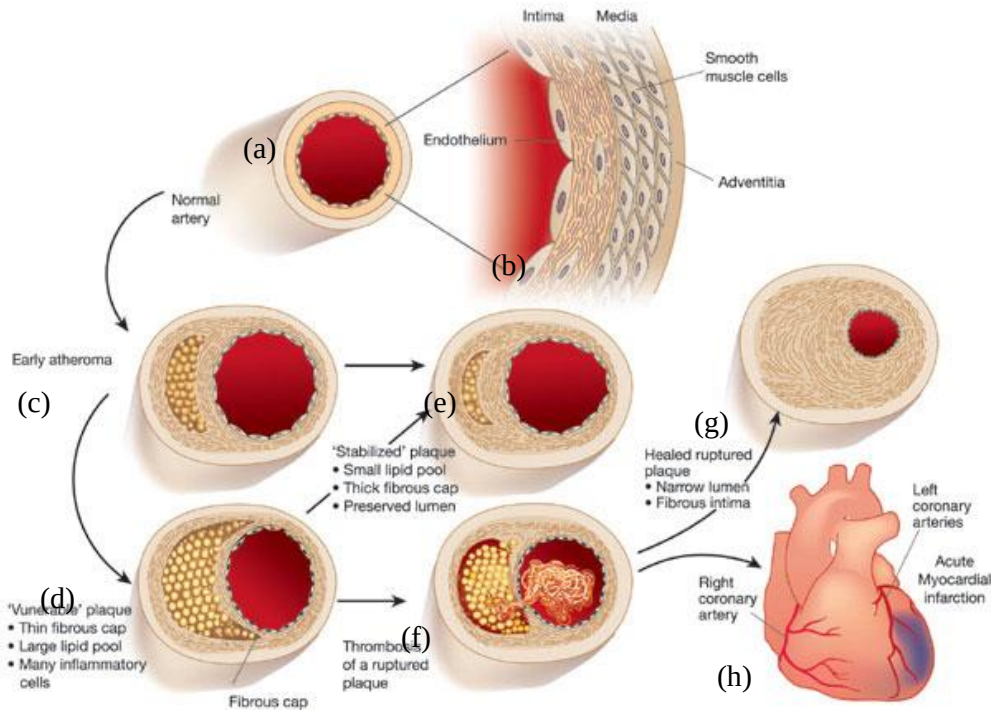

Figure 2.1 Schematic description of plaque development (Peter Libby, *Nature* 420: 868-874 (19 December 2002))

Although the mechanism of plaque initiation is not yet fully understood, studies (Giddens et al., 1995) have shown that the initiation of atherosclerotic lesion is more likely to be depended on the geometry of the arteries due to the resulted complex blood flow patterns, such as the regions with high curvature, or near bifurcations (Friedman et al., 1983). Studies (Ku et al., 1987; Ma et al., 1997) have been carried out to investigate various hemodynamic factors such as wall shear stress, macromolecules residence time, etc. and tried to link those factors to plaque initiation/growth. Ku (Ku et al., 1985) studied wall shear stress in the carotid bifurcation and proposed that the low and oscillatory wall shear stress could affect the endothelial cells' biochemistry and permeability to macromolecules and water, finally initiate plaque development. Avolio (Avolio et al., 1998) suggested that the structure alterations of arterial wall would increase the endothelial damage and dysfunction. Hansson (Hansson et al., 2002) believed that the immune response to the

accumulation and modification of lipoproteins in the arterial intima can cause the initiation of plaques. However the exact mechanism of plaque initiation still remains unclear. Other hypothesis includes high wall shear stress, cyclic stress/strain, et al.

The accumulation of oxidized low density lipids (lipoprotein, LDL) in the arterial wall forms a fatty steak, which is mainly made up of foam cells: fat-laden macrophages, and T lymphocytes (Libby et al., 2002), as shown in Figure 2.1(c). The oxidized LDL cholesterol particles can alter the biochemical environment of endothelial cells, promote them to express adhesion molecules, and secrete chemokines in the luminal surface to recruit more monocytes and T lymphocytes into the lesion region. At this stage, the thrombogenic lipid core is covered by a strong and thick fibrous cap from luminal side, therefore the risk for plaque rupture could be low.

The continued inflammation will cause the further development of the lesion, as shown in Figure 2.1(d). The increased macrophages and smooth muscle cells in the lipid region will secrete enzymes, such as Matrix Metalloproteinase (MMPs) for degrading elastin and collagen to facilitate the movement of macrophages towards the lesions. SMCs will continually synthesize and organize fibers in the lesion in order to provide the fibrous cap with sufficient strength under mechanical loads. However, the increased inflammation activities may cause more thinning and eroding of the fibrous cap, which brings a shift from extra cellular matrix (ECM) production to ECM degradation.

As the disease develops, plaques may cause clinical syndromes in two different ways. (a) plaques can gradually narrow arterial lumen size, resulting in a reduction of blood supply, which may precipitate symptoms of ischemia during periods of high oxygen demand (for example during exercises); (b) when the weakened fibrous cap covering the lipid region is not strong enough to withstand the physiological loading from the

pulsating pressure, the mechanical stresses concentrated in the plaque region might contribute to the plaque instability, shown in Figure 2.1(f). The components from lipid region are highly thrombosis and will activate the blood clotting process if it is in contact with blood, which leads to downstream artery blockage, causing subsequent stroke or heart attack (Figure 2.1(h)). Casscells (Casscells et al., 2003), found that approximately 60% of myocardial infarctions are caused by rupture of plaques with subsequent thrombus formation.

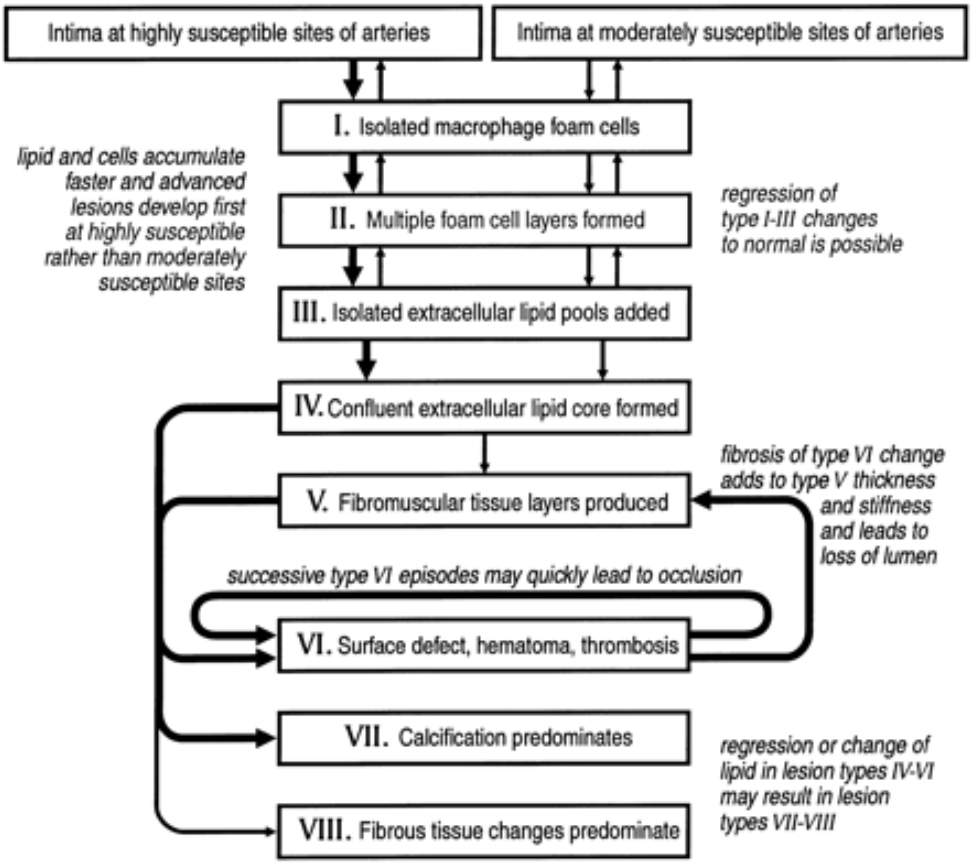

Figure 2.2 Stages of plaque progression (Stary et al., 2000)

Based on morphological features of plaques in the process of plaque development, a classification scheme has been proposed by the American Heart Association (AHA) (Stary et al., 1995a) as shown in Figure 2.2. Details can be found in these papers (Stary et al., 1995b; Stary et al., 2000; Virmani et al., 2000).

2.2 Plaque Rupture Hypothesis and Evidence

A vulnerable plaque is usually characterized by the presence of a large lipid region, covering by a thin fibrous cap, infiltrated by dense inflammatory cells. However the underlying mechanism for plaque rupture is not fully understood and it may occur without obvious clinical symptoms. Several rupture mechanisms have been proposed, usually in two categories. One is the biological abnormalities in the plaque components; the other is the biomechanical factors. The biological factors can cause weakening of plaques at the regions of extreme stress situations, which in turn extreme stress can affect the biological disorders at those regions (Arroyo et al., 1999).

Biological abnormalities in the plaques have been well considered to be related to plaque vulnerability, such as enhanced inflammatory activities, accumulation of macrophages, extracellular matrix degradation (Lendon et al., 1991; Shah et al., 1995; Ashwini et al., 2003). The study (Moreno et al., 1994) on macrophage content in coronary plaque tissue from patients with stable and unstable coronary syndromes showed that macrophage-rich areas are more frequently found in patients with unstable angina, suggesting that macrophage is a marker of unstable atherosclerotic plaques and may play a significant role in plaque rupture. Libby (Libby et al., 1996) demonstrated that ruptured plaques usually have thin fibrous cap overlying a large thrombogenic lipid core rich in lipid-laden macrophages, those monocyte-derived macrophages assume critical roles in plaque stability. Plaque macrophages are capable of expressing a variety of matrix-degrading enzymes that can contribute to the weakening of the fibrous cap, finally influence the lesion stability. Stefano Di (Stefano Di et al., 2009) discussed the potential role of intra-plaque angiogenesis as a risk factor for plaque vulnerability, because those immature blood vessels are viable source of intra-plaque haemorrhage providing erythrocyte-derived phospholipids and free cholesterol. A recent study (Dunmore et al., 2007) has found that symptomatic carotid plaques contain abnormal, immature micro-vessels, contributing to plaque

stability by acting as sites of vascular leakage for inflammatory cell recruitment. Thin cap atheroma has also been believed to be the precursor of plaque rupture, which may account for a majority of coronary thrombi (Virmani et al., 2003). Still there is a lot of research continuing to find the biological factors which could be linked to plaque vulnerability.

Biomechanical factors also have been considered to be important triggers in plaque rupture. Many studies have been carried out to associate extreme biomechanical stress situations with plaque rupture since 1990s.

- **Local maximum stress**: the local maximum stress in fibrous cap region, which is higher than the critical stress value which fibrous cap tissue can sustain, usually is considered to be the main reason of rupture in terms of biomechanics factors (Cheng et al., 1993; Tang et al., 2005a&b). A critical value of 300kPa has been proposed by Cheng (Cheng et al., 1993) for coronary arterial plaque, based on their 2D stress analysis with ruptured and stable atherosclerotic lesions.
- **Fatigue failure**: Bank (Bank AJ, 2000) hypothesized that mechanical fatigue on fibrous cap caused by pulstile blood flow may be an important factor causing plaque rupture. The growth of plaque fatigue crack based on this hypothesis has been simulated by evolving stress distribution in plaques (Versluis et al., 2006).
- **Extremely high wall shear stress**: Recently extremely high wall shear stress has been linked to plaque rupture (Groen et al., 2007; 2008) based on the findings that plaque ulceration occurs at the high wall shear stress location.
- **De-bonding effect by micro-calcification**: The hypothesis for vulnerable plaque rupture due to stress-induced de-bonding around cellular micro-calcification in thin fibrous caps was proposed (Vengrenyuk et al., 2006) based on the fact that cellular-level micro-calcifications in a thin cap can cause

local stress concentrations that lead to interfacial de-bonding. It should be mentioned that the 'De-bonding effect' also can be categorized into the hypothesis of 'Local maximum stress' because of extremely high stress caused by micro-calcifictions.

- **Other hypotheses:** include injury due to turbulent flow in the stenosis (Loree et al., 1991), rupture of vasa vasorum (Barger et al., 1984), etc.

Comparing with the others, the local maximum stress hypothesis is the most wildly accepted one which is also the one that we are working on. Several studies have been carried out to correlate high stress regions with rupture sites to provide evidence for plaque rupture caused by extreme stresses. Cheng (Cheng et al., 1993) studied the stress concentration locations compared with the rupture sites based on 2D histological plaque samples, they found that the circumferential stress concentrations had a good correlation with rupture sites in their study. However, plaque rupture may not always occur at the region of highest stress. Lee (Lee et al., 1993) used *in-vitro* balloon angioplasty to cause plaque rupture after the intravascular ultrasound imaging of the plaque. By correlating with structure analysis, they found that 82% fractures occurred in the regions with high circumferential stress. Ohayon (Ohayon et al., 2001) found that the peak circumferential stress areas correlated well with plaque rupture sites by comparing the plaque rupture locations on post-angioplasty intravascular ultrasound images with 3D structure stress analysis. However the biomechanical factors related rupture hypothesis has not been fully verified *in-vivo*, due to the difficulties such as (1) there is no technique that can directly measure wall stress in the plaque *in-vivo*, (2) the geometry of a specific plaque at pre- and post- rupture status is practically unachievable. Nonetheless, to work on any stress related hypothesis, obtaining accurate stress distribution on the specific plaque is essential.

2.3 Morphological Features Related to Plaque Vulnerability

Morphological features are considered to be key features in determining plaque stability (Li et al., 2008). It is believed that a plaque with thin fibrous cap, large lipid pool is more vulnerable to rupture (Arroyo et al., 1998). Furthermore there are some other features which may relate to plaque vulnerability: stenosis severity, calcifications, and inflammation cell contents. The study by Kumar (Kumar et al., 2005) demonstrated that the extreme stress situation in plaque had a direct relation with the thickness of the lipid pool and an inverse relation with cap thickness and lumen stenosis, and stress in a positively remodeled vessel is significantly greater than more negative remodeling plaques. Positive remodeling (compensatory enlargement) is defined as the enlargement of an artery to keep the lumen area to be the same as the normal condition with plaque accumulation in the arterial wall. The negative remodeling is referred to the plaques with narrowed lumen area. The term of positive remodeling was first introduced by Glagov (Glagov et al., 1987). Figure 2.3 schematizes positive and negative remodeling with plaques. Ohayon (Ohayon et al., 2008) proposed that the combination of fibrous cap thickness, necrotic core thickness and arterial wall remodeling index should be considered together for evaluating the risk of plaque rupture.

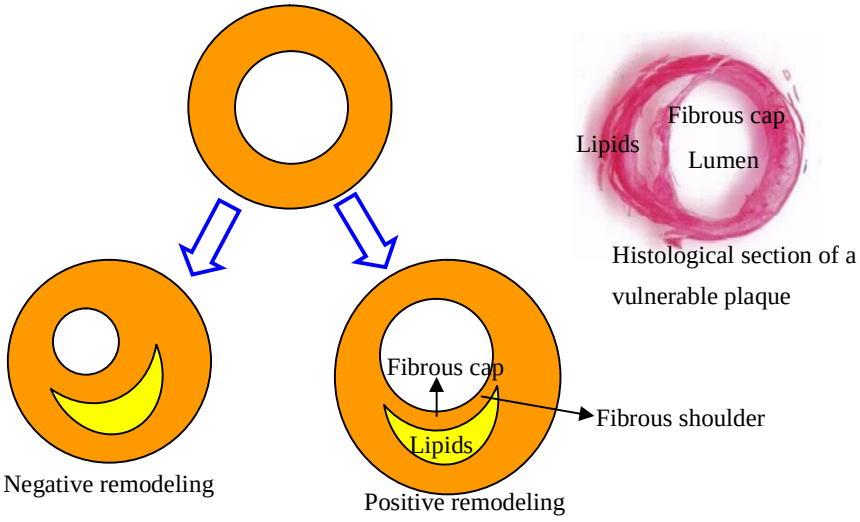

Figure 2.3 Positive and negative remodeling with plaques

Minimum Fibrous Cap Thickness: It has been well accepted that a thin fibrous cap specifically associates with plaque stability, and is one of the key features of unstable plaques. Based on a study of coronary plaques from 113 men, a cap thickness of 65μm has been suggested as a criterion of instability for coronary plaques (Burke et al., 1997). They found that the mean cap thickness of rupture plaques was 23±19μm and 95% of that cap thickness was less than 65μm. While the critical fibrous cap thickness in carotid plaques was much greater than coronary plaques, from the study of Redgrave (Redgrave et al., 2008), a minimum cap thickness <200μm and a representative cap thickness <500μm were identified in ruptured plaques based on histological assessments of 526 human carotid plaques. Although to detect the minimum fibrous cap thickness *in-vivo* is very hard, efforts have been made in *in-vivo* imaging to detect thin fibrous cap thickness. A new ultrasound system based on boundary detection was developed to measure the fibrous cap thickness in internal carotid artery plaques under *in-vivo* scanning (Devuyst et al., 2005). However there is a long way to go for accurately imaging thin fibrous cap.

The presence of a thin fibrous cap is not the only factor to predict rupture. Hangartner (Hangartner et al., 1986) found that 40% of 448 studied plaques with thin fibrous caps were rupture free. From Farb's (Farb 1996) study, 30% death out of 80 patients was not associated with plaque rupture, though thin fibrous cap were present. Virmani (Virmani et al., 2000) did a study over 200 sudden death cases. They found that approximately 120 patients (60%) died of acute thrombi which resulted from the rupture of thin fibrous caps, while 70% of these 120 patients, thin fibrous cap atheromas without rupture were found. From above studies, not all plaques with thin fibrous caps rupture.

Lipid Content: lipid size has been considered to be another key feather associated with plaque vulnerability. The lipid core mainly consists of crystalline cholesterol,

cholesteryl esters, phospholipids, and cellular debris from apoptotic or necrotic foam cells (Schroeder et al., 1995). From biomechanical aspect, the lipid core is much softer than the surrounding arterial wall tissue. It is several orders of magnitudes softer than fibrous cap tissue. Therefore, lipid core can not bear any loading, but causes stress concentrations in thin fibrous cap region or shoulder region (Figure 2.3). Studies (Richardson et al., 1989; Davies et al., 1990) have shown that lipid rich lesions are more likely to rupture and cause myocardial infarctions than the lesions containing few lipids. This is because lipid is a highly potent thrombogenic component (Wilcox JN., 1992). If ruptured, the thrombolic formation will likely block downstream blood supply. Studies have demonstrated that ruptured plaques have significantly higher lipid contents than stable plaques. However there is no significant difference in lipid contents between plaques with thin fibrous caps and ruptured plaques (Virmani et al., 2005).

Inflammation Burden: Inflammation in plaques has received much attention recently as a critical factor contributing to plaque instability (Libby P., 1995; Biasucci et al., 2000). Studies have shown that plaques often contain many inflammatory cells, including macrophages (Falk et al., 1995), the main inflammatory cells, and mastocytes. Dense macrophage infiltration has been found at the immediate sites of ruptured plaques. The role of macrophages in destabilizing plaque is by releasing MMPs, which is able to weaken fibrous cap, and promote plaque instability (Newby et al., 1999; Lee RT., 2000). Studies (Bezerra et al., 2001) demonstrated that macrophage content positively correlates with lipid content. Hallow (Hallow et al., 2009) has attempted to compare spatial distributions of inflammation and mechanical stress, and it was found that there is limited relationship between inflammation activity and extreme mechanical situation.

Stenosis Severity: Stenosis degree has been used as one of indices for predicting plaque stability in clinic, calculated by the ratio of lesion area to the total area of lesion and lumen. A high stenosis degree usually could cause a more disturbed flow around the plaque, greater pressure drop, and higher wall shear stress in plaque throat. However studies have found that stenosis degree is not a reliable predictor for plaque stability. Angiographic studies have shown that most plaques responsible for rupture are minimally occlusive prior to the clinical event, less than 50% stenosis (Giroud et al., 1992). Based on 300 ruptured plaques in 257 arteries of 254 patients, Maehara (Maehara et al., 2002) reported the correlations between the clinical and angiographic results with which plaque rupture was detected by intravascular ultrasound. The correlations showed the plaque rupture site contained the minimum lumen area site in only 28% of patients; rupture sites were more likely to have larger arterial, lumen areas and more positive remodeling. Carr (Carr et al., 1996) studied atherosclerotic plaque ruptures in 44 carotid artery plaques (25 asymptomatic and 19 symptomatic patients) with pentachrome staining and light microscopy. Patients with symptomatic carotid artery plaque were found to have more frequent of plaque rupture, however the two groups had similar average percentage of stenosis (77% vs 74%). Furthermore, IVUS studies (Tuzcu et al., 1995) have shown that segments of coronary arteries with less stenosis degree may still have large plaques due to the positive remodeling. Although positive remodeling may not narrow the lumen area significantly, plaques with positive remolding can still have larger lipid pool, higher macrophage contents and thinner fibrous cap than the plaques with negative remolding (Schoenhagen et al., 2000; Varnava et al., 2002). Therefore stenosis severity is not a reliable predictor for plaque vulnerability.

Morphological studies indicate that the detection of a vulnerable plaque is not in itself enough to predict plaque rupture, which means not all plaques with a large lipid pool and thin fibrous cap will rupture. Plaques with extreme mechanical stress conditions

combined with those morphological features may be more vulnerable. Therefore other relevant characteristics apart from morphological features must also be involved on assessing plaque rupture vulnerability, such as biomechanical factors. Current research has supported the theory of rupture that plaque rupture is a mechanical instability event within the fibrous cap and shoulder region of plaques combining with biological abnormalities of inflammatory activities (Cheng et al., 1993; Ohayon et al., 2005). In order to predict stress distributions in atherosclerotic plaques, accurate mechanical models must be developed.

2.4 Biomechanical Study of Plaque Vulnerability

The hypothesis behind this group of studies is that plaque rupture is a mechanical failure of thin fibrous cap. The tendency of a plaque to rupture is due in part to increases in mechanical stress in fibrous cap (Richardson et al., 1989; Cheng et al., 1993; Huang et al., 2001). Various studies (Ohayon et al., 2005) have revealed that plaque rupture often occurs in the shoulder regions of plaques, the high stress concentration region due to the significant difference in stiffness between fibrous cap and underlying lipid pool (Cheng et al., 1993; Huang et al., 2001). Since there is no better way to accurately measure the stress in the plaque, numerical methods have been extensively applied to obtain the stress in the plaque region, especially finite element method (FEM). The realistic plaque geometry with multi-components including lipid region, fibrous cap, et al. is generally used to construct a FEM model together with physiological mechanical loading to predict the mechanical stress distribution in a plaque.

Finite element models have been developed from 2D to 3D, from idealized models to patient specific plaques in terms of geometrical accuracy, from structure analysis only to fluid structure interaction (FSI) analysis in terms of physical phenomenon reality. There are normally five main tasks involved in building a plaque mechanical stress

analysis model which include: (a) to acquire plaque components, (b) to reconstruct plaque geometry; (c) to apply mechanical load and dynamic boundary conditions; (d) to define suitable material constitutive models; and (f) to perform FEM simulation and post processing. Table 2.1 lists breakdowns of each task for different levels of complexity of simulations. The following sections provide a brief review of the simulation technique developments, in the order of 2D structure-only stress analysis, 3D structure-only stress analysis, 3D fluid-only models and results, and 2D/3D FSI results.

Main tasks in plaque stress analysis	
Plaque components acquisition	1, Arterial wall geometry(multi-layers) 2, Fibrous cap structure(shape, size, components, thickness) 3,Lipid core(shape, size, components) 4,Calcification(size, location) 5,Hemorrhage 6,Inflammation activities(fibrous cap weakening/ erosion) 7, Angiogenesis
Plaque Geometry reconstruction	1, Idealized/realistic model 2, 2D/3D model 3, Imaging source for plaque reconstruction 4, *In-vivo/ ex-vivo* model 5, Accuracy/reproducibility of plaque reconstruction
Loading and boundary conditions	1, Pulsating blood pressure 2, Wall shear stress 3, Axial/circumferential residual stress/strain 4, Motion caused by surrounding tissue
Material Properties	1, Existed experimental data for plaque components 2, Proper material model(isotropic/anisotropic, linear/nonlinear)

	3, Patient-specific/general material model 4, Stiffness variation(heterogeneous material property)
Stress prediction	1, Plane stress/strain calculation(2D) 2, 3D structure-only analysis 3, 3D fluid-only analysis 4, 2D fluid-structure interaction analysis 5, 3D fluid-structure interaction analysis

Table 2.1 Main tasks in plaque stress analysis

2.4.1 Two Dimensional Structure-only Stress Analysis

Since 1990s, 2D structure stress analysis has been extensively applied to plaque models for predicting stress distributions from idealized models to patient-specific models. The advantage of using idealized models is that they allow easy changing of geometrical parameters to investigate effects of individual plaque features. Loree (Loree et al., 1992) studied the effects of plaque structure features including stenosis severity and fibrous cap thickness on stress distributions based on idealized plaque models. They found that decreasing the fibrous cap thickness considerably increased the peak circumferential stress, while increasing the stenosis severity decreased peak stress, suggesting that ruptured plaques may not associate with high stenosis degree. Cheng (Cheng et al., 1993) studied the relation between the locations of peak stress in ruptured plaques and rupture sites for the same plaque. The results showed that most plaque rupture sites occurred very close to regions of high stress, however, the peak stress did not always coincide with the rupture site. They also found the maximum circumferential stress in plaques that ruptured was significantly higher than maximum stress in stable specimens, a critical stress value of 300kPa has been proposed for predicting plaque rupture. Finet (Finet et al., 2004) studied the effect of fibrous cap thickness to plaque stress with 2D idealized models. They found that irrespective of plaque geometry and composition, a fibrous cap thickness of less than 60μm results stresses greater than 300kPa.

By using heterogeneous material model for stress analysis in human atherosclerotic aortas, Beattie (Beattie et al., 1998) found that the distribution of stress and strain energy was strongly influenced by plaque structure and compositions, indicating that a proper material model with multi-components in plaque stress analysis is of very importance. Williamson (Williamson et al., 2003) studied the sensitivity of wall stresses in diseased human coronary arteries to varied material properties. They showed that stresses in the artery have low sensitivities to variations in elastic modulus and comparable among isotropic nonlinear, isotropic nonlinear with residual strains, and transversely isotropic linear models. However, the stress in the stress concentration regions can vary up to 30% with different material models from the same work. Huang (Huang et al., 2001) investigated the effect of calcification towards plaque stability in human atherosclerotic coronary arteries, suggesting that calcification does not decrease the stability of the plaque. However, Veress (Veress et al., 2000) believed that the location of calcification could play an important role in plaque stability. Calcification deep in plaques could have little effect on stability, and may even stabilize the plaque from rupture, while calcification in the fibrous cap could contribute to the plaque rupture due to the great difference in stiffness, and increasing the stress in the fibrous cap, especially the interface between calcification and fibrous cap.

Stress analysis has been combined with the findings from histological analysis to study the possible interaction between inflammatory activities and extreme stress environments in fibrous cap. Lee (Lee et al., 1996) demonstrated that there are some correlations between high circumferential stress regions and MMP expression in human atherosclerotic coronary arteries, by considering that the degradation of the collagenous extracellular matrix at high stress regions will further weaken fibrous cap and promote plaque rupture. Howarth (Howarth et al., 2007) correlated the macrophage locations and plaque stress distributions by using USPIO (ultra-small

super-paramagnetic iron oxide contrast agent)-enhanced MRI in a patient with symptomatic severe carotid stenosis. Their findings supported that macrophage locations correlated well with maximal predicted stresses in the plaque. Studies from Hallow (Hallow et al., 2009) by using a 2D heterogeneous finite element model and the corresponding distributions of selected inflammatory markers, has identified the progression-dependent relationships between stress and both macrophage presence and MMP-1 expression, suggesting the role of mechanical stress in stimulating the inflammatory response, which will help explain how mechanical factors may regulate plaque remodeling.

However, many of those studies (Cheng et al., 1993; Lee et al., 1996; Beattie et al., 1998; Huang et al., 2001) are based on the geometry from histology analysis of plaques for predicting stress distribution or on idealized plaque models. The distortion caused in the histological tissue processing procedure has not been considered in the models. Plaque geometry based on histological analysis may be totally different from *in-vivo* state (Lowder et al., 2007). As the consequence, the predicted stress distribution based on the distorted/idealized geometry may not actually reflect the real stress distributions in plaques. Efforts have been made to use modern *in/ex- vivo* medical imaging techniques for more realistic stress predictions. Ohayon (Ohayon et al., 2001) used pre-angioplasty IVUS images of human atherosclerotic coronary arteries to predict plaque rupture locations. Chau (Chau et al., 2004) performed stress and strain study by using optical coherence tomography images and compared those results with models from histological images. Though the stress distributions were comparable between those two models, the maximum stress was higher in the histological models. Tang (Tang et al., 2004a) used *ex-vivo* MRI images for stress analysis and compared the results with histological models of human carotid plaques. The maximum and minimum stress values from histological models were 28% and 69% higher than those from MRI based models. From high resolution of *in-vivo*

multi-spectral magnetic resonance imaging of 5 human carotid atherosclerotic plaques, Li (Li et al., 2006) built up multi-components of 2D plaque models. Incompressible hyper-elastic material prosperities were used for the stress analysis. Results showed that the mean maximum stresses in ruptured plaques were much higher than those in un-ruptured plaques. In their following study (Li et al., 2007), they compared the stress concentrations between symptomatic and asymptomatic patients by 2D structure analysis based on *in-vivo* magnetic resonance imaging, found that maximal predicted plaque stresses in symptomatic patients were significantly higher, indicating the possibility that plaques with higher stresses may be more prone to be symptomatic and rupture in the near future. Similar results can be found in the study by Trivedi (Trivedi et al., 2007).

Although two dimensional mechanical models of atherosclerotic plaques are abundant, the findings could shed some lights on the plaque rupture mechanism, the results from such models may be inaccurate because of the assumptions of plane strain/stress, simplified material model, or distorted geometry compared to the *in-vivo* state, leading to a possible over-estimated plaque stress level. Therefore realistic 3D models are needed for accurate stress analysis in plaque region.

2.4.2 3D Structure-only Stress Analysis

3D structure-only stress analysis has been carried out based on idealized plaque models and patient specific geometries.

Idealized 3D Plaque Models: By constructing an idealized 3D plaque model, Hoshino (Hoshino et al., 2009) studied stress distributions around atherosclerotic calcifications and their effects on plaque vulnerability. Their findings suggested that the presence of a calcium deposit creates local increases in wall tensile stress, and it depends on the relative position of the deposit in the plaque region. Imoto Koji (Imoto

Koji et al., 2005) studied the structure stress distributions in an idealized 3D plaque model in a cylindrical vessel model and mapping the stress results with longitudinal IVUS plaque images, the effects of plaque size, shape, expansive remolding, calcification, and lipid core on the stress distributions were examined. Results showed that plaque shape, size and remodeling, as well as spatial configurations of plaque components have different effects on plaque stress.

***Ex-vivo* 3D Plaque Models:** Holzapfel (Holzapfel et al., 2002) have done a series of stress studies in diseased vessels by introducing a multi-layer anisotropic 3D model incorporating the histological structure of arterial wall. In their studies, MR images were used to develop 3D finite element models to simulate balloon angioplasty in atherosclerotic iliac arteries. Mechanical test was performed to provide the required raw data for the formulation of non-linear material models. They compared their 3D models with existing biomechanical models, characterized by isotropic material response, assumption of plain strain, et al. The results showed those assumptions may give a wide range of stress levels, indicating those simplifications need to be well justified when interpreting stress results with plaque rupture. By using similar nonlinear material model, Gasser and Holzapfel (Gasser and Holzapfel 2007) modeled plaque fissuring and dissection during balloon angioplasty intervention in a human external iliac artery with type V lesion. Ferrara and Pandolfi (Ferrara and Pandolfi 2008) presented three dimensional finite element simulations of damaged arteries to investigate the influence of the geometry and tissue properties on plaque rupture. The cohesive elements were used to model the fracture surface induced by the mechanical action when the tensile strength of the material is reached.

***In-vivo* 3D Plaque Models:** Ohayon (Ohayon et al., 2005) calculated the stress in a single diseased human coronary artery from IVUS images to decide the possible relation between high stress concentrations and plaque rupture sites. The diseased

arterial wall was modeled by components of adventia, media, dense fibrousis, and cellular fibrousis with isotropic materials. A physiological mean blood pressure of 13.33kPa was applied for the luminal loading. They found the peak stress locations from 3D model well coincided with plaque rupture location, but not in the corresponding 2D FE models, which may overestimate the stress levels. The stress and strain distributions using FEM and *in-vivo* patient-specific dynamic 3D coronary arterial tree reconstruction from cine angiographic images have been done by Wu (Wu et al., 2003), the local stresses were calculated in the diseased wall, results showed that a smaller vessel diameter, greater percentage narrowing, and large lesion size may result in higher stress in the fibrous cap.

Compared to 2D stress analysis, 3D structure analysis could incorporate more information in FE models, such as the multi-layers of arterial wall, anisotropic material model considering fiber directions, and no plain stress or strain assumptions as in 2D FE models. While there are still places left for improving in order to achieve a realistic plaque stress prediction. In a physiological situation, plaque is under pulsating blood pressure loading, with reduced pressure value in the stenosis throat due to the narrowing effect in the stenosis part. Therefore a uniform pressure loading applied on the luminal surface which is generally adopted in 3D FE structure only models can not simulate the realistic stress distributions. In real situation, the mechanical environment of plaques includes the blood flow dynamics and wall structure dynamics. In order to accurately predict the biomechanical environment, one must consider the hemodynamics surrounding the plaque region, and the corresponding wall dynamics under pulsating loading caused by blood flow. Therefore 3D blood flow simulation in the plaque region is required as part of plaque stress analysis.

2.4.3 3D Fluid-only Models and Results

The complex blood flow dynamics in the arterial system has been considered to be a key role in the initiation, development and even rupture of atherosclerotic plaques (Steinman DA., 2004; Chien S., 2008). Great effort has been made to calculate those hemodynamic factors and tried to link the disturbed flow features to the disease. Owing to the practical difficulties of measuring local hemodynamic factors, computational fluid dynamics (CFD) has been applied to quantify the flow patterns in diseased and non-diseased arteries via the coupling of *in-vivo* medical imaging, such as MRI, three-dimensional ultrasound. CFD combined with *in-vivo* medical imaging provides a less invasive way to identify the role of geometric and hemodynamic factors for atherosclerosis and therapeutic options. Until now, a variety of factors related to hemodynamic in plaque region have been proposed to quantify flow disturbances as potential predictors for arterial wall dysfunction, including time-averaged WSS (Caro et al., 1971), oscillatory shear index, relative residence time (Himburg et al., 2006), WSS spatial gradient, WSS angle gradient (Hyun et al., 2000), etc.

Long conducted a series of studies on patient specific flow analysis based on *in-vivo* MR images from patients (Long et al., 1997; Long et al., 2000). Their results showed that the flow pattern in the carotid bifurcation was greatly influenced by 3D bifurcation geometry. The flow and wall shear stress pattern resulted from the complex geometry features were significantly different from those found in simplified planar carotid bifurcation models. Comparison between the predicted flow patterns and MR measurement showed good quantitative agreement. Steinman (Steinman DA., 2002a; Steinman et al., 2002b) developed a new approach for reconstructing artery wall thickness and local hemodynamic at human carotid bifurcation, and correlated the artery wall thickness to the wall shear stress. 3D models were reconstructed from so called “black blood” MR images, and wall thickness was measured. The time

varying flow rate at inlet/outlet measured by phase contrast MRI was used as patient specific boundary conditions. Their results also showed good agreement between simulated and MR measured velocities and flow pattern, and a relationship could be found between wall thickening and low/oscillating wall shear in the carotid bulb, however the general relationship between wall shear stress and wall thickness was not found in their study. Augst (Augst et al., 2007) used CFD to determine wall shear stress and related hemodynamic factors in carotid artery based on geometry model generated from 3D ultrasound images, and tried to investigate possible determinants of increased intima-media thickness. However no significant correlation has been found. In a recent study, Lee Sang-Wook (Lee Sang-Wook 2009) attempted to analyze the correlations among existed indicators of disturbed flow at 50 normal carotid bifurcations. The results suggested that relative residence time can be a robust single metric of low and oscillatory flow, and may relate to atherosclerosis initiation.

Marshall (Marshall et al., 2004) compared the pulsating flow in physiologically realistic models of a normal and a moderately stenosed human carotid bifurcation by the phantom study and corresponding CFD study. Experimental flow patterns and derived WSS vectors were compared qualitatively. Moyle (Moyle et al., 2006) recommended more efforts should be given to more accurate and detailed geometry reconstructions since they have primary influence on physiologically significant indicators, from their study of the influence of inlet flow condition to the image-based CFD models of the carotid bifurcation. Nquyen (Nquyen 2008) studied carotid geometry effects on blood flow and on the risk vascular disease development. It was found the geometry of carotid bifurcation such as bifurcation angle, out-of plane angle of the internal carotid artery will affect the formation of low WSS regions on the carotid walls. Non-Newtonian fluid flow has also been studied by a few researchers (Gijsen et al., 1999; Chen et al., 2004) in carotid bifurcation models. It is found that Non-Newtonian effects may affect the hemodynamics factors in some way; however

their effects on atherosclerotic disease development need to be clarified in the future. Lee Sang-Wook and Steinman (Lee Sang-Wook and Steinman 2007) pointed out that the assumption of Newtonian fluid flow (constant viscosity) is reasonable in light of currently available levels of geometric precision.

The turbulence flow pattern recently has been revisited. Under normal healthy conditions, the blood flow in carotid artery bifurcation is laminar. However, in the presence of a high stenosis degree, the flow can transit from laminar flow to turbulence flow. The transitional *k-ω* models were used in Banks' (Banks et al., 2007) paper to investigate the complex flow pattern in stenosed arterial bifurcations. More recently, Tan (Tan et al., 2008) applied the two-equation turbulence models and transitional variants for the prediction of blood flow patterns in a diseased carotid artery, reconstructed from MR images with 70% stenosis degree. Their wall shear stress analysis showed limited differences between the laminar flow and transitional models. Lee (Lee Seung et al., 2008) did a direct numerical simulation of transitional flow in a stenosed carotid bifurcation to demonstrate the post-stenotic transitional or weakly turbulent state of the blood flow.

With the development of *in-vivo* medical imaging technology, and advanced numerical methods in fluid simulation, 3D realistic blood flow simulation can be obtained for plaque region with patient-specific models. Together with fluid dynamics, the structure stress analysis in the arterial wall and plaque region can be more accurate compared to structure-only models.

2.4.4 2D/3D FSI Results

In nature, blood flow in the arteries and arterial wall structure dynamics are interacted with each other. Blood flow provides the loading for arterial structure dynamics, such as pressure, the drag force in the wall. Arterial wall will deform under those loadings,

and correspondingly change arterial geometry which will affect the blood flow. Therefore the fluid structure interaction method simulates more accurate mechanical interaction phenomenon of artery and needs to be adopted for stress analysis in atherosclerotic plaques under physiological environment.

Zhao (Zhao et al., 2002) firstly introduced MRI-based FSI models to predict wall shear stress and wall stress patterns in healthy subjects, and tried to define regions of low wall shear stress and high wall stress. Their results demonstrated that there are certain regions with low wall shear stress and high mechanical stress, corresponding to the areas where atherosclerotic plaque develops. Younis et al (2004) used finite element simulations of fluid-solid interactions to investigate inter-individual variations in flow dynamics and wall mechanics at carotid artery bifurcations from three healthy subjects. Subject specific calculations were based on MR images of carotid artery geometries and ultrasound measured flow boundaries. Various biomechanics parameters such as wall shear stress, oscillatory shear index, and cyclic strain have been compared among subjects. Kaazempur-Morfrad (Kaazempur-Morfrad et al., 2003) proposed cyclic strain in describing the arterial wall dynamics under pulsatile blood pressure loading. They found that the regions of highest variations in cyclic strain are identified at frequent sites of atherosclerosis. In the study carried out by Kaazempur-Morfrad (Kaazempur-Morfrad et al., 2004), stress analysis was performed for 4 patients. In addition of the numerical study on the plaque models, the excised plaques were sectioned, stained for smooth muscle cells, macrophages, lipid, and collagen. Efforts have been given to correlate fluid dynamic parameters with histological markers of atherosclerosis.

Li (Li et al., 2006b) used a 2D flow-plaque interaction model and tried to answer how critical is fibrous cap thickness to carotid plaque stability. They suggested that the presence of a moderate carotid stenosis (30% to 70%) but with a thin fibrous cap can

also present a high risk for plaque rupture. Li M.X. (Li M.X. et al., 2007) constructed an idealized 3D plaque model with varying stenosis degree of 30%, 50% and 70%, to study the wall motion in plaque throat. The results suggested that severe stenosis may inhibit wall motion. The numerical study on the role of micro-calcifications in plaque vulnerability in an eccentric stenosis model (Bluestein et al., 2008) showed that the vulnerable plaque with embedded calcification spots presented higher wall stress concentration region in the fibrous cap, providing the evidence for the hypothesis that micro-calcifications could increase the plaque vulnerability. Kock (Kock et al., 2008) developed a 2D FSI model based on *in-vivo* MR images of two symptomatic atherosclerosis patients, and the longitudinal stress levels for each patient were calculated. They concluded that the longitudinal fibrous cap stresses may be useful in assessing plaque vulnerability.

Tang (Tang et al., 2004a) have developed a 3D fluid-structure interaction model from 3D *ex-vivo* MR images of a human atherosclerotic carotid artery to identify critical flow and stress/strain conditions, which may be related to plaque rupture. In the following years, Tang and colleagues did a series of studies on the stress analysis with atherosclerotic plaques from *ex-vivo* to *in-vivo* states (Tang et al., 2004b). Their results showed that large lipid pool and thin fibrous caps are associated with both extreme stress and strain levels. Large cyclic stress and strain resulted from pulsating pressure were identified, which may lead to plaque rupture by a fatigue procedure. Similarly as the results from 2D stress analysis, the plaque stress and strain conditions are affected considerably by lipid pool size, shape and position, plaque cap thickness, and axial stretch, and so on, from their 3D fluid structure interaction models (Tang et al., 2004c; 2005a). The study (Yang et al., 2007) on the comparison between fluid-wall (FSI) and wall only (or structure only) models with *in-vivo/ex-vivo* MRI-based 3D non-Newtonian FSI showed that there could be a great difference in wall shear stress, maximum principle stress between the two models. Huang (Huang et al., 2009)

has proposed a method to determine 3D zero stress state of carotid atherosclerotic plaques from *in-vivo* MRI data by a patient-specific artery shrinkage procedure in axial and inner circumferential directions. They suggested that accurate knowledge of artery shrinkage and the shrinkage process will considerably improve the accuracy of stress prediction from *in-vivo* plaque models.

Moreover, efforts have been made to use plaque stress for assessing and predicting plaque vulnerability (Tang et al., 2009). The local maximal stress hypothesis and a stress-based computational plaque vulnerability index were proposed to assess plaque vulnerability by Tang and colleagues (Tang et al., 2005b). A critical stress form in the fibrous cap was chosen to determine the vulnerability index. Their results showed the vulnerability index based on stress information was 85% agreement with the assessment given by histopathological analysis. Similarly a pilot study was also performed on assessment of plaque vulnerability by MRI and computational biomechanics by Zheng (Zheng et al., 2005). The stress/strain was calculated in plaque sections, and an index including entire plaque area, lipid-cap-thickness, and stress components was suggested for vulnerability assessment. A negative correlation between human carotid atherosclerotic plaque progression and plaque wall stress has been demonstrated by Tang (Tang et al., 2008) with *in-vivo* MRI based 2D/3D FSI models. They also suggested that both lower wall stress and lower wall shear stress may contribute to continued plaque progression. The studies linking plaque stress to plaque progression/rupture would advance the understanding of biomechanical role in atherosclerosis plaque initiation, development and rupture, providing insights in therapy options.

2.5 Factors Influencing the Simulation Accuracy of FEM Models on Plaque Stress Analysis

2.5.1 Model Reconstruction

The computational biomechanics simulation with two/three dimensional medical imaging provides a new approach for advancing our understanding between biomechanics factors and arterial disease. In order to perform biomechanical study on plaques, the first step after the image acquisition is to reconstruct the plaque model either 2D or 3D. However, the reconstruction procedure is subject to several potential uncertainties, especially for 3D models. From previous studies, it has been demonstrated that the accurate reconstruction of plaque geometry will greatly affect the biomechanics results, and more effort should be given to a more accurate and detailed geometry reconstructions, the primary influence on physiologically significant indicators (Steinman DA., 2004; Lee Sang-Wook and Steinman, 2007).

With the development of modern medical imaging technique, increasing number of different kinds of *in-vivo* images can be used for geometry reconstruction. The reconstructions of patient specific diseased artery model from medical images have been studied for a long time, the procedure has been well established, either using third party software (Shojima et al., 2004) for image analysis and geometry extraction, or in-house software based on established image processing techniques (Steinman et al., 2003). Most of the methods in existed literatures are based on the extraction of arterial cross-sectional boundaries, alignment of those boundaries in 3D context, and construction of 3D surfaces and bodies from the stack of 2D boundary profiles.

The overall accuracy of 3D luminal wall geometry reconstruction has been investigated by Moore (Moore et al., 1999) by using a carotid bifurcation phantom and a human carotid bifurcation. 5 different reconstruction procedures were applied to the reconstructions with or without smoothing. Results showed that for phantom model, all reconstructions gave acceptable results, while *in-vivo* models need to be properly smoothed for use in computational studies of *in-vivo* hemodynamics. Long (Long et al., 2003) studied the reproducibility of 3D geometrical reconstructions of

eight human carotid bifurcations from *in-vivo* MRI. Smoothed lumen contours were aligned in the longitudinal direction, B-spline interpolation was applied to reconstruct the 3D surface of carotid bifurcation, two steps of smoothing were employed to improve the quality of the 3D reconstruction, including: centerline smoothing and surface smoothing. They concluded that the geometry of common carotid artery was well reproduced by the reconstruction procedure in most of the cases, while the external carotid artery showed the worst reproducibility. 3D ultrasound also has been used for carotid geometry reconstruction for image-based CFD modeling (Glor et al., 2003).

However most of studies have been focused on the arterial luminal reconstruction and the effects on the hemodynamic factors. The stress analysis in the plaque region requires the accurate reconstructions of plaque components, which could be much harder than the reconstruction of arterial lumen. Compared to the lumen geometry reconstruction, the structures involved in the plaque structure analysis are different in size, shape, et al. especially when coming to thin fibrous cap reconstruction. A vulnerable plaque could have a thin fibrous cap less than 65um, which may be represented by one or two pixels in medical images. Therefore the relative uncertainties in fibrous cap reconstruction will be higher than other plaque components. Although structure stress analysis has been applied in plaques with modern medical imaging to assess plaque vulnerability for many years, there are few studies on assessing the plaque geometry reconstruction uncertainties and their effects on stress distributions in plaque region.

2.5.2 Material Properties

Quantifying the mechanical properties of healthy and diseased arterial tissue is essential for realistic stress prediction. Histological studies in the arterial wall have shown that arterial wall is heterogeneous, non-linear, anisotropic, and viscous-elastic.

Richardson (Richardson 2002) has pointed out that the lack of accurate plaque material properties data is possibly the most uncertain aspect in the existing literature on plaque rupture study. The main components of the plaque are lipid core, calcification, and fibrous cap tissue. While there has been many research on the healthy arterial tissue (Vito et al., 2003; Gerhard et al., 2006), studies on the mechanical properties of plaque components are much less. A review of published data showed a wide range of material properties for plaque components (Williamson et al., 2003). In general, lipid is much softer compared to other plaque components, while calcification is much stiffer. The stiffness of fibrous cap is essential to the plaque stability. Because of the complex fiber organization and content variation, the stiffness of fibrous cap shows a great range of variation. Therefore, to obtain a proper material data for structure stress analysis is a key step towards on developing biomechanical plaque models, especially for fibrous cap tissue.

Lee and colleagues (Lee et al., 1991) determined the mechanical properties of plaque fibrous cap from human abdominal aortas by static and dynamic loading tests. The stiffness of the fibrous cap was depended on its micro-structure, including calcification, collagen content and organization. They also found that fibrous cap stiffness increased with the increased frequency of loadings, indicating fibrous cap stiffness is non-linear in nature. Loree (Loree et al., 1994a) investigated the static circumferential modulus of human atherosclerotic tissue. They found that the static circumferential tangential modulus was not significantly affected by the degree of cellularity and calcification, compared to the compressive modulus. Later, Loree (Loree et al., 1994b) did the mechanical test on lipid pools with different lipid compositions by using a torsion rheometer. Results showed that the stiffness of lipid pools depended on the concentration of cholesterol monohydrate crystals.

Topoleski (Topoleski et al., 1997) used a custom-built experimental system to test segments of a whole human atherosclerotic plaque by uni-axial radial cyclic compressive testing, plaques showed nonlinear characteristic under finite deformation, related to the plaque composition and load history. Topoleski and Salunke (Topoleski and Salunke 2000) studied the mechanical behavior of calcified plaques with compression and stress-relaxation experiments, the calcified plaques are significantly different from other plaques. Holzapfel (Holzapfel et al., 2004) measured anisotropic mechanical properties of tissue components in human atherosclerotic plaque tissue, including ultimate tensile stresses/stretches. Results showed that plaque components are highly nonlinear and different in the different layers, the lowest fracture stress occurred in the circumferential direction of the fibrous cap. Ebenstein (Ebenstein et al., 2008) used nano-indentation to measure the mechanical properties of blood clots, fibrous tissue, calcified fibrous tissue from human atherosclerotic plaque tissue, demonstrated that the stiffness of plaque tissue increases with increasing mineral content. Recently Barrett (Barrett et al., 2009) measured the indentation response of 8 human carotid atherothrombotic plaque samples by fitting the experimental results to finite element simulations.

Modern medical imaging has been employed to quantify the material properties in diseased vessels recently, which provides a possibility to characterize material properties under *in-vivo* situation for realistic patient specific stress simulation. Based on 3D IVUS model, Vonesh (Vonesh et al., 1997) developed a method to estimate the regional material properties in diseased iliac and femoral arteries by using finite element method, results showed that the elastic modulus for non-diseased tissue was significantly different from plaque tissue. Karimi (Karimi et al., 2008) proposed a new method for estimation of nonlinear elastic properties of soft tissue by combining the nonlinear finite element methods for estimating tissue stiffness profile. The proposed method has been applied to realistic 2D and idealized 3D arterial plaque

models, proved the possibility for the estimation of intra-plaque distribution of nonlinear material properties. Masson (Masson et al., 2008) developed an approach to identify material properties and wall stress prediction for human common carotid arteries based on non-invasive *in-vivo* clinical data by measuring the dynamical intra-luminal pressure, medial diameter and intimal-medial thickness. The method provided a way to characterize patient-specific material parameters directly from non-invasive *in-vivo* human data.

2.5.3 Residual Stress/Strain

It is accepted that biological tissue does not become free of stress when all external loads are removed. Previous studies have shown that such residual stress/strain tends to maintain the integrity of vessel structure, and make the stress distribution more uniform throughout the arterial wall. However the effects of residual stress on plaque stability have not been well studied. Ohayon's study (Ohayon et al., 2007) showed the residual stress/strain in plaques is not negligible, and may dramatically affect the physiological peak stress in thin fibrous cap, and suggested that plaque rupture should be treated as a combination of external loading and intra-plaque residual stress/strain. The study from our group showed that the circumferential residual stress has limited effects on the actual stress distribution under normal physiological loadings (Pocaterra et al., 2009). Those controversial results indicated that more efforts need to be made to understand the residual stress/strain to plaque stability.

2.6 Summary

The summary of plaque stress analysis research is presented in the following Table 2.2. With the efforts in numerical modeling of plaque stress, combining the inputs from histological, pathological studies of plaques, more insights will be gained for the understanding of plaque initiation, development, and rupture. Better diagnosis, treatment and management could be achieved in the future.

Papers	Models Source	Results
2D structure stress analysis		
Loree et al 1992	Idealized models	Fibrous cap thickness is an critical factor affecting plaque stress
Cheng et al 1993	Histology	Plaque ruptures at high stress location
Finet et al 2004	IVUS + Idealized model	the fibrous cap thickness can greatly affect the peak stress
Beattie et al 1998	Histology	Proper material models with multi-components in plaque stress analysis is of very importance
Williamson et al 2003	Histology	Stress prediction showed low sensitivity to the chosen material models
Lee et al 1996	Histology	Significant correlation between MMP-1 and circumferential stress
Howarth et al 2007	MRI + Histology	Macrophage locations correlated with peak plaque stress
Hallow et al., 2009	Histology	A limited relation found between inflammation and extreme stress
Huang et al., 2001	Histology	Calcification may stabilize plaques
Chau et al., 2004	OCT	Realistic plaque geometry and components are important
Li et al 2006; 2007	MRI	Peak stress in symptomatic patients is much higher
Trivedi et al., 2007	MRI	Plaque stress related to plaque stability
Zheng et al., 2005	MRI + Histology	Vulnerability index was proposed based on stress analysis
Tang et al., 2009	MRI	Local critical stress was suggested for plaque vulnerability assessment
Ohayon et al., 2007	Histology	Residual stress/strain may greatly affect plaque stability
Pocaterra et al., 2009	Histology + US	Residual stress/strain may just have limited effects on the plaque stress
3D structure stress analysis		
Hoshino et al., 2009	Idealized 3D model	Calcification locations matter in plaque stability
Koji Imoto et al., 2005	Idealized 3D model	Plaque shape, size, remodeling etc. affect longitudinal plaque stress
Holzapfel et al., 2002	MRI	a nonlinear anisotropic multi-layer material model was developed
Gasser et al., 2007	Image-based 3D model	plaque fissuring/dissection could cause localized mechanical trauma
Ferrara et al., 2008	MRI	plaque rupture was simulated
Ohayon et al., 2005	IVUS	plaque ruptures at locations of high stress
Wu et al., 2003	Cine angiographic images	plaque structure/components are key issues in stress prediction
Fluid structure interaction analysis		
Zhao et al., 2002	MRI	Certain locations with high wall stress and low wall shear stress were identified in healthy carotid artery
Younis et al., 2004	MRI	Biomechanical factors effects on atherogenesis
Kaazempur-Morfrad, et al., 2003, 2004	MRI + Histology	Biomechanical factors were correlated with histological analysis
Li et al., 2006	2D idealized model	low stenosis plaque with thin fibrous cap may have high rupture risk
Li M.X et al., 2007	3D idealized model	the effects of wall motion in plaque development and rupture
Bluestein et al., 2008	3D idealized model	micro-calcification in fibrous cap could increase plaque vulnerability
Kock et al., 2008	MRI-based 2D model	plaque stress can help in vulnerability assessment
Tang,et al. 2004(a,b,c), 2005, 2008	MRI	3D FSI plaque stress with MRI has been developed and discussed
Yang, et al., 2007	MRI	Comparison between structure-only and FSI model was conducted
Huang et al., 2009	MRI	The determination of plaque shrinkage and stress-free state in plaque

Table 2.2 summary of research on biomechanical study of plaques

Chapter 3

Methodology Development: Fluid Structure Interaction

3.1 Introduction

Atherosclerotic plaque is under pulsating blood pressure loading in physiological situation all the time. The mechanical environment of plaque includes the blood flow dynamics and wall structure dynamics. In order to accurately predict the biomechanical environment, one must consider hemodynamic factors surrounding the plaque region, and the corresponding wall dynamics under the pulsating loading caused by blood flow. Therefore fluid structure interaction method is needed for plaque stress simulation to obtain the two interacted biomechanical environments in plaques.

At present, fluid-structure interaction is one of very important and popular techniques in modeling biomechanical behaviors when fluid flow and structure deformation are interacting together, especially in vascular mechanics, such as hypertension, arteriosclerosis. FSI involves the coupling of fluid mechanics and structure mechanics domains. In a FSI problem, the fluid domain is computed together with the stresses and deformations of a given structure, the main issues in FSI are: (1) fluid simulation (blood flow in carotid artery with stenosis); (2) structure dynamics simulation (wall stress in carotid plaque region); (3) interaction between fluid domain and structure domain. In the study, the FSI procedure was developed with ANSYS 11.0 SUITE (ANSYS), including Ansys Structure Mechanics (solid code) for structure analysis, CFX for blood flow simulation.

3.2 Theory on Fluid Structure Interaction (ANSYS)

3.2.1 Background of FSI

Fluid structure interaction problems usually are very complex. The discretization of the mathematical model in space and in time with time integration for both structure and fluid flow domain forms a system of algebraic equations. Considering a FSI problem, the solutions in the fluid and solid domain are defined as ξ_f and ξ_s, in which ***f*** stands for fluid

domain, *s* stands for structure domain. The equilibrium conditions in the fluid structure interface are the kinematic condition for displacement continuity: $d_f = d_s$ and the dynamic condition for stress continuity $n_f \cdot t_f = -n_s \cdot t_f$, *n* stands for the normal direction. Therefore the FSI interface values are given by $d_s = d_s(x_s)$, and $t_f = t_f(x_f)$. The system equations for the fluid-structure interaction problem can be written as

$$\begin{cases} f_f(x_f, d_s(x_s)) = 0 & [3.1] \\ f_s(x_s, t_f(x_f)) = 0 & [3.2] \end{cases}$$

Two main approaches exist for the simulation of FSI:

- Monolithic approach: the equations governing flow and displacements of the structure are combined and treated in one system, and solved simultaneously with one single solver.
- Partitioned approach: the equations governing flow and displacement of the structure are solved individually, in succession, with two or more distinct solvers. A coupling system is required for exchanging latest information among solvers.

Monolithic Solution Strategies

The monolithic approach usually requires the code developed for the combinations of physical problems in one single system. It has the advantage of solving very difficult FSI problem, such as large deformations with 'soft structure' or highly compressible flow, and it is also simpler to analyze the FSI system mathematically. However the monolithic approach does not recognize the differences between the mathematical properties of fluid and structure domains. Moreover, it will not reuse the existed software modularity for each domain which have been validated and used for a long time.

For monolithic approach, the equations (3.1 and 3.2) governing flow and structure dynamics need to be combined into to a single system, and solved simultaneously by a single preferred time-integrator (Morton et al., 1997), such as Newton-Raphson interactions as in equations 3.3 and 3.4,

$$\begin{bmatrix} \frac{\partial f_f{}^k}{\partial x_f} & \frac{\partial f_f{}^k}{\partial x_s} \\ \frac{\partial f_s{}^k}{\partial x_f} & \frac{\partial f_s{}^k}{\partial x_s} \end{bmatrix} \cdot \begin{bmatrix} \Delta x_f{}^k \\ \Delta x_s{}^k \end{bmatrix} = - \begin{bmatrix} \Delta f_f{}^k \\ \Delta f_s{}^k \end{bmatrix} \quad [3.3]$$

$$x_f{}^{k+1} = x_f{}^k + \Delta x_f{}^k; x_s{}^{k+1} = x_s{}^k + \Delta x_s{}^k \quad [3.4]$$

where ***k*** stands for the current iteration step, ***k+1*** is the next step. The interaction between fluid and structure domain has been taken into account during the solution process because of the off-diagonal blocks of Jacobian matrix in equation 3.3.

Partitioned Solution Strategies

The staggered schemes are probably the simplest and best known strategies, often used to solve the corresponding coupled systems. In staggered schemes, explicit and implicit methods can be used for the time integration. The general serial staggered procedure in a generic cycle can be described as in Figure 3.1 (Farhat et al., 2006): (1) transfer the movement ($d_s(x_s)$) of solid boundary to the fluid domain, and update the mesh for flow simulation; (2) solve the fluid domain to the next time interval (x_f); (3) transfer the loading from fluid domain ($t_f(x_f)$) to the structure, and solve structure dynamics (x_s) with latest loading boundaries to the next time interval. Therefore information is only exchanged between the domains after the increment has been performed. Inside the increment, each domain is solved individually, and independent of others. This type of staggered solution procedure usually is described as a loosely-coupled solution scheme. The improvement can be made inside the increment by carefully designed inner iterations which are performed at each time interval, and then the staggered procedure can be called as a strongly-coupled scheme.

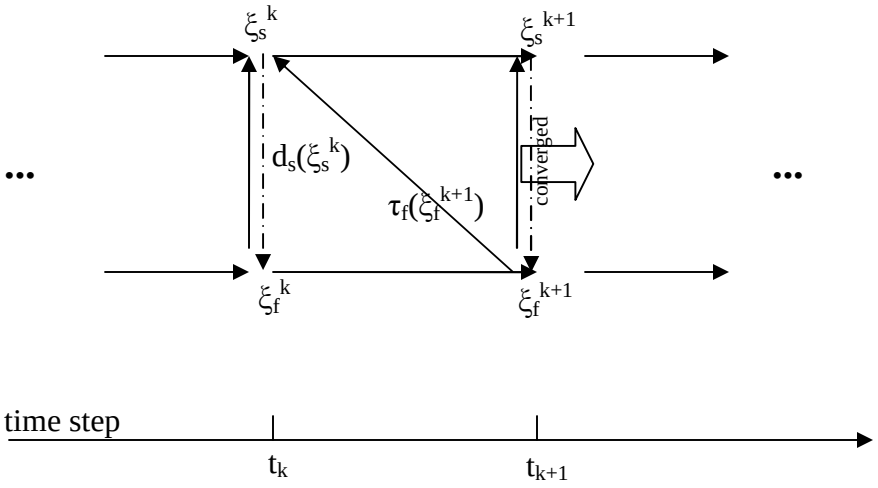

Figure 3.1 Schematic of FSI simulation with staggered scheme

The loosely coupled staggered scheme is often criticized for its lack of sufficient time-accuracy and sufficient numerical stability, therefore strongly-coupled solution and monolithic schemes are more encouraged for FSI problems. The strongly-coupled methods usually yield the solution of a nonlinear problem on the fluid structure interface (La Tallec et al., 2001), with all other variables internal to the residual operator of this problem. Some numerical methods have been proposed to solve these nonlinear equations, such as Interface-Newton method (Degroote et al., 2009), Gaussian-Seidel iterations (Gerbeau et al., 2005), etc. For example, the interface-Newton techniques will reformulate the FSI problem (equation 3.1) as

$$R(d_s) = 0 \qquad [3.5]$$

R is the residual operator. The solution of the fluid flow system $f_f(x_f, d_s(x_s)) = 0$ with given $d_s(x_s)$ can be reformulate as $t_f = j_f(d_s)$. Similarly the solution of the structure system $f_s(x_s, t_f(x_f)) = 0$ with given $t_f(x_f)$ is represented by $d_s = j_s(t_f)$, then the residual of the FSI problem in the fluid-structure interface is defined as

$$R(d_s) = j_s \circ j_f(d_s) - d_s \qquad [3.6]$$

The fluid structure coupling is achieved by solving the above nonlinear equation. There are several methods to solve equation 3.6, such as fixed point strategy, Newton methods,

etc. For example, in Newton-Raphson iterations (Degroote et al., 2009), the above nonlinear equation 3.6 is reformulated as

$$\frac{\partial R^k}{\partial d_s}\Delta d_s^k = -R^k; d_s^{k+1} = d_s^k + \Delta d_s^k \qquad [3.7]$$

Several techniques have been proposed for calculating residual matrix $\frac{\partial R^k}{\partial d_s}$ in partitioned schemes without knowledge of the Jacobians of the solvers for fluid and structure domains (Vierendeels et al., 2007), in which the solvers for fluid, structure and fluid-structure interface will be solved subsequently to reach convergence for the whole domain.

The advantages of the partitioned approach in FSI simulation lie in facts: (1) it can preserve software modularity, and reduce the computational complexity by combining existing fluid solver and structure solver with certain coupling algorithms; (2) the partitioned approach can allow to solve the flow equations and the structure equations with different, possibly more efficient techniques which have been developed specifically for either flow equations or structure equations; (3) newly developed mathematical models and methods in fluid and structure dynamics can be implemented under the framework of FSI with less pain; (4) compared with monolithic approach, it requires less memory and may be more applicable to solve very large problems. Therefore the partitioned approach is employed in the research for plaque stress analysis.

3.2.2 Fluid Simulation

The fluid simulation in FSI is identical to a conventional CFD problem with moving boundaries, that is, the mesh in fluid domain will change during simulating. For a fluid flow, the general mathematical descriptions are mass, momentum, and energy conservation equations. The continuity equation can be expressed as

$$\frac{\partial r}{\partial t} + \nabla \cdot (rU) = 0 \quad \text{in } {}^{F}\Omega(t) \qquad [3.8]$$

r : fluid density, t: time, U represents the velocity field with three components for three dimensional flows, meaning $U = (u, v, w)$.

The momentum equations (Navier-Stokes equation) are:

$$\begin{aligned}
&\frac{\partial(ru)}{\partial t}+\nabla\cdot(ruU)=-\frac{\partial p}{\partial x}+\frac{\partial t_{xx}}{\partial x}+\frac{\partial t_{yx}}{\partial y}+\frac{\partial t_{zx}}{\partial z}+r f_x\\
&\frac{\partial(rv)}{\partial t}+\nabla\cdot(rvU)=-\frac{\partial p}{\partial y}+\frac{\partial t_{xy}}{\partial x}+\frac{\partial t_{yy}}{\partial y}+\frac{\partial t_{zy}}{\partial z}+r f_y \quad \text{in } {}^{F}\Omega(t)\\
&\frac{\partial(rw)}{\partial t}+\nabla\cdot(rwU)=-\frac{\partial p}{\partial z}+\frac{\partial t_{xz}}{\partial x}+\frac{\partial t_{yz}}{\partial y}+\frac{\partial t_{zz}}{\partial z}+r f_z
\end{aligned} \qquad [3.9]$$

p : the pressure, t_{ij} : viscous stress, $f=(f_x, f_y, f_z)$ represents the body force.

The stress tensor t_{ij} is related to the strain rate by

$$t=m(\nabla U+(\nabla U)^T-\frac{2}{3}d\nabla\cdot U) \qquad [3.10]$$

m is the fluid viscosity.

Several simplifications can be made for blood flow in human arteries, such as: (1) the blood is incompressible; (2) the viscosity is constant, referred as Newtonian fluid; (3) the body force can be ignored; (4) the flow can be considered to be laminar due to the low Reynolds number; (5) the energy equation is ignored if there is no requirement on thermal information. With these simplifications, the continuity and Navier-Stokes equations become:

$$\begin{aligned}
&\nabla\cdot(U)=0\\
&\frac{\partial u}{\partial t}+\nabla\cdot(uU)=-\frac{1}{r}\frac{\partial p}{\partial x}+\frac{1}{r}m\nabla^2 u\\
&\frac{\partial v}{\partial t}+\nabla\cdot(vU)=-\frac{1}{r}\frac{\partial p}{\partial y}+\frac{1}{r}m\nabla^2 v \quad \text{in } {}^{F}\Omega(t)\\
&\frac{\partial w}{\partial t}+\nabla\cdot(wU)=-\frac{1}{r}\frac{\partial p}{\partial z}+\frac{1}{r}m\nabla^2 w
\end{aligned} \qquad [3.11]$$

For viscous, incompressible fluids, the viscosity stress tensor can be written as

$$t=m(\nabla U+(\nabla U)^T) \qquad [3.12]$$

The Reynolds number is defined as $\mathrm{Re}=\frac{rVD}{m}$, V: the mean velocity, D: the diameter of the arterial lumen. In carotid artery, the typical diameter is around 8mm, if the mean velocity is about 0.2m/s, the viscosity is taken as 0.004Pa.s, and the density is 1060kg/m^3, then Re is 427, which indicates laminar flow could be assumed for blood flow in carotid

artery in the study. However the assumption of laminar flow in carotid arteries may not be always accurate, the critical Reynolds number for laminar flow varies according to the geometry features for the studied domain, such as the stenosis degree. Therefore in this study, in order to simply the computation modeling model in blood flow, the laminar flow model is assumed even for different carotid geometries.

Since there is no analytical solution for N-S equations for complex flow such as intra arterial blood flow, numerical methods need to be developed. Now there are a number of different solution methods which are used in CFD codes to solve the continuity and momentum conservation equations. The finite volume technique, most popular method, is used in CFX (ANSYS), in which the computational domain is divided into small sub-regions, called control volumes (mesh), and the equations are discretized and solved iteratively for each control volume. In the end, the approximated values in each specific point throughout the domain will be obtained (Eymard 1997).

In finite volume method, the governing equations [3.11] are integrated over each control volume by using CFD mesh. Typical meshes are Hexahedral and Tetrahedral elements. Consider the compact form of Equation 3.11

$$\begin{aligned} &\frac{\partial r}{\partial t}+\frac{\partial}{\partial X_j}(rU_j)=0 \\ &\frac{\partial}{\partial t}(rU_j)+\frac{\partial}{\partial X_j}(rU_jU_i)=-\frac{\partial p}{\partial X_i}+\frac{\partial}{\partial X_j}(m(\frac{\partial U_i}{\partial X_j}+\frac{\partial U_j}{\partial X_i})) \end{aligned} \qquad [3.13]$$

where $U=(u,v,w)$, $X=(x,y,z)$, and $i,j\in(1,2,3)$. Gauss' Divergence Theorem is applied to convert volume integrals to surface integrals when Equation 3.13 is integrated over a control volume,

$$\begin{aligned} &\frac{d}{dt}\int_V r\,dV+\int_s rU_j dn_j=0 \\ &\frac{d}{dt}\int_V rU_i dV+\int_s rU_iU_j dn_j=-\int_s p dn_j+\int_s m(\frac{\partial U_i}{\partial X_j}+\frac{\partial U_j}{\partial X_i})dn_j \end{aligned} \qquad [3.14]$$

where V, s and dn_j represent the volume, surface regions and outward normal surface vector of the control volume. The discrete forms of the above integral equation 3.14 usually are based on series expansion approximations of continuous functions, such as the Taylor series, therefore the order-accuracy is depended on the exponents on the mesh spacing and timestep factor of the largest term in the truncated part of the series expansion. The discrete forms can be

$$\begin{aligned} &V\left(\frac{r^n - r^{n-1}}{\Delta t}\right) + \sum_{ip}(U_j \Delta n_j)_{ip} = 0 \\ &\left(\frac{r^n U_i^n - r^{n-1}U_i^{n-1}}{\Delta t}\right) + \sum_{ip} m_{ip}^n (U_i^n)_{ip} = \sum_{ip}(p^n \Delta n_i)_{ip} + \sum_{ip}(m(\frac{\partial U_i^n}{X_j} + \frac{\partial U_j^n}{X_i})\Delta n_i)_{ip} \end{aligned} \quad [3.15]$$

where V is the control volume, Δt is the time step, Δn_j is the discrete outward surface vector, the subscript ip represents evaluation at integration points. n and $n-1$ denote the current time step and previous one. m_{ip} stands for the mass flow through a surface of the control volume, defined as

$$m_{ip} = (rU_j \Delta n_j)_{ip} \quad [3.16]$$

In ANSYS CFX, those nonlinear equations are linearized and assembled into a solution matrix, and solved by using an algebraic multigrid method. A coupled solver is employed for the solution strategy, in which the hydrodynamic equations (for u, v, w, p) are solved in a single system. Furthermore ANSYS CFX uses a fully implicit discretization of the equations at any given time step, which will reduce the number of iterations required for convergence compared to segregated solvers. The details regarding discretization, CFX solution strategy, accuracy, etc, can be found in ANSYS CFX Document (CFX).

3.2.3 Structure Mechanics

The second computational domain involved in FSI is the stress/strain calculation in structure domain. Similar as the conventional solid mechanics too, the equations controlling the movement include,

(a) momentum equations:

$$r\ddot{d}_{i,tt} = s_{ij,j} + r\ddot{f}_i \qquad \text{in } {}^s\Omega(t) \quad [3.17]$$

(b) equilibrium conditions:

$$s_{ij} n_j = {}^{s}t_i \quad on\ {}^{s}\Gamma(t) \tag{3.18}$$

where r is the material density, s is the Cauchy stress tensor, $\vec{f}$ is the externally applied body force, ${}^{s}t$ is the externally applied surface traction vector, $\vec{d}$ is the solid displacement vector, ${}^{s}\Omega$ represent the structure domain, ${}^{s}\Gamma$ is the boundary surface of the structure domain ${}^{s}\Omega$, n is the normal vector at ${}^{s}\Gamma$.

The relationship between stress and strain is needed for the structure analysis, which is material model or constitutive equation. Normally, arterial wall and plaque components are considered to be hyper-elastic, isotropic, incompressible, and homogeneous, therefore there exists an elastic potential function W (strain energy density function) defined by deformation tensors, and its derivative with respect to strain components determines the corresponding stress components. The 3D non-linear 5-parameters Mooney-Rivlin model is used to describe the material properties of the arterial wall and plaque components in this study, they are

$$W = c_{10}(I_1 - 3) + c_{01}(I_2 - 3) + c_{20}(I_1 - 3)^2 + c_{11}(I_1 - 3)(I_2 - 3) + c_{02}(I_2 - 3)^2 + \frac{1}{D}(J-1)^2$$

$$I_1 = tr(C)$$

$$I_2 = \frac{1}{2}(tr(C)^2 - tr(CC)) \tag{3.19}$$

$$I_3 = \det(C)$$

Where I_1 and I_2 are the first and second strain invariants, D is the material incompressible parameter, J stands for the ratio of the deformed volume over the un-deformed volume of materials, c_{10}, c_{01}, c_{20}, c_{11} and c_{02} are material constants which need to be decided by the experimental data. C represents the deformation tensor, comprised of the products of the deformation gradient F, defined as

$$C_{ij} = F_{ik} F_{kj} \tag{3.20}$$

From the strain energy function, the Cauchy stress is obtained by

$$s_{ij} = \frac{1}{\det(F_{ij})} F_{ik} \left(2 \frac{\partial W}{\partial C_{kl}}\right) F_{jl} \tag{3.21}$$

the infinitesimal strain-displacement relation can be expressed as

$$e_{ij} = \frac{1}{2}(d_{i,j} + d_{j,i}) \quad [3.22]$$

Usually arterial wall and plaque components exhibit nonlinear structure behaviors including: (1) material nonlinearity; (2) geometric nonlinearity due to 'large' displacements and/or rotations. Ansys Structure Mechanics employs the 'Newton-Raphson' approach to solve nonlinear problems, in which the load is subdivided into a series of load increments, which can be applied over several load steps. In each load step, the calculated restoring forces are obtained by balancing with applied loads. An iterative procedure is used to update the solution based on the balanced results from the previous step until the final load step.

3.2.4 Fluid Structure Interface

After the mathematical definitions for fluid and structure domain separately, the interface between the two domains is needed to be set up for transferring force from fluid domain and deformation from structure domain. For example, the luminal surface is defined as the FSI interface in the study. Dynamic and kinematic compatibility conditions must be satisfied in the FSI interface, they are:

(a) the displacements at the interface in fluid and solid domains are the same,

$$^{F}d = {}^{S}d \quad [3.23]$$

with the assumption of no-slip wall boundary condition, it leads to the fluid velocity at the interface being defined as

$$^{F}u = {}^{S}u \quad [3.24]$$

(b) the surface force acting on the structure will be opposite to the force acting on the fluid, that is

$$^{S}f = -{}^{F}f \quad [3.25]$$

Because of the deformation of FSI interface during structure simulation, the corresponding fluid mesh needs to be regenerated after each step of structure simulation. In CFX, the remeshing of fluid domain is determined by the mesh motion model 'Displacement Diffusion' by solving

$$\nabla \cdot (\Gamma_{disp} \nabla d) = 0 \quad [3.26]$$

d is the displacement relative to the previous mesh locations, and Γ_{disp} is the mesh stiffness. This equation is solved immediately after the displacement is transferred from structure domain. 'Displacement Diffusion' model has the ability to preserve the relative mesh distribution of the initial mesh.

The mesh node location at the FSI interface from fluid and structure might be different. An interpolation method must be used to map the loading data from the mesh points of one domain to the other. Two types of interpolation are implemented in ANSYS: 'Profile Preserving' and 'Conservative'. The profile preserving interpolation simply takes the profile of the variables on one mesh, and matches or maps it to the other mesh as best as it can; the conservative interpolation ensures the profile is interpolated in such a way to ensure that a total quantity passing across the interface is conserved. Usually profile preserving is used for displacement transfer, conservative method for forces.

3.2.5 FSI Realization by ANSYS SUIT

The multiple code coupling is available for FSI simulation by using two ANSYS Multi-field solvers (ANSYS Structure Mechanics for arterial wall and plaque components, ANSYS CFX for corresponding blood flow). These two field solvers are coupled using coupling iterations method, shown in Figure 3.2. During each iteration, every field solver collects loads in the FSI interface from other field solvers, and proceeds to solve its own physics field individually. Iterations continue until all physical field solutions and loads converge.

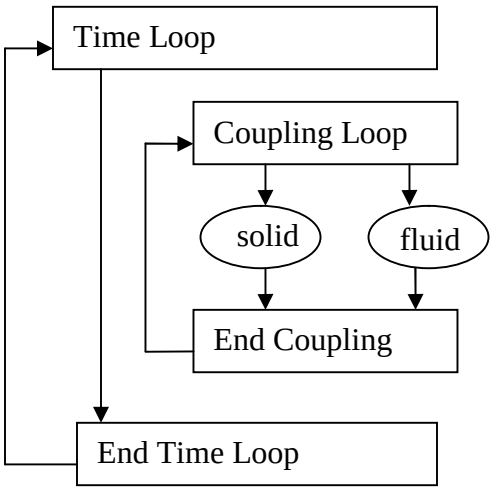

Figure 3.2 FSI procedure by ANSYS

There are two types of coupling: one-way (loose-coupling) and two-way (strong-coupling). **One way coupling**: when one field strongly affects the other fields, but not be affected by other fields, then the coupling between the solution fields can be assumed to be one-directional, as shown in Figure 3.3. Therefore there is no iteration between the two field solutions. In the case of a one way FSI simulation of plaque stress analysis, the fluid and structure are decoupled from each other, only one direction of load transfer occurs, either the fluid pressure loading from blood flow, or the lumen wall deformation from structure analysis. Usually the resulted deformation of the carotid artery wall is small, therefore the effects caused by wall deformation is small on the general blood flow pattern; on the other hand, due to stenotic effect in plaque region, there could be a great pressure drop in plaque region. Therefore there is a need to transfer pressure loading to the structure domain for more accurate plaque stress analysis, rather than uniform pressure loading as used in structure only simulation.

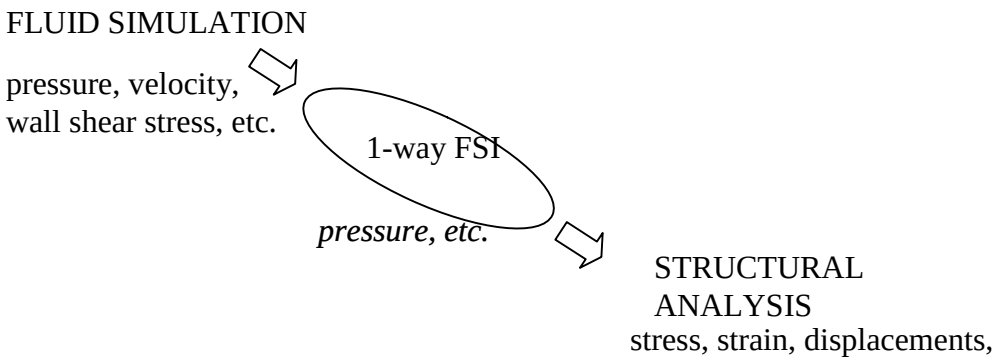

Figure 3.3 Diagram of one-way FSI

Two way coupling: for stress analysis in plaque region, when the accurate fluid results are needed, the displacements from structure deformation are required to feedback to fluid simulation with moving boundary conditions. In ANSYS, the loadings are exchanged in loops of iterations until all field solutions and loads converge. The displacements in FSI surface are the moving boundaries for CFD simulation of blood flow. In turn, the resulted pressure and wall drag forces are fed back as the loading boundary conditions for solid domain, shown in Figure 3.4.

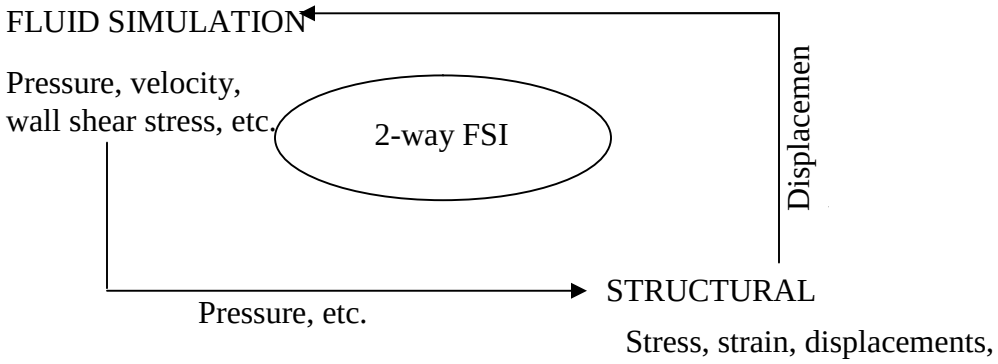

Figure 3.4 Diagram of two-way FSI

During FSI simulation in ANSYS, the Solid code for structure dynamics functions as the master and CFX code as the slave. The master performs the coupling setup, reads the coupling commands, collects the interface mesh from the slave, and maps the nodes of

two different meshes. CFX code will receive the coupling information and send the interface results to the master. The solution consists of two main loops for transient simulation: (a) the outer time loop (time step iteration), (b) the multi-field coupling loop. Within each time step there is the stagger loop, allowing the coupling of multi-fields. In one stagger iteration, the solid code and CFX will run sequentially. For example, CFX can run first with boundary conditions obtained at the beginning of coupling iteration, after several coefficient loop iterations until convergence, CFX will stop and transfer the pressure and wall drag force to solid domain. After receiving the data from CFX, the Solid code will start for the structure dynamics simulation until the convergence. Data exchange between fields occurs at each coupling loop, the global convergence of the load transfer between fields will be checked to decide whether the multi-field coupling reaches convergence at the end of each coupling loop. If it is converged, the computation will proceeds to the next time step; otherwise, a new coupling loop will be lunched. The exact solution procedure can be found in Figure 3.5.

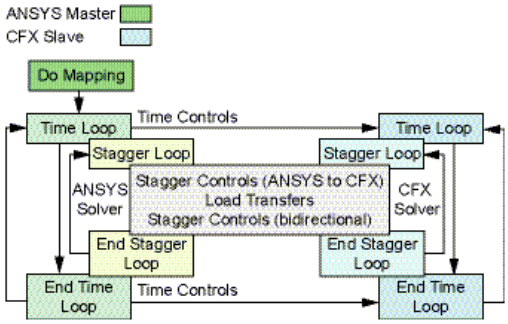

Figure 3.5 The solution procedure of two-way FSI (ANSYS). Stagger loop stands for coupling loop in ANSYS

3.3 Application of FSI to Carotid Plaques

The general procedure for setting up the FSI simulation with ANSYS Solid and CFX for carotid plaque stress analysis is showed in Figure 3.6. The plaque geometry from one studied subject is chosen for demonstration.

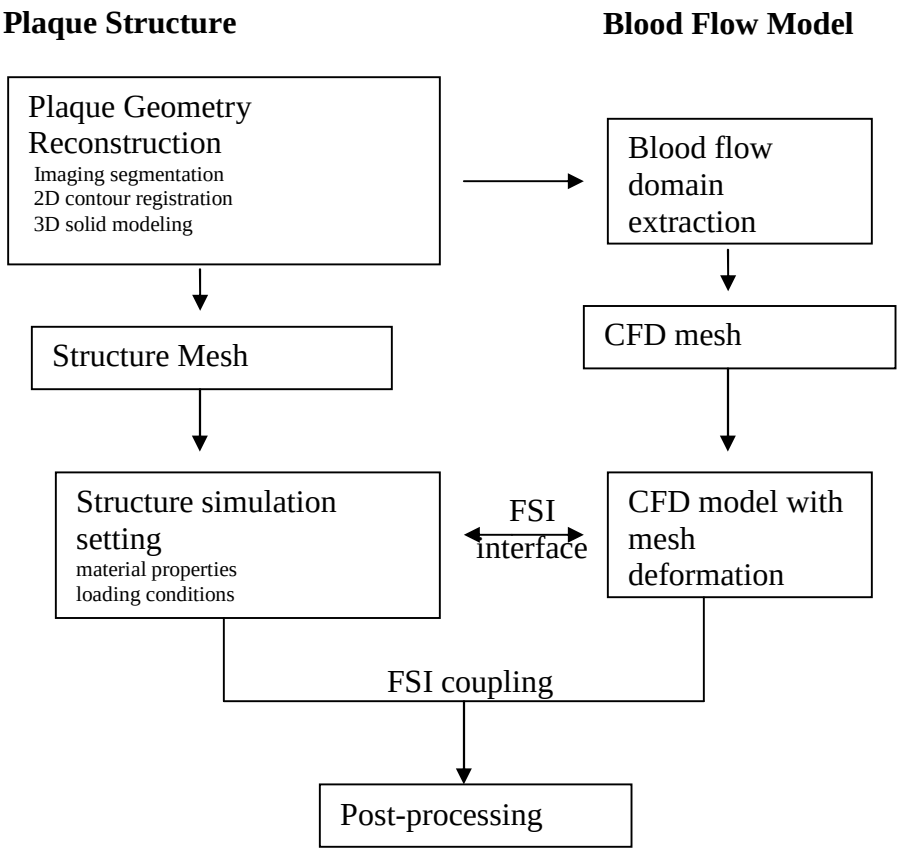

Figure 3.6 General FSI procedure for Carotid Plaque Stress Analysis

3.3.1 Blood Flow Model in Carotid Artery

The fluid domain was meshed in ICEM CFD11.0 with 3D tetra cells shown in Figure 3.7. Blood was treated as an incompressible, Newtonian fluid with a viscosity of $4*10^{-3}$ $Pa.s$ and a density of $1{,}067 kg.m^{-3}$. The flow was assumed to be laminar with a mean Reynolds number of around 500. Transient simulations were carried out with time-dependent pressure at the inlet of common carotid artery (CCA) and mass flow rates at the internal carotid artery (ICA) and external carotid artery (ECA) as the CFD simulation boundary conditions.

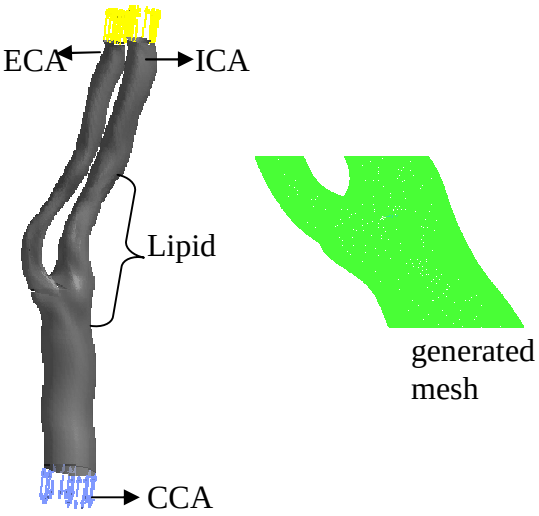

Figure 3.7 Blood flow domain and mesh

The values of mass flow rate at the CCA and ICA were computed from the phase-contrast cine images of the subject. Figure 3.8 shows the corresponding magnitude and phase image for CCA, the lumen region is indicated by the arrow.

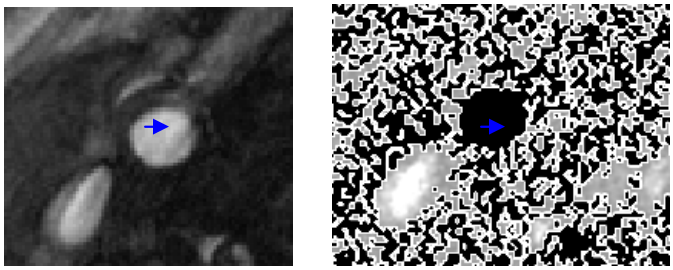

Figure 3.8 Phase contrast images at CCA

The velocity was calculated by

$$v = \frac{phase\_image}{magnitude\_image} * \frac{venc}{vencscale * 10.0 * PI} \qquad [3.27]$$

venc: the encoding velocity, vencscale: the scale for velocity encoding used by MRI machine. PI equals 3.14. By integrating the velocity over the lumen region, mass flow rate can be obtained throughout the whole cardiac cycle for CCA and ICA (Figure 3.9(a)). Due to the relatively small lumen region of ECA, the mass flow rate at ECA was derived from the difference between CCA and ICA. The cross-sectional area changing curve during a cycle measured by phase-contrast cine image was used as Pressure_Time curve in CCA, the pressure value in CCA was rescaled linearly to the Pressure_Time curve

with a range of 80-110mmHg based on the assumption that lumen area change for a healthy artery is linearly related to corresponding blood pressure change (Figure 3.9(b)).

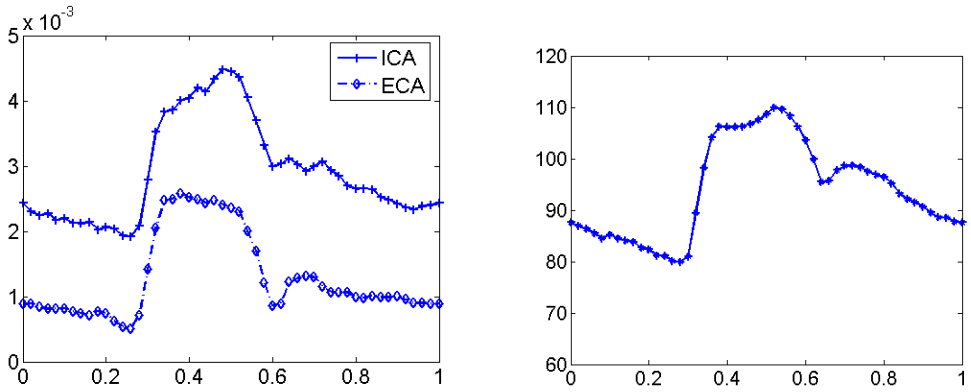

Figure 3.9 Boundary conditions for blood flow domain. (a): mass flow rate for ICA and ECA; (b) pressure profile for CCA.

In order to obtain reliable simulation results, the mesh sensitivity, time-step size, and the total simulation time were tested on this subject. Two different mesh densities were used for mesh sensitivity test (1,000,000 cells and 1,300,000 cells), the maximum velocity was compared for the whole cardiac cycle, and the absolute difference was under 2%. Furthermore, 30 points in the lumen at plaque region were selected for comparison of velocity and pressure, numerical difference in calculated velocities was found to be less than 2%. Therefore the mesh consisting of 1,000,000 cells was used for all blood flow simulation. To decide the total simulation time, one simulation with 1,000,000 cells was conducted with 3 cardiac cycles with repeated boundary conditions. The velocity difference between the second and the third cardiac cycle was compared. The results showed that the difference was less than 2%, indicating the periodic results can be reached after one cycle. Therefore in order to save the simulation time, the total simulation time was set to be 2 cardiac cycles, the results in the second cardiac cycle were used for post-processing. Two different time step sizes (50 and 100 time steps per cycle) were used for the simulation with the 1,000,000 cell model, the velocities at selected locations were compared and showed that the difference was less than 1%, the time step of 50 per cycle was then chosen for the simulation.

3.3.2 Plaque Structure Model

The reconstructed 3D plaque geometry (including arterial wall and lipid region) was imported into ANSYS workbench for structure simulation setting. The carotid arterial wall was assumed to be nonlinear, isotropic, and incompressible. A 5-parameters Mooney-Rivlin model (refer to section 3.2.3) was used to describe its material properties. The strain energy function is given by:

$$W = c_{10}(I_1 - 3) + c_{01}(I_2 - 3) + c_{20}(I_1 - 3)^2 + c_{11}(I_1 - 3)(I_2 - 3) + c_{02}(I_2 - 3)^2 + \frac{1}{d}(J - 1)^2 \quad [3.28]$$

The material constants are c_{10} =50.445kPa, c_{01} =30.491kPa, c_{20} =40kPa, c_{11} =120kPa, c_{02} =10kPa, and d=1.44e^{-7} according to the published experimental results (Yang et al., 2007), the corresponding strain-stress curve can be found in Figure 3.10. The lipid core was assumed to be very soft, and incompressible. Its stiffness is around 100 times less than arterial wall (Finet et al., 2004). The property of fibrous cap was assumed to be the same as the arterial wall.

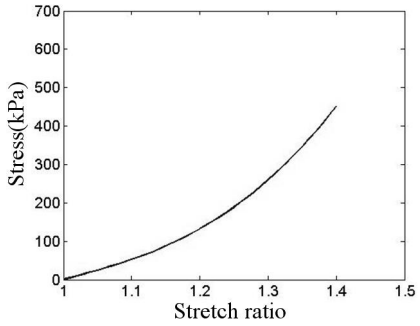

Figure 3.10 Strain-stress curve derived from the 5-parameters Mooney-Rivlin model

The structure model was meshed with an unstructured mesh consisting of 3D tetra elements. The interface between lipid core and arterial wall was treated as a so-called "always bonded" contact. The pure penalty method was employed for the contact connection. The nodes at the ICA and ECA planes were fixed in all directions to keep the carotid plaque in space, nodes at the CCA plane were stretched by applying the prescribed displacement, due to the fact that when artery is cut into sections, it will shrink longitudinally. The detailed boundary settings can be found in Figure 3.11.

Figure 3.11 boundary settings for structure analysis

The lumen surface was defined as the pressure loading for non-FSI simulation, or FSI interface for data exchange in FSI simulation. The numerical simulation was carried out by ANSYS Structure Mechanics 11.0 with finite element method (the Solid code). Mesh density sensitivity analyses was performed until stress differences between solutions from two consecutive meshes at 30 selected points in plaque regions with static simulation less than 2%. In detail, a model with about 90,000 tetras meshes and another one with 120,000 tetras meshes were used for the purpose, with 11% pre-stretch in CCA, 110mmHg pressure loading at the lumen surface. The Von Mises stress differences (30 points in the plaque region) between the two meshes were less than 2%; therefore the mesh number of around 90,000 tetras was used for structure stress simulation. It should be mentioned that the mesh independence study has not been fully studied with at least 3 mesh profiles or more, also including mesh independence study with the whole FSI domain but separately within fluid and structure domains in the PhD project. Some references can be helpful regarding those issues (Hubner B 2006, Veshkina 2010).

3.3.3 Stress Factor Definitions

In order to describe the stress distribution in fluid and structure domains, several mechanical factors need to be defined, such as wall shear stress, wall tensile stress. The temporal mean WSS (WSS_tmean) and the maximum WSS in the whole cardiac cycle ($WSS\_t\max$), were used to represent fluid domain results. Their definitions are:

$$WSS\_tmean(x,y,z) = \frac{1}{T}\int_0^T |\vec{t}_w(x,y,z,t)|dt \qquad [3.29]$$

$$WSS\_t\max(x,y,z) = \max(|\vec{t}_w(x,y,z,t)|),t \subset (0,T) \quad [3.30]$$

Where $\vec{t}_w(x,y,z,t)$ is the instantaneous WSS vector, T is the cardiac cycle, t is the time, and $|\vec{t}_w(x,y,z,t)|$ is the WSS value at time *t*. Since the stress in the arterial wall is a second-order tensor which has six components (Figure 3.12), the Von Mises stress form, named VWTS, was chosen to represent the wall tensile stress distributions and levels in the diseased plaque, defined by

$$VWTS = \sqrt{\frac{(s_1 - s_2)^2 + (s_2 - s_3)^2 + (s_3 - s_1)^2}{2}} \quad [3.31]$$

σ_1, σ_2, and σ_3 are the first, second and third principle stresses, which are calculated from the stress components by the equation:

$$\begin{vmatrix} s_x - s & s_{xy} & s_{xz} \\ s_{xy} & s_y - s & s_{yz} \\ s_{xz} & s_{yz} & s_z - s \end{vmatrix} = 0 \ , \ s = [s_1, s_2, s_3] \quad [3.32]$$

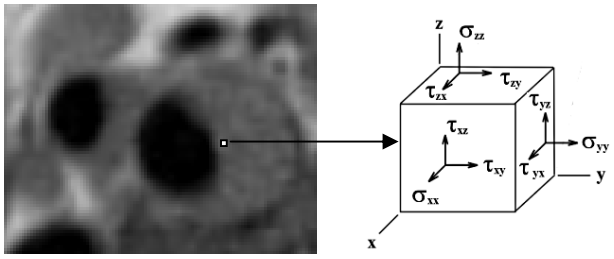

Figure 3.12 Stress components in structure domain

The temporal maximum VWTS in a cycle (VWTS_tmax), the spatial maximum VWTS at a time (VWTS_smax), spatial and temporal maximum VWTS (mVWTS) and relative cyclic VWTS (rcVWTS) at each computational node also were used to represent the plaque stress distributions. The mathematical definitions are:

$$VWTS\_t\max(x,y,z) = \max(VWTS(x,y,z,t)),t \subset (0,T) \quad [3.33]$$

$$VWTS\_s\max(t) = \max(VWTS(x,y,z,t)),t \subset (0,T) \quad [3.34]$$

$$mVWTS = \max(VWTS(x,y,z,t)),t \subset (0,T) \quad [3.35]$$

$$rcVWTS(x,y,z) = \frac{(VWTS\_t\max(x,y,z) - VWTS\_t\min(x,y,z))}{VWTS\_tmean(x,y,z)}, t \subset (0,T) \quad [3.36]$$

where $VWTS\_t\max$, $VWTS\_t\min$ and $VWTS\_tmean$ represent maximum, minimum and average VWTS in a cardiac cycle in a specific region. The first principle stress σ_1 also was used in the study for representing stress distributions.

3.4 Parameter Study with Fibrous Cap Thickness and Lipid Core Size

3.4.1 Introduction

Clinical and biomechanical studies have identified plaque components and morphology features as the main predictors for plaque vulnerability, including thin fibrous cap, large lipid region with highly active inflammation, etc. The stress in plaque regions also are highly influenced by plaque components and morphology features (Loree et al., 1992; Finet et al., 2004). So far, there is no systematic study on the influence of gradually varied lipid core volume and fibrous cap thickness to the stress distribution changes in 3D carotid bifurcation – one of the most important sites for plaque rupture. In this section, based on a realistic multi-component arterial plaque geometry, a total of 13 carotid bifurcation models were manipulated with varied combinations of fibrous cap thickness and lipid core volume but fixed degree of stenosis. One-way Fluid structure interaction simulations were performed on the cases to investigate the impacts of the specific combination of fibrous cap thickness and lipid core volume to the stress distribution. Part of the work has been published in the paper (Gao & Long, 2008).

3.4.2 Model Geometry Reconstruction

Figure 3.13 shows a carotid arterial plaque reconstructed from a sequence of histological slides of a carotid endarteroctromy specimen in our lab which has 55% of luminal area reduction at the narrowest region. The plaque specimen was obtained from a carotid endarterectomy (CEA) patient. The specimen was sliced into about 5mm length blocks along axial direction to fit in a pinkset for tissue processing. A special tissue marking dye was applied on the outer surface of the specimen before the slicing to keep the correct 3D orientation for each block. After conventional tissue processing and waxing, the waxed block containing the sample was reshaped in a way that the corners of the wax block point to the mark line made by the tissue marking dye. The wax block shape will remain on the 6μm histological section. A glass marker pen was used to make marks on the

microscope slide at the wax corners corresponded to the tissue marking dye. Therefore, the orientation information is recorded on each histology section. The sections were stained with Picrosirius Red with hematoxylin, and viewed under polarized light microscope to provide collagen and lipid core geometry information (Figure3.13). The regions that change colors and light intensity with varied polarized angle reveal the collagen. The segmented lipid core and lumen boundary were input into Solidworks™ 2006 for 3D reconstruction. The total axial length of the reconstructed plaque was 48mm (Figure 3.13(a4)).

A 3D geometry of carotid bifurcation with a multi-component plaque (named Case2 in the study, shown in Figure 3.13(b)) was then generated from the original plaque geometry by:

1. increasing the plaque severity from 55% to 85% by pushing the fibrous cap and lipid toward the lumen centre to create a thicker arterial wall in the plaque region and allow a large range of variations of lipid core volume and fibrous cap thickness;
2. the common carotid artery, internal carotid artery and external carotid artery were artificially extended based on the published general carotid bifurcation geometry (Steinman et al., 2002b; Long et al., 2003), to allow one-way FSI simulation.

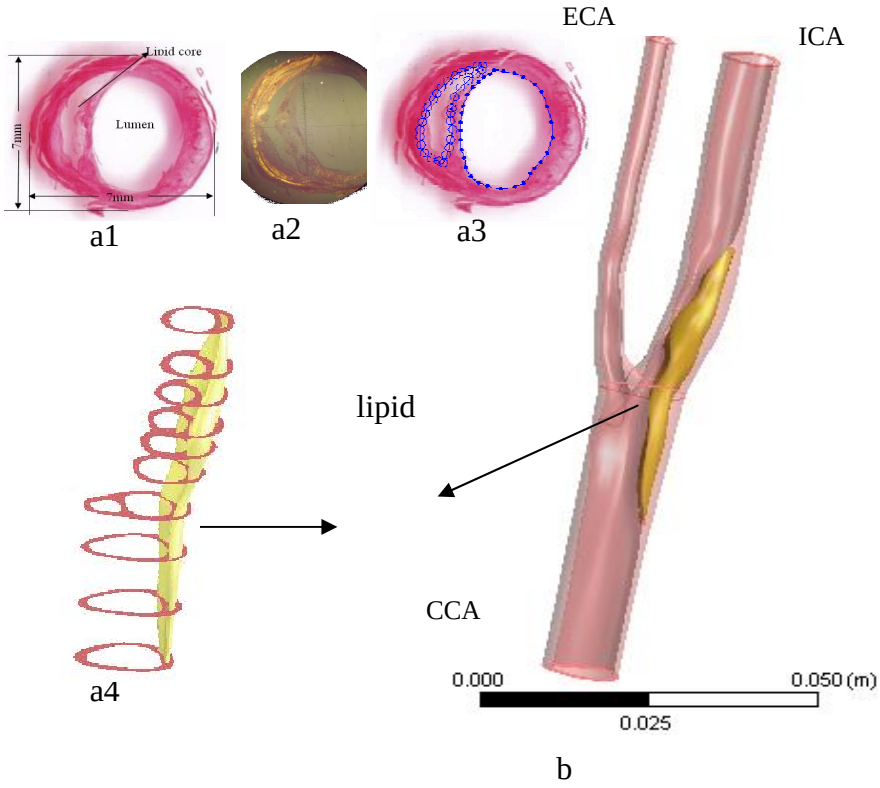

Figure 3.13 The reconstructed carotid arteries with plaque. (a1) histological image of the plaque; (a2) a polarized light microscope image of the plaque; (a3) the segmentation of the plaque boundary; (a4) original plaque geometry with 55% luminal area reduction; (b) manipulated 3D carotid bifurcation with 85% area reduction.

Based on the model for Case2, 12 cases were manipulated, with fixed inner and outer surfaces of arterial wall but varied volumes and locations of lipid core to provide different combinations of fibrous cap thickness and lipid core volume (Figure 3.14(b)). Table 3.1 presents the study case matrix. For the cases with the same fibrous cap thickness, the surface of lipid core at the luminal side was fixed, the rest parts were moved proportionally to change lipid core volume as shown in Figure 3.14(b) “i" from Cases 2 to 4;

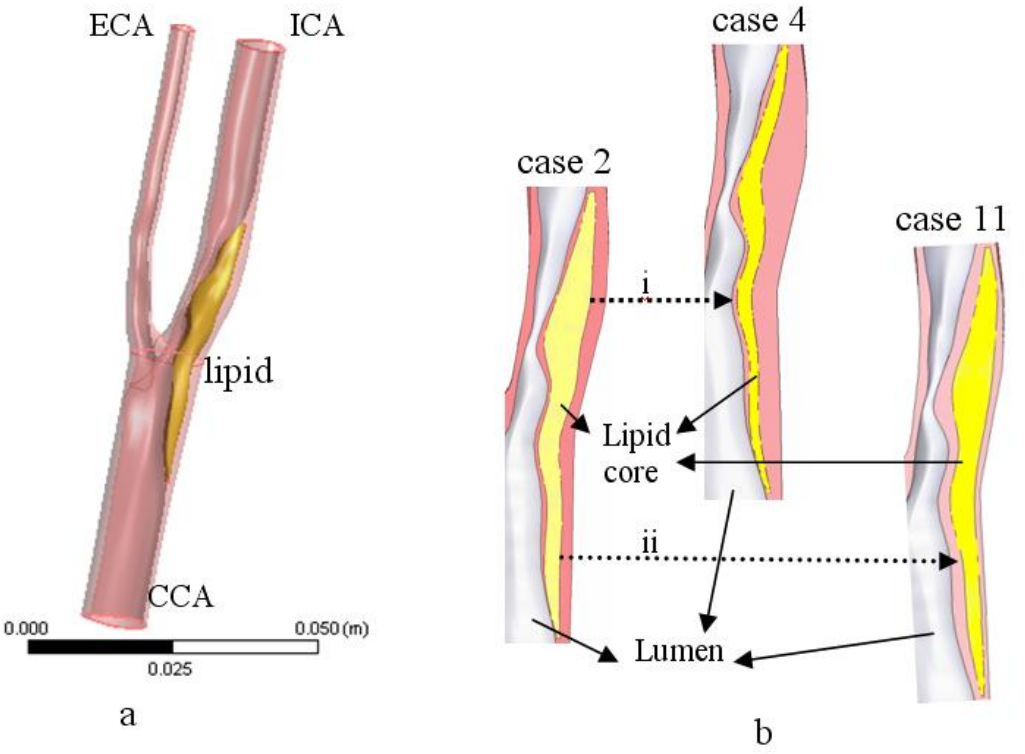

Figure 3.14 Diagrams of arterial model reconstruction and manipulation of simulation cases. (a) The reconstructed geometry for case2 (base model). (b) Schematic reconstruction of simulation cases: (i): fibrous cap thickness remains constant and lipid core volume is reduced proportionally, from case2 to case4; (ii): lipid core volume remains constant, and the fibrous cap thickness is increased proportionally, from case2 to case11.

for the cases with the same lipid core volume and different cap thickness, the surfaces of lipid core were moved proportionally towards or away from the luminal surface, as shown in Figure 3.14(b) "ii" from Cases 2 to 11. The shape of the fibrous cap will remain similar for the cases through the manipulation procedure, while fibrous cap thickness will not be the same throughout the plaque for the same case. The minimum value of the fibrous cap thickness for each case is presented in Table 3.1, from 0.15mm to 0.64mm. This manipulation process is purely for simulation purpose of creating geometry models with varied cap thickness or lipid core volume. It does not mean that the plaque will grow in this way in reality.

Lipid Core Size / Fibrous cap thickness(mm)	26.46%	22.4%	18.15%	12.23%
0.15	Case1	Case2	Case3	Case4
0.35		Case5	Case6	Case7
0.58		Case8	Case9	Case10
0.64		Case11	Case12	Case13

Table 3.1 Descriptions of the plaque geometry of the simulation cases constructed in the study

The lipid core size was defined as the percentage of the lipid core volume of the plaque volume.

$$Normalized \quad lipid \quad core\, volume = \frac{V_{lipid\_core}}{V_{plaque}} \qquad [3.37]$$

V_{plaque} was the total volume of the lipid core, V_{plaque} was the plaque volume which remains constant in all simulation cases. All the 13 cases cover the changes of lipid core size from 24.46% to 12.23%, and the fibrous cap thickness from 0.15mm to 0.64mm. For the largest lipid core case, only one case with the thinnest fibrous cap can be generated (Case1), because a thicker cap with a larger lipid core will push the lipid core very close to the arterial outer wall causing simulation difficulties.

3.4.3 Material Properties and Boundary Conditions

The carotid arterial wall was assumed to be nonlinear, isotropic, and incompressible, the 5-parameters Mooney-Rivlin model was used to describe the material properties of the arterial wall. The strain energy function is given by equation [3.28]. The lipid core was assumed to be very soft with 2kPa Young's Modulus and 0.49 for Poisson's ratio.

The interface between lipid core and arterial wall was treated as a so called "always bonded" contact. Computational nodes at the inlet plane of CCA were fixed in all directions to keep the geometry stable in space, and an axial pre-stretch 5% was applied at the outlet plane for the structure analysis. However the zero-stress conditions were not included in the study. The structure model was meshed with an unstructured mesh consisting of nearly 100,000 10-node 3D tetra elements.

The fluid domain was meshed in ICEM CFD11.0 with a much finer grid of 850,000 3D tetra cells. Blood was treated as an incompressible, Newtonian fluid with a viscosity of $4*10^{-3}$ $Pa.s$ and a density of $1{,}067 kg.m^{-3}$. The flow was assumed to be laminar with a mean Reynolds number of 400. Transient simulations were carried out with time-dependent pressure at the inlet of the CCA and mass flow rates at the ICA and ECA as the CFD simulation boundary conditions. The waveforms for pressure and mass flow rates were obtained from (Zhao et al., 2000) as shown in Figure 3.15. The boundary conditions were the same for all simulations.

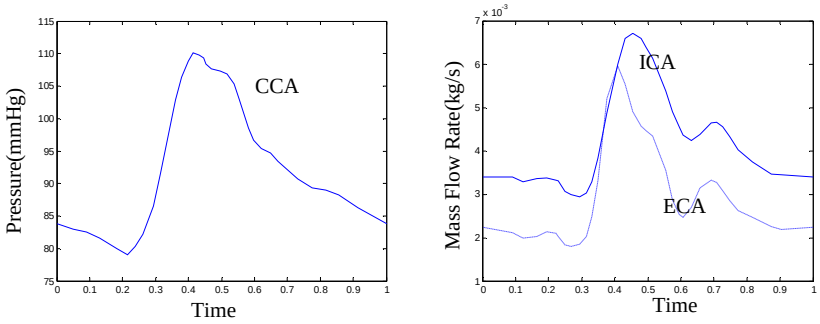

(a) (b)

Figure 3.15 Fluid boundary conditions for the inlet and outlet planes. Time is normalized by the cardiac period in x-axis. (a) Pressure for CCA; (b) mass flow rates for ICA and ECA respectively

One-way FSI coupling was employed for stress analysis, which requires the CFD code to pass pressure to structure analysis.

3.4.4 Stress Distributions for Case1.

The stress in the hemodynamic domain was calculated first, including wall shear stress (WSS) and pressure, shown in Figure 3.16(a) and (b) at t=0.4, which is the peak systole phase. In general WSS is much higher in the stenosis part and relatively lower at upstream and downstream part of the plaque. WSS in the throat shows the highest value because of the highest stenosis degree, about 34Pa. This high value of WSS might be strong enough to cause endothelial cells damaged and followed by platelet deposition and thrombus formation, contributing to the instability of the plaque, and even rupture. The pressure distribution along the plaque region is non-uniform with the lowest value at the most stenosis part. The maximum pressure drop in the plaque is about 20%.

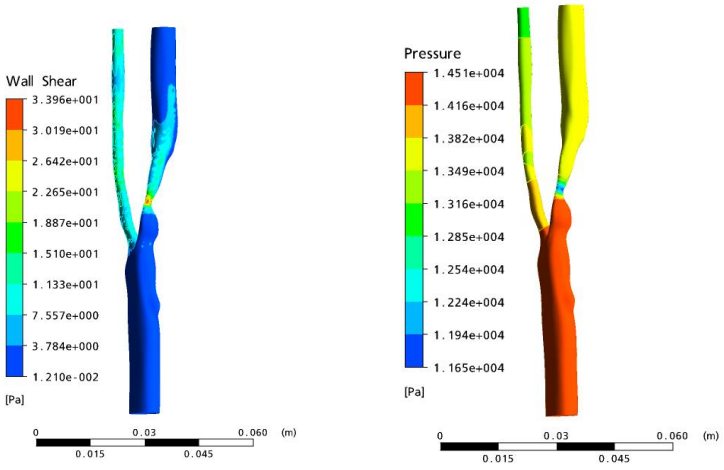

(a) (b)

Figure 3.16 Hemodynamic results. (a) WSS distribution for Case1 at 0.4; (b) Pressure distribution for Case1 at peak systole

The pressure profile in the lumen wall was applied to the structure analysis as boundary loading condition. The combined stress formation – Von Mises stress (VWTS as defined in equation 3.31) was used to describe stress distribution on the fibrous cap. Figure 3.17(a) shows the VWTS distribution in the fibrous cap at the lumen side for Case1. VWTS is much higher in the plaque region than that in the rest of the model. Within the plaque regions, higher VWTS can be found on the fibrous cap near lipid core boundary, lower value of VWTS appears at the center of the fibrous cap, and a stress concentration region can be found upstream of the plaque. Figure 3.17(b) is the VWTS distribution in a

transversal plane of the plaque, the higher stress value is at the fibrous cap while low stress can be found in the lipid core region.

Six points, P1 to P6 representing different regions from upstream to the downstream (shown in Figure 3.17 (a)), were selected to describe the VWTS change in a cardiac cycle. In detail, P1 and P6 are located at the outside of the plaque or health part of the arterial wall. P2, P3 and P5 are at the local stress concentration regions, among which, P2 and P5 are at up- and downstream boundaries of the plaque respectively, and P3 is at the middle of the plaque (longitudinally). P4 is also at the middle of the plaque and the circumferential centre of plaque fibrous cap. Figure 3.17(c) shows the VWTS changes at those 6 locations in one cycle. VWTS at P2, P3 and P5 are always at very high levels in a cycle and the curves are similar to the pressure waveform imposed at the inlet of the ICA with slight phase variations, especially at P2, for the whole cardiac cycle, VWTS is greater than 250kPa; P5 has the similar trend with a stress level of 200kPa. The values at P1 and P6 are significantly lower than the values at other points. Stress concentrations can be found around P2, P3 and P5, they all locate in the fibrous shoulder region, the frequent rupture sites. The high stress region around P2 is greater than those in P3 and P5, which may indicate the rupture risk in upstream shoulder of the plaque is higher than the downstream shoulder of the plaque.

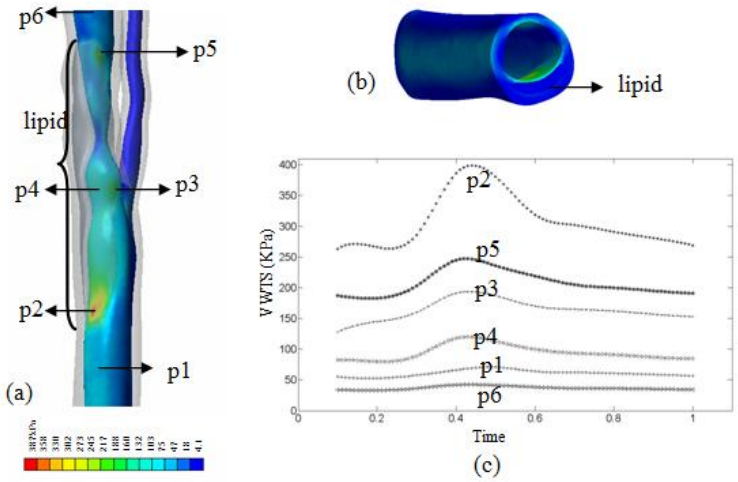

Figure 3.17 VWTS distribution for case1. (a) VWTS distribution at the lumen side at time 0.4; (b) VWTS distribution in a cross section cut of the plaque at t=0.4; (c) VWTS at 6 chosen points as shown in (a) in one cardiac cycle

3.4.5 Maximum VWTS Values for All Simulation Cases

The maximum value of VWTS over the plaque for a cardiac cycle is usually recognized as a critical parameter to predict the rupture of the plaque. Figure 3.18(a) presents the VWTS_smax curves in one cardiac cycle for Cases 1, 2, 3 and 4 which have the same minimum fibrous cap thickness of 0.15mm. The VWTS_smax value is generally higher than 300kPa for Cases 1, 2, 3 in peak systole. For Case4, the maximum value is close to 300kPa. Among the cases, the VWTS_smax value decreases gently for the cases with smaller lipid core.

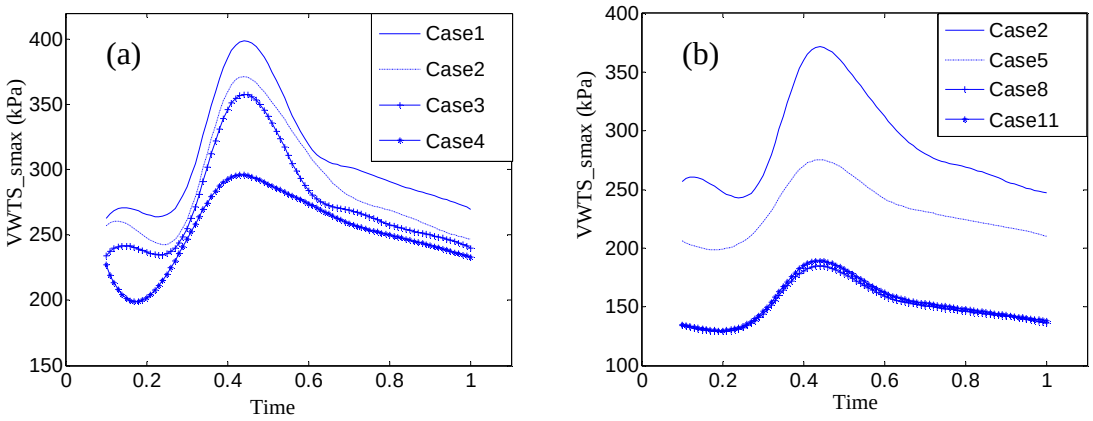

Figure 3.18 VWTS_smax distributions in one cycle in the selected cases. (a) cases have the same fibrous cap thickness of 0.15mm; (b) cases have the same lipid core size with volume ratio of 22.4%

Figure 3.18(b) presents the VWTS_smax distribution for Cases 2, 5, 8, and 11 which have the same lipid core volume. VWTS_smax decreases dramatically with the increased fibrous cap thickness. The VWTS_smax value exceeds 300kPa only in Case2. The VWTS_smax curve and almost the same values are for Cases 8 and 11 with the peak value smaller than 200kPa. It is also found that the differences of VWTS_smax value between the cases are similar throughout the cardiac cycle for all cases as in Figure 3.18(a) and 3.18(b).

time / Cases	0.1	0.2	0.3	0.4	0.5	0.6	0.7	0.8	0.9	1.0
Case1	263	266	287	**386**	**381**	**319**	**302**	291	281	270
Case2	257	248	262	**360**	**356**	**312**	280	269	257	247
Case3	234	237	255	**346**	**341**	284	269	258	250	240
Case4	227	202	247	293	289	274	259	250	242	233
Case5	206	199	222	270	267	242	231	224	218	210
Case6	184	178	198	245	242	217	207	200	195	188
Case7	165	160	178	213	210	194	185	179	175	169
Case8	134	129	144	181	178	159	151	146	142	136
Case9	137	134	143	178	175	157	149	145	141	138
Case10	172	168	181	212	209	193	186	182	178	174
Case11	135	130	146	185	182	162	153	148	143	138
Case12	126	122	136	171	169	150	143	138	134	129
Case13	128	124	138	174	172	153	145	140	136	131

Table 3.2. VWTS_smax distribution at different time of a cycle for 13 cases. Bold font was applied on the cases with VWTS_smax larger than 300kPa. Unit for stress: kPa

Table 3.2 presents the VWTS_smax values at the fibrous cap region for all 13 cases at 10 time phases in a cycle. It can be seen that the VWTS_smax value is much more sensitive to the changes of fibrous cap thickness than the lipid core volume. With same fibrous cap thickness, the maximum stress is nearly in the same range. However for the same lipid core size, the stress changes greatly from thinner fibrous cap to the thicker one. Those changes can be found in Figure 3.19, mVWTS represents the spatial and temporal maximum value of VWTS in the plaque region.

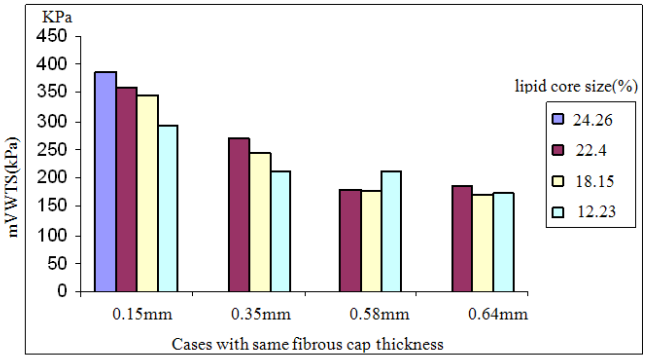

Figure 3.19 mVWTS changes among different groups

Figure 3.20 shows the general rupture risk assessment by the combination of the influences of the lipid volume and fibrous cap thickness for the 3D carotid bifurcation

cases. If 300kPa can be used as a critical rupture stress value (Cheng et al., 1993), the simulation cases can be classified into the high and the low rupture risk cases which are presented as '*', 'o' , and '+' respectively and separated by a curve as shown in the Figure 3.20. It is shown that the cases with mVWTS larger than 300kPa are all located at the upper-left corner of the Figure. According to the above separation: Cases 1 to 3 are more likely to rupture because of the high mVWTS values (>300kPa), and Cases 4 and 5 are less unstable because they are close to the separating line, a transition region from stable plaque to vulnerable one; Cases 6 to 13 are more stable than other cases.

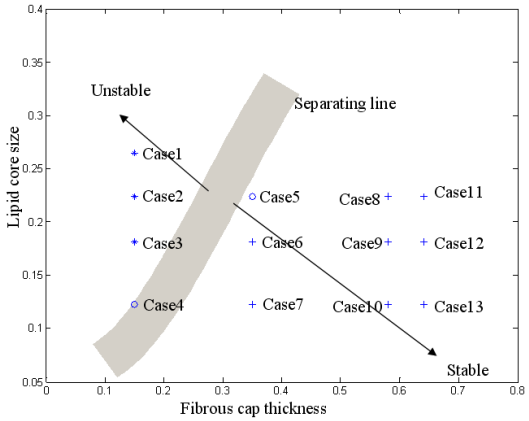

Figure 3.20 General rupture risk assessment for all cases.

3.4.6 VWTS Distributions for All Cases

The occasional high VWTS values presented above caused by local stress concentrations may trigger fibrous cap rupture; however the overall level of VWTS on the fibrous cap will also contribute to the general rupture risk. Cumulative histograms of VWTS at the computational nodes on the luminal surface at the fibrous cap at peak systole were calculated and presented in the Figure 3.21(a) for all cases. The y-axis represents the accumulated normalized number of nodes per unit stress while the x-axis represents the VWTS value. It can be found that the majority of regions on fibrous cap experience a relatively low VWTS (below 100kPa) while only a few nodes experience higher VWTS than 300kPa. The turning points of the cumulative histogram curves occur at 90% for most cases. A significant increase of the stress range and value were experienced by only the top 10% nodes for all cases. A stress level named as VWTS_90 was introduced representing the cutoff VWTS value at 90% of cumulative histogram, and VWTS_90(n)

is for the case "n" as shown in the Figure 3.21(b). Inserted panels 1 and 2 present more details of the curves at 90% and the node distributions which possess stress higher than 300kPa, respectively.

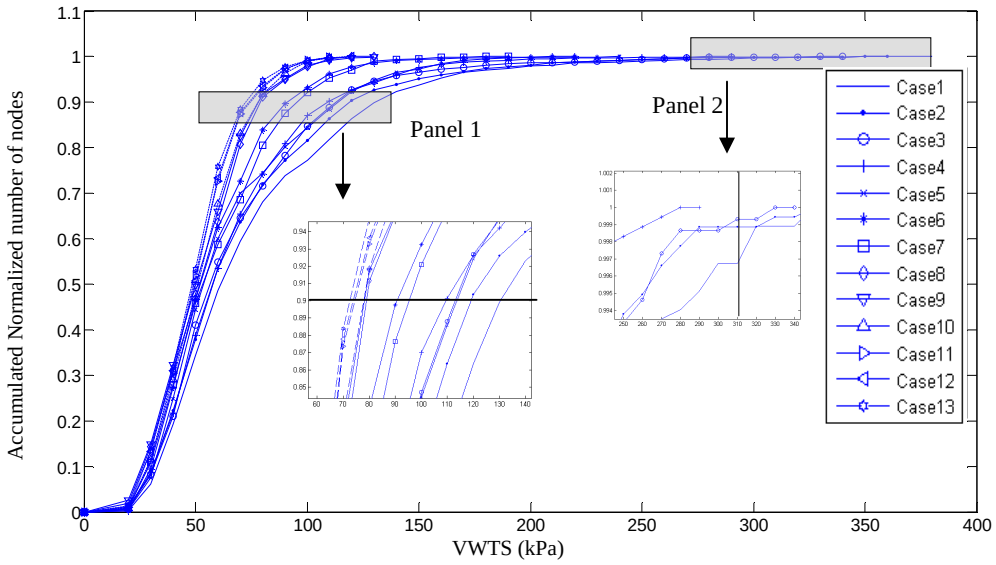

(a)

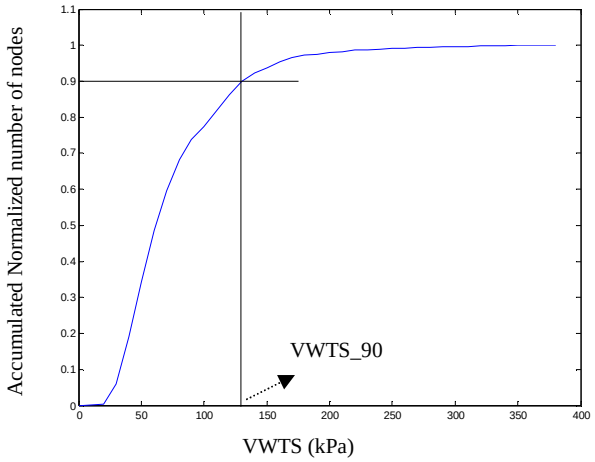

(b)

Figure 3.21 Cumulative histogram of VWTS experienced by the computational nodes on the luminal surface at fibrous cap. (a): all cases, inserted panels 1 and 2 present details of the curves at 90% and the node distributions which possess VWTS higher than 300KPa, respectively; (b): the definition of VWTS_90 for Case1

Table 3.3 (upper part) presents the detailed locations and areas of nodes possessing stress higher than 300kPa. The total areas that experience stress higher than 300kPa decreases gradually from Cases 1 to 3. These nodes are generally located around the P2 region (defined in Figure 3.17(a)) due to the local stress concentration. From Table 3.3 lower part, it can be seen that the VWTS_90 values also decrease gradually from Cases 1 to 13. The nodes which experience stress higher than VWTS_90 are generally located around lipid boundary regions in the upstream of the throat.

	C1	C2	C3	C4	C 5	C 6	C 7	C 8	C 9	C10	C11	C12	C13
300kPa Distribution													
area(mm^2)	6.9	2.15	2.18	--	--	--	--	--	--	--	--	--	--
Location	P2	P2	P2	--	--	--	--	--	--	--	--	--	--
VWTS_90 (kPa)	**130**	**119**	**113**	*110*	*114*	91	95	78	77	77	73	72	72
Location	L1+	L1	L1	L1	L2	L2	L2	L2	L2	L2	L2	L2	L2

C1 represent Case1, the same for others;

* P2 is the same as in Figure 3.16;

\+ L1 represents the area locates in the upstream fibrous cap boundary region and a small region around P5. L2 represents the area mainly locates in the upstream fibrous cap boundary region.

Table 3.3 summarized stress results (location, area, and value)
(Upper part): corresponding area and locations experiencing stress higher than 300kPa for all cases; (lower part): VWTS_90 values and the distribution of nodes experiencing stress higher than VWTS_90 for each case.

3.4.7 Discussion

Arterial plaque rupture is a complex process. Among others factors, fibrous cap thickness and lipid core volume are the most important geometry factors influencing plaque rupture risk. 2D simulation studies (Li et al., 2006) showed that the combinations of thin fibrous cap and large lipid core normally produce high VWTS in fibrous cap which will increase the rupture risk. In this 3D study, similar trends of VWTS changing with different combinations of cap thickness and lipid core volume have been demonstrated. In addition,

the study also demonstrates the quantitative progressions of mVWTS with the decrease of the cap thickness and increase of lipid core volume, or both. Usually, the size of the lipid core was measured by the percentage of the overall cross-sectional area of the plaque (Jessica M. Mann, 1996), thus in the study, the lipid core size in the atherosclerotic throat section was also calculated for reference, the size changes in the order of 42.55%, 38.5%,30.45% and 24.05%. A rupture risk assessment is proposed for the combined risk factors of cap thickness and lipid core volume. The simulation results from (Loree et al., 1992) based on the 2D models suggested that very thin (<100 μm) fibrous cap is needed to produce a peak stress larger than 300kPa. In the present study, the peak stress could be larger than 300kPa even when the fibrous cap thickness is 350μm for the Case5. The possible reason of the high VWTS for the cases could be that the stress analyses in the 2D models do not consider the longitudinal deformation, tethered effects, and axial local curvature.

Based on the critical rupture stress of 300kPa proposed by Cheng et al (1993), a general rupture risk state for all the cases was presented in the Figure 3.20. It is understood that 300kPa may not be a universal value for fibrous cap rupture. Furthermore, the critical values was derived from 2D stress analysis with coronary plaques, the critical stress in carotid plaques could be different from coronary plaques. At present there is no other research regarding the threshold value of the plaque ruptures, thus we used 300kPa only for a reference purpose. However the mVWTS values may be influenced by numerical errors, or local stress concentration due to local geometry. The value of VWTS_90 is more robust on presenting the general stress level for the plaque. In table 3, VWTS_90 is significantly higher for the high rupture risk group based on the mVWTS assessment (cases 1 to 5), above 110kPa, and lower for the more stable plaque group. A double t-test was performed on the mean value of VWTS_90 in the two groups, a significant difference exists between the two groups with $p<0.005$.

Due to the massive computational resource required by FSI simulation, even the one-way FSI simulation, the question may be raised that do we really need the FSI simulation for plaque stress analysis? For Case2, an extra simulation was performed with uniform

pressure load on the arterial inner wall at peak systole, named Case2_constant. The stress distributions in general are nearly the same. However the maximum VWTS with the one-way FSI model is slightly higher than Case2_constant, around 8%, the average VWTS for Case2_constant in the fibrous cap is about 5% higher, and the maximum stress concentration region is close to P2 as in Figure 3.17(a) for One-way FSI, while for Case2_constant, the maximum stress concentration region is close to P3 as in Figure 3.17(a). Therefore the answer to the question will be depended on the study aims: (1) FSI simulation can provide a more realistic pressure loading on the lumen surface, thus the predicted stress will be more precise; (2) FSI will also provide solutions in fluid domain such as flow patterns and WSS. A fully coupled FSI simulation will provide more accurate solutions in fluid domain, the extra simulation for Case11 with fully coupled FSI showed that the pressure variation is less than 5%, which results 6% and 3% variation in maximum and average value, but with the same stress distributions, therefore one-way FSI is a good compromise providing more realistic loading conditions in structure analysis.

Although the original plaque geometry was subject specific, the manipulations afterwards make the model geometry more general. For all simulation cases, the high stress regions show general patterns which are at the fibrous cap near the lipid core boundaries. The local stress concentration zones may be caused by the specific plaque geometry. For example, P2 and P5 are at the regions with large local curvature or the thinner fibrous cap. However, the graduate changes of the total areas possess higher stress than 300kPa and VWTS_90 values from vulnerable plaque cases to more stable plaque cases indicate that the overall results generated from this study represent a more general trend. It is worth mentioning that the findings in the study should be interpreted with cautions when comes to the biological and clinical significance. The study aims to provide some insights into the plaque vulnerability with proposed constant changing in geometry parameters. Although the model geometry will not be necessarily the same as an individual patient; the model geometry in general does provide similarity to the realistic cases. As mentioned above, in realistic cases, there were many variables in plaque geometry which could influence the stress analysis results and make the parameter study extremely

difficult. The manipulated models in the present study are able to provide more uniform changes of the geometry, making the comparison feasible.

A thin fibrous cap region may cause a high stress value. However, a higher stress concentration may not always relate to a much thinner fibrous cap. Other local geometry features, such as the local Gauss Curvature may also cause high stress value locally, which will be discussed in Chapter 6. In this study, the model was created from the 2D slices using a surface loft technique in SolidWorks, the final 3D surface will be the surface interpolation results which can not be controlled locally. Therefore, the cap thickness can not remain constant throughout whole fibrous cap. However for the cases with different fibrous cap thickness, the one with thinner fibrous cap will be always thinner than the thicker one in the same position. It would be nice to analysis the correlation of the fibrous cap thickness and the stress value. However, the post processing software does not provide the fibrous cap thickness at every point automatically. It is not feasible to measure the cap thickness distributions throughout 3D fibrous cap manually. We have tried to extract the cap thickness for one case (Case1) by the procedure as: two point sets were defined, one was on the fibrous cap surface in the lumen side, the other was on the fibrous cap surface near the lipid core. A searching algorithm was used to calculate the minimum distance between the two point sets. The minimum distance at every point was used to represent the fibrous cap thickness at that point. It should be mentioned that the value found by the above algorithm may not be the actual fibrous cap thickness. The corresponding wall tensile stress VS fibrous cap thickness found by the procedure for the Case1 was shown in Figure 3.22.

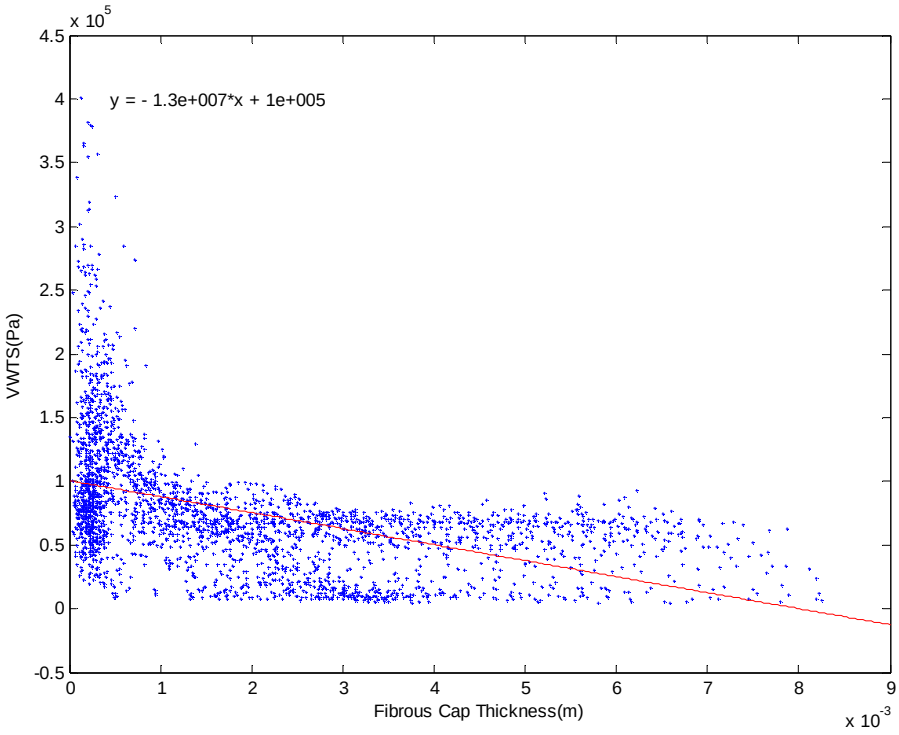

Figure 3.22 wall tensile stress VS fibrous cap thickness

From Figure 3.22, it shows that higher wall tensile stress is associated with thinner fibrous cap, while the maximum wall tensile stress is not necessarily located at the thinnest fibrous cap region, which may explains why plaque ruptures not always occur at thinnest fibrous cap region. Generally with decreased fibrous cap thickness in the fibrous cap, wall tensile stress increases dramatically.

In conclusion, one way 3D FSI is employed to perform stress analysis based on 13 carotid bifurcation cases, with fixed stenotic degree, varied lipid core size and fibrous cap thickness. Values of mVWTS and VWTS_90 based on the cumulative histogram VWTS experienced on the computational nodes on the fibrous cap are used to assess the plaque rupture risk for the cases. Both parameters are capable of separating the simulation cases into vulnerable and more stable plaque groups, while the VWTS_90 value is more robust for plaque rupture risk assessment. The results also show that the stress level on the fibrous cap is much more sensitive to the changes of cap thickness than the lipid core

volume. A slight decrease of cap thickness can cause a significant increase of stress. For all simulation cases, high VWTS appears at the fibrous cap near the lipid core regions.

3.5 Summary

Fluid structure interaction has been developed in this section for plaque stress analysis based on ANSYS SUIT 11.0, and applied to carotid plaques successfully with parameters from existed literature. The study on morphological features shows that stress levels on the fibrous cap is much more sensitive to the changes of cap thickness than the lipid core volume, therefore more attention needs to be paid for fibrous cap reconstruction.

Recently, the developed *in-vivo* high resolution MRI has gained popularity for carotid plaque imaging, providing a way for patient specific plaque modeling with realistic geometry and boundary conditions, rather than assumed geometries. In the next chapter, plaque geometries will be reconstructed from *in-vivo* MRI, and followed by plaque stress analysis. It is one of the main aims of the PhD project.

Chapter 4

3D Plaque Geometry Reconstruction from *in-vivo* MRI

4.1 Introduction

A major application of multi-component arterial plaque images obtained by multi-spectral MRI is to analyze plaque stress on anatomically realistic arterial models and provide critical information for predicting plaque rupture (Tang et al., 2004a; 2004b; 2004c; 2005a; 2005b; Li et al., 2007) by finite element (FE) modeling. Uncertainties in MR imaging and 3D reconstruction may be acceptable for visualization purposes, but can be significant in influencing the stress analysis results. Based on the results in chapter 3 and published results (Loree et al., 1992), plaque stress analysis results are highly sensitive to fibrous cap thickness variations. Therefore the study of plaque geometry reconstruction reproducibility based on *in-vivo* MRI would then give a level of confidence when applying the procedure to assess plaque stress based on MRI-based realistic plaque geometry.

This chapter includes three main tasks, they are (1) the development of a procedure of 3D plaque geometry reconstruction from *in-vivo* multi-spectral MR images; (2) the inter-observer reproducibility assessment of image segmentation and plaque 3D reconstruction uncertainties from *in-vivo* MR images on different geometry parameters, and sensitivity assessment of image processing and 3D reconstruction uncertainties to the plaque stress analysis. However, the assessment of reproducibility on MR imaging is not included in the study. Part of the work has been summarized in the paper (Gao et al., 2009a); (3) the FSI stress analysis on 4 human subjects with carotid plaques, part of the work has been published in the paper (Gao et al., 2009b).

4.2 3D Plaque Geometry Reconstruction

4.2.1 MR Image Acquisition

Patients with carotid arterial plaques, recruited from a specialist neurovascular clinic, were chosen for the study. Multi-spectral MRI scans were performed on the subjects to

provide plaque morphology. The protocol was approved by the local ethics committee, and written informed consent was obtained from each patient before the study.

Multi-contrast imaging was conducted using a 1.5 T MRI system (GE Diagnostic Imaging, Waukesha, WI) and a 4-channel phased-array neck coil (PACC, Machnet BV, Elde, The Netherlands). Movement artifacts were minimized using a dedicated vacuum-based head restraint system (VAC-LOK Cushion, Oncology Systems Limited, UK) to fix the head and neck in a comfortable position and allow close apposition of the surface coils.

After an initial coronal localizer sequence, axial 2D time-of-flight (TOF) MR angiography was performed to identify the location of the carotid bifurcation and the region of maximal stenosis on each side. Axial images were acquired through the common carotid artery 12 mm below the carotid bifurcation to a point 12 mm distal to the extent of the stenosis identified on the TOF sequence to cover a large range of carotid bifurcation. The following 2D, ECG-gated, blood-suppressed, fast spin echo pulse sequences were used in the plaque region: intermediate T_2 Weighted (ImT2W_FatSat: TR/TE: 2*RR/46) with fat saturation; T_2 Weighted (T2W: TR/TE: 2*RR/100); short T_1 inversion-recovery (STIR: TR/TE/TI: 2*RR/46/150). The field of view was 10x10cm^2, matrix size 256 x 256, slice thickness was 3mm. It made the pixel size of 0.39x0.39x3mm in all cases except the TOF images. These images were used to delineate the various plaque components such as fibrous cap, lipid core.

4.2.2 3D Carotid Bifurcation and Arterial Plaque Reconstruction

The artery and plaque geometries were obtained from the multi-spectral MR scans. An in-house program developed in Matlab was used to facilitate the segmentation of lipid core, arterial wall and lumen, which have different signal characteristics when imaged using multi-spectral protocol. The plaque region was identified and reconstructed based on T2W, ImT2W_FatSat, STIR images (if existed), and the healthy arterial part was reconstructed based on TOF images. The detailed image segmentation and 3D

reconstruction procedures described below as in Figure 4.1 were for one subject. The whole procedure was explained based on the subject.

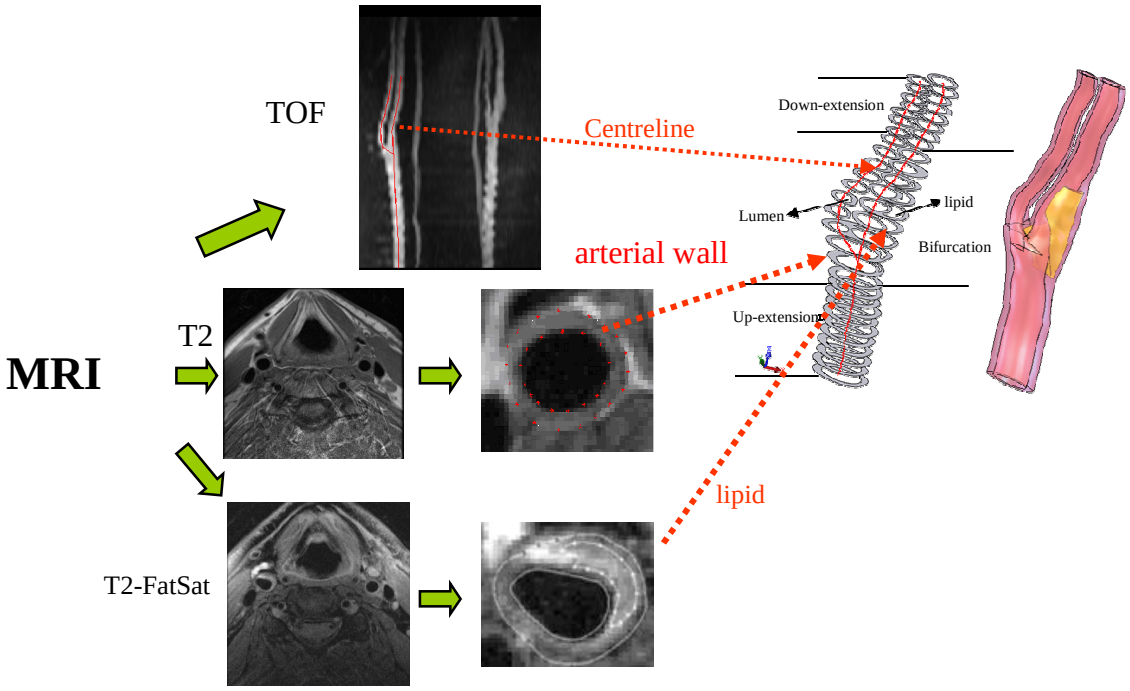

Figure 4.1 General Procedure of 3D plaque geometry reconstruction

4.2.3 Arterial Lumen Surface, Outer-wall Boundary Segmentation

The lumen area in T2W images appears with very low intensity, forming a dark region compared with the arterial wall. As shown in Figure 4.2, the arterial wall can be defined by the band region around the lumen. Though the lumen boundary can be easily segmented by methods such as region growing or active contour, the arterial outer wall boundary does not show significant contrast from the surrounding tissue. Therefore, after delineating the lumen region, the arterial wall thickness is considered to be 2-4 pixels (0.8mm to 1.6mm) in the healthy part, which can be used to facilitate delineation of the artery boundary when the wall boundary is obscure. Because of the relative thin arterial wall, and also the need for segmentation of lipid region inside arterial wall, one pixel of segmentation error may impose great uncertainty in the stress analysis which is based on the reconstructed geometry. Therefore the manual method was used to define all the boundaries (arterial wall, lipid core) for better control of segmentation quality. A total of 11 T2W images were acquired for the reconstruction of the whole bifurcation geometry.

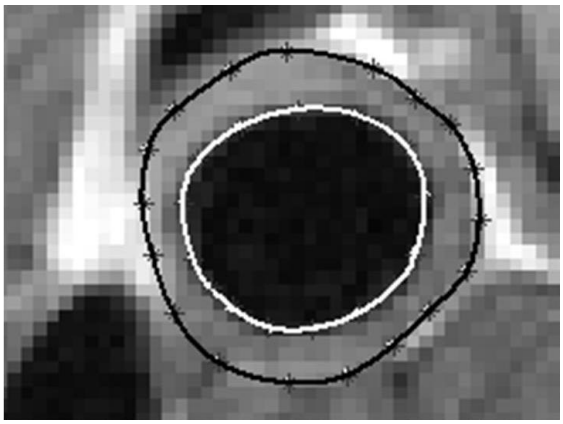

Figure 4.2 Segmentation of the T2 Weighted images for lumen and arterial outer boundary

4.2.4 Lipid Core Segmentation

ImT2W_FatSat images were mainly used for lipid core segmentation. In total, seven 2D images were available for the subject for the definition of lipid core. Regions of lipid core, fibrous cap and lumen appear slightly darker, brighter and black respectively (Toussaint et al., 1995; Saam et al., 2005; Trivedi et al., 2006). In addition, the corresponding STIR images can provide further proof on the plaque component segmentation. In STIR images the area of very high signal adjacent to the lumen was classified as fibrous cap, while areas of low signal intensity below the fibrous cap were classified as lipid core. The signal intensity characteristics of the major components on different MR sequences have been summarized as in Table 4.1. Figure 4.3 shows T2W, ImT2W_FatSat, STIR images of the plaque. Part of fibrous cap can be identified in STIR and ImT2W_FatSat, the missing part was assumed to have a thickness of less than 1 pixel which will produce less contrast due to partial volume effect. In these cases, a thickness of one pixel (about 0.39mm) was allocated for the fibrous cap thickness.

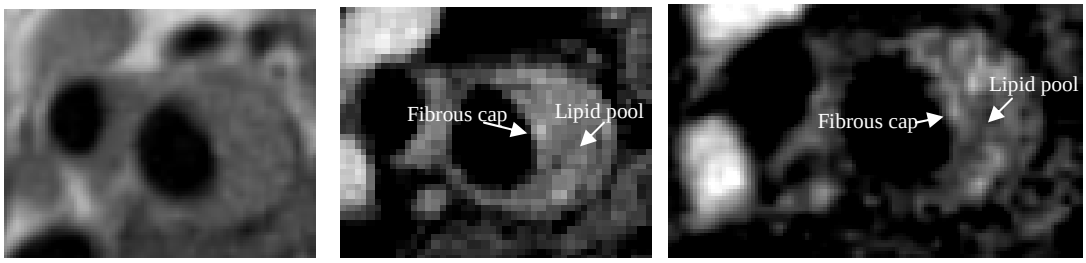

T2W ImT2W_FatSat STIR

Figure 4.3 T2W, ImT2W_FatSat, and STIR sequences for one cross section

	T1W	Intermediate T2W	Long T2W	STIR
Fibrous cap	+/-	++	++	+++
Lipid Core	+	+/-	+/-	-
Calcium	-	-	-	-
Haemorrhage	++	+/-	+/-	+/-

Table 4.1 signal intensity characteristics of the major plaque components on different MR sequences (+ indicates high signal; - indicates low signal). Usually the STIR can give the better tissue classification between lipid core and the fibrous cap (Trivedi et al., 2004).

Combining the artery geometry from T2W images, the lipid core could be segmented manually. Since the arterial inner/outer walls and lipid core boundary were delineated by T2W, ImT2W-FatSat, STIR images respectively, it was necessary to perform a registration procedure between images obtained from T2W and ImT2W-FatSat, STIR sequences. A linear transformation method (Goshtasby A.Ardeshir, 2005), was employed. In detail, specific regions which have very high contrast and can be easily identified between the paired images (T2W image and the corresponding ImT2W-FatSat image) were chosen. Region growing method was used to calculate the centre point for each region. The registration transformation matrix can be calculated according to the associated centre point movements. As shown in Figure 4.4, there were 6 pairs of points available for the purpose of registration. P1 represents the set of points from T2W image; P2 represents the set of points from ImT2W_FatSat image.

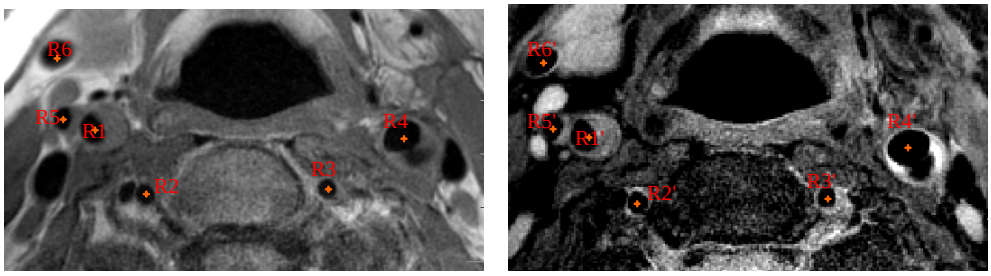

Figure 4.4 the definition of pairs of centre points for co-registration

A linear transformation matrix was calculated based on the two sets of points, the spatial transformation was assumed to only include translation, rotation, and scaling. The equation can be:

$$\begin{aligned} sc &= scale * \cos(angle) \\ ss &= scale * \sin(angle) \\ [P1] &= [P2] * \begin{bmatrix} sc & -ss \\ ss & sc \end{bmatrix} + [tx \quad ty] \end{aligned} \tag{4.1}$$

Where "*scale*" is the scaling factor from P2 to P1, "*angle*" represents the rotation, $[tx, ty]$ is the translation vector. The boundary information from ImT2W_FatSat and STIR was projected back to T2W sequence, and combined together. Figure 4.5 shows the segmentation of flow lumen, arterial wall and lipid core by the combination and co-registration of T2W, ImT2W-FatSat, STIR images.

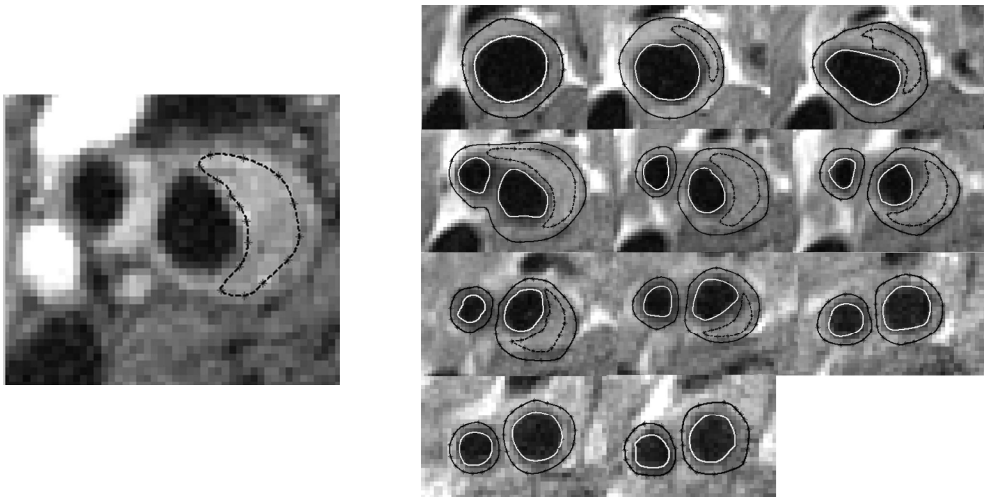

(a) (b)

Figure 4.5 Segmentation results (a) the segmentation of the lipid core region; (b) the combination of segmentation of arterial wall and lipid core.

4.2.5 Carotid Bifurcation 3D Reconstruction

Reconstruction of the arterial regions beyond the plaque segment was based on the TOF images. The centre points of the lumen provided by TOF and T2W images were used to construct the centre lines for the common carotid artery, internal carotid artery, and external carotid artery, shown in Figure 4.6(a). The 2D slices from different MRI series can be aligned along the centre lines, with axial coordinates assigned. For the regions upstream and downstream of the plaque, only luminal surface information was available from the 2D TOF scan. A constant wall thickness was assigned for these regions to construct the arterial wall. After 2D segmentation and registration, the region boundary points were imported into SolidWorks^{TM} 2006 for each slice. The complete contours were generated using a B-spline interpolation.

Geometry model shrinkage procedure. The *in-vivo* MR measured plaque is subject to physiological pressure loading, while stress simulation normally starts from zero loading condition. Therefore, a proper shrinkage procedure should be applied during the geometry reconstruction from *in-vivo* MRI data, which represents physiological loading condition, to perform FSI simulation. The shrinkage procedure was: (a) 10% shrinkage in the axial direction from reconstructed geometry, and (b) lumen area shrinkage determined by trial and error manor to best match with *in-vivo* geometry under mean pressure loading condition (100mmHg). It was found that 10% area shrinkage or about 5% shrinkage in diameter fits the MRI geometry best. The details for lumen area shrinkage rate are as followings: one cross section in CCA was chosen, the arterial wall was reconstructed for 2D structure analysis, and the shrinkage rates from 0 to 20% were applied to the reconstructed 2D arterial wall. During the shrinkage procedure, the vessel wall cross-section area remained constant due to the wall material incompressibility. A pressure of $(p_s+p_d)/2$, where p_s and p_d represent systolic and diastolic pressures respectively, was applied to the lumen. The deformed arterial wall with different shrinkage rates was compared with *in-vivo* morphology, the rate which had the best match was chosen for the shrinkage procedure of 3D plaque geometry. In addition, the outer wall was also reduced proportionally to match the plaque volume in the *in-vivo* state.

3D reconstruction was carried out by the loft method as shown in Figure 4.6(b). Finally, the complete plaque model contains two parts: (a) lipid core (indicated in Figure 4.6) and (b) arterial wall region. The fibrous cap was treated as part of arterial wall (the same material property) located in the regions between the lumen and lipid core. Therefore the fibrous cap was indirectly decided by the relative lipid region location.

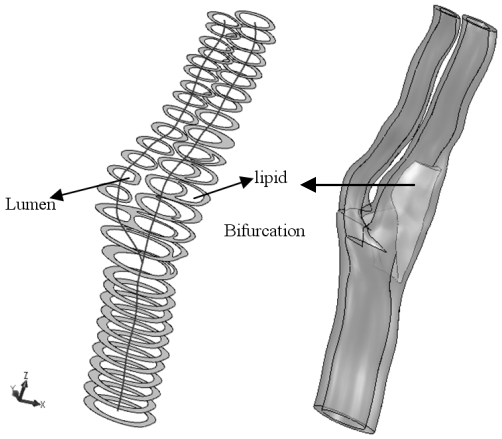

(a) (b)

Figure 4.6 Reconstructed Geometry. (a) Stack of 2D contours of one subject; (b) 3D geometry reconstruction

4.3 Study of Reproducibility of Human Arterial Plaque Reconstruction

4.3.1 Study Methodology

Plaque measurements using MRI and histology are generally in good agreement for revealing plaque structures (Von Ingersleben et al., 1997; Yuan et al., 1998; Yuan et al., 2001). Several studies reported good accuracy and reproducibility of reconstruction of carotid artery lumen from MRI images (Moore JA et al., 1999; Long et al., 2003). However, measurement uncertainties become significant when attempting to define a thin plaque fibrous cap, with a thickness at one pixel size, i.e. 0.39mm or less, which is common for a vulnerable plaque. Cai (Cai et al., 2005) quantitatively measured the fibrous cap and lipid-rich necrotic core size with *in-vivo* MRI imaging, and compared this with histology data. The MR images and histology slices showed moderate to good agreement for the fibrous cap length and area and the lipid core area. The difference between them became significant when a very thin fibrous cap was studied. Emmanuel

Touze (Emmanuel Touze et al., 2007) also showed that the inter-operator disagreements in lipid core area measurement from MRI data could be high.

Because of the limited resolution and accuracy in MR imaging and 3D reconstruction, there is a need to assess (a) image processing reproducibility and (b) the impact of the 3D plaque geometry reconstruction uncertainty to the plaque stress analysis (Gao et al., 2009a) as discussed in Chapter 2.

4.3.2 Reproducibility Study

For the first purpose, three investigators (IV1, IV2, IV3) were invited to segment the MRI images to define the lumen wall, arterial outer wall and lipid core boundary independently following the above protocols on the data from two subjects (subject 1: S1 and subject 2: S2) by using the same in-house program. The primary segmentation data from IV3 was used as the baseline. The plaque geometries for the two subjects from IV3 are shown in Figure 4.7.

As shown in Figure 4.8, a centre point (centre of gravity) of the lumen area was defined by a region growing algorithm. A polar coordinate system was then created based on the centre point. Uniformly distributed locations along the circumferential direction with a constant angular distance of 3.6 degree interval, were obtained on the boundaries of lumen, arterial outer wall and lipid core. Four parameters were defined to quantify the inter-operator segmentation results. They were: (a) arterial wall thickness, which is the distance between lumen and arterial outer wall; (b) lipid core thickness, or the distance between the lipid core boundaries along the same radius direction; (c) lipid core area; (d) fibrous cap thickness. The definitions for the parameters are shown in Figure 4.8.

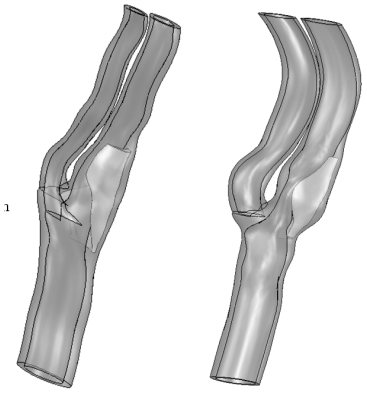

(a) (b)

Figure 4.7 3D geometries for 2 studied subjects. (a) 3D plaque geometry for subject 1 (S1); (b) 3D plaque geometry for subject 2 (S2)

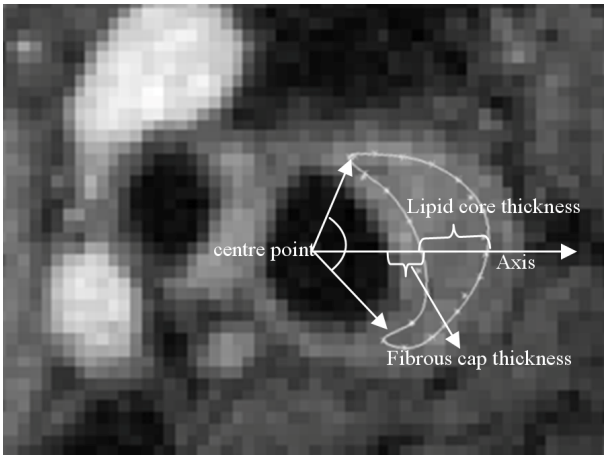

Figure 4.8 The definition of wall thickness, lipid core thickness and fibrous cap thickness.

4.3.2.1 Plaque Components Reconstruction Reproducibility Analysis

For subject 1, a total of 11 T2W images and 7 ImT2W_FatSat images were available for arterial wall and lipid core segmentation respectively, and 9 T2W images and 6 ImT2W_FatSat images for the subject 2. Linear correlation analysis was performed for all parameters except for lipid core areas. The geometry parameter values measured at the same axial and circumferential locations of a subject from different observers were compared. The results show that estimation of wall thickness is highly consistent between different investigators (correlation coefficients > 0.9 with $P<0.05$), however correlations

of lipid core thickness and fibrous cap thickness were much poorer with correlation coefficients of about 0.5($P<0.05$).

	Wall thickness difference(Pixel)		lipid core thickness difference (pixel)		lipid core area difference(mm^2)		Fibrous cap thickness difference (pixel)	
	Mean	SD	Mean	SD	Mean	SD	Mean	SD
Subject 1								
IV1 Vs IV3	1.19	0.83	1.51	1.01	3.39	2.46	0.96	0.96
IV2 Vs IV3	1.16	0.83	1.50	0.93	4.39	5.71	1.07	1.03
Subject 2								
IV1 Vs IV3	0.85	0.63	1.32	0.86	6.0	6.1	0.84	0.92
IV2 Vs IV3	0.82	0.61	1.41	0.89	6.95	5.21	0.88	0.87
Mean Value	1.0	0.7	1.4	0.9	5.2	4.9	0.94	0.95

Table 4.2 Inter-observer disagreement for wall thickness, lipid core thickness, lipid core area and fibrous cap thickness on subjects 1 and 2.

Table 4.2 shows the differences in calculated parameters between IV1 and IV3, and IV2 and IV3, of all images in the plaque region for subjects 1 and 2. The averaged disagreements on arterial wall thickness between the operators are generally around one pixel (or 0.39mm) and the standard deviation is about 0.7 pixel. The mean value of the difference for lipid core thickness is 1.4 pixel, with a standard deviation of around 0.9 pixel; the disagreement on lipid core area, is about 5.2 mm^2 between different investigators. It is worth mentioning that the mean lipid core area difference and standard deviation is in the same range as the difference between MRI and histology measurements reported by Cai (Cai et al., 2005). The differences in fibrous cap thickness obtained by different investigators are around one pixel, with a standard deviation of 0.95 pixel. From the above analysis, the segmentation uncertainties for wall thickness and fibrous cap thickness are around 1 pixel. For lipid core, the uncertainty is larger than 1 pixel. Because of the thin fibrous cap, the relative segmentation uncertainty of fibrous cap thickness is much bigger.

4.3.2.2 3D Reconstruction Error Evaluation

During the reconstruction procedure in Solidworks, a 3D surface smoothing step was carried out for the geometry. The minor variations in transverse plane (2D arterial contour) and along the axial direction were smoothed out, causing 3D reconstruction uncertainty, especially in the bifurcation bulb region due to the fast change in geometry. The difference between the smoothed and unsmoothed contours in CCA and ICA was analyzed here for subject 1. Parameters such as arterial wall area difference, including the lipid region, were calculated for the contours from smoothed and unsmoothed models. The area difference, defined as $(Area_{smoothed}-Area_{unsmoothed})/Area_{unsmoothed}$, is presented in Figure 4.9. In Figure 4.9(a), the continuous line and dashed line represent the contour obtained from the smoothed and unsmoothed models respectively. The main features of the unsmoothed contour were preserved in the smoothed contour; however, the difference between the two contours is noticeable. The arterial wall area difference caused by the smoothing procedure, shown in Figure 4.9(b), is usually below 7% for the 11 slices. Since the arterial lumen diameter is about 8mm, and the wall thickness is 1mm, a 7% variation of the arterial wall area represents a range of ±0.06 mm for the arterial wall thickness variation, i.e. 0.15 pixel in the MR images.

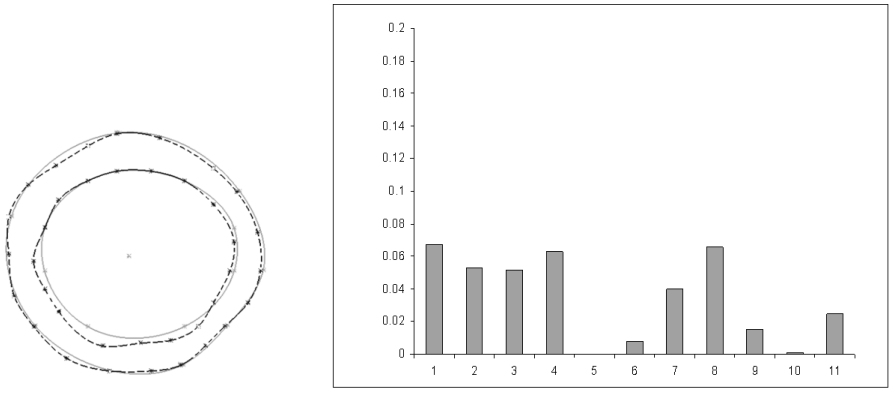

a b

Figure 4.9 Comparisons between smoothed and unsmoothed results (a) Smoothed(continuous) and unsmoothed(dashed) contours for the arterial wall boundary; (b) Arterial wall area difference between smoothed and unsmoothed wall for 11 slices.

4.3.3 Study of Segmentation Uncertainty on Stress Analysis

From the plaque reconstruction reproducibility study in previous section (4.3.2), the disagreements for arterial wall reconstruction usually are very small (< 1 pixel) due to the relatively clear contrast of the wall boundary. However, for the lipid core region, because of the low contrast between the lipid core and the surrounding tissue, artificial adjustments are made on the reconstruction of the lipid core region which will affect the fibrous cap delineation accuracy accordingly. Because the fibrous cap thickness is derived from the lipid boundary, the uncertainty of the lipid segmentation will directly affect the fibrous cap definition. Since the stress analysis results are highly sensitive to fibrous cap thickness variations (Loree et al., 1992), uncertainties in fibrous cap thickness measurement and their impact on stress analysis results needs to be quantified. This section aims to study the geometry reconstruction uncertainties' impact on plaque stress analysis, including stress distribution patterns, maximum plaque stress locations.

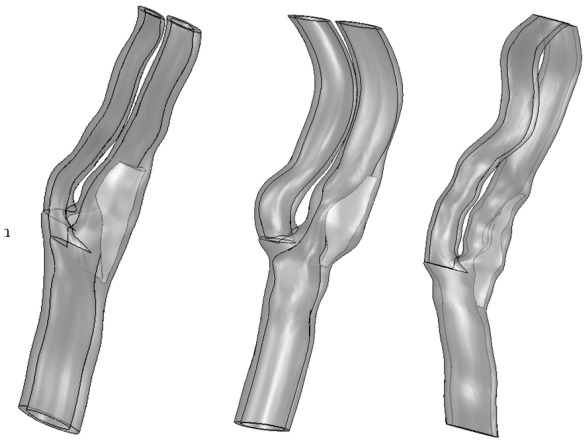

(a) (b) (c)

Figure 4.10 3D plaque geometries from 3 subjects. (a) Subject 1; (b) Subject 2; (c) Subject 3

Three subjects were selected (Subject 1, Subject 2, and Subject 3), shown in Figure 4.10. Structure only stress analysis was applied for those plaques. In detail, the carotid arterial wall was assumed to be nonlinear, isotropic, and incompressible, with the 5-parameters Mooney-Rivlin model being used to describe its material properties (Equation 3.28 in Chapter 3), the lipid core was assumed to be very soft with a 1KPa Young's Modulus and a 0.49 Poisson ratio. The structure model was meshed with an unstructured mesh

consisting of nearly 90,000 10-node 3D tetra elements. Nodes at the both upstream and downstream ends of the arteries were fixed in all directions. A pressure of 110mmHg was applied at the lumen side. The residual stress and pre-stretch were not included in the model, and the numerical simulation was carried out by ANSYS Workbench 11.0.

4.3.3.1 Baseline Stress Analysis for the Subjects

The computed VWTS for Subject 1 in the whole structure is shown in Figure 4.11(Panel 1(a)). The local maximum stress concentration could be found in the plaque region, indicated by the black arrow within the fibrous cap. In the plaque region, the stress is at a higher level with more complex distributions. The stress in the lipid core is much lower, due to the soft characteristic of the lipid core. Figure 4.11(Panel 1(b)) is the stress distribution on the lumen wall surface. Figure 4.11(Panel 1(c)) shows the first principle stress (FPS) which represents the circumferential component of stress or the strongest stretching force in the whole structure. The local maximum FPS concentration could also be found in the plaque region, with a similar distribution pattern to VWTS. Figure 4.11(Panel 2) shows the results for Subject 2 while Figure 4.11(Panel 3) shows the stress analysis results for Subject 3. The local maximum stress concentrations are indicated by the black arrows in the Figures. Similar stress distributions of VWTS and FPS in plaque regions are found in subjects 2 and 3, however the local maximum stress concentrations in the plaque region are not the same as global maximum stress level as in Subject 1, and the global maximum stress can appear in the healthy part of the carotid artery.

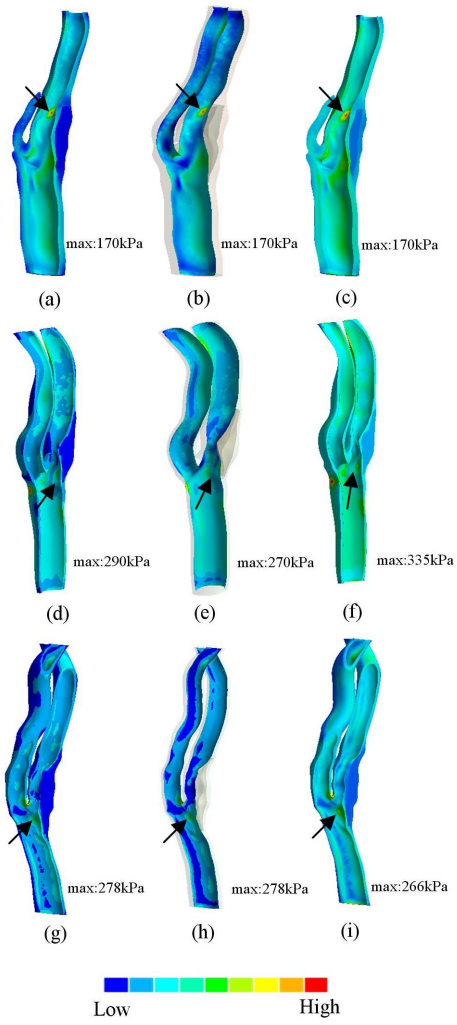

Figure 4.11 Stress for the studied 3 subjects. (a) VWTS in the whole structure of Subject 1; (b) VWTS in the lumen surface of Subject 1; (c) The first Principle Stress in the whole structure of Subject 1. (d) VWTS in the whole structure of Subject 2; (e) VWTS in the lumen surface of Subject 2; (f) The first Principle Stress in the whole structure of Subject 2. (g) VWTS in the whole structure of Subject 3; (h) VWTS in the lumen surface of Subject 3; (i) The first Principle Stress in the whole structure of Subject 3.

4.3.2.2 The Impact of Model Reconstruction Uncertainties on Stress Analysis

From the analysis in section 4.3.2, the arterial/lipid size can be overestimated (enlarged) or underestimated (reduced) by one pixel or more during model reconstruction. In this section, the impacts of these geometry-reconstruction errors on the stress analysis were

assessed systematically. In doing so, the model geometry was modified to represent different scenarios. They were:

a) *model with overestimated boundaries*: if the region boundaries (arterial wall or lipid) were not clear (with the image intensity gradient less than a threshold of 100 (intensity range: 0-65536 in MRI images), one pixel was added outside of the regions from the base model. If the boundaries were clear, or there was not enough space for the adjustment, no modification was made. Figure 4.12 shows the over-estimation of arterial wall and lipid region boundaries.

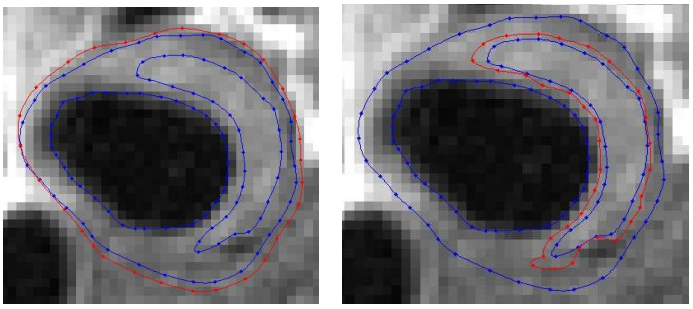

Figure 4.12 Schematic of over-estimation of arterial wall and lipid region, blue line: original segmentation; red line: over-estimation of boundaries

b) *model with underestimated boundaries*: adding one pixel inside the regions of the base model when region boundaries (arterial wall or lipid) were not clear; if the boundaries were clear, or there was no enough space for the adjustment, no modification was made. Figure 4.13 shows the under-estimation of arterial wall and lipid region boundaries.

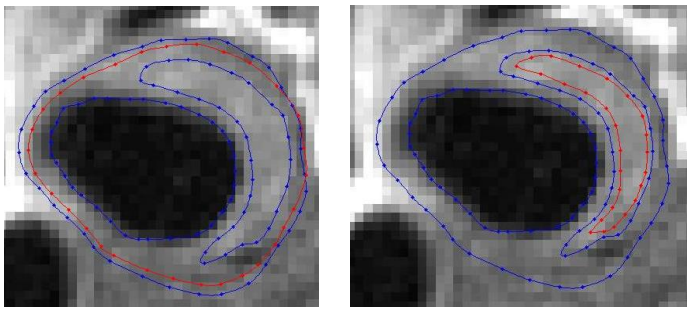

Figure 4.13 Schematic of under-estimation of arterial wall and lipid region, blue line: original segmentation; red line: under-estimation of boundaries

Because of the generally high contrast at the lumen wall, no adjustment was made to the lumen boundary. Therefore, for each subject, a total of 4 models were constructed: Wall+, one pixel added in the outer wall (or overestimated arterial wall); Wall-, one pixel subtracted in the outer wall (or underestimated arterial wall); Lipid+, one pixel added in both lipid core boundaries—inner boundary close to the lumen and outer boundary (or overestimated lipid core); Lipid-, one pixel subtracted in both lipid core boundary too (or underestimated lipid core). In models Lipid+ and Lipid-, the corresponding decrease or increase of the fibrous cap thickness would be one pixel.

The structure analysis was performed on Subjects 1, 2 and 3 individually. The stress analysis for Subject 1 is shown in Figure 4.14 (Panel 1), Subject 2: Figure 4.14 (Panel 2), Subject 3: Figure 4.14(Panel 3). The stress distribution for the baseline models can be found in Figure 4.11(Panel 1(a), Panel 2(a) and Panel 3(a)). For Wall+ cases, the stress distribution pattern is nearly the same as the baseline model; the local stress concentrations occur in the plaque region, and becoming more easily to be identified in Subject 2(Panel 2(a)) and 3(Panel 3(a)) in Figure 4.14; while the maximum VWTS (mVWTS) value is lower than in the baseline model. In the Wall- cases, the mVWTS is higher. The stress concentration area may appear in the healthy part of the arteries, due to the thinner arterial wall, indicated in Figure 4.14(Panel 1(b), Panel 2(b), and Panel 3(b)). In the Lipid+ cases, the fibrous cap becomes thinner and a clear local maximum stress concentration, induced by the thinner fibrous cap, can be found in the plaque region, and the mVWTS is much higher than in the baseline model. For the Lipid- cases, the stress distribution patterns are almost the same as those in the base model because the morphology change only occurs at the plaque region. Stress in the plaque region is lower for the cases because of the thicker fibrous cap.

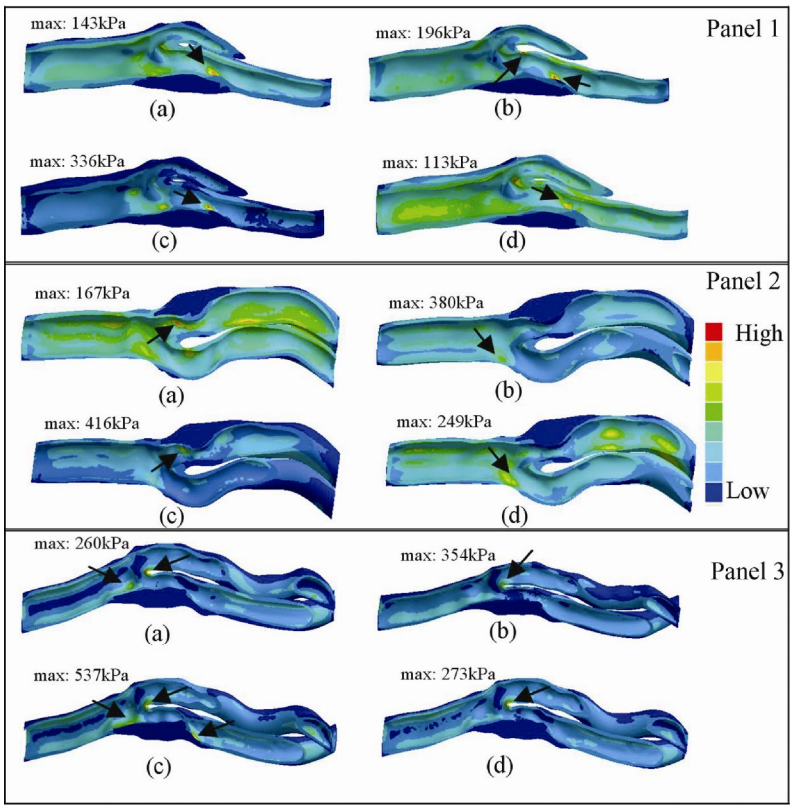

Figure 4.14 VWTS distribution and mVWTS value for models. (a)(e)(i) Wall+ model; (b)(f)(j) Wall- model; (c)(g)(k) Lipid+ model; (d)(h)(l) Lipid- model.

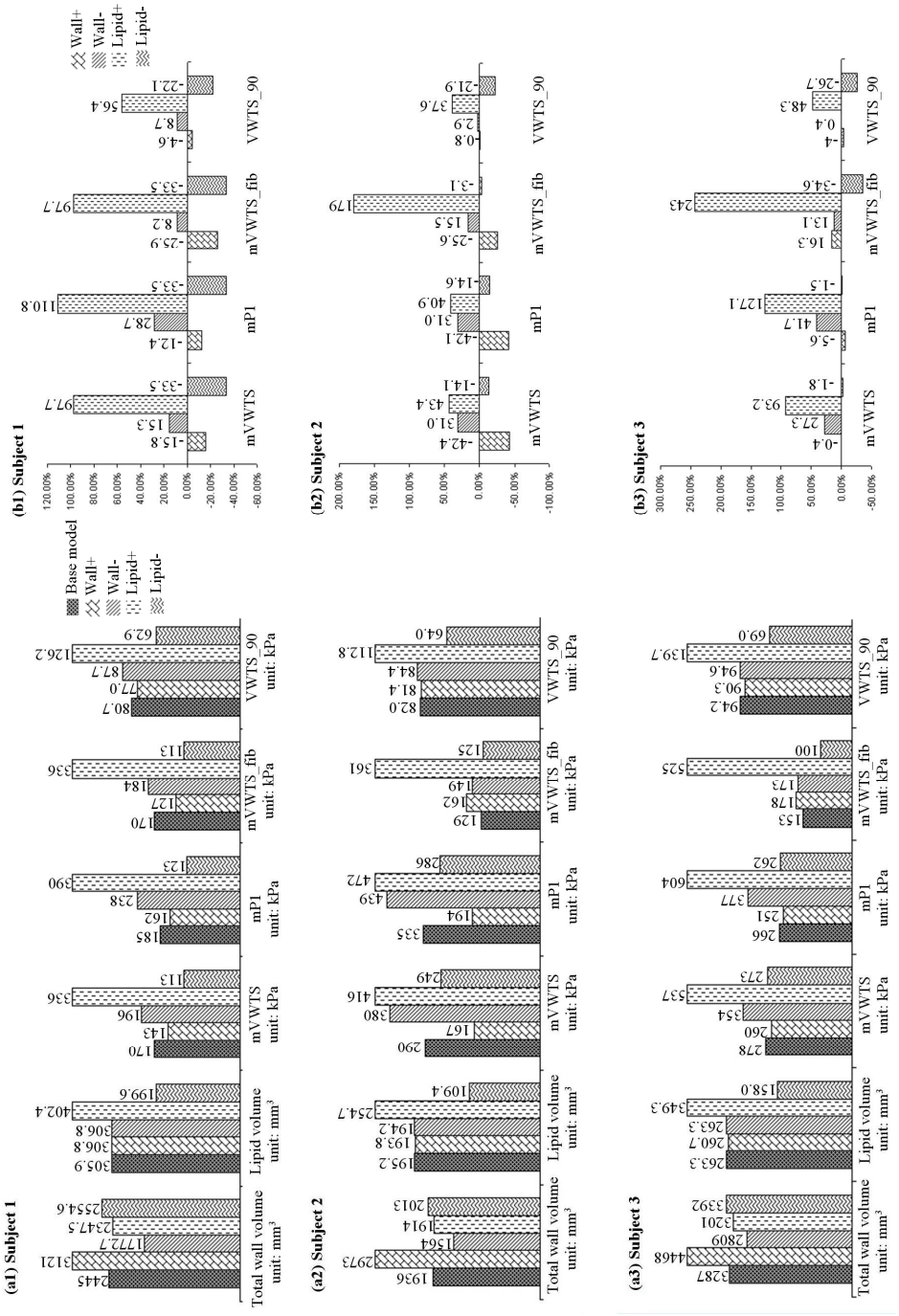

Figure 4.15 (ax) The impact of model reconstruction uncertainty on stress analysis and (bx) relative stress variation compared to the baseline model for the three subjects, including mVWTS, 1st principle stress, and mVWTS, VWTS_90 in the fibrous cap surface.

In Figure 4.15, both mVWTS and maximum FPS (mP1) in the arterial wall were presented for comparison with those in the baseline models for all cases. Since mVWTS represents the global maximum stress, which may not always be located in the fibrous cap, a local maximum stress on the fibrous cap named mVWTS_fib was calculated and presented in Figure 4.15. A stress value named VWTS_90 was also defined and presented to represent the general stress level in fibrous cap which may indicate a general rupture risk. In doing so, cumulative histograms of VWTS at the computational nodes on the luminal surface at the fibrous cap were calculated; the VWTS_90 is the 90% cut-off value of the histogram. Figure 4.15(a1,a2,a3) shows the stress values for all models of the 3 subjects, Figure 4.15(b1,b2,b3) shows the stress variations compared to the corresponding baseline model for each subject.

In Subject 1, with increased arterial wall thickness (Wall+ models), the mVWTS and mP1 decreased to a lower level, 15.8% and 12.43% respectively, compared to the baseline model; the reduction in mVWTS_fib was 25.9%, greater than the global maximum value change. The VWTS_90 value only reduced by about 4.6%. For the model with a decreased arterial wall thickness (Wall- models), the mVWTS, mP1, mVWTS_fib, and VWTS_90 values increased to 15.3%, 28.7%, 8.2%, and 8.7%, respectively. With decreased fibrous cap thickness (Lipid+ cases), the mVWTS, mP1, mVWTS_fib and VWTS_90 increased significantly by 97.7%, 110.8%, 97.7% and 56.4% respectively. With increased fibrous cap thickness (or Lipid- cases), the stress value decreased 33.5%, 33.5%, 33.5%, and 22.1% for mVWTS, mP1, mVWTS_fib, and VWTS_90 respectively. Similar trends can be found in subjects 2 and 3. The relative variations for each subject are shown in Figure 4.15 (b1, b2, b3).

Based on the above analysis, cases of Wall+ and Lipid- have smaller values of mVWTS and mP1 in the whole bifurcation, while for the cases of Wall- and Lipid+, mVWTS and mP1 will be larger. Among the cases, the greatest stress variation occurs in cases of Lipid+. The results show that mVWTS_fib and VWTS_90 experienced a small change in the cases of over/under-estimation of the arterial wall, and a much greater change for over/under-estimation of the lipid region, especially for the Lipid+ cases. For the general

stress level in fibrous cap, VWTS_90 increased significantly in cases Lipid+ (>40%) due to the thin fibrous cap, and decreased in Lipid- cases (about 20 to 30%). Therefore stress analysis result is much more sensitive to the segmentation accuracy of the lipid core and fibrous cap, and less sensitive to the arterial wall segmentation uncertainties.

4.4 FSI Procedure to 4 Patients

4.4.1 Study Purpose and Methodology

So far, the studies on applying FSI simulation procedure to the 3D multi-patient cases to provide cross-case comparisons of the stress predictions are limited. It is an important step forward of applying the procedure on a small group of patients in order to apply it to proper clinical study. This section used the developed FSI procedure for 3D stress analysis on a mini group of patients to: (1) demonstrate the applicability of the procedure to multi-patient cases by using *in-vivo* MRI images; (2) analyze stress in individual plaque; (3) compare the differences in stress distributions among different patients (Gao et al., 2009b).

4 plaque samples were selected for the stress analysis, shown in Figure 4.16.

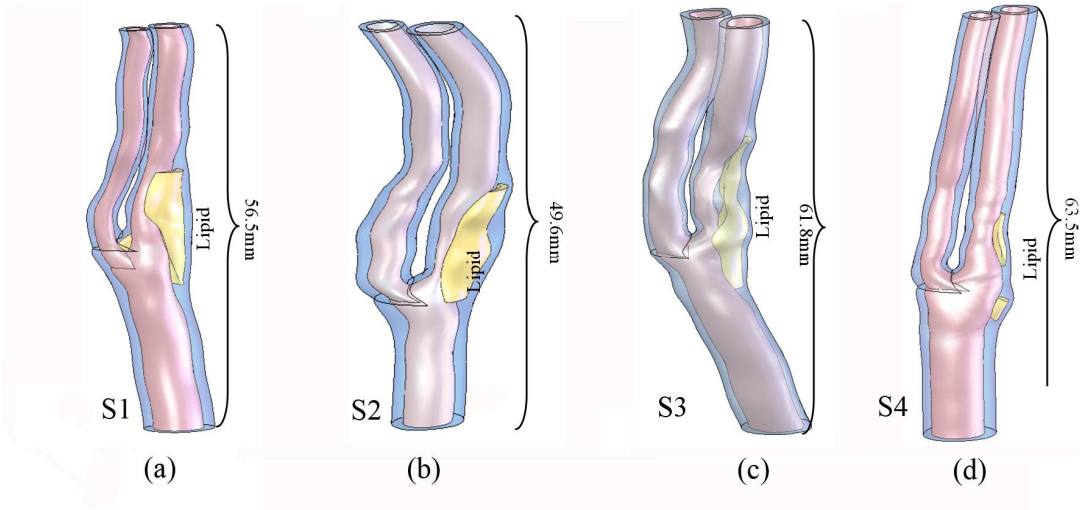

Figure 4.16 3D plaque geometry reconstructions for 4 subjects. (a) to (d): 3D geometry reconstruction of S1, S2, S3 and S4 respectively

The carotid arterial wall was assumed to be nonlinear, isotropic, and incompressible, with the 5-parameters Mooney-Rivlin model being used to describe its material properties

(Equation 3.28 in Chapter 3). The lipid core was assumed to be very soft with a 1kPa Young's Modulus and a 0.49 Poisson ratio (Finet et al., 2004). The interface between lipid core and arterial wall was treated as a so called "always bonded" contact; the pure penalty method was employed for the contact connection. Computational nodes at the outlet plane of ICA and ECA were fixed in all directions. An axial pre-stretch of 11% based on the shrunk geometry was applied at the inlet plane of CCA for the structure analysis. The structure model was meshed with an unstructured mesh consisting of nearly 100,000 10-node 3D tetra elements. The fluid domain was meshed in ICEM CFD11.0 with a much finer grid of around 1,000,000 3D tetra cells. Blood was treated as an incompressible, Newtonian fluid with a viscosity of $4*10^{-3}$ $Pa.s$ and a density of $1{,}067 kg.m^{-3}$. The flow was assumed to be laminar. Transient simulations were carried out with time-dependent pressure at the inlet of the CCA and mass flow rates at the ICA and ECA. In this study, the boundary conditions for the 4 subjects were assumed to be the same.

The fully coupled FSI simulation details can be found in chapter 3.

4.4.2 Results in Fluid Domain

Fluid pattern for subject 2 with high stenosis degree is showed in Figure 4.17 at systole phase. Due to the stenosis effect in the plaque region, a jet flow can be found at plaque throat, the reverse flow zone can be found right after plaque throat, shown in Figure 4.17(b). In order to present detailed velocity contours in plaque region, 10 planes were inserted with velocity contours plotted at those planes as in Figure 4.17(c). Strong secondary flow can be found after plaque throat. For plaques with high stenosis degree, the fluid flow shows more complex patterns in post plaque region, compared to the flow pattern in less stenosis plaques.

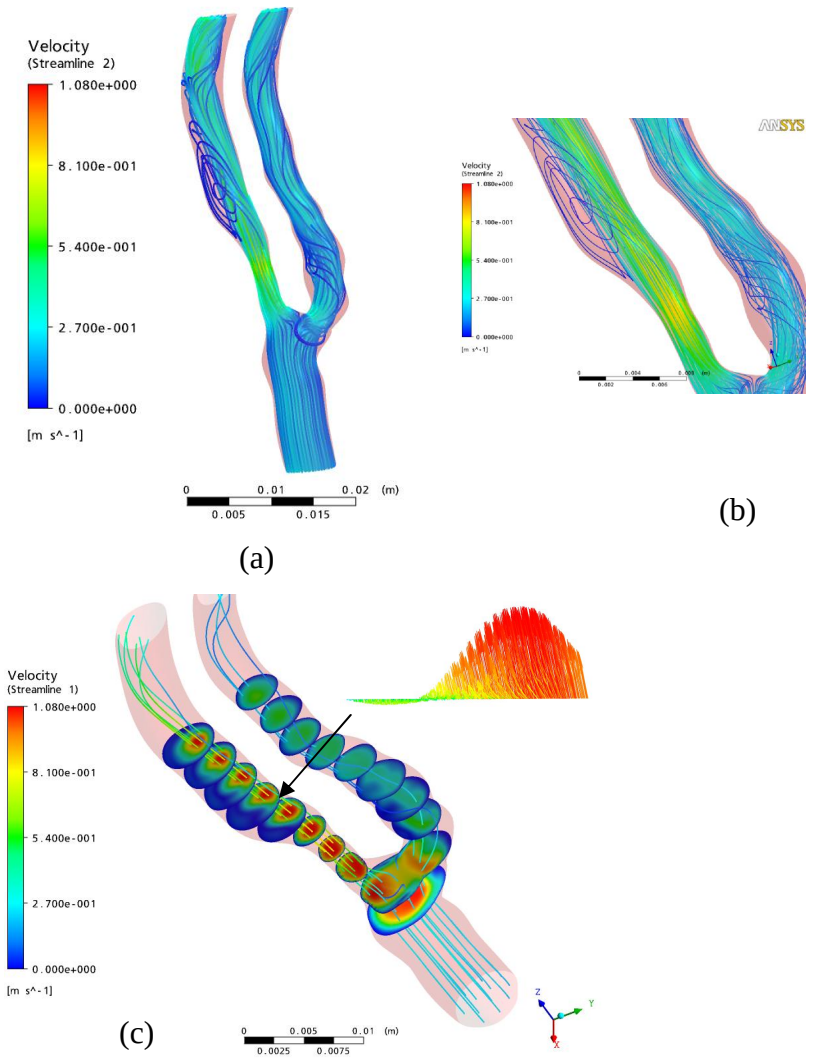

Figure 4.17 Flow pattern in Subject 2. (a) streamline for the whole plaque; (b) detailed flow pattern in plaque region; (c) velocity contours in selected planes along the plaque

The distributions of WSS_tmean and $WSS\_t\max$ (Equation 3.29 and 3.30 in Chapter 3) for the 4 subjects are shown in Figure 4.18. Because of the minor area reduction, WSS values in S1 and S4 are much lower compared to S2 and S3, which had medium stenosis. In the stenotic region, WSS values are generally high, which are much lower at upstream and downstream regions. A large post-stenosis recirculation zone can be found immediately distal to the stenotic region in S2, and S3 from the WSS results.

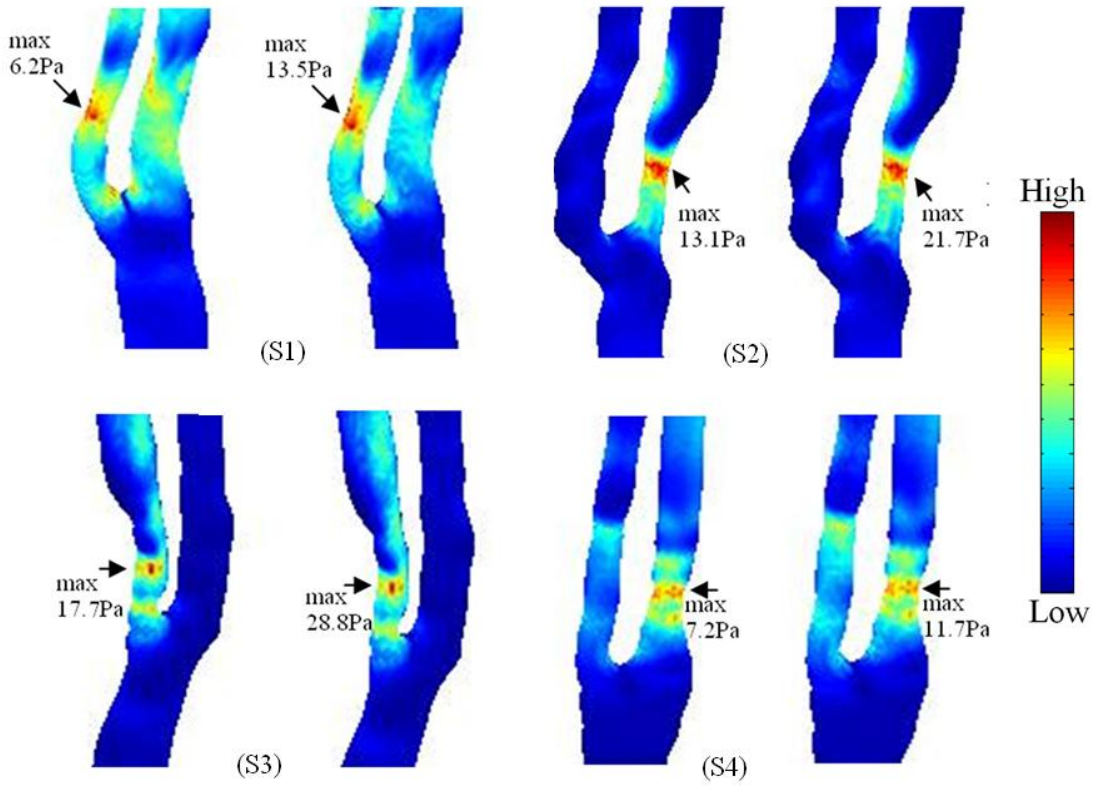

Figure 4.18 WSS_tmean , and WSS_tmax distributions for the subjects S1, S2, S3 and S4, only showing the stenotic region, the maximum value locations are indicated by arrows.

4.4.3 VWTS Distributions for the Four Subjects

Figure 4.19(a) shows the VWTS distribution for subject 1 in the lumen surface at systole phase. A local high stress region can be found downstream of plaque, just on the fibrous cap, indicated by an arrow. The stress at three locations for a cardiac cycle was extracted, shown in Figure 4.19(a1, a2 and a3). By examining the whole cardiac cycle, the region downstream of plaque for subject 1 always experienced higher VWTS than other plaque regions. Figure 4.19(b) shows the maximum principle stress distribution for the subject which is similar as VWTS. Figure 4.19(c) shows the equivalent strain at the lumen surface. Again a similar distribution pattern can be found as VWTS distribution. The correlation analysis between VWTS and maximum principle stress, equivalent strain showed that they are significantly correlated.

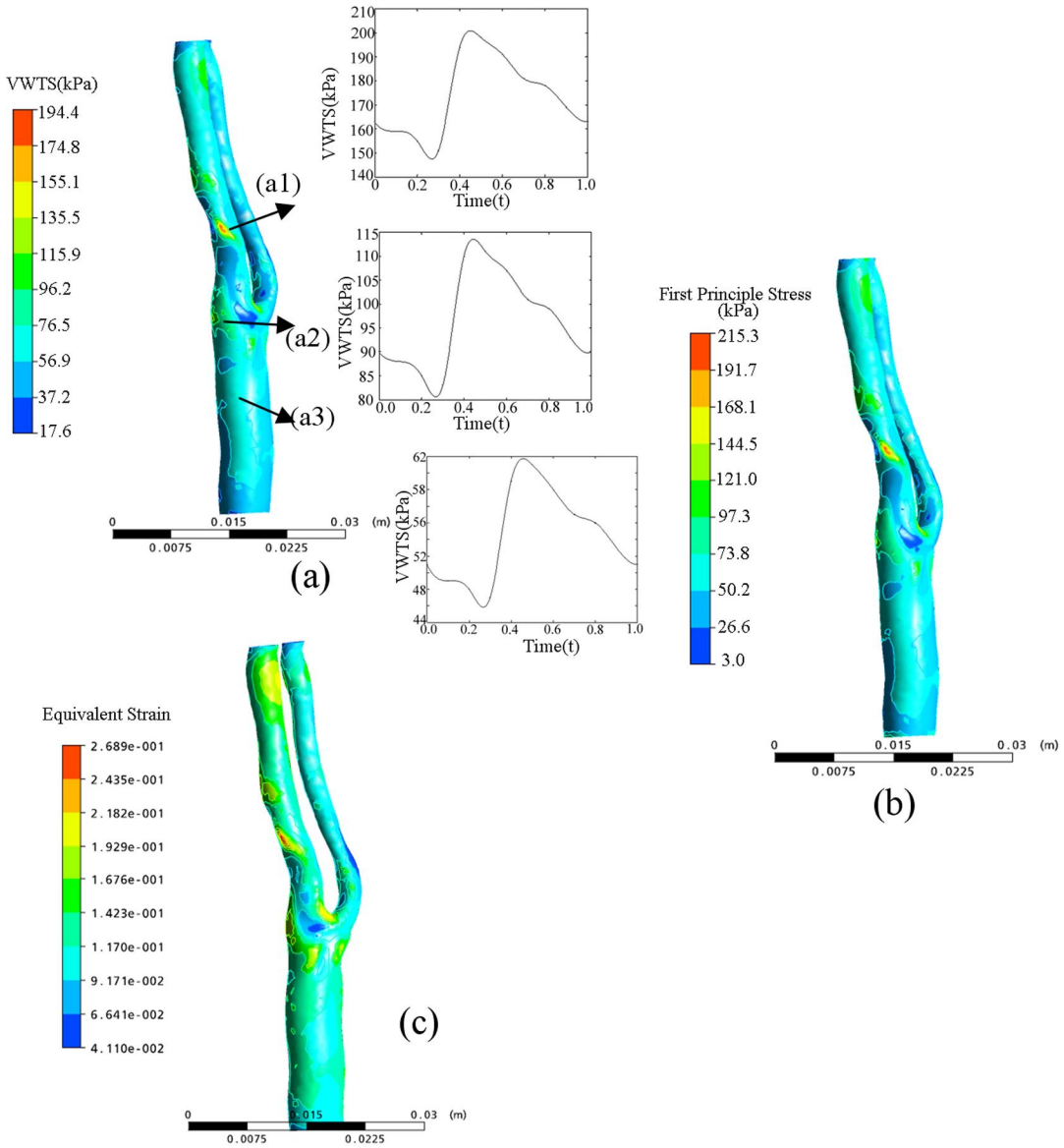

Figure 4.19 Stress/strain distribution for subject 1 in the lumen surface at systole phase. (a) VWTS; (b) First principle stress; (c) equivalent strain

Figure 4.20 shows stress distributions for the four subjects at peak systole. In the left column of each row, the general stress distribution contour is presented for the whole plaque. The VWTS distribution on the chosen transversal planes with 3mm interval throughout the plaque starting from CCA, is shown in the middle column. The maximum VWTS value at each transversal plane is shown in the right column. In general, VWTS is higher at the luminal wall, lower at the outer arterial wall and lowest in the lipid region.

Compared to the other subjects, S4 has more uniform distributions of VWTS along the circumferential direction due to its small lipid core. Also, in the transversal plane for all cases, high VWTS values can be located at the healthy side of the wall when the fibrous cap is thick; for the sections with a thin fibrous cap, the stress concentration regions appear at one or both edges of the lipid core (or plaque shoulders). Longitudinally, two peaks of VWTS can be found at either side of the lipid boundary for S1, S2, and S3, while for S4, VWTS peaks at the location between the two lipid cores, which is in the healthy part.

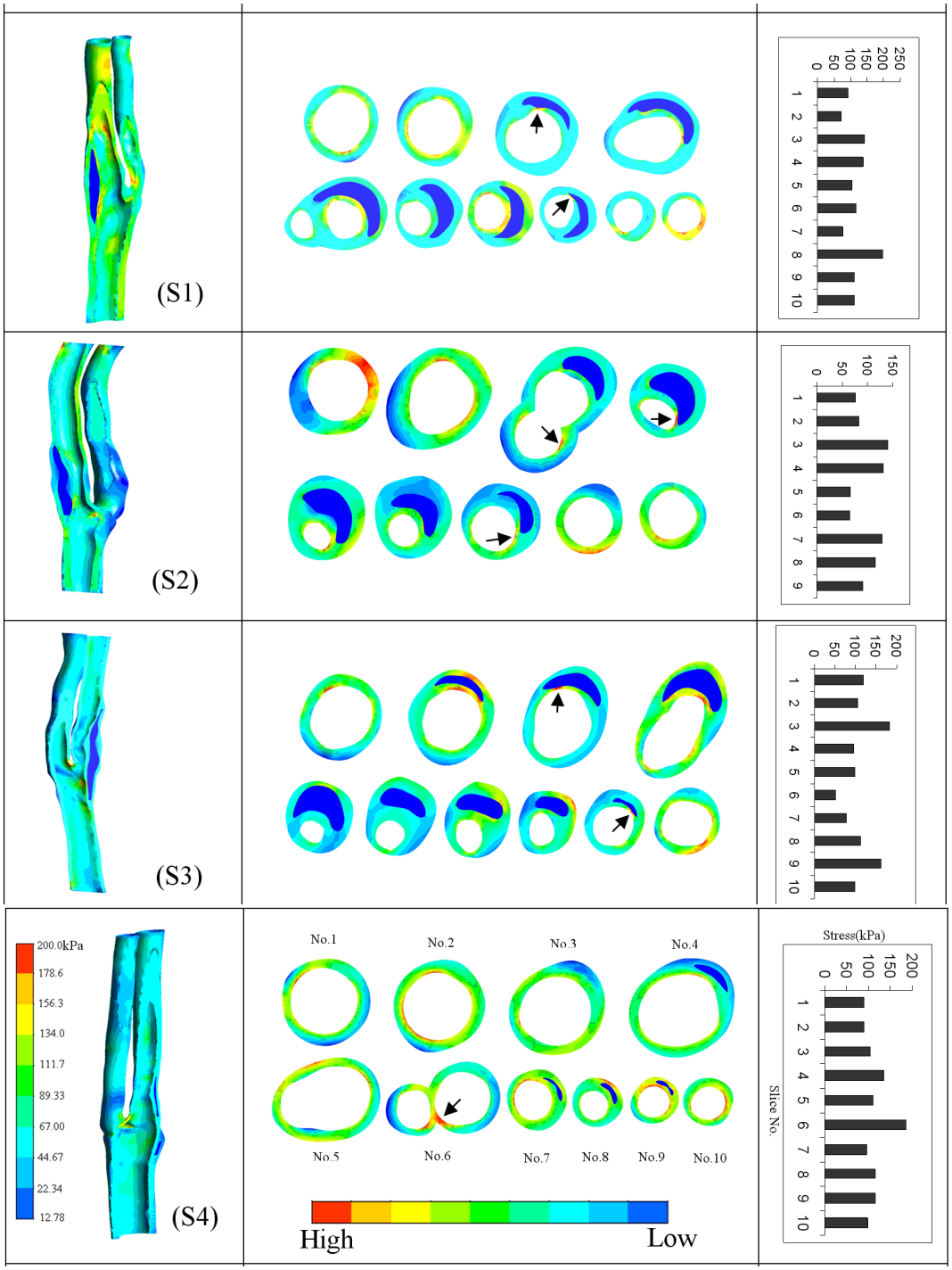

Figure 4.20 Stress distributions for 4 subjects at peak systole. The first column: general stress distribution in the whole geometry with cutting views; The second column: stress distribution on selected transversal sections; The third column: maximum VWTS for the planes in the second column of the corresponding case. The arrows in column 2 indicate the longitudinal peaks presented in column 3.

4.4.4 VWTS in the Fibrous Cap

Stress distribution in the fibrous cap has been considered to be closely related to plaque rupture (Tang et al., 2005a). Figure 4.22 shows more details of the distributions of temporal maximum VWTS (VWTS_tmax in the third column) within a cycle, and relative VWTS variation (rcVWTS in the fourth column) on the fibrous cap at the luminal side during a cycle. The fibrous cap thickness, defined as the shortest distance between the fibrous cap surface (lumen side) and lipid region, is shown in the second column of Figure 4.21. Although the MR image spatial resolution is 0.39mm, the 3D surface interpolation during model reconstruction can still produce fibrous cap regions with a thickness less than 0.39mm. The minimum fibrous cap thickness is 0.18, 0.29, 0.23 and 0.34mm for cases S1 to S4 respectively.

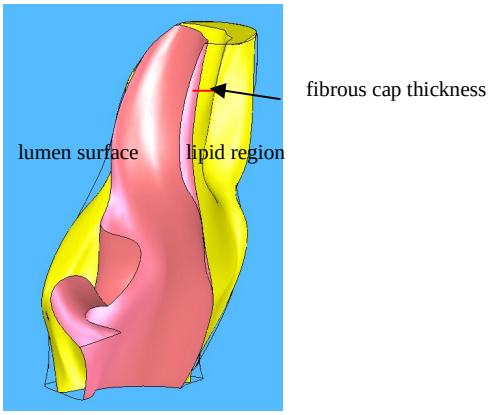

Figure 4.21 fibrous cap thickness definition

Generally, a thin fibrous cap is associated with a high VWTS (Finet et al., 2004). This trend has been followed in cases of S1, S2 and S3: for example, in the Figure 4.22 column 3, the stress concentration regions at (1) downstream left and upstream right for S1; (2) upstream left and right side for S2; (3) upstream left and downstream right for S3, were all related to thin fibrous caps. However, the stress concentration region in S4 seems not to follow the trend due to the small lipid core size and large fibrous cap thickness. With regards to the VWTS_tmax distribution for all cases, stress concentrations are more likely to occur at the left or right boundaries of the fibrous cap, which represent the shoulder regions of the plaque at the transversal plane instead of near the middle of fibrous cap, except in S3. In S3, there is a large high stress zone in the upstream-middle

region closely associated with a thin cap. The rcVWTS maps in the fourth column of Figure 4.22 provide information about the relative VWTS variations during a cycle. It is found that high rcVWTS regions negatively correlate with high VWTS zones in S1, S2 and S3, with high rcVWTS regions close to the middle in the circumferential and longitudinal directions of the fibrous cap. It can also be seen that some high rcVWTS are located immediately next to a high VWTS zone as in S2.

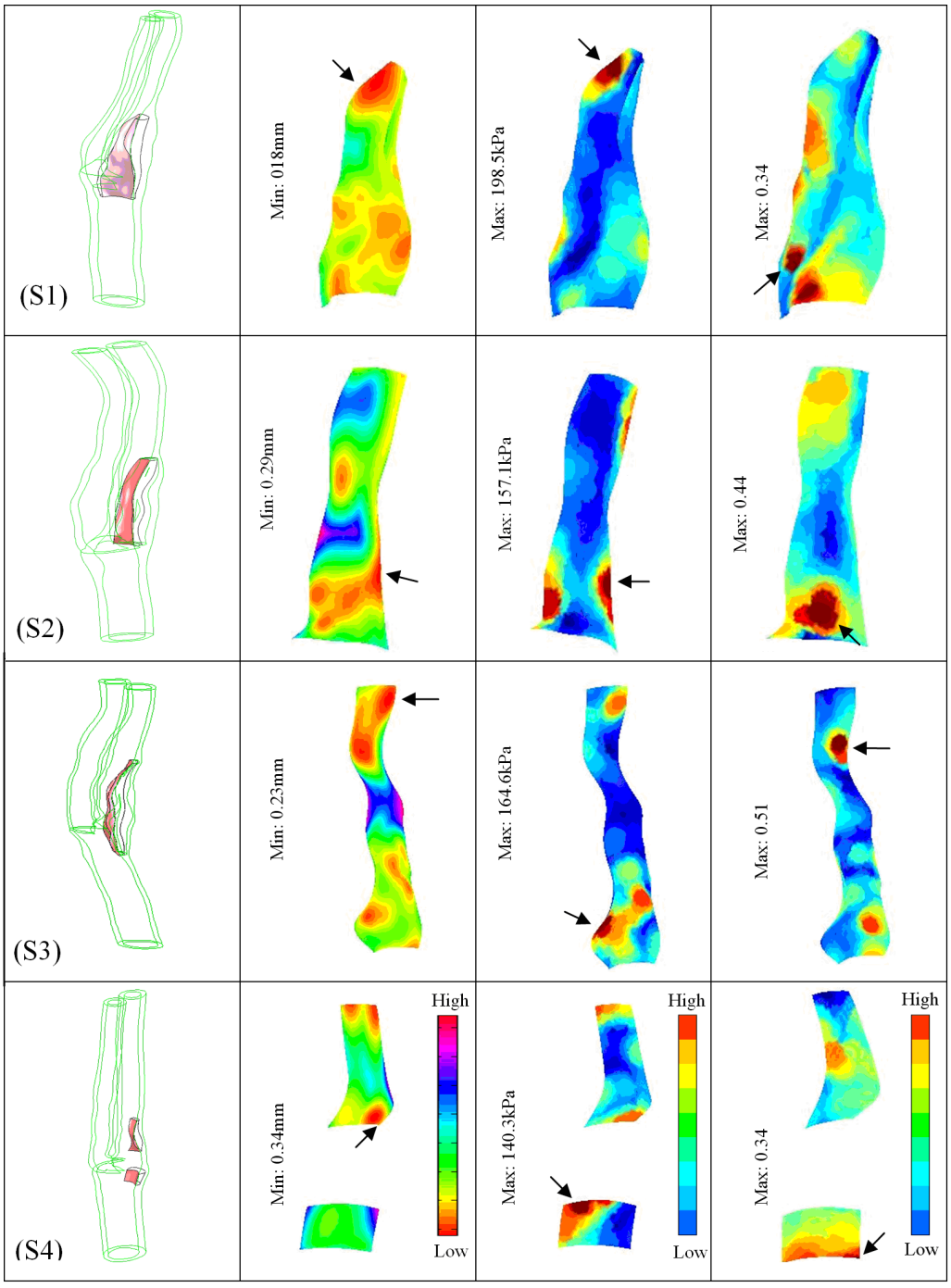

Figure 4.22 Stress distribution on the fibrous cap. The first column shows the fibrous cap surface in the whole geometry; the second column represents the fibrous cap thickness; the third column is VWTS_tmax distribution in the fibrous cap, the maximum VWTS_tmax locations are indicated by arrows; the fourth column is rcVWTS distribution, the maximum rcVWTS locations are indicated by arrows.

4.4.5 Comparisons among the Four Subjects

Table 4.3 summarized several stress and geometry factors for all subjects in the plaque region. They are the maximum/mean value of WSS_tmax, WSS_tmean, VWTS_tmax, rcVWTS in the defined fibrous cap surface and the minimum fibrous cap thickness (min_FT), maximum degree of stenosis (max_SD) in the plaque region. From Table 4.3, the stress factors derived from WSS are highly correlated with the degree of stenosis; a higher degree of stenosis will induce a higher WSS in the maximum and mean values. However, the maximum VWTS_tmax values do not appear to be dependent on the degree of stenosis; they are more closely related to the fibrous cap thickness (min_FT). The rcVWTS values are similar in all subjects, with a higher level in S2 and S3. When combining minimum fibrous cap thickness with VWTS factors, S1 possesses both the highest local maximum stress value, and very thin fibrous cap, indicating a higher rupture risk than the other subjects. In summary, the plaque stability order from high risk to low risk could be S1, S3, S2, and S4.

4.5 Discussion & Conclusion

4.5.1 Reproducibility Study on Plaque Geometry Reconstruction

By using multi-spectral MR imaging, the main features of carotid plaques, including fibrous cap status, lipids, intra-plaque hemorrhage, and vessel thickness, can be imaged noninvasively, and the technique is highly reproducible (Von Ingersleben et al., 1997; Yuan et al., 1998; Yuan et al., 2001; Cai et al., 2005). Saam (Saam et al., 2005) compared the major plaque components classified by ***in-vivo*** MRI with measurements of plaque components from histology, demonstrated that MRI measurements of plaque components were statistically equivalent to the measurements from histology analysis. By comparing the wall thickness from MRI and B-mode ultrasound, Underhill (Underhill et al., 2005) suggested it is possible to use carotid MRI for assessing atherosclerotic disease. Recently the contrast-enhanced MR in distinguishing plaque components has also been developed and applied clinically. For example, a gadolinium contrast agent has been used to enhance the contrast between lipid core and surrounding tissue (Yuan et al., 2002a). 3-T MR scanner is under the way for plaque imaging and diagnosis, which can significantly improve the signal-to-noise ratio, also spatial resolution (Yarnykl et al., 2006). Efforts

also have been made to differentiate plaque components according to MR signal intensities (Rogers et al., 2000; Trivedi et al., 2004).

Subjects / Stress Factors		S1	S2	S3	S4
WSS_tmax(Pa)	max	6.9	21.7	28.8	11.4
	mean	3.6	8.6	8.2	4.03
WSS_tmean(Pa)	max	4.1	13.1	17.7	6.9
	mean	2.2	5.3	5.0	2.4
VWTS_tmax(kPa)	max	198.5	157.1	164.6	140.3
	mean	80.7	69.1	82.9	80.5
rcVWTS	max	0.34	0.44	0.51	0.34
	mean	0.26	0.28	0.29	0.21
Morphological Factors					
min_FT(mm)	min	0.18	0.29	0.23	0.34
max_SD	max	22%	73%	72%	10%

Table 4.3 Stress results and morphological factors for 4 subjects. WSS_tmax: temporal maximum wall shear stress; WSS_tmean: temporal mean wall shear stress, VWTS_tmax: temporal maximum wall tensile stress, rcVWTS: relative cyclic wall tensile stress, min_FT: minimum fibrous cap thickness, max_SD: and maximum degree of stenosis.

In this chapter, MR images of carotid plaques from several sequences were used together for generating the necessary boundaries. The first step was the registration of multi-images with one fixed frame. Due to the possible movement of patients during MR scanning, the MR images of same locations could have some distortions when scanned at different time. Therefore a registration procedure was needed for using multi-sequence MR images. While it is possible that there are nonlinear distortions occurring at different MR sequences, the linear transform method used in the study would not be enough for the registration purpose, certain no-linear methods are desired, such as deformable registration.

The resolution of the MRI images was 0.39mm/per pixel, which may be enough for presentation purposes, however it is not adequate for assessing the fibrous cap thickness (Jahnke et al., 2007), especially when the data is to be used for stress analysis. The detection of arterial inner and outer wall has been well studied, several semiautomatic image processing methods have been proposed for boundary detection based on active contour or 'snakes' (Ladak et al., 2001), which utilize the intensity gradient information. Because of the high contrast of lumen region and arterial wall, shown in Figure 4.2, it makes possible to apply 'snakes' to the boundary detection with high accuracy. However, when detecting plaque components, it becomes much more difficult: (1) multiple contrast weightings are needed to detect plaque components, rather than single MRI sequence, therefore the registration is needed to align different contrast weighting MR images to the same location; (2) segmentation of tiny plaque components into distinct regions according to signal characteristics is very hard and noise-sensitive. A computer-aid system for cardiovascular disease evaluation (CASCADE) has been developed and applied to the segmentation of carotid plaques recently (Kerwin et al., 2002). However, plaque imaging analysis still requires experienced reviewers to help in defining plaque components and even arterial wall. Due to the high accurate requirement of 3D plaque geometry reconstruction for stress analysis, the manual segmentation methods were used in the project for arterial wall, plaque components segmentation. Furthermore, the low contrast between lipid region and the arterial wall makes the segmentation of lipid region/fibrous cap to be hard. An assumption was proposed for the detection of thin fibrous cap, at least one pixel thickness was reserved when the fibrous cap can not be differentiated from surrounding lipids, though it is possible the real fibrous cap thickness is greater than one pixel or less than one pixel. The newly developed MRI technology for imaging the atherosclerotic plaque, such as the post-contrast enhanced T1 weighted (Phan et al., 2006; Boussel 2008), can be very helpful in accurately defining lipid region/fibrous cap, and consequently enhancing following stress analysis accuracy.

From the study of reproducibility of human arterial plaque reconstruction, the disagreements for arterial wall reconstruction usually were very small around one pixel

due to the clear definition of the wall boundary. However, for the lipid core region, because of the relatively low contrast between the lipid core and the surrounding tissue, more artificial estimations are made on the reconstruction of the lipid core region which will affect the fibrous cap delineation accuracy accordingly. In Emmanuel Touze's (Emmanuel Touze et al., 2007) study, it was concluded that the inter-observer reproducibility for quantitative area measurements such as arterial wall area and luminal area was generally high. However, it was relatively low for the lipid core area with a mean difference ranging from -9.8 to 8.2mm^2. In our study, the mean lipid area differences were 3.89 and 6.47mm^2 for subjects 1 and 2 respectively, which lie in the same range. Since the fibrous cap thickness is derived from the lipid boundary, the uncertainty of the lipid segmentation will directly affect the fibrous cap definition. Therefore it can be concluded that the reproducibility of the arterial wall segmentation is high, while relatively large uncertainties are associated with the fibrous cap and lipid core segmentation.

Finite element analysis could provide the stress distribution and local maximum stress concentration regions on the arterial wall, including plaque. Numerous studies have been carried out in this area based on histology data (Cheng et al., 1993) or *ex- vivo* MR images. The uncertainties of the geometry reconstruction on different plaque components have varied impacts on the stress analysis. Over/Underestimation of the arterial wall (models Wall+ and Wall-) will only introduce a minor stress variation in the fibrous cap region, especially for VWTS_90, about 10%. However, Over/Underestimation of lipid region (models Lipid+ and Lipid-) has significant effects on stress values, especially on the Lipid+ models in which a general increase of 100% on mVWTS_fib and 50% on the values of VWTS_90 can be found. Since the absolute stress value is affected by many factors, such as the material properties, local geometry features and so on, the VWTS_90 value change is more representative and robust, which can also be evidenced by the more uniform change in VWTS_90 values for different subjects in Figure 4.15 (b1, b2, b3).

The impacts on the stress distribution in the plaque region caused by over/under-estimation of arterial wall are much less and insignificant comparing with the variations

caused by the over/under-estimation of the lipid region. It would be expected that a higher spatial resolution and better image contrast between lipid region and fibrous cap, which could be provided in the future MRI technical development, will generate more accurate and reliable plaque morphology and stress prediction. Therefore the accuracy of stress analysis based on plaque geometry is subject to MR image quality. The improved resolution/quality in plaque imaging with newly-developed MRI protocols would generate more realistic stress predictions.

4.5.2 FSI Simulation with 4 Subjects

With anatomically realistic plaque geometry, FSI simulation is able to provide detailed stress analysis for the plaque which has been demonstrated with individual case studies (Yang et al 2007, Tang et al 2008). However, the procedure can only be useful when the result can be compared across subjects and provide statistics meaningful rupture risk assessments. For a multi-case study more restrictions may be applied to the simulation algorithms since the study with single case only deals with a specific geometry, which makes the model generation and simulation condition to be more flexible and the final convergence can also be achieved easily. In multiple cases situation, due to the significant plaque geometry variations from one case to another, more robust and consistent approaches need to be adopted or developed to obtain simulation results under similar conditions and make the cross-case comparison meaningful. In the present study, specific concerns were (1) similar assumptions were applied in model reconstruction especially on segmentation to all cases so that the 3D model geometry reconstruction error margins were in the same range. (2) Interactions between arterial wall and lipid region need to be defined in the similar way, and (3) consistence in post-processing procedure, et al. Other conditions, which were important to provide realistic simulation results such as the patient specific material property and fluid flow boundary conditions, were not applied here due to data limitation.

Based on the stress analysis, plaque rupture risks among the 4 subjects were made. The results showed that higher stress (indicating a more vulnerable plaque) is associated with a thinner fibrous cap and a large lipid region which is in agreement with previous studies

(Richardson et al., 2002). In terms of morphology features, the lipid volume size from large to small for the four subjects is S1, S3, S2, S4 and the fibrous cap thickness from thin to thick is S1, S3, S2, S4 while the degree of stenosis from high to low is S2, S3, S1, S4. The predicted stress level on the fibrous cap from high to low is: S1, S3, S2, S4 which followed the similar trend from morphological analysis. It also indicated that varied morphological features of the plaque components and the induced stress factors could provide more information of the rupture risk, rather than the degree of stenosis (Nighoghossian et al., 2005). It must be stated here that the rupture risk assessment cannot be concluded with only local stress data since rupture of the fibrous cap is a very complex process (Casscells et al., 2003). It is not only the mechanical factors that matter, but other abnormalities in tissue and cells, such as elevated inflammatory activity, degraded collagen structures can also influence the rupture process (Richardson et al., 2002).

Generally, the extremely high stress value occurred at the thinnest fibrous cap thickness among the four subjects. When looking at individual plaques, stress concentration regions are confined to the thinner fibrous cap regions, with high stress values located at the shoulder regions. These are the major rupture risk regions responsible for 60% of plaque ruptures according to Shah (Shah et al., 2003). On the other hand, during the long development period of a plaque, with constant remodelling, a constantly high stress region in the fibrous cap may be associated with a strengthened collagen structure. As a result, rupture critical stress would be increased in the region. It may partially explain the fact that not all plaque ruptures occur at the shoulder regions. The pulsatile nature of arterial pressure and the consequent cyclic arterial wall stress/strain not only modulates the cellular function of endothelial cells (Kaissis et al., 2004), but also causes fatigue damage in the fibrous cap (Versluis et al., 2006). Cyclic strain has been shown to affect endothelial and smooth cells' activity, promoting proliferative response or mitosis (Cheng et al., 1997). Li (Li et al., 1994) demonstrated that there exists an optimal cyclic strain range for endothelial cell proliferation, which if exceeded will cause mitosis. Kaazempur-Mofrad (Kaazempur-Mofrad et al., 2003) suggested the cyclic strain as a factor for atherogenesis, which is defined by $e_{vm,cyclic} = e_{vm,systolic} - e_{vm,diastolic}$ based on Von Mises

strain. Though there are growing studies on cyclic strain effects' on early atherogenesis, the cyclic strain/stress pattern on vulnerable plaques are still need to be investigated. The introduction of rcVWTS in the study aims to assess VWTS oscillation levels on the fibrous cap, which has similar formation as cyclic strain in Kaazempur-Mofrad's work (Kaazempur-Mofrad et al., 2003), while the relative change was introduced rather than the absolute change. A higher rcVWTS represents a high variation of VWTS in a cycle, which indicates a high probability of fatigue damage in the region. The results show that high rcVWTS regions occur in the middle of the fibrous cap which agrees well with Lovett's result in which 16.9% of ruptures occur in the middle of the plaque in symptomatic patients (Lovett et al., 2003). However, histological evidence of plaque fatigue is needed to support the correlation of the rcVWTS value with rupture probability.

From Williamson's study (Williamson et al., 2003), the stress analysis may be used with confidence because the uncertainties in material properties cause relatively small errors in the stress prediction. In this study, two plaque components were considered in the plaque region, they are arterial wall (including fibrous cap), and lipid region. Based on the baseline model of subject 1, material properties for arterial wall and lipid region were changed from -100% softer to 100% stiffer (one material was changed while the other one was kept the same as the baseline model). Static simulations were performed with different material properties, the boundaries conditions were: 11% axial pre-stretch in CCA plane, 110mmHg luminal loading. Local maximum VWTS at fibrous cap increased by about 8% with a 100% increase in vessel stiffness, and decreased by about 5% with a 100% decrease in vessel stiffness; for the variation of lipid core stiffness, it led to less than 10% changes for local maximum VWTS at fibrous cap. The stress distributions at plaque region were similar for all the simulations with different material properties. The results had confirmed the finding from Williamson (Williamson et al., 2003). Therefore the same material models were used for all simulations in the section. However, it should be pointed out that the patient-specific material models still are needed in the future stress studies, without the accurate material properties, the predicted stress needs to be carefully examined especially when linking stress results to biological abnormalities. How to derive patient specific material model will be revisited in Chapter 6.

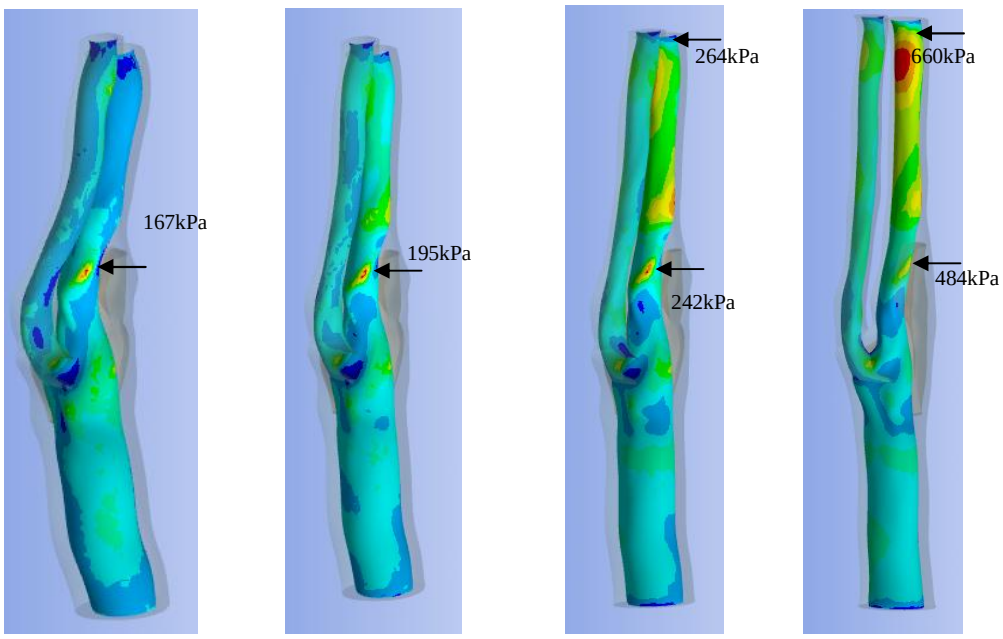

(a) (b) (c) (d)

Figure 4.23 VWTS distribution in the luminal surfaces with different axial pre-stretch, 0%, 10%, 20% and 30% respectively. (a) simulation 1; (b) simulation 2; (c) simulation 3; (d) simulation 4

It has been well accepted that the arteries experience significant axial stretch in *in-vivo* situation. Because of lack of direct methods to measure the axial stretch in-vivo, the data regarding axial stretch in human carotids are not available. Studies have demonstrated that axial stretch plays an important role in plaque stress/strain prediction (Tang et al., 2004a). In order to quantify the effects caused by axial stretch in the study, simulations with different axial stretch were carried out to investigate the influence caused by axial stretch. The simulations were done with the static model, 110mmHg pressure loading in the lumen surface, and with different axial stretch in the CCA plane, they were 0%, 10%, 20% and 30%. The VWTS distribution in the luminal surfaces were chosen to examine the stress distributions, shown in Figure 4.23.

For simulation 1, without axial stretch, the maximum stress can be found in the plaque region, indicated by the arrow. When 10% axial pre-stretch was applied to the CCA plane, the maximum stress still can be found in the lipid region, with 17% increase in value compared to the simulation 1 without axial stretch. In simulation 3, the maximum stress location changes to the healthy part of ICA, with 58% value increase compared to simulation 1. In the plaque region, a local maximum stress concentration region still can be found, and VWTS at that local stress region is 242kPa, 45% higher than the stress at the same location for simulation 1. For simulation 4, which had 30% axial pre-stretch, the maximum stress is significantly higher than the other three simulations. It is nearly 3 times higher than that in simulation 1, and the location of maximum stress has also moved to the healthy part as in simulation 3, local extreme VWTS at plaque region is around 484kPa, 1.89 times higher than that in simulation 1. Maximum VWTS in the whole geometry and plaque region was summarized in Table 4.4.

Simulations	Axial stretch	Global Max VWTS(kPa)	Higher than Sim1	Local Max VWTS in Plaque(kPa)	Higher than Sim1
Sim1	0%	167	--	167	--
Sim2	10%	195	17%	195	17%
Sim3	20%	264	58%	242	45%
Sim4	30%	660	295%	484	189%

Table 4.4 the comparison of stress results with different axial pre-stretch

The above study indicates that the axial pre-stretch can have great influence on stress distribution in plaque region. A large axial pre-stretch can cause extreme stress condition in the healthy part, and the maximum values also are highly different. Therefore in the plaque stress simulation, the axial pre-stretch needs to be added in order to have a realistic stress prediction. For *in-vivo* MRI based model, the pre-stretch condition is inherited in the image information, therefore a geometry adjustment is needed as discussed in the section 4.2.5, a proper shrinkage procedure needs to be applied. By using non-invasive *in-vivo* clinical data, the axial pre-stretch was estimated for two human

subjects, around 10% was reported in a recent study (Masson et al., 2008). Due to lack of subject specific axial stretch data, a pre-stretch around 11% was applied in the study, corresponding 10% shrinkage in the shrinkage procedure. It is believed that the accurate knowledge of axial stretch data will significantly improve the accuracy of stress predictions from those *in-vivo* computational plaque models.

4.6 Summary

In sum, the procedure of patient-specific models of carotid bifurcations with plaque constructed from *in-vivo* multi-spectral MR images was established, and successfully applied to 4 subjects.

Plaque reconstruction reproducibility was studied by comparing the imaging segmentation results from three independent investigators. Inter-operator reproducibility for the arterial wall reconstruction based on T2W images was high, with the disagreement among the operators being at one pixel level. The reproducibility was lower for the segmentation of lipid core and fibrous cap. The uncertainties caused during 3D surface interpolation and smoothing, and 3D reconstruction were minor and negligible. The followed stress analysis showed that accurate fibrous cap reconstruction has great effects on the predicted stress distributions and levels. It would be expected that a higher spatial resolution and better image contrast between lipid region and fibrous cap, which could be provided in the future MRI technical development, will generate more accurate and reliable plaque morphology and plaque stress predictions.

The developed FSI was performed for four subjects based on *in-vivo* multi-sequence MRI images. For all studied cases, wall shear stress distributions are highly related to the degree of stenosis, while the level of its magnitude is much lower than the VWTS in the fibrous cap. Wall stress is higher in the luminal side and lower at the outer wall, with the lowest stress at the lipid region. Local stress concentrations are well confined in the thinner fibrous cap region. The introduction of relative stress variation in the fibrous cap during a cycle can be a potential indicator for fibrous cap fatigue damage. According to stress analysis of the four subjects, a risk assessment in terms of mechanical factors was

made with a ranking of rupture risk possibility among the cases, which could be helpful in clinical practice.

Chapter 5 Applications (1)

Stress Analysis of Carotid Atheroma in Transient Ischemic Attack (TIA) Patients

5.1 Introduction

Up until now, the direct evidence between stress and plaque rupture is still not available. If plaque geometry is available at both pre- and post- rupture for a plaque, it would be possible to provide some kind of validation of the plaque rupture hypothesis based on plaque specific stress analysis, which we are working on. However, there is no way to know for sure of plaque geometry both before and after the rupture event. *In-vivo* MRI has been used to detect the ruptured fibrous cap in carotid plaques. With the plaque geometry information immediately after rupture by scanning the patient after a TIA, it may be possible to reconstruct the plaque geometry just before ruptured with some adjustments. Applying stress analysis with the ruptured and corresponding non-ruptured plaques, it could provide some evidence for the hypothesis on plaque rupture caused by extreme stress. The general procedure of such is illustrated in Figure 5.1.

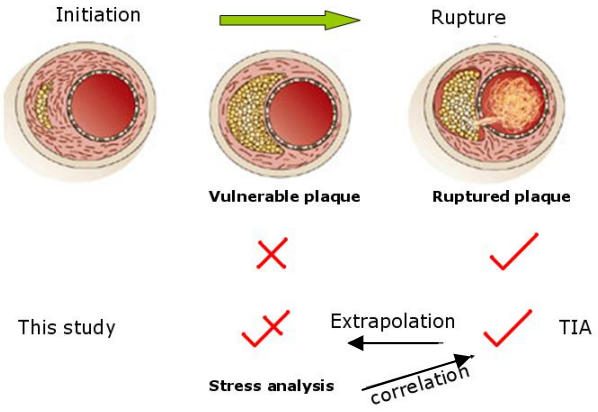

Figure 5.1 General Procedure of stress analysis with TIA patients

In this study, ruptured plaques from 3 TIA patients (TIA1, TIA2, and TIA3) were scanned by *in-vivo* multi-spectral MR imaging, based on which the pre-rupture plaque models were constructed by repairing the ruptured fibrous cap. One-way FSI simulation was performed to enable stress prediction in both fluid and structure domain. The correlation between local stress and plaque rupture was examined. Furthermore, the

uncertainties in the plaque reconstruction in the rupture sites were examined to study the local stress variation against the plaque rupture sites. Part of the work has been reported in the paper (Gao et al., 2010).

5.2 Imaging Method

Three patients were recruited from a specialist neurovascular clinic. The patients suffered a recent TIA and underwent carotid MRI within 72 hours. High resolution MR imaging was performed to obtain the plaque geometries. Arterial and plaque geometry was obtained from the multi-sequence MRI. An in house program developed in Matlab^{TM} was used to segment the regions of lipid core, arterial wall and lumen, which have different signal characteristics when imaged by the multi-spectral protocol, shown in Figure 5.2. The detailed MR imaging and plaque segmentation procedure can be found in Chapter 4, section 4.2.

5.3 Baseline Cases Simulation

5.3.1 Geometry Reconstruction

Attention needs to be paid for the segmentation of fibrous cap for all cases. In the ruptured plaques, the fibrous cap is not intact, and shows no signal in MR images. In detail, if the images has blur boundary for the fibrous cap, one pixel (0.39mm) was reserved for the fibrous cap thickness as in the cases in section 4.2.4 in Chapter 4. Special attention was paid to the segmentation in the rupture site of the plaque. The ruptured fibrous cap was deemed present if there was a clear defect, discontinuity or ulceration within the fibrous cap (Hatsukami et al., 2000; Yuan et al., 2002b). In this situation, the fibrous cap is absent in STIR images with a dark lipid core region connected with luminal area (demonstrated in Figure 5.2(c)). A constant fibrous cap thickness of 0.39mm (one pixel) was assumed for the fibrous cap reconstruction in the region. Figure 5.2(d) shows the segmentations at the rupture site based on STIR image. It should also be noted that according to Figure 5.2(c), it is not clear where the initial rupture site located, which can be either at the middle of the fibrous cap, or at the shoulder region. Longitudinally, the rupture site was further assumed to cover the range from the upstream to the downstream section of Figure 5.2(d) with a distance of 1.5mm on each side (which is the slice

thickness). A linear transformation was applied for the registration of images obtained from different sequences. The whole segmentation for the bifurcation region is shown in Figure 5.2(e) with the lipid region from STIR images. The reconstructed 3D plaque models are shown in Figure 5.3, and the rupture sites are indicated by arrows, the stenosis degree for all 3 subjects is moderate, around 25%.

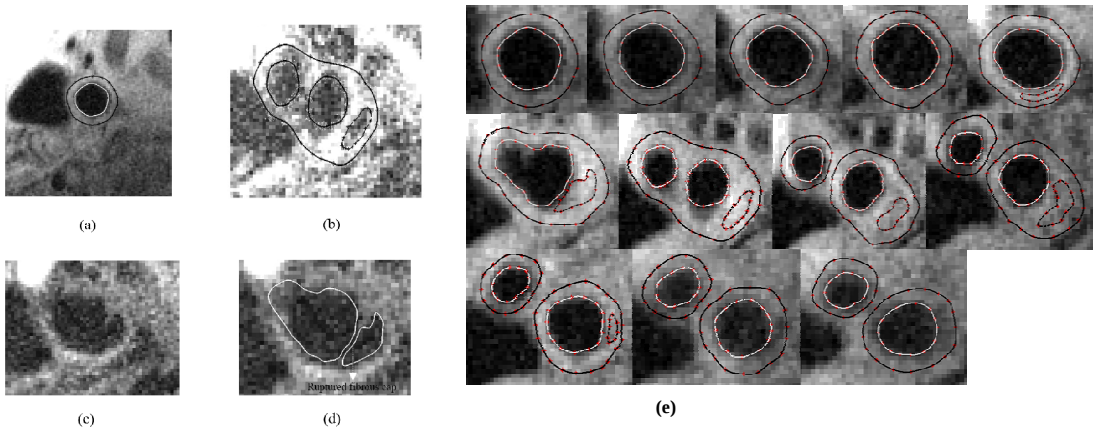

Figure 5.2 Segmentation results. (a) arterial wall segmentation with T1-weighted images, (b) lipid region segmentation with STIR images, (c) rupture site in the STIR image, (d)lipid and lumen segmentation in the rupture site, (e) the whole segmentation based on T1 weighted and STIR images, superimposed in the T1-weighted images.

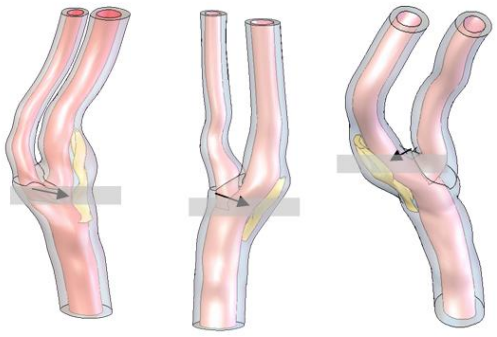

Figure 5.3 Geometry of the 3 subjects (TIA1, TIA2, TIA3), the rupture site is indicated by the arrow with gray brand. The length of each subject is 52mm.

The detailed description of material property and one way FSI procedure can be found in Chapter 3. In brief, the carotid arterial wall was assumed to be nonlinear, isotropic, and

incompressible with the 5-parameters Mooney-Rivlin model (Ansys^{TM}) being used to describe its material properties. The lipid core was assumed to be very soft with a 2kPa Young's Modulus and a 0.49 Poisson ratio. Computational nodes as the efferent plane of ICA and ECA were fixed in all directions, and an axial pre-stretch of 11% was applied at the afferent plane of CCA for the structure analysis. The structure model was meshed with an unstructured mesh consisting of nearly 90,000 10-node 3D tetra elements. The fluid domain was meshed in ICEM CFD11.0 with a much finer gird of 1 million 3D tetra cells. Blood was treated as an incompressible, Newtonian fluid with a viscosity of $4*10^{-3}$ $Pa.s$ and a density of $1{,}067 kg.m^{-3}$. The flow was assumed to be laminar; transient simulations were carried out with time-dependent pressure at the inlet of the CCA and mass flow rates at the ICA and ECA. The boundary conditions for the 3 subjects were assumed to be the same, and obtained from Chapter 3. One-way FSI coupling was used for stress analysis. The inner surface of the carotid arterial wall and the corresponding fluid boundary were defined as the fluid-structure interface.

5.3.2 Results

WSS results are shown in Figure 5.4 for the 3 subjects at systole phase of a cardiac cycle. Because of the minor lumen reduction in the plaque region, the luminal area reduction was around or less than 25% for the 3 subjects, WSS in the plaque region is not very high. To clearly demonstrate WSS in the plaque region, the fibrous cap surface at the luminal side was defined for each subject, just covering the lipid region. Then WSS is projected to the fibrous cap surface as shown in Figure 5.4 (a.2, b.2, c.2). The maximum WSS in the fibrous cap surface for the 3 subjects is less than 6 Pa. For all 3 subjects, the relatively high WSS regions can be found close to plaque throat.

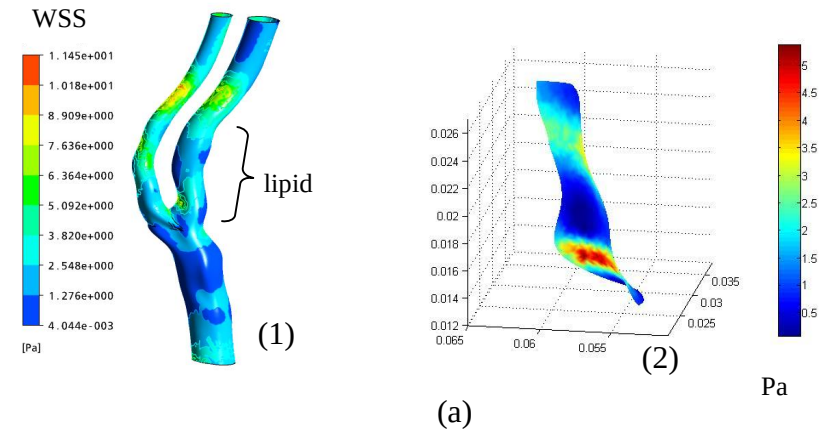

(a)

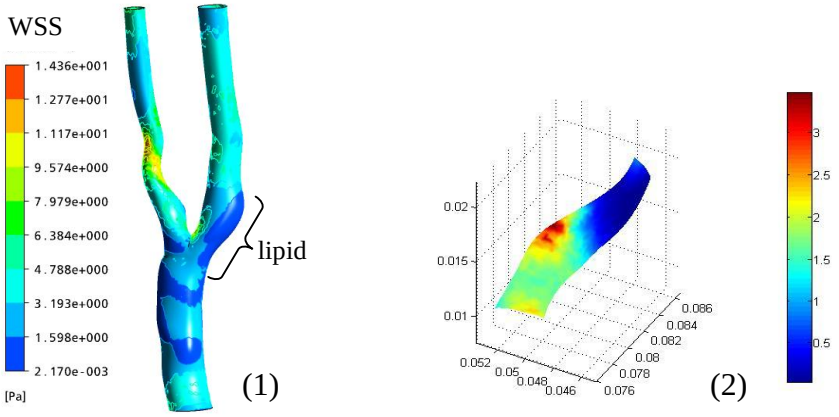

(b)

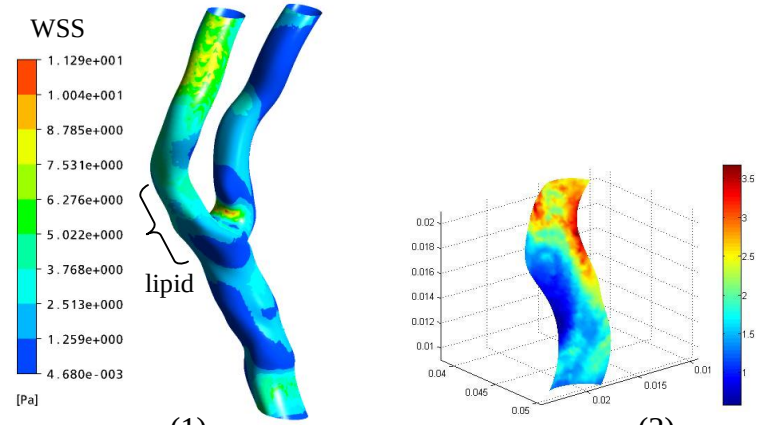

(c)

Figure 5.4 WSS distribution at peak systole for the 3 subjects

Wall tensile stress is believed to be an important factor to rupture the thin fibrous cap. First-principle stress (FPS), which is the highest stretching stress in the wall, was used

here to represent the wall stress distribution for the 3 subjects at the systolic cardiac phase. Figure 5.5(a.1) shows the stress results for TIA1. In general, FPS is higher in the plaque region, and much lower in the lipid region. A high FPS concentration region can be found in the fibrous cap, especially when the fibrous cap is thin. Figure 5.5(a.2) shows FPS distributions in cross-sections from CCA to ICA, covering the whole plaque region. Figure 5.5(a.3) shows FPS stress distributions in the lumen surface. The local maximum stress regions can be found in the plaque region, indicated by the arrows, which are around the rupture region of the plaque. The similar results can also be found in cases TIA2 and TIA3, the local stress concentrations can be found around the rupture sites.

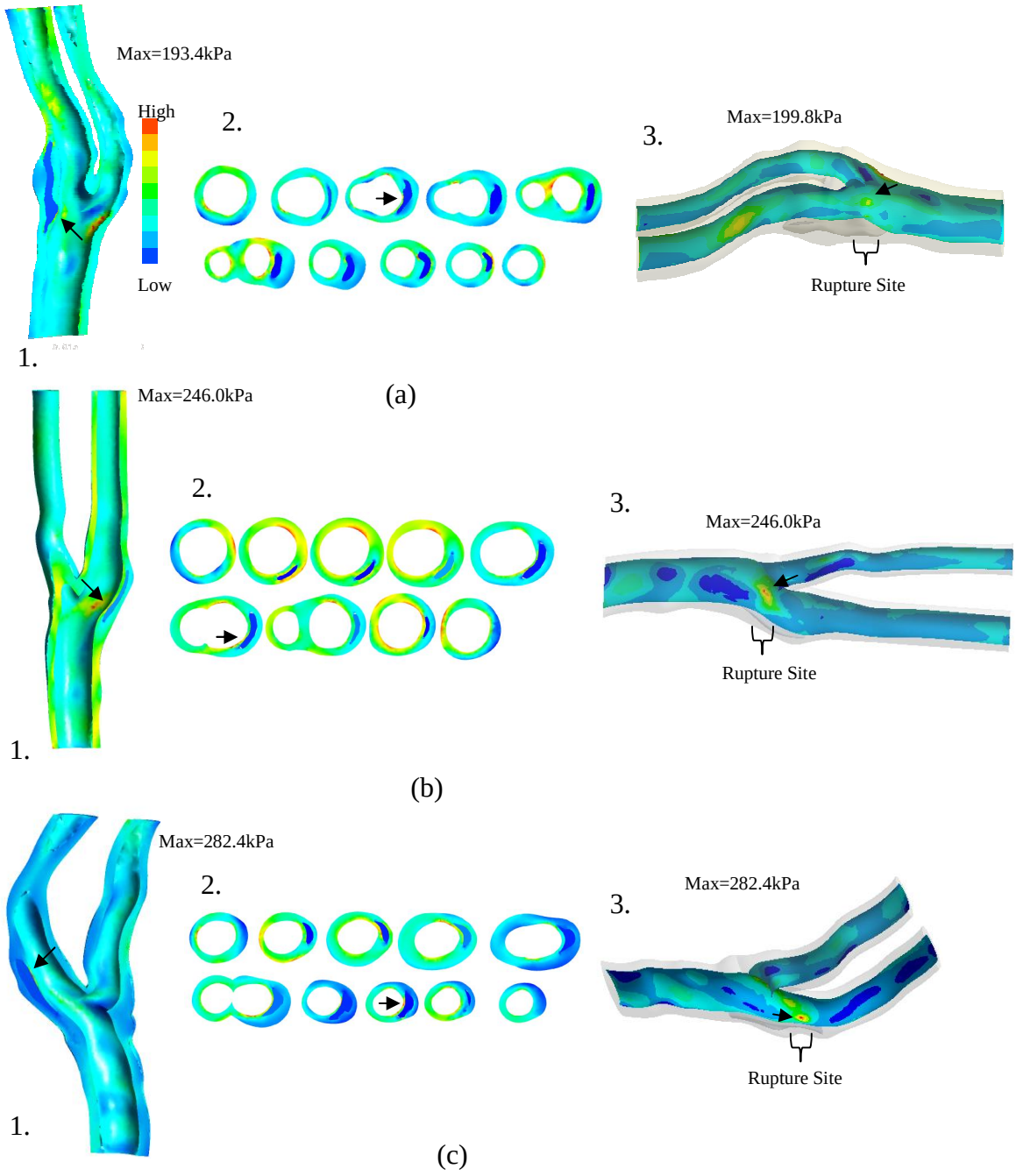

Figure 5.5 General stress distributions for TIA1, 2 and 3

5.4 Additional Simulation with Varied Fibrous Cap Geometry

5.4.1 Model Geometry Construction

Although STIR images can provide information of lipid region in rupture site, assumptions must be made on the thickness of fibrous cap in order to construct a pre-

rupture geometry. The baseline model constructed above is one of the possible configurations, which may not represent the real lipid pool and fibrous cap geometry. In order to study the impacts of the rupture site local geometry variation to the stress analysis, for each subject, a total of 6 models were created with varied fibrous cap and lipid pool sizes which can be divided into two groups. The difference between the groups is that the luminal size in the rupture plane is slightly larger in the group 2. In each group three models with an incremental fibrous cap thickness of half pixel in the rupture site. Therefore the models were BL_Fth (baseline), BL_Fth+ and BL_Fth++ for group 1, and SL_Fth, SL_Fth+, SL_Fth++ for group 2.

Group 1

(1) BL_Fth can be found in the previous section

(2) the same lumen segmentation as BL_Fth but with thicker fibrous cap in which half pixel thickness was added in the fibrous cap at lipid pool side, named BL_Fth+, showing in Figure 5.6(a.2)

(3) based on BL_Fth+ geometry, another half pixel thickness was added in fibrous cap at the lipid pool side, named BL_Fth++, showing in Figure 5.6(a.2)

Group 2

(4) The luminal area was enlarged by pushing fibrous cap towards lipid core region. The same criteria for the fibrous cap segmentation was applied as the baseline model, named SL_Fth, showing in Figure 5.6(b.1&2)

(5) Thicker fibrous cap than the SL_Fth, named SL_Fth+, showing in Figure 5.6(b.3). In these cases, a half pixel size thickness was added on the original fibrous cap from SL_Fth, at the lipid core side.

(6) based on SL_Fth+, the fibrous cap thickness was increased another half pixel at the lipid core side, named SL_Fth++, showing in Figure 5.6(b.3)

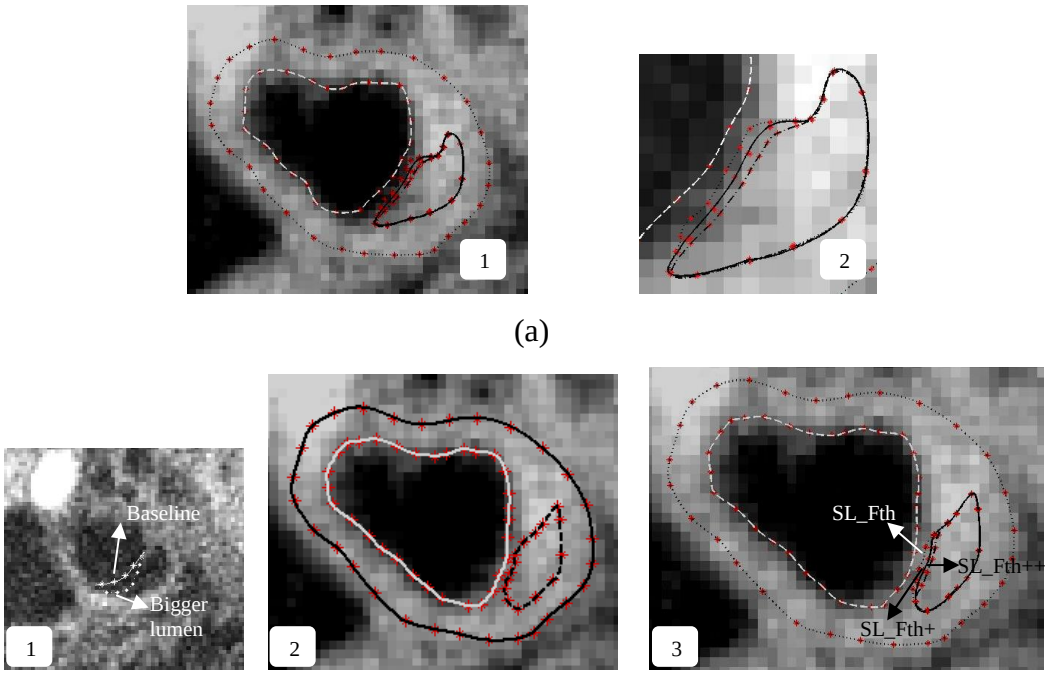

Figure 5.6 Models variation (a) Models(BL_Fth+ and BL_Fth++) with thicker fibrous cap based on BL_Fth, (b.1) bigger lumen region segmentation based on STIR image, (b.2) segmentation for SL_Fth, (b.3) Models(SL_Fth+ and SL_Fth++) with thicker fibrous cap based on SL_Fth

Because of the lumen region was changed in SL_Fth, SL_Fth+, SL_Fth++, the CFD study of blood flow was performed again for those models to provide the pressure loading for the corresponding structure stress analysis. The geometry change was limited to the rupture site, therefore the result in the blood flow domain only has minor change with similar distributions and levels in WSS and pressure. The fibrous cap thickness in order is BL_Fth < BL_Fth+ < BL_Fth++, and SL_Fth < SL_Fth+ < SL_Fth++.

5.4.2 Results

Figure 5.7 shows the wall tensile stress distributions in the fibrous cap surface of lumen side for 6 models of each subject. They are similar among the models with same group. The stress concentration regions can be easily identified for each model, and generally

located at the original rupture sites of the plaque, regardless the local geometry variations. Figure 5.8 shows the maximum FPS value in the fibrous cap surface corresponding to Figure 5.7. With increased fibrous cap thickness, the maximum FPS decreases for each group, the same trend can be found for the group 2 cases as well.

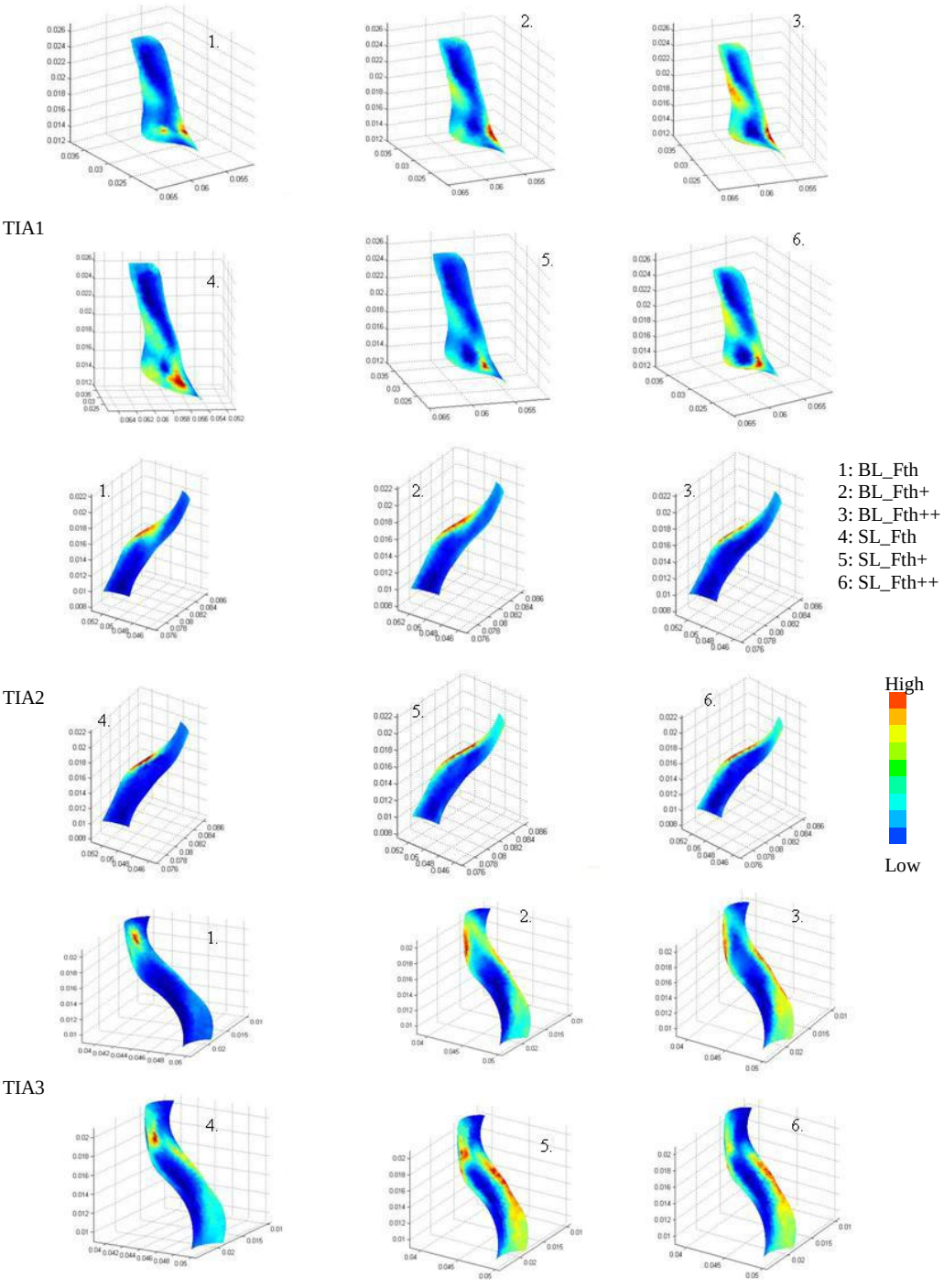

Figure 5.7 FPS distributions for 6 models of TIA1, 2 and 3

Different segmentations in the lumen region at rupture sites cause slightly different lipid pool size, it results different stress distribution and especially the stress level, which indicates the lipid pool size and shape also play an important role in the stability of the plaque rupture. With different fibrous cap thickness and lipid region configurations in the rupture region, the local maximum FPS concentration regions can be found close to or at the rupture site. The locations vary slightly from the middle of the fibrous cap to the shoulders of the fibrous cap. The stress distribution pattern will change between the models with a thinner fibrous cap and or a thicker one. For example in TIA3, for a thinner fibrous cap model (SL_Fth), the stress concentration region locates in the middle of fibrous cap, while for a thicker fibrous cap model (SL_Fth++) the stress concentration region mainly locates in the shoulder region (figure 5.7).

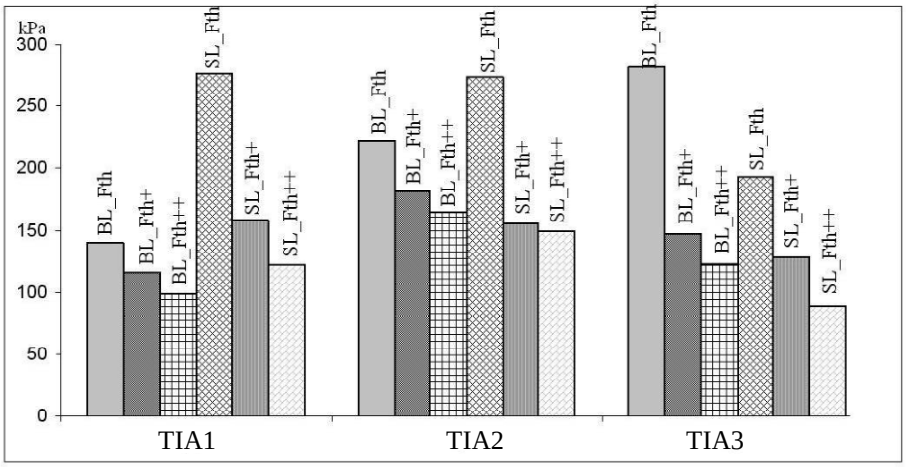

Figure 5.8 Maximum FPS in the fibrous cap surface

5.5 Discussion

5.5.1 Stress Related to Plaque Rupture

The usual reason for the transient ischemic attack is caused by small blood clot blocking some small blood vessels in the brain, and the clot mainly comes from the patches of atheroma in the main arteries, such as carotid artery, even from the heart chamber. TIA patients could provide the plaque morphologic information with the rupture site from which the blood clot is from. It is generally difficult to obtain plaque morphology information just before its rupture. However, MRI scan of the patient who suffered TIA recently can always be performed which will provide the critical plaque morphologic

information of the rupture sites. If the pre-rupture plaque geometry can be constructed, combining with the stress analysis, it will provide a possible way to study the plaque rupture with stress distribution retrospectively.

WSS was believed to play an important role in the plaque initiation and development; recently Groen (Groen et al., 2007) proposed that the high WSS in the fibrous cap could rupture the vulnerable plaque. From earlier studies (Piet et al., 1986), WSS with a level above 40Pa is able to cause structure change or even damage in the endothelial cells in the lumen side. However, in our study WSS is generally at low level ranges even in the fibrous cap region, with less than 6Pa for the 3 subjects. Although the direct link between the plaque rupture and high shear stress has not been established and is not supported from this study results, it is proposed that high WSS could induce thinning of the fibrous cap and unstablizing the plaque (Groen H.C et al., 2008).

Local extremely high wall stress value occurred around the rupture sites for the 3 subjects regardless the fibrous cap construction variations. When looking at individual plaques, stress concentration regions are locating at the proximal site for TIA1, circumferentially one at the plaque shoulder, the other at the middle of fibrous cap; In TIA2, the only stress concentration region locates mainly at the plaque shoulder (circumferentially) and in the middle part of the plaque (longitudinally); and in TIA3, the stress concentration region locates at the plaque shoulder (circumferentially) and in the distal part of the plaque (longitudinally). According to Shah's (Shah 2003) study, the major rupture risk regions are locating in the plaque shoulder, responsible for 60% of plaque rupture, while Lovett's(Lovett et al., 2003) result indicates that 16.9% of ruptures occur in the middle of the plaque in symptomatic patients. In this study, the high stress region in the shoulder can be found in TIA1 and TIA2 and in the middle of fibrous cap for TIA3. However without the structure information, it is hard to reach the conclusion where the exact plaque rupture site is.

5.5.2 Fully Coupled FSI vs One-way Coupled FSI

Based on the baseline model for TIA1, the fully coupled FSI was applied for plaque stress analysis to investigate the stress distribution pattern related to plaque rupture. Figure 5.9 shows stress distributions for the subject at peak systole from fully coupled FSI simulation. The general stress distribution contour is presented for the whole plaque in Figure 5.9(a). The FPS distribution on transversal planes through the plaque, starting from CCA, is shown in Figure 5.9(b1) from C1 to C11 with different legends on each panel. The maximum FPS value at each transversal plane along axial direction is shown in Figure 5.9(b2). Figure 5.9(c) shows FPS distribution in the luminal surface.

In general, the fully coupled FSI has similar FPS distribution as one-way coupled FSI as in Figure 5.5(a), but with slightly different stress levels. From the distributions at selected transversal planes, high FPS values may locate at the healthy side of the wall when the fibrous cap is thick (in C2 and C3). For the sections with a thin fibrous cap, the stress concentration regions appear at one or both edges of the lipid core (or plaque shoulders) as in C4 and C6. Longitudinally, one main peak of FPS can be found at proximal part of the plaque from C3 to C5 in Figure 5.9(b2). Two local stress concentrations could be found in the luminal surface of plaque region, just locating around the rupture site of the plaque, as shown in Figure 5.9(c).

The surface of the fibrous cap in the luminal side was extracted, and stress values were projected to that surface. The definition of the fibrous cap surface is presented in Figure 5.10(a), which covers the whole lipid region. Figure 5.10(b) shows more details of the distributions of maximum FPS within a cardiac cycle. From Figure 5.10(b), the stress distribution varies greatly in the fibrous cap surface, the stress level at upstream is much higher than downstream. Two stress concentration regions can be found, one is in the middle of the fibrous cap circumferentially (indicated by "A" in Figure 5.10(b)), and the other "B" is locating in the shoulder region of the fibrous cap. The high stress region was corresponding to the rupture site of the plaque, indicating the high stress can be responsible of plaque rupture. The findings from fully-coupled FSI was same as those from one-way coupled FSI, therefore one-way FSI was a good approximation for fully-

coupled FSI simulation when lots of simulations need to be done, which will save lots of computational time.

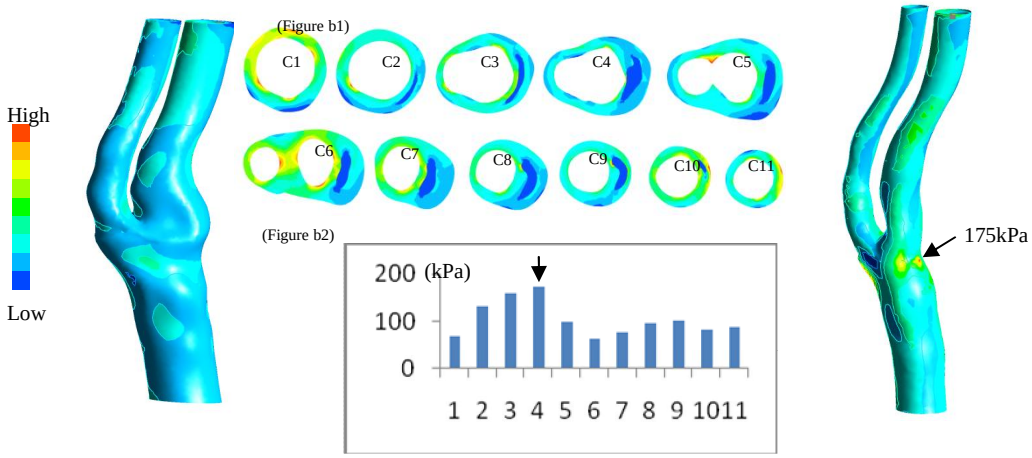

(a) (b) (c)

Figure 5.9 (a) general stress distribution for FPS; (b1) FPS stress distributions in the selected planes with different color scale at panels, (b2) maximum FPS on selected planes; (c) FPS distribution in the lumen surface. (Time: peak systole)

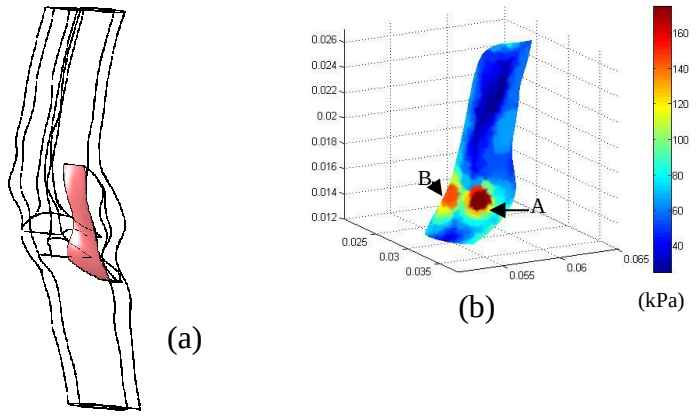

(a) (b)

Figure 5.10 Stress in fibrous cap surface. (a) the definition of fibrous cap surface in the lumen side; (b) maximum FPS distribution in the fibrous cap surface;

One of the main difficulties in the study is that the plaque geometry before TIA was unknown. In order to account for the possible plaque morphologies, 5 models for each subject were assumed, and the stress analysis on the 5 possible geometries shows that the

local stress concentration region could always be found around the rupture sites, no matter with a thicker fibrous cap, or a smaller lipid pool. Therefore based on this study it may indicate that the local wall tensile stress concentration in the fibrous cap could be a nice predictor for the plaque rupture. However the stress level changes significantly from a thin fibrous cap model to a model with a thicker fibrous cap.

5.6 Summary

In this chapter, one-way FSI was performed in the patients who had a TIA recently. The assumed pre-rupture plaque geometry was constructed based on the *in-vivo* plaque MR images. The stress analysis provides the stress distributions in the ruptured plaque region. Generally, the local maximal stress concentrations are found collocated with plaque rupture site. It is not influenced by the geometry variations in the rupture sites which were introduced artificially during model reconstruction. The good correlation between local maximal stress concentrations and plaque rupture site in the studied subjects could provide an evidence for the local maximal stress concentration hypothesis on plaque rupture.

Chapter 6 Applications (2)

STRESS ANALYSIS ON CAROTID ARTERY PATIENTS: A COMPARISON BETWEEN SYMPTOMATIC AND ASYMPTOMATIC PATIENTS

6.1 Introduction

From previous chapters 3, 4 and 5, it is demonstrated that stress analysis in plaques will provide critical information regarding plaque vulnerability, which can be helpful in clinic. In this chapter, the aim is to study the stress distributions among symptomatic and asymptomatic patients to investigate whether the stress level can be a possible predictor for plaque vulnerability, one of the main objectives of the PhD research project. If there are differences existing between symptomatic and asymptomatic patients, then it might be possible in the future that stress analysis procedure can be applied before the further treatment, and personalized care can be provided based on plaque stress levels.

20 carotid plaque models were reconstructed from *in-vivo* MR images, the fully coupled FSI simulation was performed on each subject, and followed a detailed stress analysis. Lastly, the stress results between the two groups were compared, including plaque morphological features, such as lipid core size, minimum fibrous cap thickness, and stenosis severity to provide insights into plaque rupture mechanism and clinical application.

6.2 Methods

6.2.1 MR Image Acquisition

Patient selection and image acquisition were performed by investigators who were not involved in the stress analysis. The protocol was approved by the local ethics committee, and written informed consent was obtained from each patient before the study. Informed written consent was gained from all patients before the study. *In-vivo* multi-spectral MRI scanning was performed on 20 nonconsecutive individuals (12 symptomatic and 8 asymptomatic) recruited from a specialist neurovascular clinic. The basic information regarding the two groups can be found in Table 6.1. The median time from symptoms to carotid endarterectomy in the symptomatic cohort was 12 weeks (range, 7 to 18 weeks).

All symptomatic subjects had recently experienced either a retinal or cortical transient ischemic attack and were scanned less than 6 months of the event. Asymptomatic patients had not experienced any symptom before imaging. MR imaging protocols can be found in Chapter 4.

Characteristic	Symptomatic	Asymptomatic
Number of Patients	12	8
Mean age	69±9 years	68±7 years
Female	4	0
Hypertension	8	7
Diabetes mellitus	2	2
PTCA/CABG	1	1
Peripheral vascular operations	1	0
Current smokers	3	3
Past smokers	6	5
Never smoked	3	1
Hypercholesterolemia	2	3
Cholesterol	4.2±1.02	4.0±0.9
Triglycerides	1.5±0.8	0.9±0.4
Statin Use	10	8
Antiplatelet agent	11	8

PTCA: Percutaneous Coronary Angioplasty

CABG: Coronary Artery Bypass Graft

Table 6.1 Information for symptomatic and asymptomatic patients

6.2.2 3D Plaque Geometry Reconstruction and FSI Simulation Set Up

An in-house program developed in Matlab was used to segment the regions of lipid core, arterial wall and lumen in the plaque, which have different signal characteristics when imaged by the multi-sequence protocol. The image segmentation and 3D reconstruction procedure can be found in Chapter 4.

The detailed description of material property and FSI procedure also can be found in Chapter 3 and 4. After the stress analysis, the maximum wall tensile stress in the plaque region was extracted for each subject in the two groups. A non-paired student t test was used to determine the significance of any differences in the maximum stress among plaques from symptomatic and asymptomatic patients.

6.3 Results

6.3.1 Stress Analysis

The first principle stress (FPS) was used to represent the WTS, the strongest stretching stress. Figure 6.1 shows an example of the stress distributions between symptomatic (column 1) and asymptomatic (column 2) subjects. Figure 6.1(a1, b1) shows the FPS distribution in the whole plaque with longitudinal cutting view. Generally FPS is higher at the luminal wall, lower at the outer arterial wall and lowest in the lipid region. The local high stress concentrations could be identified in the plaque region at both patients, indicated by arrows. The maximum FPS value is higher in the symptomatic patient than the asymptomatic subject. Figure 6.1(a2, b2) presents FPS distributions in the transversal planes covering the whole plaque region. For the sections with a thin fibrous cap, the stress concentration regions appear at one or both edges of the lipid core (or plaque shoulders).

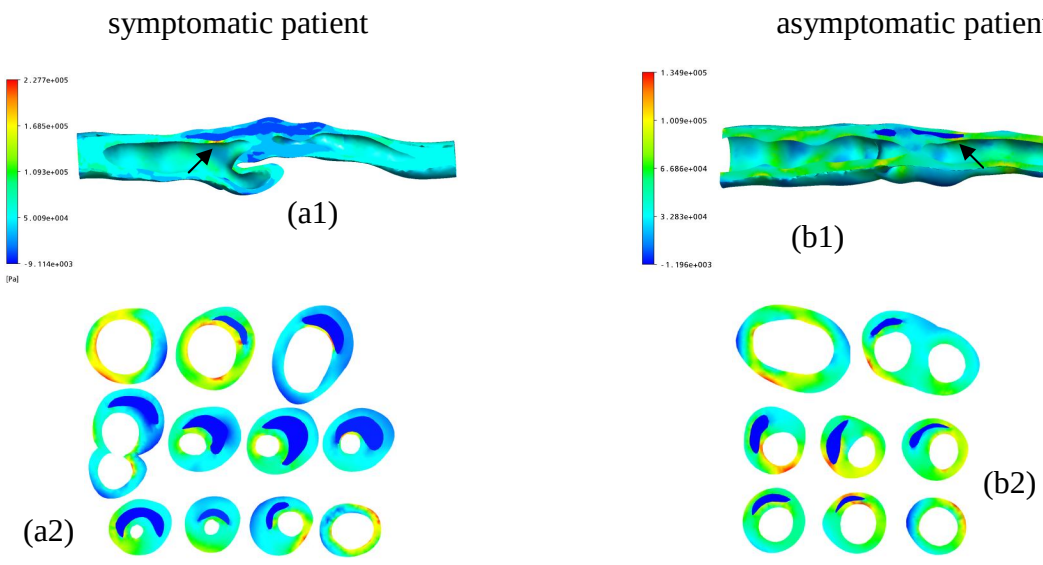

Figure 6.1 FPS distributions for one symptomatic patient (a) and one asymptomatic patient (b).

Stress distribution in the fibrous cap has been considered to be closely related to plaque rupture. The fibrous cap surface in the lumen side was extracted, covering the lipid core, to clearly show the stress distribution in the plaque region. The fibrous cap thickness (FCT), defined as the shortest distance between the fibrous cap surface (lumen side) and lipid region, is shown in Figure 6.2(a1, b1). Although MR image spatial resolution is 0.39mm, the 3D surface interpolation during model reconstruction can still produce fibrous cap regions with a thickness less than 0.39mm. The minimum FCT in the symptomatic subject is much smaller than the asymptomatic subjects (0.087mm Vs 0.177mm). Figure 6.2(a2, b2) shows corresponding FPS distributions in fibrous cap surfaces. Generally, the high stress regions are well correlated with the thin fibrous cap regions, especially for the asymptomatic patient, the high stress region upstream is corresponding to a very thin fibrous cap location. While in symptomatic patient, the highest stress region does not locate in the thinnest fibrous cap region (downstream plaque), this may be resulted in part from the blood pressure drop at downstream plaque.

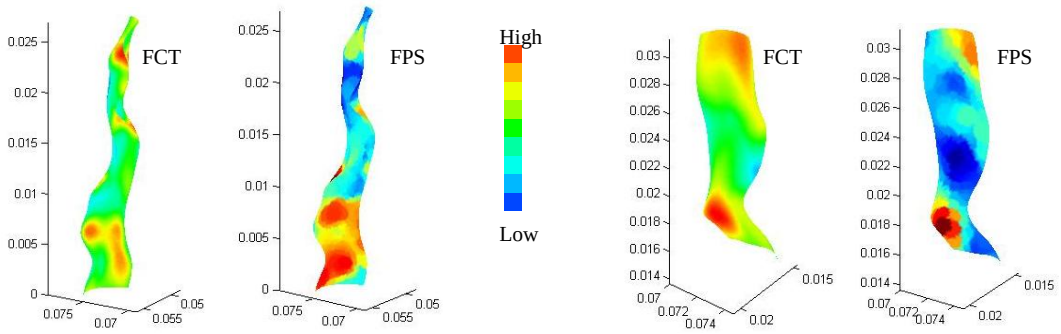

(a1) (a2) (b1) (b2)

Figure 6.2 FCT and FPS distributions for symptomatic(a) and asymptomatic(b) patients, same patients as Figure 6.1

6.3.2 Statistical Analysis

FSI simulation was performed on all 20 plaques; the maximum FPS in one cardiac cycle at the fibrous cap surface was extracted. Table 6.2 summarized the comparison between the asymptomatic group and symptomatic group, including lipid core size, stenosis degree, minimum FCT and maximum FPS. The symptomatic group usually has a thinner fibrous cap (mean value of 0.2±0.1mm) and large lipid core (mean value of 139±80mm^3);

the stress is much higher than that in the asymptomatic group (199±45kPa VS 122±42kPa). However stenosis degree between the two groups has similar level.

	Lipid size (mm^3)	Stenosis (0-1)	Min fThk (mm)	Max FPS (kPa)
Asymptomatic	78±77	0.47±0.2	0.37±0.25	122±42
Symptomatic	139±80	0.4±0.27	0.20±0.1	199±45

Table 6.2 the comparison between the asymptomatic group and symptomatic group

Parametric statistical analysis was undertaken using a non-paired t test (Matlab 7.0) and considered at the 5% significance level. The maximum stresses in the plaques of symptomatic patients were significantly higher than those of asymptomatic patients (199±45 VS 122±42 kPa, P=0.002). Figure 6.3 shows the box and whisker plot of median peak stress (red bar), interquartile ranges (whiskers) in the two groups. The median peak FPS in the symptomatic group is 187kPa, much higher than that in asymptomatic group, 129kPa. However there is no significant difference for the severity of stenosis, defined as the lumen area reduction between symptomatic (0.4±0.27) and asymptomatic groups (0.47±0.2), indicating stenosis severity is not a good predictor for the plaque vulnerability. There is difference in the minimum fibrous cap thickness (0.20 vs 0.37mm, P=0.052), and actual lipid size (139 vs 78mm^3, P=0.1) between the symptomatic and asymptomatic groups.

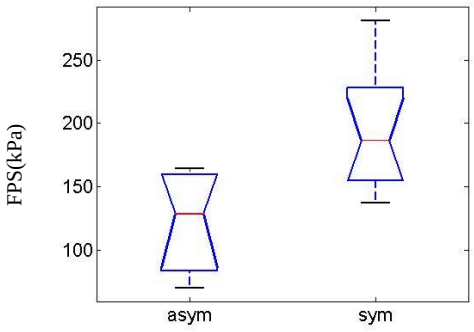

Figure 6.3 the box and whisker plot of median peak stress

The local stress concentration in the fibrous cap can occur upstream of the plaque or downstream, at shoulder region or beyond the shoulder region, as shown in Figure 6.4.

The stress distributions for all 20 plaques were extracted after the stress analysis. 10 subjects were found to have main local maximum stress concentrations upstream of the plaque, named G1; the other 10 cases with the stress concentration mainly locate downstream or in the middle longitudinally, named G2. The averaged stenosis degree for G1 is 51±27%, higher than the average value for G2, 36±20%. Although there is no significant difference in stenosis degree between the two group, 6 out of 7 plaques with high stenosis degree (>60%) have stress concentration regions upstream of the plaque. It indicates that critical stress condition is more likely to happen in the proximal part of the plaque for a plaque with high stenosis degree. It can be partially explained by the greater post-stenosis pressure drop in high stenosis plaques. The local maximum stress concentration in the plaque shoulders can be found in 17 out of 20 plaques, which is 85% in the studied subjects.

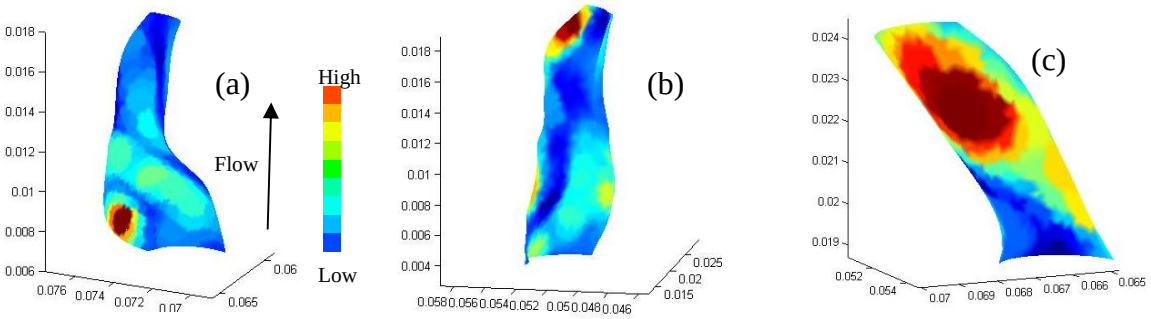

Figure 6.4 local maximum stress concentrations in fibrous cap surface in the luminal side, (a) upstream; (b) downstream; (c) middle

The maximum VWTS and maximum Von Mises Strain (VMStrain) in the fibrous cap during the whole cardiac cycle also were obtained for the groups of subjects. The average value of maximum VWTS is 184±43kPa for symptomatic group, 117±32kPa for asymptomatic group; the average value of VMstrain is 0.26±0.03 for symptomatic group, and 0.2±0.03 for asymptomatic group. Parametric statistical analysis showed that both max VWTS and VMStrain are significantly different for the two groups with $p<0.05$. The linear correlation analysis among different stress factors (FPS, VWTS, and VMStrain) showed that they are highly correlated with each other, shown in Figure 6.5. Therefore either FPS or VWTS can be used for the extreme stress representation in plaques, which also can represent the strain distributions.

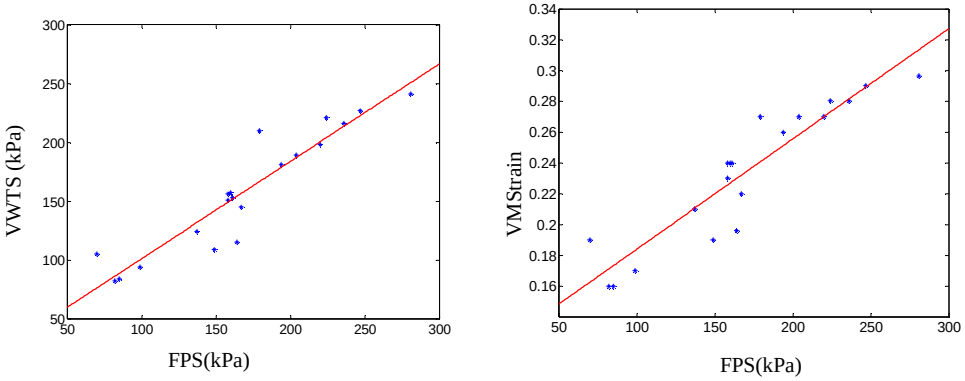

Figure 6.5 Correlation among VWTS, FPS and VMstrain in the fibrous cap

6.4 Discussion and Conclusion

6.4.1 Stress Comparison between Symptomatic and Asymptomatic Groups

In this Chapter, 20 plaque models were reconstructed from *in-vivo* carotid MRI for the comparison of symptomatic and asymptomatic patients. From the comparison of the two groups, our 3D stress analysis confirmed the conclusion that the maximum stress in the symptomatic group is much higher than the asymptomatic group (199±45 VS 122±42 kPa, P=0.002). According to Li's study (Li et al., 2007), which was based on 2D *in-vivo* MRI, the stress in asymptomatic patients is lower than that in symptomatic patients (269.6±107.9kPa vs 508.2±193.1, p=0.004). However in Li's study, 2D stress model may not accurately predict the stress in the plaque region, and also the pressure loading was not realistic which did not consider the pressure drop in the plaque region.

6.4.2 Morphological Features VS Plaque Stability

Fibrous cap thickness A vulnerable plaque usually is associated with a thinner fibrous cap and a large lipid region (Richardson, et al., 2002). The comparison between the two groups in minimum fibrous cap thickness and actual lipid core size shows that symptomatic patients had a thinner fibrous cap thickness and larger lipid core size than asymptomatic patients. Fibrous cap thickness is a very critical morphological feature associated with plaque rupture. A very thin fibrous cap usually indicates a more vulnerable plaque. The correlation analysis is showed in Figure 6.6 between fibrous cap thickness and maximum wall tensile stress, in which minimum fibrous cap is negatively related to the stress conditions. According to Burke's (Burk et al., 1997) study on 133

men coronary plaque, a cap thickness of 65μm was defined as a critical value of instability. However, the critical cap thickness of coronary plaque can not directly be applied to the carotid plaque. Redgrave (Redgrave et al., 2008) studied the critical cap thickness and rupture in symptomatic carotid plaques, suggesting that the optimum cut-offs for discriminating between ruptured and non-ruptured plaques were a minimum cap thickness<200μm. In the study, the mean minimum cap thickness for symptomatic group is around 200μm, in the same range as Redgrave's study, indicating a carotid plaque with a thin fibrous cap less than 200μm is more prone to rupture, the value is larger than the critical value in the coronary plaque (65μm). Although a thin fibrous cap usually associates with a high stress level in the plaque region, the thin fibrous cap does not always induce extreme stress condition to rupture the plaque from this study. It suggests that thin fibrous cap is only one of the factors which will contribute the plaque rupture.

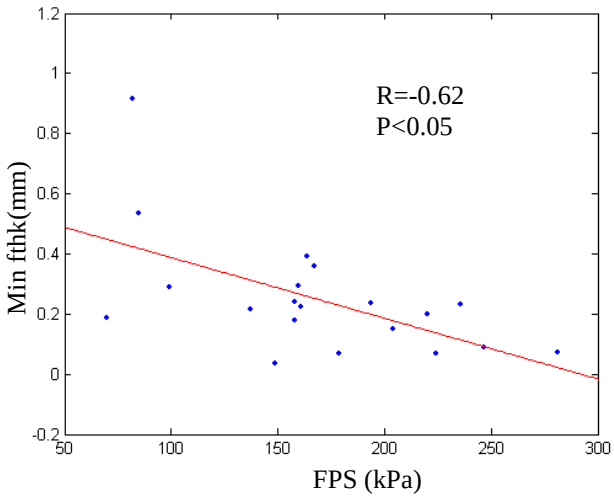

Figure 6.6 the correlation between minimum fibrous cap thickness and maximum WTS

Lipid core size Lipid core size is also considered to be an important factor influencing the stability of plaque. Studies have shown that lipid rich plaques are more likely to rupture and cause myocardial infarction than lipid poor lesions (Richardson 1989; Davis 1990). Until now, there is no clear indication of the threshold value for lipid core size above which the plaque will become unstable, as for the cases of fibrous cap thickness, 65μm is the critical value for coronary plaques. From a 2D study, Ohayon (Ohayon et al., 2008) suggested that plaque instability is to be viewed as a consequence of the

combination of fibrous cap thickness, lipid core thickness and remodeling index, and the lipid core thickness is more important than its area in determining plaque stability. When we consider the lipid core in 3D context, it is expected that the morphological feature is much harder to be represented. It includes the volume, the shape occupied by lipids, interface smoothness between fibrous tissue and lipids, lipid core depths, and so on. Therefore only lipid core volume is compared between the two groups. The soft characteristic of lipid will cause extreme stress concentrations in plaque shoulder region, a frequent location of plaque rupture. Although there is no significant difference in actual lipid size between the two groups in the study, symptomatic group usually has a larger lipid core than asymptomatic group (139 vs 78mm^3, P=0.1). The correlation analysis is showed in Figure 6.7. A general trend can be found that the larger the lipid core, the greater the resulted plaque stress.

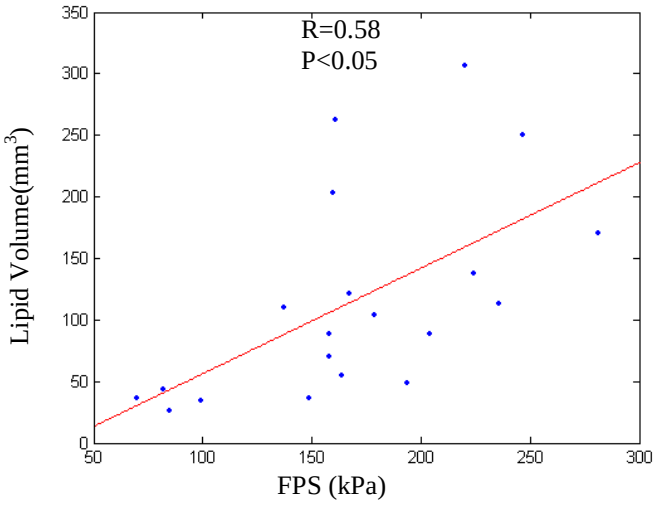

Figure 6.7 correlation analysis between lipid volume and maximum FPS

Luminal stenosis degree Luminal stenosis has been used as the traditional clinical measure of the plaque rupture risk, which is based on the fact that an increased degree of stenosis indicates a higher plaque burden. However, research has also shown that a large number of ruptured coronary plaques are in vessels less than 70% stenosed (Casscells et al., 2003). In the present study, the results show that a plaque with a minor luminal area reduction can still induce critically high stress on the fibrous cap. The stenosis severity between symptomatic and asymptomatic patients lies in the same level. Therefore plaque

rupture risk assessment based only on the degree of stenosis may lead to underestimate the rupture risk of some plaques with lower degree of stenosis.

Local stress concentration distributions in fibrous cap surface Generally, the extremely high stress value occurred at the thinnest fibrous cap thickness among the subjects. When looking at individual plaques, stress concentration regions are confined to the thinner fibrous cap regions, with high stress values located at the shoulder regions. These are the major rupture risk regions responsible for 60% of plaque ruptures (Shah et al., 2003). In this study, 85% of patients had main stress concentration in the plaque shoulder region. Due to lack of plaque rupture information, the correlation between extreme stress condition and plaque rupture locations were not known for all patients. On the other hand, during the long development period of a plaque, with constant remodeling, a constantly high stress region in the fibrous cap may be associated with a strengthened collagen structure. As a result, rupture critical stress would be increased in the region. It may partially explain the fact that not all plaque ruptures occur at the shoulder regions. In the study, the local stress concentration locations were studied for all subjects, suggesting the plaques associated with a higher stenosis degree usually have extreme stress concentrations upstream. If a degree of stenosis 60% is set as a critical value, then 86% of those plaques in the study have local maximum stress concentrations upstream. Therefore, a plaque with high stenosis degree, such as greater than 60%, the upstream of the plaque may be more vulnerable to rupture, since the extreme stress conditions are more likely to happen at that region.

Other Concerns in Plaque Stress Analysis

6.5 Residual Stress Effects on Plaque Stress

Residual stress is the stress existing within a body in the absence of external loadings. It is well known that residual stresses are present in a variety of biological tissues, such as the arteries (Chuong et al., 1986). In normal vessels, the residual stress/strain tends to make stress distribution more uniform throughout normal arterial wall (Guo et al., 2005). Although the residual stresses have been well acknowledged for the normal function of arterial wall, the effects caused by residual stress in plaque stress distribution have not been well studied. Williamson (Williamson et al., 2003) firstly introduced residual strain in their plaque stress computation study. It was found that the introduce of residual strain could produce a model with smaller radial stress gradients at normal arterial pressure, and the changes of stresses are much smaller between simulations with and without residual strain. Ohayon (Ohayon et al., 2007) studied the residual stress/strain distribution on human coronary plaques by using an 'Open-Close' procedure. They found that if the stress computation without residual stress/strain, the peak stress may still locate in the same locations as the case with the residual stress, even under normal physiological loading. The stress level may be over-estimated by around 4 times compared with stress prediction with residual stress. Therefore the stability of vulnerable plaques is needed to be viewed as the result of a balance between intra-plaque residual stress and external loading. The above results obtained from Williamson (Williamson et al., 2003) and Ohayon (Ohayon et al., 2007) are controversial regarding the residual stress effects on plaque vulnerability, therefore the residual stress in carotid plaques and the effects on plaque stress distributions will be studied in this section.

6.5.1 Plaque Sample Preparation and FEM Analysis

A specimen of the diseased carotid arterial plaque with a longitudinal cut was obtained in carotid endarectomy (CEA) from a local hospital. A General Electric Logic 9 Ultrasound (US) system was used to scan the specimen, which was immersed in a water tank at room temperature. A 5-10 MHz linear transducer was selected for optimum penetration and resolution. Images were saved in a format that 4D view^{TM} can be used to derive 2D slices from the 3D data set. From the 3D US image of the cut specimen (Figure 6.8), it was

clearly seen that the open angle changed significantly throughout the specimen. It is started with a small angle in the common carotid artery (CCA) and became larger in the bifurcation region and getting smaller when approaching the internal carotid artery plaque region. As known from previous studies, open angle values were generally related to the magnitude of residual stress in arterial wall. The longitudinal non uniformity of the open angle may be related to different plaque components, such as lipid region and calcification which lead to a non-uniformity of arterial wall mechanical properties and wall thickness.

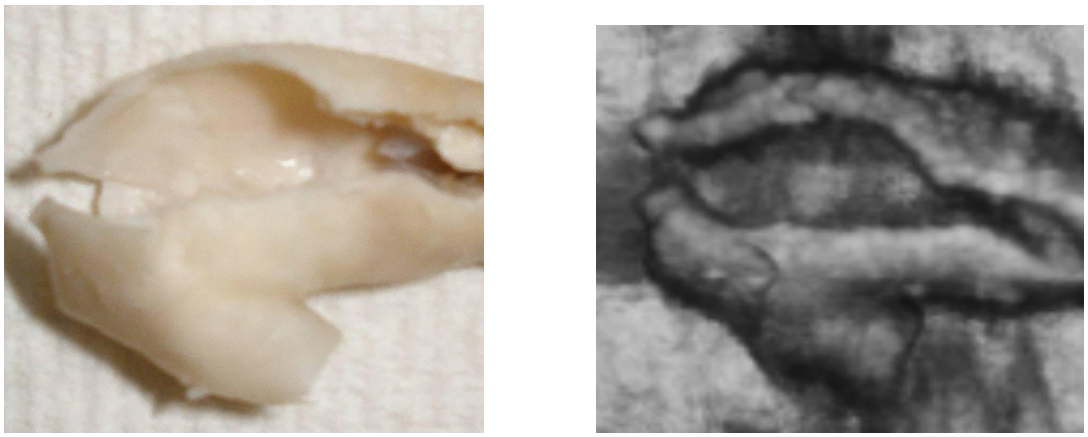

Figure 6.8 (a) CEA sample; (b) CEA sample under US scan

A conventional histology analysis was applied to the plaque sample for revealing plaque components. Tissue marking dye was applied on the outer wall of the specimen to provide the circumferential relationship of the histology sections, while landmarks on the axial direction, such as bifurcation apex, were used to provide axial information of the sections compared with US images. The specimen was subject to a conventional paraffin wax histology process and sliced sequentially into 7 μm sections in 250 μm intervals along the axial direction. Sections were stained using Picrosiris Red and Hematoxylin to reveal the collagen content and general structure of the plaque. Corresponding 2D US transversal images of the plaque were obtained from the 3D scan data set by 4D VIEW^{TM}.

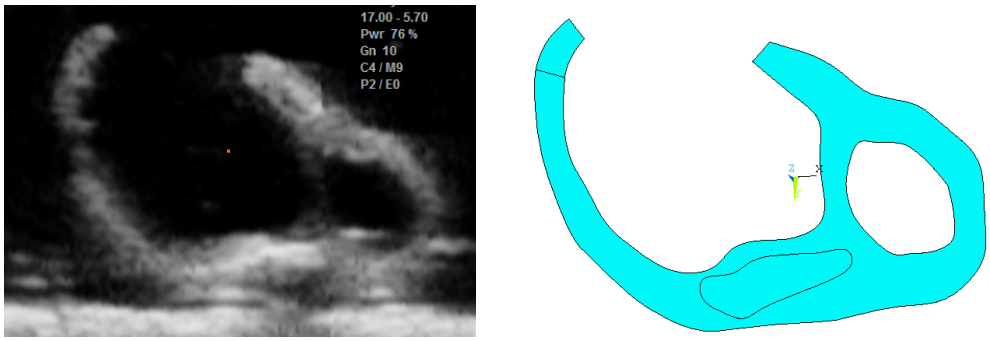

Figure 6.9 (a) Ultrasound image with cross sectional view, (b) reconstructed 2D plaque slice

The 2D images from US and corresponding histological analysis were segmented with an in-house software coded with Matlab to generate region contours including arterial outer wall, luminal wall and lipid region. The boundary information was imported into ANSYS 11.0 to generate arterial wall, lipid region, as shown in Figure 6.9(b). The simulation was divided into two steps: (1) closing procedure: by pushing the open boundaries in arterial wall together, the residual stress/strain in the plaque will be obtained. With the absence of blood pressure, this step corresponds to the unloaded physiological configuration, in which the residual stresses and strains are present. (2) Physiological loading: a normal physiological loading of 110mmHg will be applied to the luminal surface with the closed plaque sample. The material properties for arterial wall can be found in Chapter 4, that is hyper-elastic, homogeneous, with a much softer lipid region, here a Young's Modulus of 10000Pa was chosen with 0.49 for Poisson ratio. The finite element model was solved under the assumption of plane and finite strains.

6.5.2 Results

Figure 6.10 shows the residual stress distribution for the plaque by pushing the open boundaries back. Figure 6.10(a) shows the first principle stress, the stretching force. The outer layer of arterial wall experiences a much higher stretching force than the inner layer, with a maximum value of 28kPa. The inner layer experiences a much higher compression stress than the outer layer; the maximum compression stress is locating in the thinner fibrous cap, with a value of 47.5kPa, shown in Figure 6.10(b). For this plaque sample, the

fibrous cap is subject to compressive stresses and strains; the lipid is subject to neither high compressive stress nor high stretching stress.

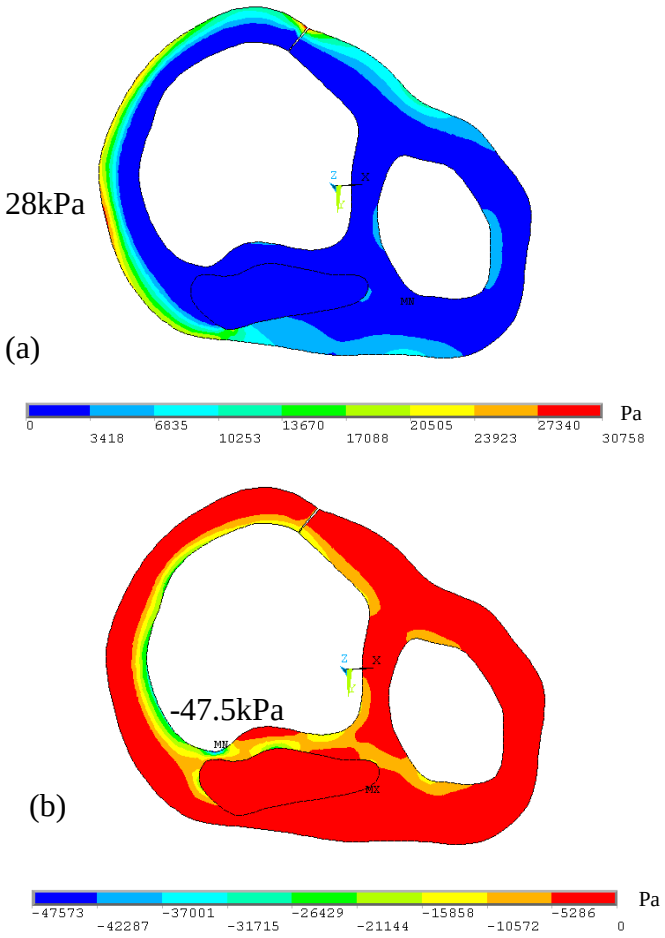

Figure 6.10 Residual stress distributions, (a): First principle stress distribution (stretching); (b): Third principle stress distribution (compression).

Figure 6.11 shows the first principle(a) and third principle stress(b) distributions in the plaque region under the physiological pressure loading of 110mmHg. The compressed inner layer has been stretched greatly under the pressure loading, shown in Figure 6.11(a), a local high stress region could be found in the thinner fibrous cap region, indicated by the arrow. The stress distribution has similar pattern as the existed literatures about stress analysis with 2D plaque samples (Cheng et al., 1993; Finet et al., 2004).

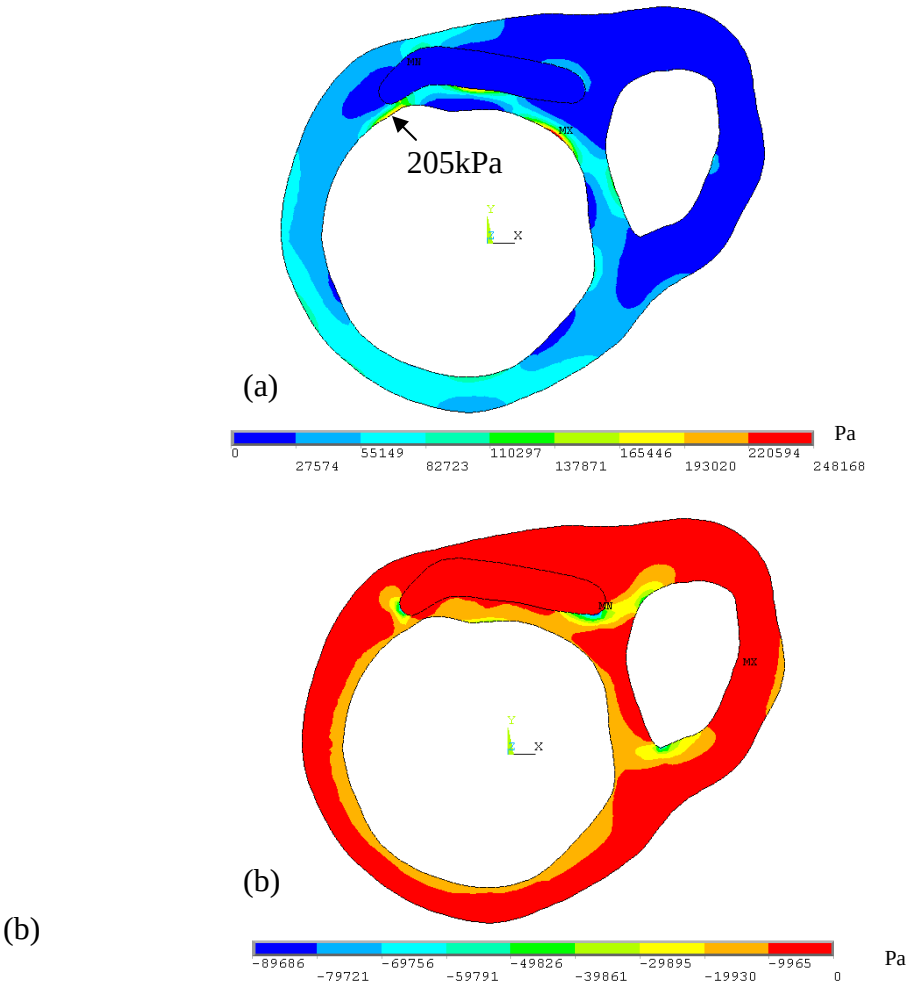

(b)

Figure 6.11 Stress distributions with residual stress/strain.

(a) First principle stress; (b) Third principle stress

Figure 6.12 shows the stress distribution without residual stress/strain during the simulation. The comparison (the first principle stress) between the simulations with and without residual stress/strain shows that the stress patterns for both simulations are similar. A local higher stress concentration can be found in the thin fibrous cap region, and stress in the lipid region is much lower. However the stress level shows certain difference between the two simulations, the local maximum fibrous cap stress without residual stress/strain is slightly higher than that with residual stress/strain(221kPa VS 205kPa). Therefore the residual stress/stain tends to lower the stress levels in the inner layer, however the absolute stress levels do not change significantly between the simulations with and without residual stress/strain with a less than 10% difference. Figure

6.13 shows the residual stress analysis on another section, similar results can be found as the previous simulation.

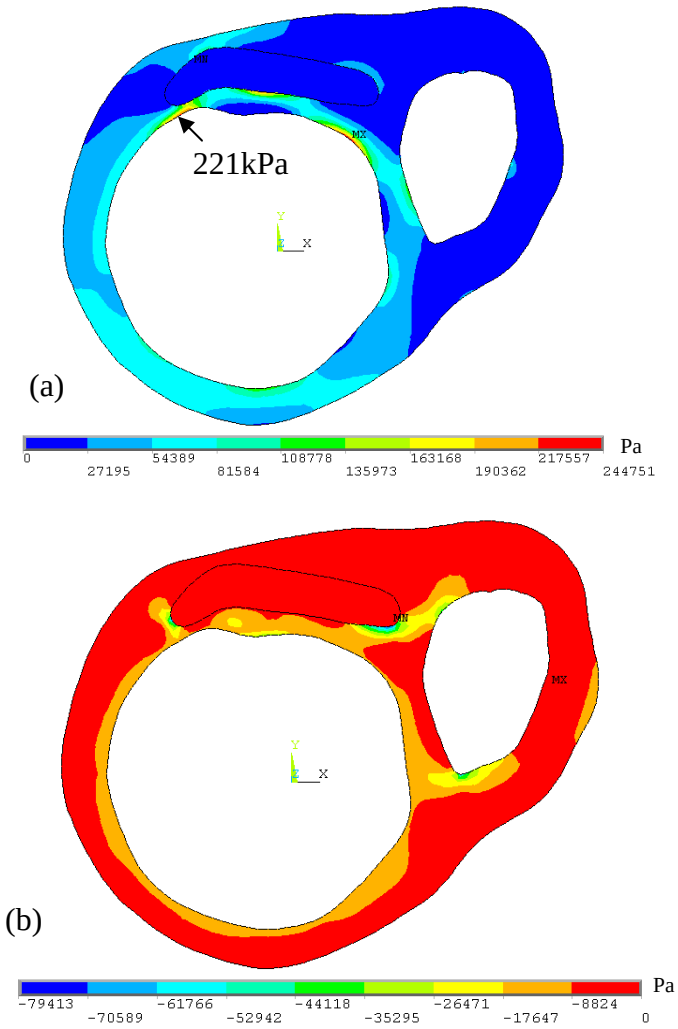

Figure 6.12 Stress distributions without residual stress/strain. (a) First principle stress; (b) Third principle stress

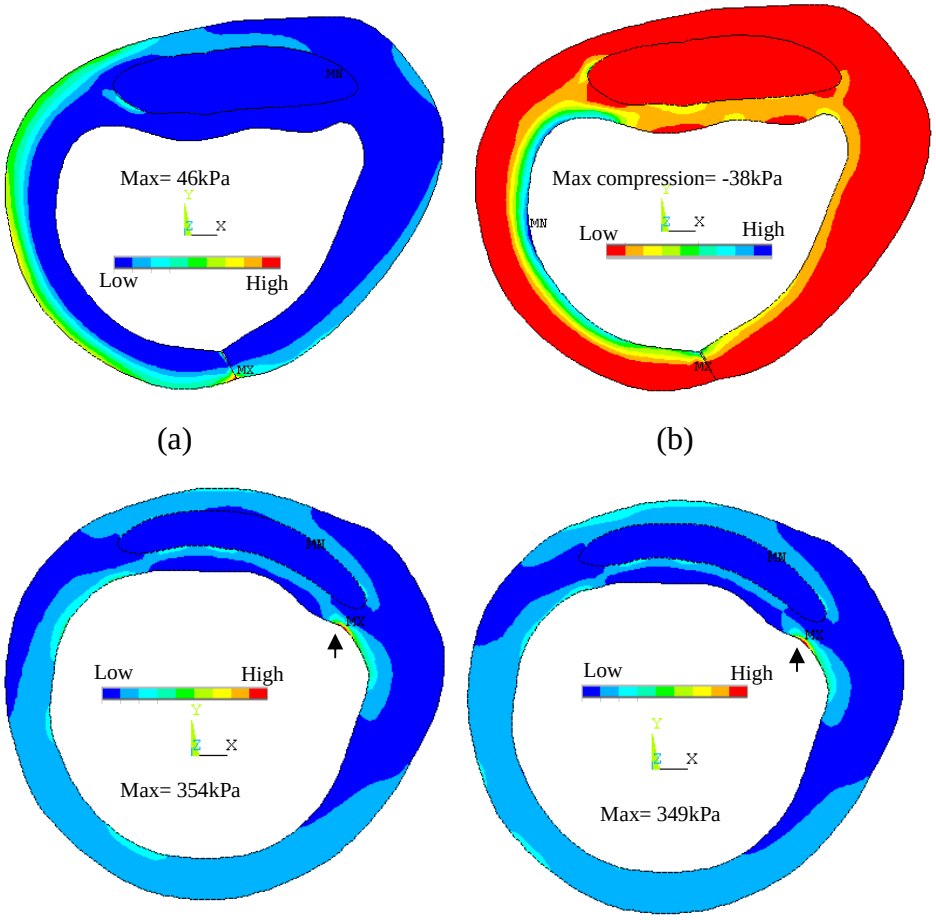

Figure 6.13 residual stress distribution on another plaque model. (a) the first principle stress distribution without pressure loading; (b) the third principle stress distribution without pressure loading; (c) the first principle stress distribution without considering residual stress under pressure loading; (d) the first principle stress distribution with residual stress under pressure loading.

6.5.3 Discussion and Conclusion on Residual Stress Study

One of important issues in plaque stress analysis is to calculate the stress pattern and levels in the plaque region accurately with mimic loading as *in-vivo*. Here we combined the experimental and computational approaches together to investigate the residual stress patterns and their effects on the finial stress levels.

In order to obtain the residual stress information, the opening angle technique was used to release the existed residual stress in the carotid plaque sample, which has been widely used for approximating the stress-free state of arterial walls (Fung YC, 1993). Usually by closing the stress-free arterial wall, the inner layer will be compressed, and outer layer will be stretched. When pressurizing the closed artery, the compression in the inner layer will be released. Therefore the residual stress in the inner layer of arterial wall tempts to minimize the stress/strain level under physiological pressure loading. For carotid plaques, due to the multi-components nature which include soft lipid pools, stiff calcifications, and the bifurcation geometry, the residual stress can be more complex than that in a normal straight artery. In this study, the open configuration of carotid plaque was assessed by the cutting in the healthy part of the artery, the resultant open geometry was assumed to be free of stress. Since the carotid plaque in axial direction still kept intact, the residual stress/strain may not be released totally, therefore the open angle might be under-estimated. It would be expected a proper sectioning technique would generate more realistic results for residual stress/strain patterns.

The local maximum stress distributions in plaque region with/without residual stress do not show significant difference, always can be found in the thinner fibrous cap region. It may be overestimated slightly by the exclusion of residual stress effects. However the absolute stress levels are not influenced significantly by the incorporation of residual stress, same as the findings by Williamson (Williamson et al., 2003). While from Ohayon's (Ohayon et al., 2007) study, the stress can be overestimated by 4 times, which significantly affects the stress level in plaque region when residual stress is included. The different findings may partially because of thinner fibrous cap in their study, which was 89.40±14.69μm, and greater opening angles. In this study, the thinnest fibrous cap thickness is around 200 μm, and open angle is around 30 degree. Those different results may suggest that the effects of residual stress/strain to the plaque stress can be more complex than we originally thought. It will be influenced by plaque morphology features, components, etc. If the lipid region was replaced by the calcification, the residual stress/strain patterns were much different from the plaques with soft lipid regions. The

interface between calcification and surrounding tissues experienced a much higher level residual stress/stain due to the great stiffness difference.

In summary, FEM simulations were performed on an atherosclerotic plaque to assess circumferential residual stress distribution variations in the plaque based on open angles measured from 3D ultrasound image. It was found that the residual stress is more uniform along circumferential direction in healthy part of the artery. The fibrous cap was compressed much more with the presences of soft lipid regions. The influence of the residual stress to the final stress distribution under physiological blood pressure load was minor. If the stress pattern is the concern, then the inclusion of residual stress will not make any difference, while if the quantity of maximum stress value of the parameter to be obtained, an inclusion of residual stress may lead to a 10% decrease of the absolute stress value from this study. Therefore the inclusion of residual stress in plaque stress prediction will depend on the application and accuracy requirement.

6.6 Relationship between Curvedness of Fibrous Cap Surface and Plaque Stress

Studies of the coronary and carotid arteries demonstrated that plaques with irregular surfaces are more prone to cause cardiac infarction and stroke (Ledru et al., 1999). A local high curved surface will induce a much higher stress under pressure loadings based on the mechanical analysis principle. Li (Li et al., 2008) studied 2D finite element plaque models from 20 symptomatic and 20 asymptomatic patients, found that lumen curvature was one of the main determinants of plaque stress, and was significant different between symptomatic and asymptomatic patients. However fibrous cap surface is in 3D context. The curvature analysis based on 2D sections can not represent the curvedness of a 3D surface. The 3D curvedness should be defined and studied, and its effects and correlation with local stress distribution may yield useful information in plaque rupture risk assessment.

6.6.1 Methodology

The mesh in fibrous cap surface of the luminal side was extracted for curvature computation. In order to obtain the curvatures at a given point in one mesh, a local surface fitting step was applied to the given point and its surrounding points (Mcivor et al., 1996). For a give point ***p(x,y,z)***, the surface around ***p*** can be approximated by a quadratic polynomial function with parameter ***du*** and ***dv***, which can be considered as a Taylor expansion at the point ***p*** by omitting the higher terms.

$$p(u+du, v+dv) = p_{00} + p_u du + p_v dv + (p_{uu} du^2 + 2 p_{uv} du dv + p_{vv} dv^2)/2 \qquad [6.1]$$

p_{00}, p_u, p_v, p_{uu}, p_{uv} and p_{vv} are the zero, first and second derivatives with respect to u and v, (u, v) are the basic parameters of the fitted surface. For the considered surface patch, the original point (0, 0, 0) will be moved to the given point p, that is $x' = x - x_0$, $y' = y - y_0$ and $z' = z - z_0$. The second-order polynomial form

$$z' = c_1 + c_2 x' + c_3 y' + c_4 x'^2 + c_5 x' y' + c_6 y'^2 \qquad [6.2]$$

was used to fit the surrounding surface of the given point p. The six coefficients of equation 6.2 are obtained by least-squares solution of an overestimated system of linear equations. Therefore at least 6 surrounding points are needed for the fitting process. For such a quadric, the surface normal at p is given by

$$n(p_0) = \frac{1}{(1+c_2^2+c_3^2)^{0.5}} \begin{bmatrix} -c_2 \\ -c_3 \\ 1 \end{bmatrix} \quad [6.3]$$

A rotation based on $n(p_0)$ could be done to align z' axis with the new surface normal. Then a new quadric can be fitted to the points under the new coordinate system resulted from the rotation process. The calculated coefficients can be used to calculate the curvatures as:

$$K = \frac{4c'_4c'_6 - c'^2_5}{(1+c'^2_2+c'^2_3)^2}$$
$$H = \frac{c'_4 + c'_6 + c'_4c'^2_3 + c'_6c'^2_2 - c'_5c'_2c'_3}{(1+c'^2_2+c'^2_3)^2} \quad [6.4]$$

Usually the commonly used descriptors for quantifying 3D surface shape are Gaussian curvature ($K = k_1 \cdot k_2$) and the mean curvature ($H = (k_1 + k_2)/2$). (k_1, k_2) is the two principle curvatures at a given point which can be obtained from K and H. The Gaussian curvature has been widely used for surface shape characterization. However it is unable to describe the surface bending, for example the cylindrical surface, which has zero Gaussian curvature as a flat plane. The mean curvature, on the other hand, can not describe the surface shape properly too. For example, a surface with the same H can have different combinations of k_1 and k_2. Koenderink (Koenderink et al., 1992) proposed a more proper measure of local shape, known as curvedness, which was used in this study. The curvedness defined by Koenderink (Koenderink et al., 1992) could be used to measure the extent of which a region deviates from flatness, that is

$$C = \sqrt{\frac{k_1^2 + k_2^2}{2}} \quad [6.5]$$

6.6.2 Results

Figure 6.13 shows the curvature distributions for one plaque in the fibrous cap surface((a): the maximum principle curvatures k_1; (b) the minimum principle curvatures k_2; (c) curvedness; (d) FPS distribution. The principle curvatures vary greatly in the fibrous cap surface. In Figure 6.14 (a), a region of high k_1 can be found downstream of

the plaque, compared to FPS distribution in Figure 6.14 (d), the same region experiences a very high plaque stress, which is marked by the arrow (RA). Curvature k_2 shows a different distribution from curvature k_1. In the middle region of the fibrous cap surface, two high curved regions can be identified(Figure 6.14 (b)), marked by RB, and RC, which still have higher stress levels than its surrounding. Figure 6.14 (c) shows the curvedness of the fibrous cap, the combination of the principle curvatures, 4 high curved regions are identified as RA, RB, RC and RD.

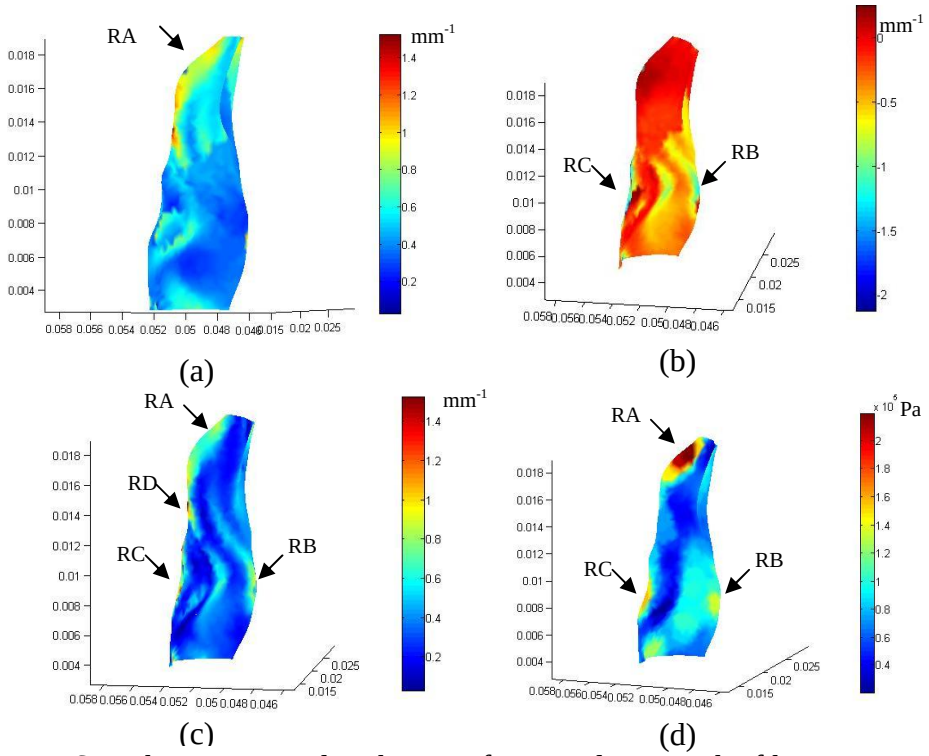

Figure 6.14 the curvature distributions for one plaque in the fibrous cap surface((a): the maximum principle curvatures; (b) the minimum principle curvatures; (c) curvedness; (d) FPS distribution)

The comparison between curvedness and FPS distribution shows that a highly curved region will normally associate with a high stress level, although the relationship may not be always true. For example, in Figure 6.14 (c), the high curved region, marked by RD, does not experience a high stress level. The linear correlation analysis was performed between curvedness C and FPS, shown in Figure 6.15, the stress is moderately related

with local curvedness, suggesting the irregularity of the fibrous cap can contribute to the extreme stress conditions in vulnerable plaques.

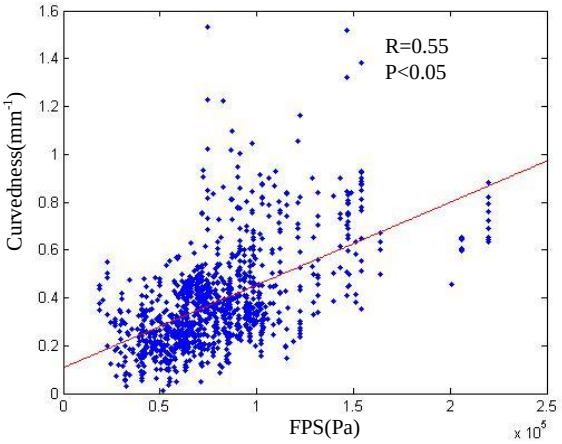

Figure 6.15 correlation between FPS and curvedness C

Figure 6.16 (a,b,c) shows the results for other 3 plaques for the curvature distributions, FPS distribution, and their relations. Based on these result, it can be found that the curvedness in the fibrous cap shoulder is higher than other regions, the fact may partially explain why the stress concentration could often be found in the fibrous cap shoulder region, as shown in Figure 6.14 and 6.16.

In total, 20 subjects were analyzed for the curvature distributions and the relations with FPS distributions. There is a significantly positive relation between curvature and FPS distribution among 14 subjects, that is 70%, with $p<0.05$, however the correlation coefficient does have a large variation in a range from 0.13 to 0.76. The average value of the correlation coefficients is 0.33±0.2. Four subjects (out of 20) did not show such correlation, and two subjects show negative correlation with a small coefficient. In general, the curvature could affect the stress distributions in the fibrous cap surface, the greater of the curvature, the greater of the stress. However, high stress regions can still occur in areas having low curvature.

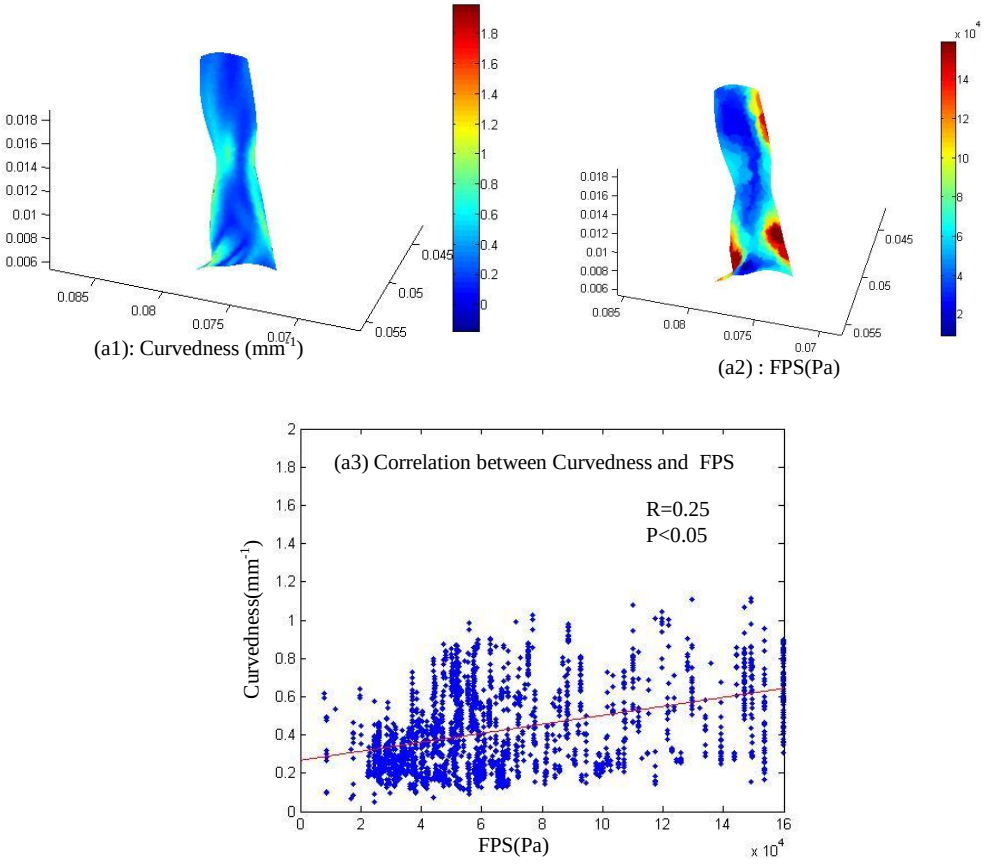

(a): the curvature distribution (a1), FPS distribution (a2), and their relations (a3)

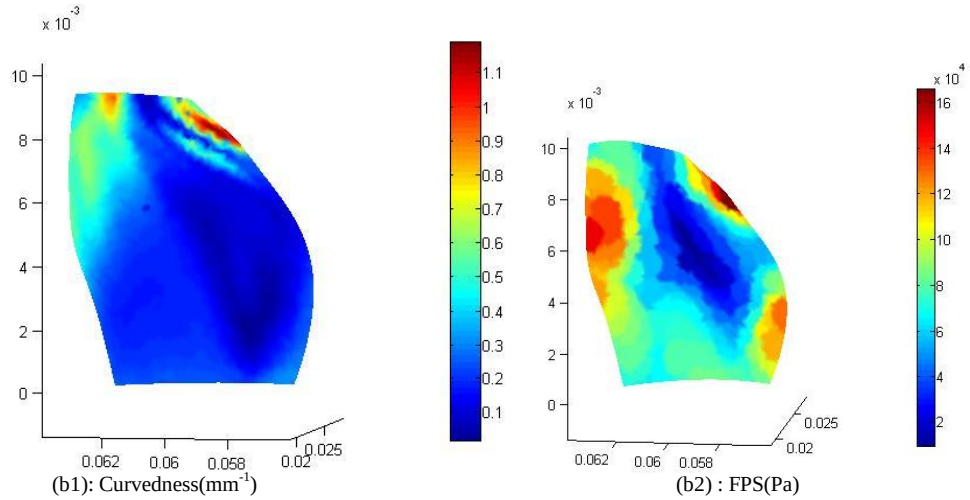

(b1): Curvedness(mm^{-1}) (b2) : FPS(Pa)

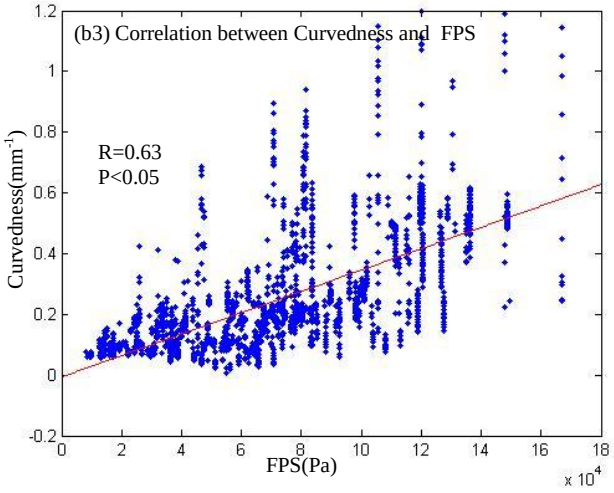

(b): the curvature distribution (b1), FPS distribution (b2), and their relations (b3)

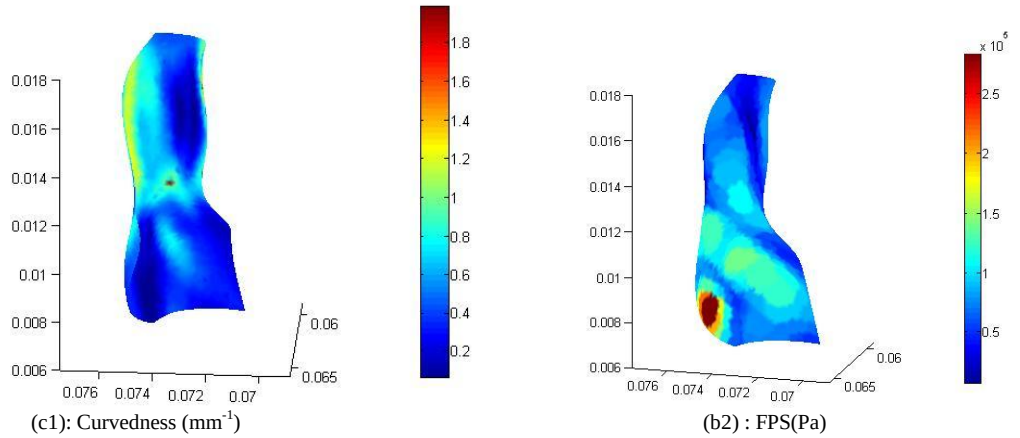

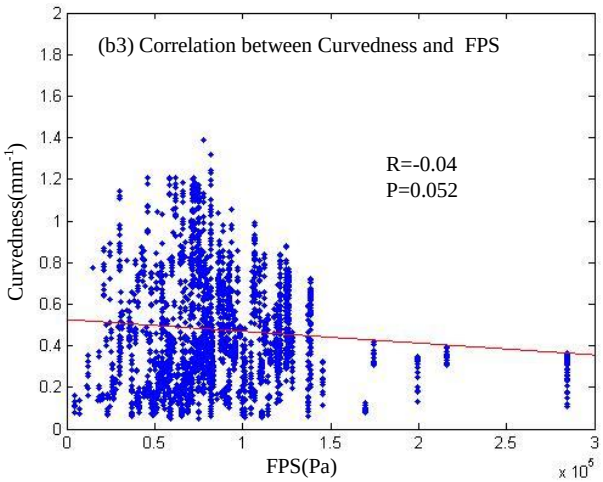

(c): the curvature distribution (c1), FPS distribution (c2), and their relations (c3)

Figure 6.16 the curvature distribution, FPS distribution, and their relations for 3 plaques (a, b, c).

From Li's study (Li et al., 2008), the lumen curvature of the plaques of symptomatic patients was significantly larger than those of asymptomatic patients. To analyze the difference between the symptomatic and asymptomatic plaques, the average curvedness in those mesh points experiencing the maximum FPS were averaged to represent the curvedness for plaques. The averaged curvedness (named Cur_ave) was summarized for the two groups of symptomatic and asymptomatic subjects (in total 20). Cur_ave is $0.45\pm0.20mm^{-1}$ for symptomatic patients and $0.49\pm0.20mm^{-1}$ for asymptomatic patients. The difference between the two groups is not significant. The different results compared to Li et al's study from 2D MRI derived plaque models, may lie in the facts: (1) the

curvature in this study is from 3D shape analysis, rather than 2D curvature; (2) the choice of curvature representations in 3D and 2D are different. For 3D surface, there are 2 principle curvatures; a proper combination of the two curvatures is needed. In this study, the curvedness C was chosen. (3) Not the global maximum curvedness in the fibrous cap was chosen for the comparison between two groups, but the averaged curvedness associated with extreme stress conditions was chosen for the comparison. We tried to compare the global maximum curvedness in the fibrous cap surface, defined by the curvedness which 1% mesh points have higher curvedness than. Still, there is no significant difference between the two groups of subjects.

Stress distribution simulation in an anatomically realistic plaque normally requires long computational time and manual processing hours. Usually for a 3D FSI simulation of one carotid plaque, the computational time is 3 weeks in a Dell Workstation with 2.3GHz Xeon CPU and 8 GB of RAM in our Lab. It is impractical to apply the stress analysis procedure in clinical as it is done in this research. However the structure determinants from plaque morphology are much easier to compute, and need less computational time. If the stress could be indirectly assessed from certain structure determinants, it will be more quickly and easily to identify the most vulnerable plaques, and the most dangerous regions in plaques. From Chapter 3 and 4, the fibrous cap thickness is one of the most important factors affecting stress distribution in the fibrous cap surface. In this section the curvedness also shows a positive correlation with plaque stress distributions. A combined analysis of the relationships among fibrous cap surface, curvedness, and FPS distribution may produce more accurate predictions from geometrical feature to rupture risks. Those results for one subject are shown in Figure 6.17.

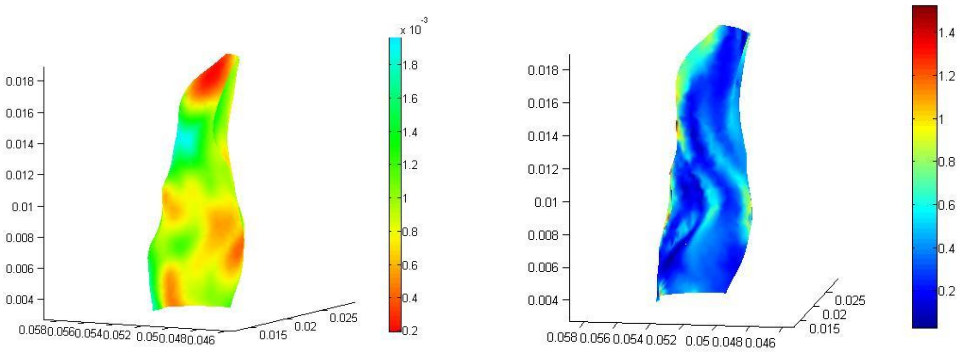

(a): fibrous cap thickness(mm) (b): Curvedness(mm^{-1})

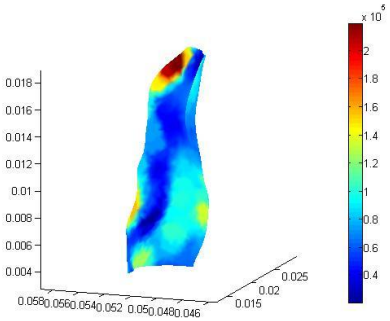

(c): FPS distribution(Pa)

Figure 6.17 fibrous cap surface, curvedness, and FPS distributions for one subject

From Figure 6.17, it can be found that a thinner fibrous cap region with higher curvatures experience higher stress levels for this subject. The multiple regression is applied to fibrous cap thickness, the curvedness and FPS. The model is assumed as

$$FPS(kPa) = b0 + b1 * fThk(mm) + b2 * curvedness(mm^{-1}) + b3 * fThk * curvedness \quad [6.6]$$

95% confidence level is chosen for the regression analysis, $b0$, $b1$, $b2$, $b3$ are the parameters which are needed to be determined. Figure 6.18(a) shows the multi-regression analysis for the subject.

$$FPS = 58.623 - 16.446 * fThk + 149.75 * curvedness - 62.149 * fThk * curvedness \quad [6.7]$$

With a 95% confidence interval, parameters b were: b0= [49.57, 67.676]; b1= [-25.484, -7.4068]; b2= [131.38, 168.11]; b3= [-79.505, -44.793]. The predicted FPS according to the equation [6.7] is shown in Figure 6.18(b). Comparing with 6.17(c) which is FSI simulation result for the plaque, the general patterns of stress have been captured by the predicted FPS. Figure 6.18(c) shows the difference between predicted stress and original FPS. The coefficient of multiple determination among fibrous cap thickness, curvedness, and FPS is 0.47, which means that the amount of variance in FPS is accounted for by the

variation in the predictor variables fibrous cap thickness and curvedness. Figures 6.19 and 6.20 show the regression results for two other subjects. For the three subjects, the FPS predictions by fibrous cap thickness, surface curvedness are comparable to the simulated results by fully coupled FSI. The average coefficient of multiple determination for the 20 subjects is 0.36±0.17.

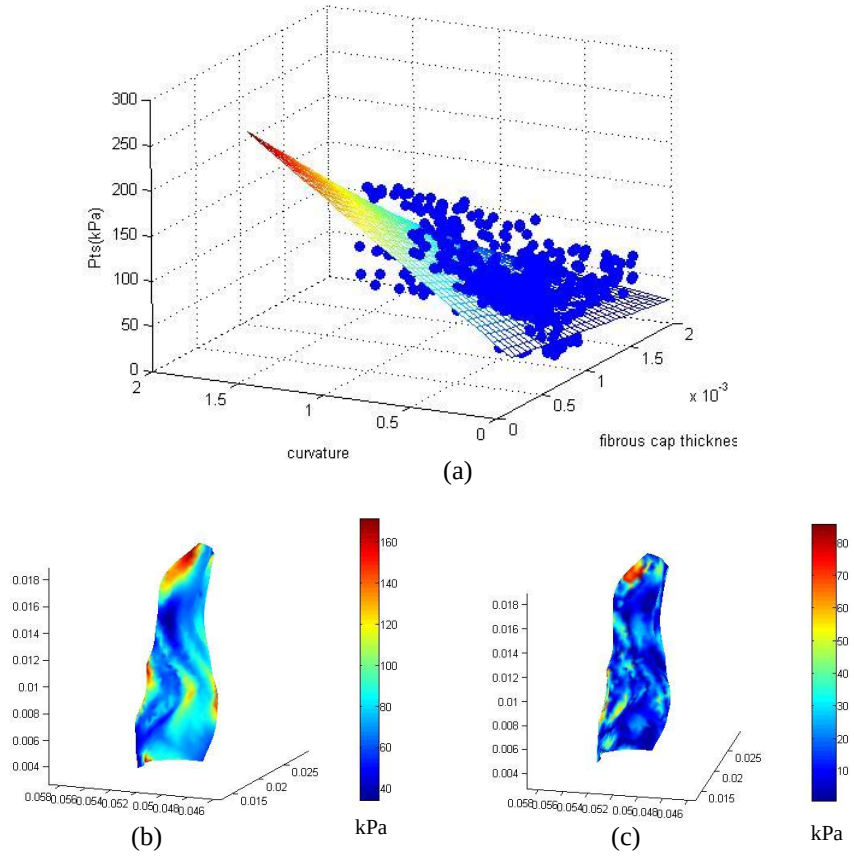

Figure 6.18 Multi-regression results. (a) Multi-regression with fibrous cap thickness, curvedness, and FPS; (b) predicted FPS; (c) The difference between predicted value and simulated results (the simulated result can be found in Figure 6.17)

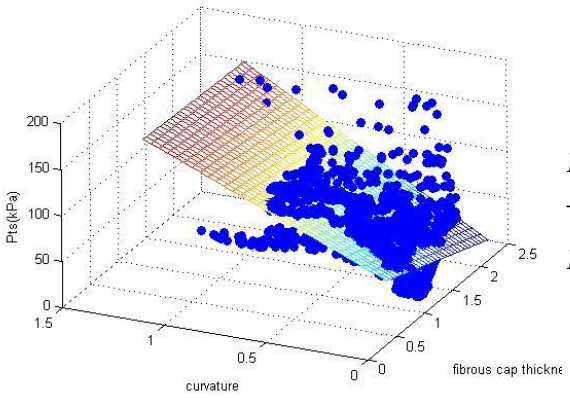

(a)

$$FPS = 76.225 - 26.09 * fThk + 85.21 * curvedness + 18.24 * fThk * curvedness$$

$$R^2 = 0.45$$

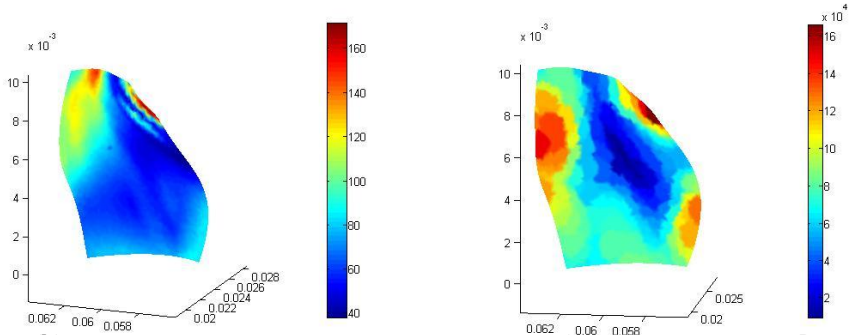

(b) (c)

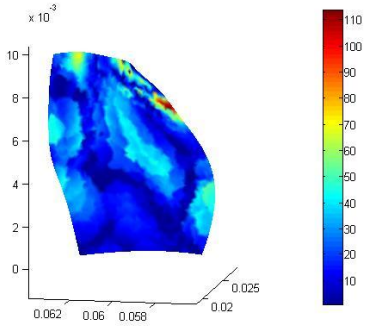

(d)

Figure 6.19 results for another symptomatic subject (a) Multi-regression with fibrous cap thickness, curvedness, and FPS; (b) predicted FPS; (c) the simulated FPS; (d) difference between predicted and simulated FPS.

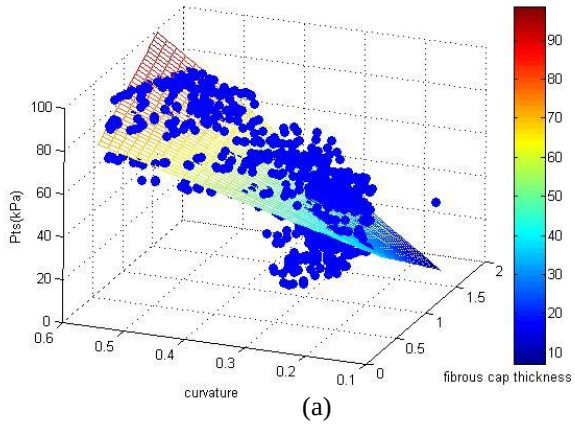

(a)

$$FPS = 51.68 - 46.24 * fThk + 5.54 * curvedness + 125.9 * fThk * curvedness$$

$$R^2 = 0.58$$

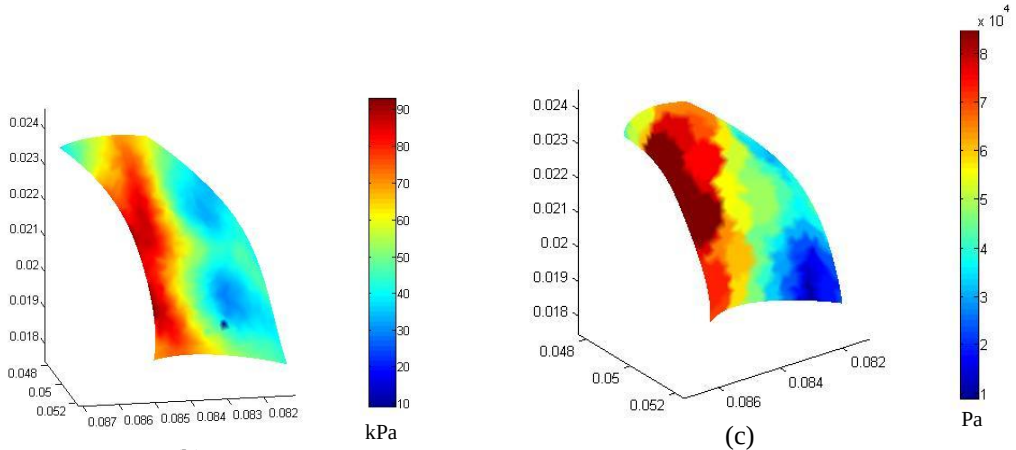

(b) (c)

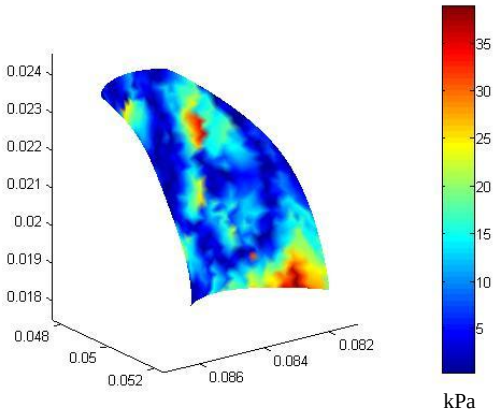

(d)

Figure 6.20 Results for the third chosen subject (asymptomatic) (a) Multi-regression with fibrous cap thickness, curvedness, and FPS; (b) predicted FPS; (c) the simulated FPS with FSI; (d) difference between predicted and simulated FPS

FPS prediction by fibrous cap thickness and surface curvature has a moderate agreement with the stress simulated by FSI, around 40% variation of FPS can be accounted by the

variations from the two morphological features. Some other plaque geometry features may need to be defined for a better prediction, such as lipid core size, inflammation information, micro-structure of fibrous cap, and calcification deposits. Until now there is no conclusion on how to characterize the lipid core features on the effects to plaque stress. Ohayon (Ohayon et al., 2008), used the lipid core thickness, rather than lipid core area in determining plaque stability in their 2D study. For 3D plaque stress analysis, there are more features associating with lipid core, such as the lipid core volume, dimensions, et al. It would be expected with more plaque features included, the predicted FPS will be much closer to the simulated results.

6.7 Patient Specific Material Model Determined from *in-vivo* MRI

Recent studies have demonstrated that it is possible to obtain patient specific material model from *in-vivo* human data (Masson et al., 2008), which enable plaque stress analysis to be much closer to the real situation rather than a general material model from existed literatures or obtained by *ex-vivo* experiments. Therefore in this study, the method proposed by Masson (Masson et al., 2008) was used to determine arterial properties from *in-vivo* data, and applied the material properties for plaque stress analysis for one subject. An idealized 3D arterial wall section representing CCA was constructed based on *in-vivo* Phase contrast MR images, residual stress, perivascular stress, and fiber-reinforced, hyper-elastic effect of arterial tissue were included in the mechanical model. The fitted material parameters were applied to the real plaque stress analysis. It is believed that the procedure of using patient specific material model will yield more realistic plaque stresses, which may play an important role in understanding plaque development and rupture.

6.7.1 in-vivo Data

A subject with carotid plaque was chosen for the study. Phase contrast MR images at common carotid artery was obtained to provide the luminal area change over one cardiac cycle as in Figure 6.21(a), the bright region, indicated by the arrow, is the lumen region, however there is no information regarding arterial wall. Figure 6.21(b) shows the luminal radius change of the CCA section over one cardiac cycle. Due of lack of pressure information, a pressure profile(denoted as measured pressure) was chosen as in Chapter 3 by rescaling the pressure range of 80~110mmHg according to luminal area change over time at CCA, shown in Figure 6.21(c).

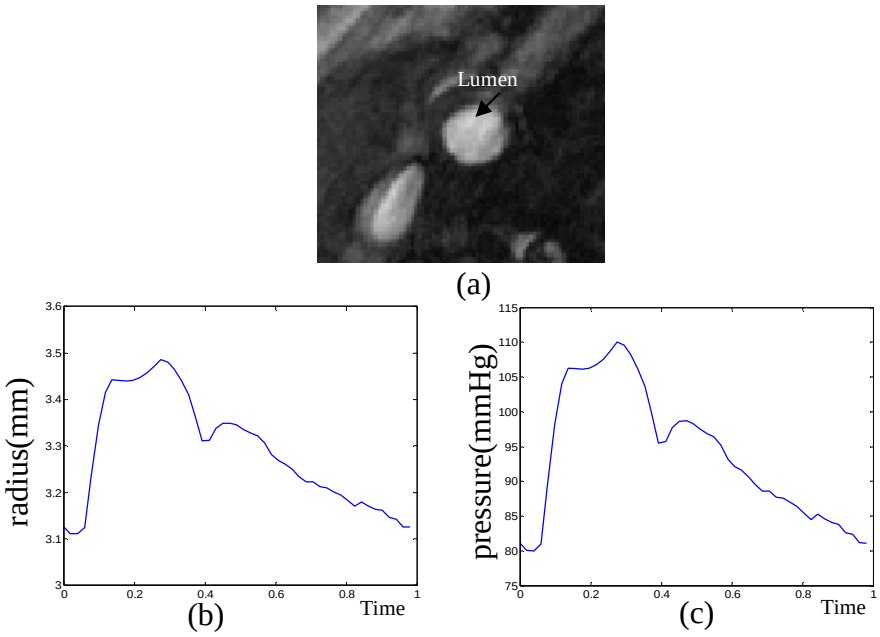

Figure 6.21 *In-vivo* data in CCA. (a) Phase contrast MRI of a CCA section; (b) luminal radius change; (3) intra luminal pressure profile

6.7.2 Kinematics of Idealized Arterial Wall

CCA section in Figure 6.21(a) was considered to be a thick-walled circular cylinder in order to theoretically calculate stretch ratio in radial and circumferential directions by using a cylindrical coordinate system, that is (e_r, e_q, e_z). Therefore the deformation field of the CCA section over one cardiac cycle could be calculated from two successive motions (Humphrey 2002). Three configurations were considered as: Ω_0: stress free and excised configuration (R, Θ, Z); Ω_1: intact and unloaded configuration (r, f, x); Ω_2: *in-vivo* loaded configuration (r, q, z). The three configurations can be found in Figure 6.22.

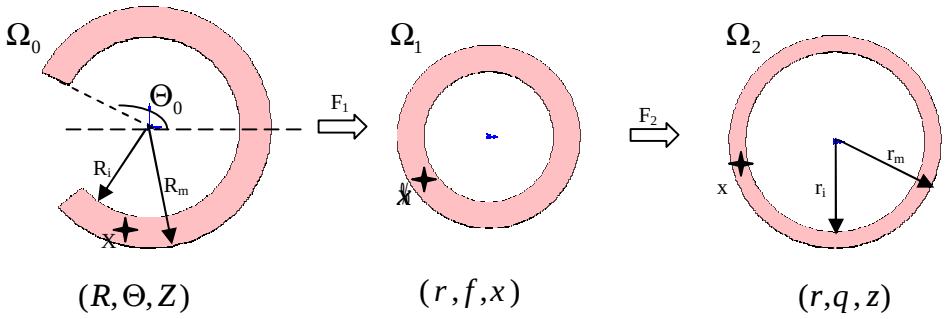

Figure 6.22 three different configurations of the intact CCA from stress free to load free and loaded state

If a material particle is considered in the arterial wall, such as the particle indicated by '✦' in Figure 6.22, then $X(R,\Theta,Z)$, $x(r,f,x)$, $x(r,q,z)$ are the configurations of Ω_0, Ω_1, and Ω_2 respectively. By employing the relations from Humphrey (Humphrey 2002),

$$r = r(R), f = \left(\frac{p}{\Theta_0}\right)\Theta, x = \Lambda Z \qquad [6.8]$$

$$r = r(r,t), q = f, z = l\,x \qquad [6.9]$$

where t is the time, Θ_0 is the open angle when arterial wall is excised. Λ is the axial stretch accounting for axial residual stress from Ω_0 to Ω_1. l is the *in-vivo* load-induced axial stretch, which is assumed to be constant over cardiac cycles. R_i and r_i are the inner radiuses in Ω_0 and Ω_2; R_m and r_m are the radiuses at the medial-adventitial interface.

The deformation gradient tensor from Ω_0 to Ω_2 can be defined as $F = \partial x(X)/\partial X$, that is

$$F = \begin{bmatrix} \frac{\partial r}{\partial R} & & \\ & \frac{p\,r}{\Theta_0 R} & \\ & & l\Lambda \end{bmatrix} = \begin{bmatrix} l_r & & \\ & l_q & \\ & & l_z \end{bmatrix} \qquad [6.10]$$

where l_r, l_q and l_z are principle stretch ratios in radial, circumferential and axial directions. The left and right Cauchy-Green tensors are

$$B = FF^T, C = F^T F \quad [6.11]$$

The local volume ratio is

$$J = \det(F) = l_r l_q l_z \quad [6.12]$$

Generally arterial wall is considered to be impressible, therefore $J = 1$. Then by applying equation 6.10 to equation 6.12 with $J = 1$,

$$R\partial R = \frac{p l \Lambda}{\Theta_0} r\partial r \quad [6.13]$$

integrating from r_i and R_i to r and R respectively,

$$R = \sqrt{(R_m^2 - \frac{p l \Lambda}{\Theta_0}(r_m^2 - r^2))} \quad [6.14]$$

therefore the stretch ratio in radial direction is

$$l_r = \frac{\Theta_0}{p l \Lambda} \cdot \frac{R}{r} = \frac{\Theta_0}{p l \Lambda} \cdot \frac{\sqrt{(R_m^2 - \frac{p l \Lambda}{\Theta_0}(r_m^2 - r^2))}}{r} \quad [6.15]$$

6.7.3 Constitutive Modeling of Arterial Wall

The mechanical response of the CCA section is considered to be anisotropic hyper-elastic. Because the material properties in adventitial layer is different from medial layer, and different collagen fiber configurations compared to medial layer, in order to simplify the solution procedure, as in Masson's study (Masson et al., 2008), only medial and intimal layer was studied in this study. The strain energy function proposed by Gasser (Gasser et al., 2006) was used to model the CCA section with two families of collagen fibers embedded in a soft incompressible ground matrix, which is also available in Abaqus 6.8. The associated strain energy function W is

$$W = a(I_1 - 3) + \frac{k_1}{2k_2}\sum_{f=1}^{N}(e^{k_2 < E_f >^2} - 1) + \frac{1}{D}(\frac{(J)^2 - 1}{2} - \ln J) \quad [6.16]$$

$$E_f = k(I_1 - 3) + (1 - 3k)(I_{4(ff)} - 1) \quad [6.17]$$

a, D, k_1 and k_2 are material parameters. k denotes the level of dispersion in the fiber directions, in this study $k = 0$, which means fibers from one family are perfectly aligned along one direction. f represents one fiber family, N is the total number of fiber families. Two families of fibers (f_1, f_2) are considered in this study ($N=2$), and the fibers only distribute in circumferential and axial directions, no fiber in radial direction, as shown in Figure 6.23. The angles of f_1 and f_2 with circumferential direction are j_1 and j_2. In this study, j_1 is equal to j_2.

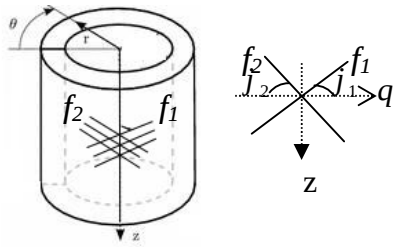

Figure 6.23 two families of collagen fibers in medial layer of artery

The fiber orientations can be defined in the reference configuration by unit factor $A_{f_1}(0, \cos(j_1), \sin(j_1))$ and $A_{f_2}(0, \cos(j_2), \sin(j_2))$, which depend on the angle of j_1 and j_2. I_1 is the first strain invariants, defined as $I_1 = trace(C)$. $I_{4(ff)}$ is the pseudo-invariants of C combined with A_{f_1}, and A_{f_2},

$$I_{4(f_1 f_1)} = A_{f_1} C A_{f_1}^T \qquad [6.18]$$

$$I_{4(f_2 f_2)} = A_{f_2} C A_{f_2}^T \qquad [6.19]$$

The first term in the strain energy function 6.16 represents the contributions of the non-collagenous isotropic ground material; the second term represents the contributions from the different families of collagen fibers; and the third term is the contributions from volumetric change. A basic assumption of the model is that the fibers can only support tension, therefore, the anisotropic contribution in the second term appears only when the strain of the fibers is positive, that is $E_f > 0$, enforced by the term $< E_f >$, where the operator $<*>$ stands for the Macauley bracket and is defined as $< E >= \frac{1}{2}(|E| + E)$. The

second Piola-Kirchoff stress S for nonlinear elastic incompressible material from strain energy equation is

$$S = -pC^{-1} + 2\frac{\partial W}{\partial C} \quad [6.20]$$

where p is the hydrostatic pressure, then the Cauchy stress tensor s can be computed from S as

$$s = FSF^T J^{-1} \quad [6.21]$$

From equations 6.16 to 6.21, and $j_1 = j_2 = j$, the components of Cauchy stress tensor s are

$$s_{rr} = -p + 2a\,l_r^{\,2} \quad [6.22]$$

$$s_{qq} = -p + 2a\,l_q^{\,2} + 4k_1 e^{k_2 E_4^{\,2}} E_4 \cos(j)^2 \quad [6.23]$$

$$s_{zz} = -p + 2a\,l_z^{\,2} + 4k_1 e^{k_2 E_4^{\,2}} E_4 \sin(j)^2 \quad [6.24]$$

$$E_4 = A_{f_1} C A_{f_1}^{\,T} = A_{f_2} C A_{f_2}^{\,T} = l_q^2 \cos(j)^2 + l_z^2 \sin(j)^2 - 1 \quad [6.25]$$

6.7.4 Equilibrium of Arterial Dynamics

From Humphrey's (Humphrey & Na, 2002) study, if no body force is included, the motion equation of the idealized CCA section as shown in Figure 6.22 at Ω_2 configuration can be expressed as

$$\frac{\partial s_{rr}}{\partial r} + \frac{s_{rr} - s_{qq}}{r} = r\,a_r \quad [6.26]$$

r is the density of the CCA section. a_r is the radial acceleration, due to the insignificant contribution of inertial term, the quasi-statically assumption is applied (Humphrey and Na, 2002). Equation 6.26 can be solved by numerical integration over r from the inner wall r_i to the interface between media and adventitial layers r_m .

$$P_i(t) = P_a(t) + \int_{r_i(t)}^{r_m(t)} \frac{s_{qq}(r,t) - s_{rr}(r,t)}{r} \quad [6.27]$$

where $P_i(t)$ is the computed luminal pressure, $P_a(t)$ is the pressure-like contribution from the adventitial layer on the medial layer (perivascular stress). Equation 6.27 can allow the computation of luminal pressure by given information of arterial wall motion, residual

stress effects, and pressure contribution from adventitial layer. The exact form of equation [6.27] can be obtained from Matlab by Symbolic Math Toolbox.

6.7.5 Material Parameters Fitting

The material parameters are estimated based on non-invasive *in-vivo* data. The residual stress-related axial stretch Λ is chosen to be 1 from existed literatures (Chuong and Fung 1983). The *in-vivo* loading induced axial stretch ratio l is assumed to be 1.1 as in previous chapters. Θ_0 is assigned to be 130 degree, a static pressure of 2kPa is assigned to $P_a(t)$ (Masson et al., 2008). In order to define r_m, which is not available in phase contrast MR images, an assumed thickness (0.6mm) of medial and intima was assigned in the beginning of the cardiac cycle, then the change of r_m over one cardiac cycle can be calculated by applying the constraint of constant area of arterial wall because of incompressibility. Therefore the undetermined parameters are a, k_1, k_2, j, and R_m. Best-fit values for those parameters can be obtained using a nonlinear least-square minimization of the difference between predicted and measured luminal pressures over one cardiac cycle. The function *lsqnonlin* in Matlab was used for the fitting procedure.

The best fitted parameters from *lsqnonlin* is

$$[a, k_1, k_2, j, R_m] = [32.1kPa, 9.6kPa, 3.8, 45.7, 4.8mm]$$

Figure 6.24(a) shows the predicted pressured compared to the assumed measured pressure, the predicted pressure agrees well with measured pressure, no noticeable difference can be identified. The residual of the fitted procedure is in Figure 6.24(b), the maximum difference between predicted and measured pressure is about 0.288mmHg. Figure 6.25 shows s_{qq} under uni-axial stretch in circumferential direction. s_{qq} increases dramatically when stretch ratio increases because of the engagement of fibers in circumferential direction.

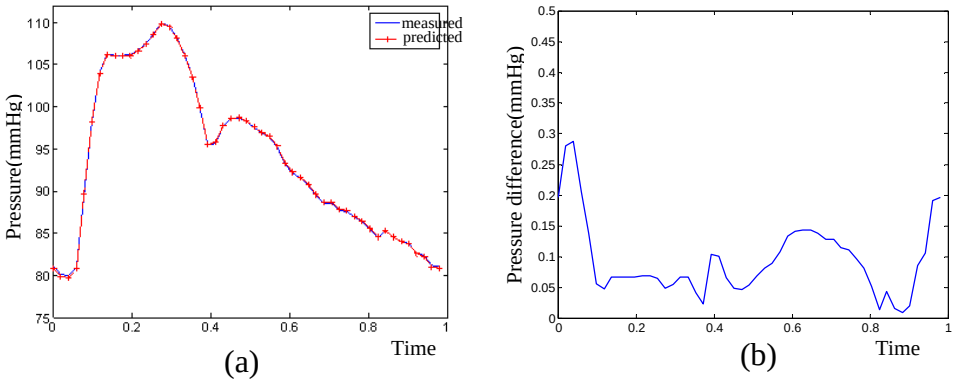

(a) (b)

Figure 6.24, (a) predicted pressure compared to the real pressure profiles; (b) residual between predicted and real pressure profiles

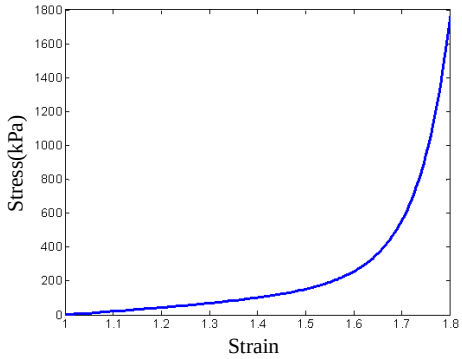

Figure 6.25 s_{qq} response under uni-axial stretch

A cross-section of plaque sample with lipid from the same subject was chosen for stress analysis with the fitted material parameters for arterial wall material model. Static stress analysis was performed in Abaqus 6.8, which has implemented the strain energy function 6.16. The geometry is shown in Figure 6.26, the cross-section was extruded to construct the 3D plaque geometry, a cylindrical coordinate system was created in the luminal centre. A pressure load of 110mmHg was applied in the luminal surface. Lipid was considered to be very soft with 2kPa for Young's modulus and 0.49 for Poisson ratio.

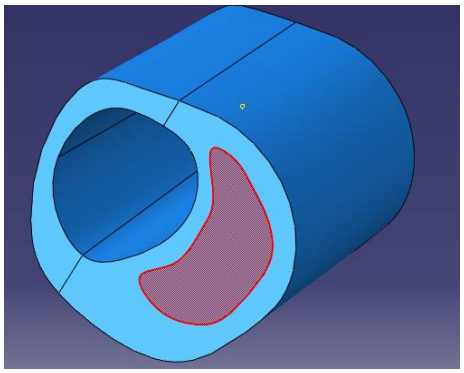

Figure 6.26 3D plaque geometry

Figure 6.27 shows the first principle stress distribution. The stress distribution pattern from the patient-specific material model is similar as existed literatures on plaque stress analysis, however the stress levels and detailed distribution pattern would be much closer to the real situation. In Figure 6.27, a local high stress concentration can be found in the thin fibrous cap region, indicated by an arrow. Due to the thin wall region in the opposite side of lipid core, a high region of stress appears.

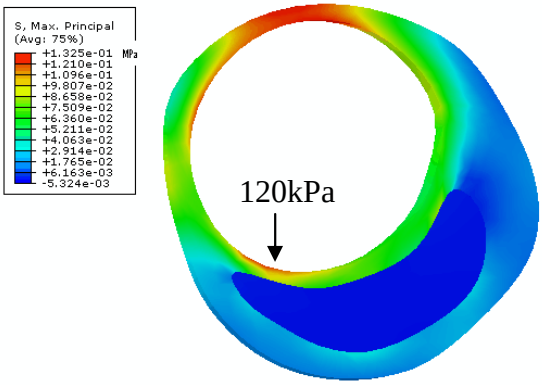

Figure 6.27 Maximum Principle stress distribution

6.8 Summary

In this study, fully coupled FSI simulation was performed on 20 carotid plaques reconstructed from high resolution *in-vivo* MR images. The extreme stress conditions could be found in the fibrous cap region, and most happen in the plaque shoulder. Local maximum stress predicted in the plaque region are found to be significantly different between symptomatic and asymptomatic groups, and much higher in the symptomatic group, which suggests a higher stress in the plaque region may indicate a high vulnerable

risk. Though there is no significant difference in minimum fibrous cap thickness and lipid core size, symptomatic group has thinner fibrous cap and larger lipid core size. Plaques with a higher stenosis are more likely to have extreme stress conditions upstream. The stress analysis and plaque morphological feature study will be helpful in the identification of high rupture risk patients.

2D FEM simulations were performed on an atherosclerotic plaque to assess circumferential residual stress distribution variations in the plaque based on open angles measured from 3D ultrasound image. The stress analysis without residual stress may overestimate the stress level around 10%, while the influence of the residual stress to the final stress distribution under physiological blood pressure load was minor. Therefore the inclusion of residual stress in the plaque stress analysis will depend on the application and accuracy requirement.

By quadratic surface fitting, the curvedness in fibrous cap surface was extracted analytically for 20 subjects. In general, curvedness is higher in the fibrous cap shoulder. It is also found that the greater of curvedness, the higher of the stress level. The combined analysis of curvedness, fibrous cap thickness, and wall tensile stress leads to wall stress to be predicted by plaque morphological features with multi-regression. The predicted stress shows similar patterns as the stress distributions from FSI simulation. With more morphological features included in the stress calculation formula, the stress may be calculated directly from the geometry information for a quick solution in the future, rather than a more costly fully coupled FSI.

Based on the *in-vivo* MR images of carotid plaques, it is possible to characterize material properties of arterial wall, which has been studied in the research. The patient specific material model will greatly advance plaque stress analysis in terms of patient specific model. However there is still a long way to go for robust and reliable material model characterization, and application to real 3D patient specific plaque models.

Chapter 7

Further Development of plaque stress analysis

7.1 Plaque Stress Analysis on Element Based Material Property Model

7.1.1 Introduction

The stress distributions in the coronary and carotid arteries with plaque have been studied by many researchers on idealized or realistic 2-D and 3-D multi-component arterial models (Finet et al., 2004; Tang et al., 2004a, 2004b; Zheng et al., 2005). In these conventional finite element stress analysis models, model geometry was divided into different regions in order to assign different material properties to the regions to represent plaque components such as normal wall, fibrous cap, calcified region, lipid pools. Within a region, for example fibrous cap, a homogenous material property was usually assumed. This simulation method is called region based finite element method or RB_FEM in this section. Stress analysis results have shown that stress distributions in the plaque region are sensitive to the model geometry, collagen fiber structure (Gasser et al., 2006), material variations among different plaque components. Although the majority plaque rupture occurs at the plaque shoulder region where RB_FEM predicts maximum tissue stress, contradiction results also show that 40% of ruptures occur in the other parts of the cap. It may indicate that for these cases, the rupture location can not be fully predicted by conventional RB_FEM in terms of the maximum tissue stress.

Soft biological tissue in general and the arterial wall in particular are considered as a hybrid fibrous material. In addition to the ground substance and the cells of smooth muscles, it contains fibers of different stiffness. Figure 7.1 shows that in the fibrous cap the content and structure of the collagen vary greatly, which can be seen from the polarized light microscope (Borges et al., 2007). On the boundary of the fibrous cap and lipid core, the collagen fibers become loosely structured and gradually disappear, the spaces are occupied gradually by the increasing number of foam cells and finally by the extra-cellular lipids as shown in Figure 7.1(a). This change of collagen structure will

introduce a graduated decrease of material stiffness from the fibrous cap towards the lipid core. However, in the conventional stress analysis model, a clear boundary of fibrous cap and lipid core has to be defined in order to assign proper material properties to the regions. This process will introduce an artificial stress change or even a local stress concentration if a dramatic geometry change occurs in the boundary. Also, the collagen fiber distribution in the fibrous cap varies along the circumference. Figure 7.1(a) and 7.1(b) show two different fiber distributions in the fibrous cap circumferentially. In Figure 7.1(a), collagen fibers are well structured in the shoulders of the fibrous cap, and loose in the middle; while in Figure 7.1(b), collagen fibers are loose in the shoulders and well structured in the middle.

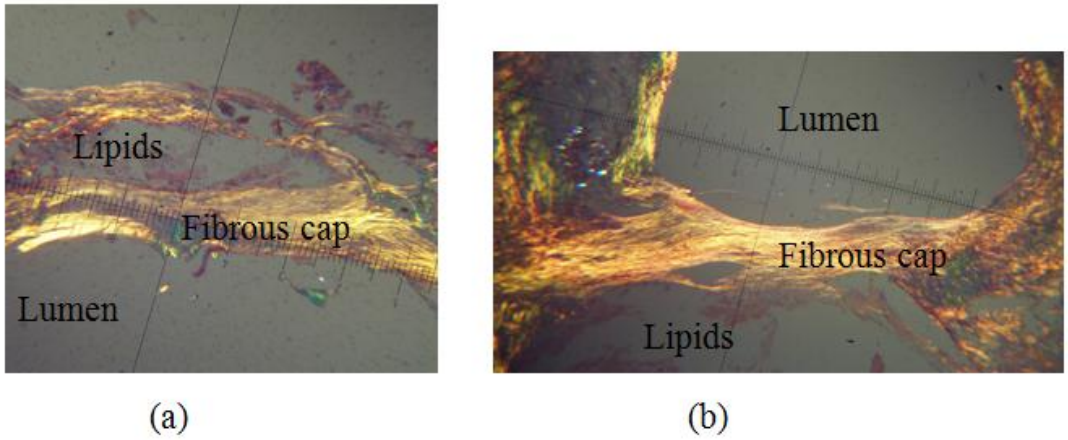

Figure 7.1 Polarized light microscope of the plaque sample, the highlight region relates to the collagen content and structure, brighter, denser. (a) Collagen fibers are denser in the shoulder and looser in the middle of the fibrous cap, also denser near the lumen and looser near the lipids. (b) Collagen fibers are denser in the middle of the fibrous cap and looser in the shoulder.

To deal with the heterogeneous material property in the biological tissues, one may generate more small regions and still apply the conventional stress analysis. However, it is a very time consuming process and may still not be able to catch the graduated change of the local material property. Another way to define the material property in FEM may be introduced to cope with the problem. An element based material property assignment model, proposed in this section, is able to deal with the simulation with heterogeneous material properties. It abandons the idea of defining regions in a geometry model all

together but assigning the material property to each numerical element automatically from a material property map.

The ideas of incorporating the local material property changes into FEM simulation were not totally new. In bone mechanic study, a similar method was introduced several years ago, called voxel-based finite element method (Niebur et al., 1999 and 2000). With their high-resolution finite element models, the studies were capable of assigning a unique modulus value to each element and performing analyses on geometrically identical models with different modulus distributions (Jassma et al., 2002), and the modulus value for each element could be obtained from the specimen CT attenuation (Benjamin et al., 2004). However, in bone mechanics, the material is much stiffer, usually 20GPa, than the soft tissue. The deformation of the bone is also much smaller compared with soft tissue such as arterial plaque; furthermore the model geometry and loading condition in the arterial plaque are totally different from those in bone. Therefore, there is a need to address the reliability and accuracy issues when applying the procedure on the arterial plaque simulation.

The purpose of this part of study is to develop a simulation procedure to incorporate the local material property changes in the current FEM model for the stress analysis in the arterial plaque, named Element Based Finite Element Method or EB_FEM. As a methodology development study, intensive test cases providing validations of the procedure form the first part of the chapter. These will be followed by some case studies to demonstrate the abilities of the procedure, the second part.

7.1.2 METHOD

Three major steps are needed to generate EB_FEM models for simulation. They are:

1. **Model geometry reconstruction and numerical mesh generation:** a single region will be used to define the entire arterial wall geometry. An FEM mesh will then be generated in the geometry.
2. **Material property map generation:** a corresponding material property map is obtained with the same geometry as in step 1. The value of each pixel in the

material property map comes from other sources, for example: polarized light microscope images of histology section of the plaque sample can provide quantitative description of the fibres content and structure in the arterial wall.

3. **Element material property interpolation:** each individual FEM element generated in step 1 will be assigned a material property by interpolating the property value from the property map according to the element location.

After defining the material model for each element, the structure equations are assembled for the whole geometry and solved by conventional FEM solver ANSYS^{TM}. In addition the mesh can be refined after the material property assignment to provide a more accurate result. The procedure is shown as Figure 7.2.

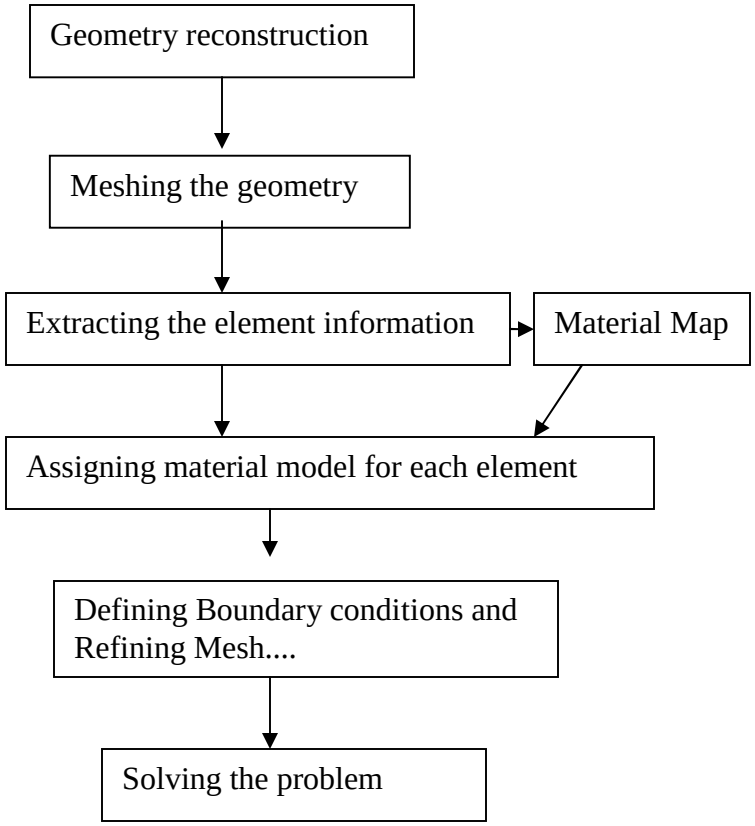

Figure 7.2 Diagram of simulation procedure for EB_FEM

The conventional RB_FEM stress analysis on simple geometry has been validated intensively in the early stage of the simulation technique development. In this part of the study, EB_FEM simulations were validated by comparing the simulation results with RB_FEM. Idealized and realistic models were included in the tests.

Based on the realistic plaque sample, the varied material property models were built for the application of EB_FEM.

7.1.3 Validation with Region Based FEM

7.1.3.1 Geometry Sensitivity Test Based on Idealized Models

The first set of validations was to test the simulation uncertainties caused by different model geometry. Three models were built with different geometries for the purpose. Model A: three layered structure; Model B: a small rectangle embedded within a large rectangle; and Model C: a small circle embedded within a large rectangle as shown in Figure 7.3. Table 7.1 provides the detailed information for the simulation of the three models including boundary conditions and material properties. RB_Model A, B and C were solved by ANSYS^{TM} 11.0. A Matlab^{TM} based program was used to interpolate the material property from the material map to each element. The material maps for the models were the same as the regional model geometry with only two (or three) different material property values. An ANSYS Parametric Design Language program was built to re-assigning the material property automatically for each element in EB_FEM simulations. The solution procedure was also performed in ANSYS^{TM} 11.0.

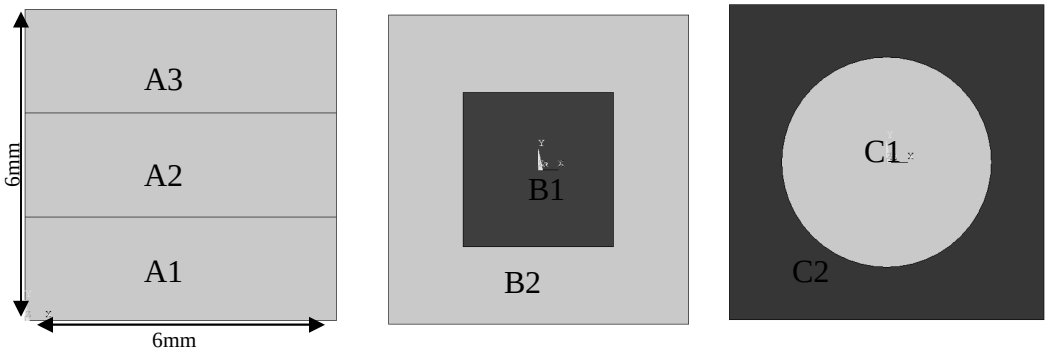

Figure 7.3 Model A with three layers A1, A2, A3; Model B with two rectangles B1 and B2; Model C with the rectangle C2 and the circle C1.

Models	Material Properties	Boundary Conditions
Model A	A1: Young's Modulus: 1E6Pa Poisson Ratio: 0.45	(1) the bottom line was fixed (2) the up line was pressured with 110mmHg (3) element number: 3600
	A2: Young's Modulus: 1E3Pa Poisson Ratio: 0.49	
	A3: Young's Modulus: 1E6Pa Poisson Ratio: 0.45	
Model B	B1: Young's Modulus: 1E3Pa Poisson Ratio: 0.49	(1) the bottom line was fixed (2) the up line was pressured with 110mmHg (3)element number: 3755
	B2: Young's Modulus: 1E6Pa Poisson Ratio: 0.45	
Model C	C1: Young's Modulus: 1E3Pa Poisson Ratio: 0.49	(1) the bottom line was fixed (2) the up line was pressured with 110mmHg (3)element number: 3953
	C2: Young's Modulus: 1E3Pa Poisson Ratio: 0.45	

Table 7.1 Material properties and boundary conditions for the three test models

Figure 7.4 presents the contours of Von Mises stress of the models A, B and C. The left and right panels in Figure 7.4 represented the results from region-based and element-based simulations respectively. It showed that the results from the two methods were almost identical. The distribution and the maximum values of Von Mises stress were nearly the same. The stress values on selected points were also the same. Although not presented in Figure 7.4, the results for the first principle strain were identical for different geometry models between the two kinds of simulations.

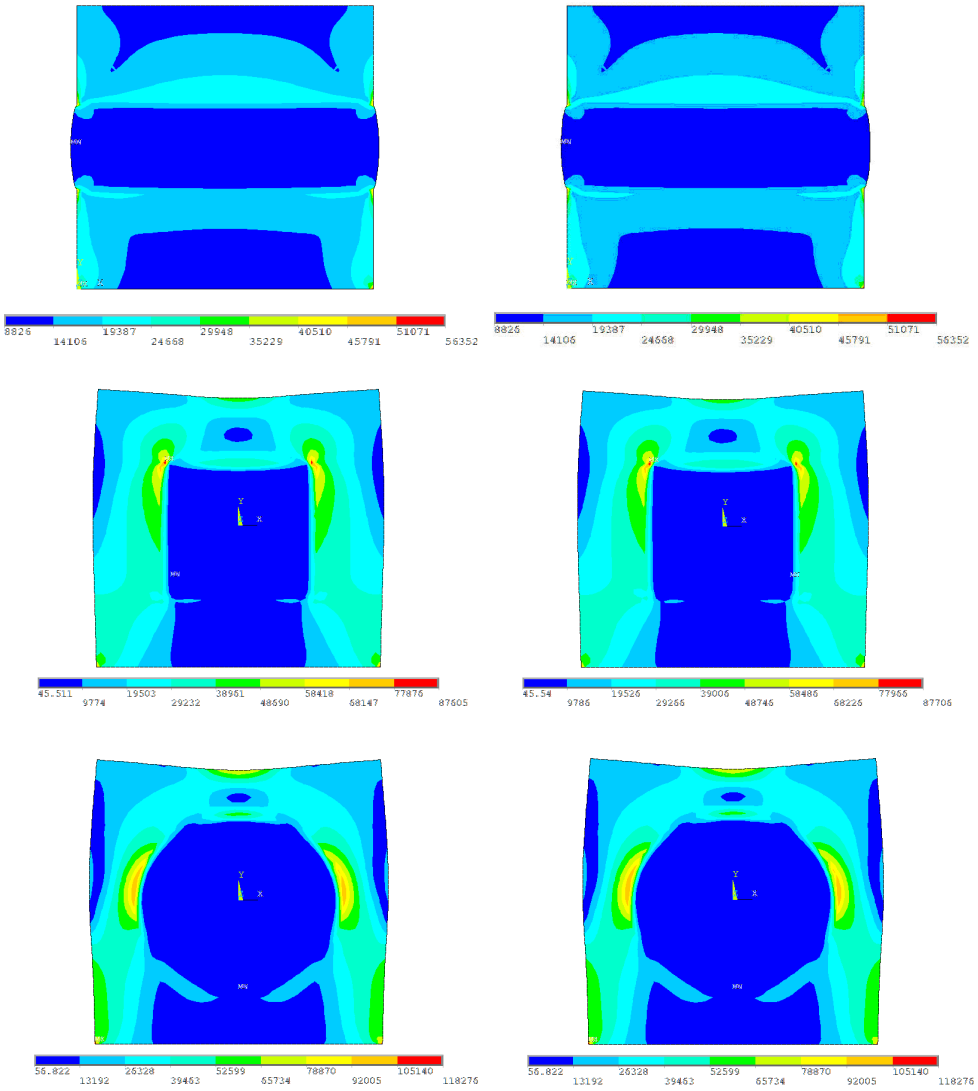

Left Column: Region-Based Right Column: Element-Based

Figure 7.4 Distributions of Von Mises stress of the three models. Left panel: region-based simulation; Right panels: element based simulations. (unit: Pa)

For the idealized model C, more tests were carried out, they were

1. **Boundary condition variation test**: the bottom boundary was fixed in the vertical direction, and could freely move in the horizontal direction. The upper boundary was compressed by 0.5mm. The simulations indicated that the element-based method could produce the same results as that in region based method.

2. **Element type test**: triangle element mesh rather than quad, which was used in the original simulation, was used for meshing. Simulations were carried out (a) at the original boundary conditions (Table 7.1) and (b) the one proposed in test step 1. The results showed that the maximum stress difference between the two mesh methods was less than 1%, and the stress distribution was identical.
3. **Mesh independence test**: A total of 7 meshes were tested with the mesh number increased from 3953 to 44196, in which the corresponding element size decreased from 100μm to 30μm. The boundary conditions proposed in test step 1 were used in the tests. The maximum stress difference between the two successive meshes decreased to 2% in L2 norm with increased mesh density for EB_FEM simulations. In the following realistic geometry, the element size was chosen to be 30μm since the sizes of geometry were comparable.

7.1.3.2 Geometry Sensitivity Test with Realistic Model

A histology image of a plaque was selected for the case study, which was obtained from a section of a human carotid endarectomy specimen through conventional wax histology procedures (Hematoxylin and Eosin staining). The plaque geometry was segmented manually and reconstructed for the FEM analysis, shown in Figure 7.5 (a) and (b). A thinner fibrous cap covered the lipids from the blood flow. The outer wall of the artery was extended to provide an artificial adventitial layer with a wall thickness of about 1.2mm at healthy part. First, a EB_FEM analysis was performed with only two material properties, they were the soft lipid region, with 1kPa Young's Modulus and 0.49 Poisson Ratio; the rest of the regions, including the arterial wall and fibrous cap, with a Young's Modulus of 1MPa and Poisson Ratio=0.45. In the simulation, the outer wall was fixed, and the luminal wall had a constant and uniform pressured load of 110mmHg. The geometry model and numerical mesh used in RB_FEM simulation were used directly to generate the EB_FEM model. Again, the regional geometry model (Figure.7.5 (b)) was used as the material property map. The element size was chosen to be 30μm for the realistic case.

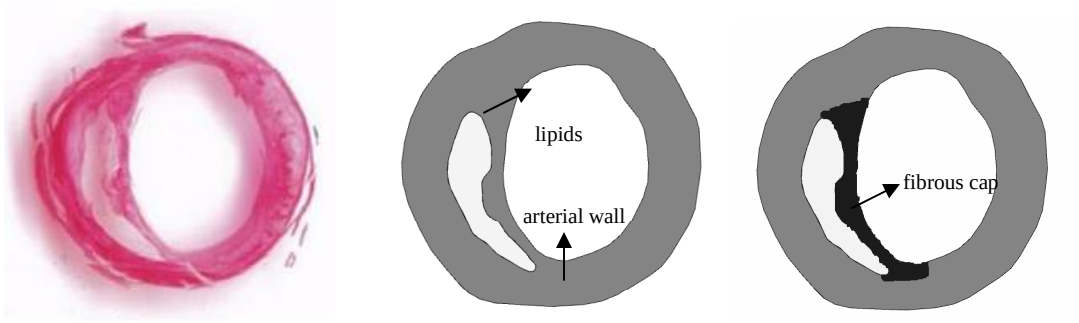

(a) (b) (c)

Figure 7.5 Geometry models based on a histology section of a human CEA specimen. (a) Histology image of a plaque sample; (b) segmented geometry of the plaque sample; (c) the definition for the fibrous cap shape.

The von Mises stress contours for the realistic model are presented in Figure 7.6(a,b). The stress distributions for RB_FEM (Figure 7.6(a)) and EB_FEM (Figure 7.6(b)) are nearly the same, with several stress concentration zones locating at the shoulder and the middle of the fibrous cap. However, the maximum stress value in the EB_FEM model is about 17.5% higher than those in RB_FEM. It may be caused by the discontinue boundary between the regions in EB_FEM as shown in Figure 7.6 (b) which will introduce an addition stress increase in the elements. Since the mesh was generated from the predefined region boundary in RB_FEM, the boundary is very smooth in RB_FEM model as shown in Figure 7.6 (a).

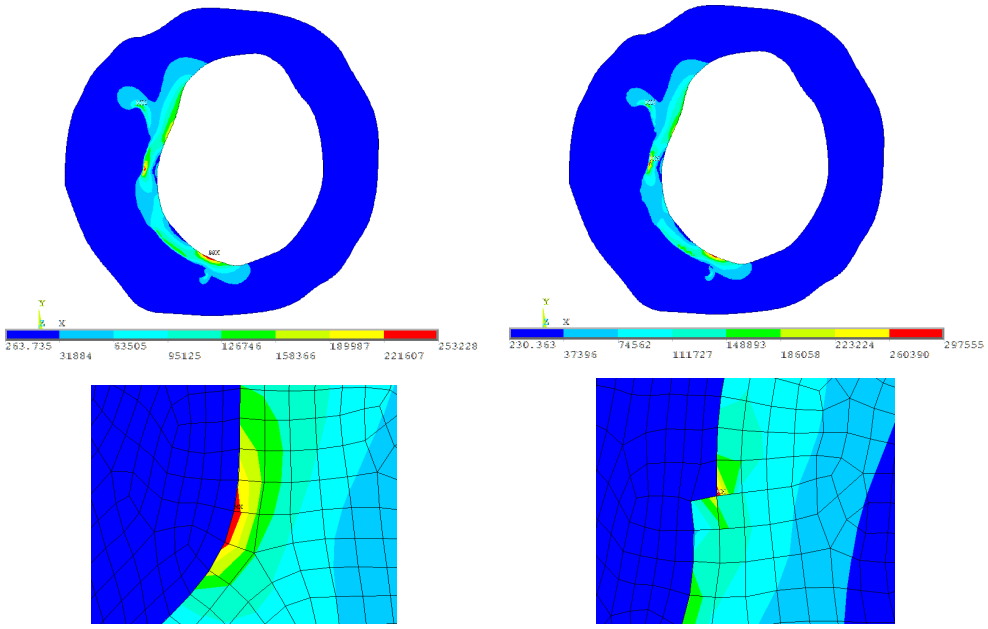

(a) (b)

Figure 7.6 Von Mises stress distribution for the realistic model. (a) Region based FEM with a zoom in; (b) Element based FEM with a zoom in. Unit: Pa

From the above analysis, if the RB_FEM and EB_FEM have the same material property map, mesh profile, and boundary conditions, the simulation results are almost identical.

7. 2 2D Plaque Stress Analysis with Real Human Carotid Plaque Samples

7.2.1 Plaque Geometry Preparation

Three plaque samples were selected for the stress analysis, which were obtained from the sections of human carotid endarectomy specimen through conventional wax histology procedures (Hematoxylin and Eosin staining), named sample 1, sample 2 and sample 3 respectively. The plaque geometry were segmented manually and reconstructed with 2D models. For each subject, the lipid and arterial wall boundary were defined by the HE microscope image(Figure7.7.a(1)) and polarized light microscope images as Figure 7.2.a(2) and a(3), the reconstructed geometries were shown in Figure 7.7.a(4), b(4) and c(4) for the three samples. The fibers in the arterial wall showed high intensity under polarized light microscope, while the lipid region usually was transparent with lower

intensity. In sample 1, there is a large lipid with a thin fibrous cap; in sample 2, a big lipid region with a thicker fibrous cap; and in sample 3, 2 small lipid regions with a thick fibrous cap. Due to the lack of adventitial layer in the endarectomy specimen, the arterial wall was expanded for a thickness of 1-1.4mm. In sample 2, due to the distortion of histology processing, the arterial wall was broken, thus in the reconstruction process, the broken part was restored to reconstruct the intact lumen.

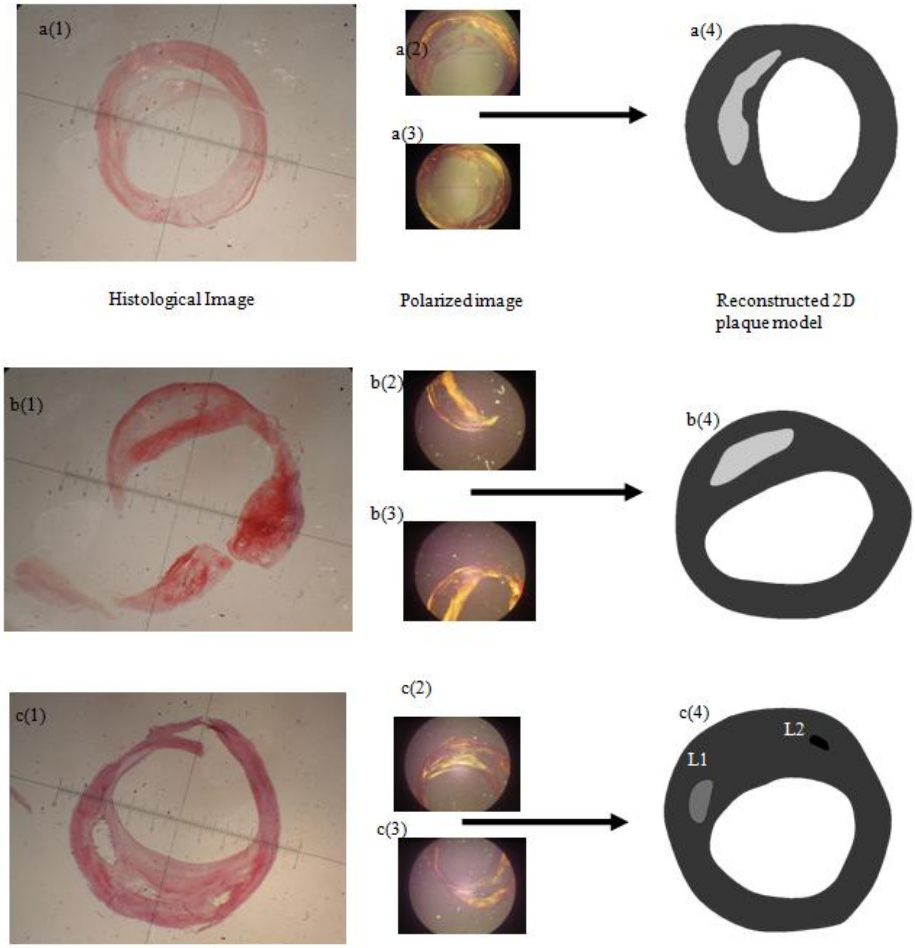

Figure 7.7 Plaque Geometry Reconstruction for 3 samples. (a): sample 1; (b): sample 2; (c):sample 3

7.2.2 Material Map Generation

The collagen distribution could be studied under the polarized light microscope, which had high intensity as shown in Figure 7.7(a(2),a(3)). The stability of the fibrous cap is the key factor of the plaque rupture, which is largely relied on the collagen fibres. Therefore

a region of interest was defined for each subject (ROI), surrounding the lipid region, including the fibrous cap. The red component of the polarized light microscope images was used to identify the existence of fibres. Since there were two or more polarized light microscope images to cover the whole lipid region, a linear registration procedure was performed to obtain the collagen information for the tissue surrounding lipid regions. The collagen distributions for the 3 samples around lipid regions are shown in Figure 7.8.

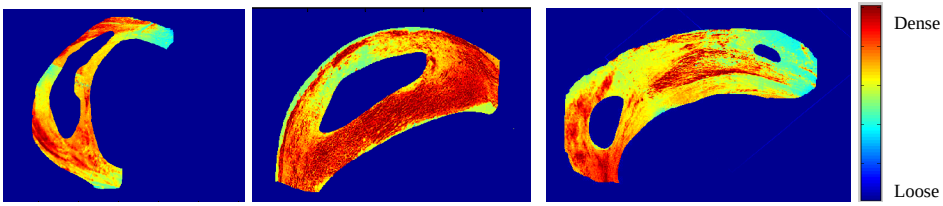

Figure 7.8 collagen distributions for the 3 samples around lipid regions

The lipid region was assumed to be isotropic linear with 1000 Pa for Young's Modulus with Poisson ratio of 0.49, the material properties in the arterial wall beyond the ROI was treated to be homogeneous, the transversal orthotropic model was used as in Table 7.2.

Parameters	E_x (MPa)	E_y (MPa)	G_{xy} (MPa)	u_{xy}	u_{yz}
Values	0.1	1	0.5	0.01	0.27

x: the direction vertical to the collagen orientation, y: collagen orientation; z: axial direction

Table 7.2 Transversal orthotropic material model

In the study, the collagen orientation was assumed to be circumferential according to the centre point of the lumen region, therefore, the collagen orientation in each location can be defined by the centre point. In ROI, the material properties will change according to the collagen content obtained by polarized light images as in Figure 7.8. Because of lack of the mathematical relationship between collagen content and material properties, several assumptions were made to obtain those material coefficients:(1)linear orthotropic material model was used; (2) Poisson ratio would keep constant no matter the changes of collagen content, (3) along the collagen orientation, E^*_y changed with collagen content, denser collagen, higher E^*_y , (4) E_x was also assumed to be constant which was

perpendicular to the collagen orientation, (4) G_{xy} was assumed to be half of E^*_y. A mathematical relation was proposed for assumption (3) as following in sample 1:

$$E^*_y = \begin{cases} E_y e^{0.0144*130-2.6} & 130 \geq I \\ E_y e^{0.0144*I-2.6} & 130 < I < 180 \\ E_y e^{0.0417*I-7.5} & 180 < I < 255 \end{cases} \quad [7.1]$$

I was the intensity value in Figure 7.8, range 0-255. Therefore for the most stiffness location, E^*_y was about 23MPa, and 0.48MPa for the softest part. Similar material map generations were conducted for sample 2 and sample 3, and E_y maps were shown in Figure 7.9. Sample 2 has a very stiff fibrous cap among the three samples.

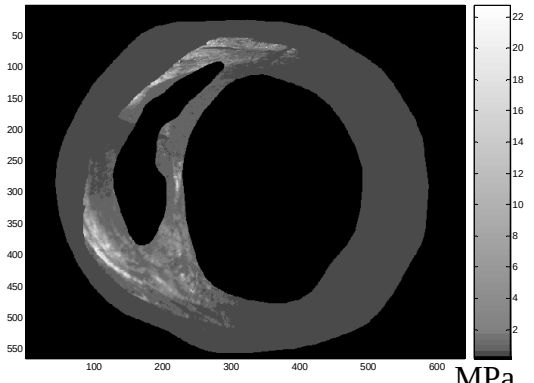

sample 1

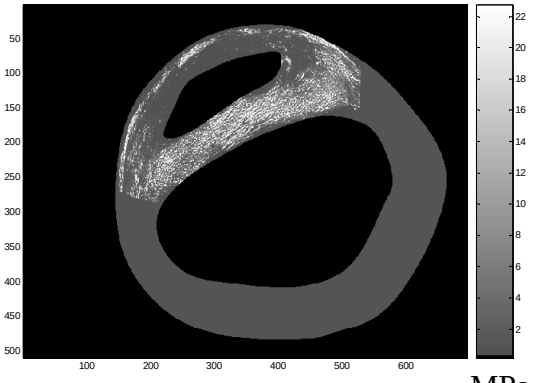

sample 2

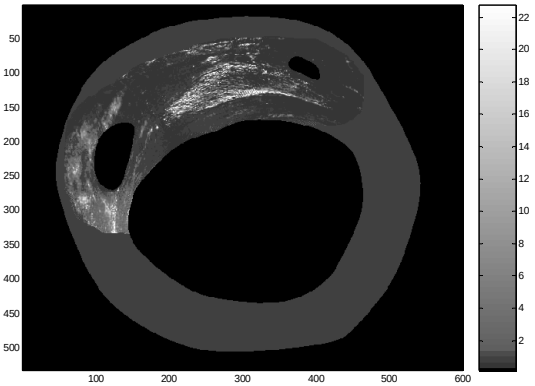

sample 3

Figure 7.9 E_y maps for 3 samples

7.2.3 Boundary Conditions

Each element in the computational domain was assigned a material model according to the collagen orientation and content. The outer wall was fixed to keep the sample in the

space, and a load of 110mmHg pressure was applied in the lumen wall. The homogeneous material model was also applied to 3 plaque samples to compare the difference, in which $E_y = 1MPa$.

7.2.4 Stress Distribution

The stress analysis results were shown in Figure 7.10

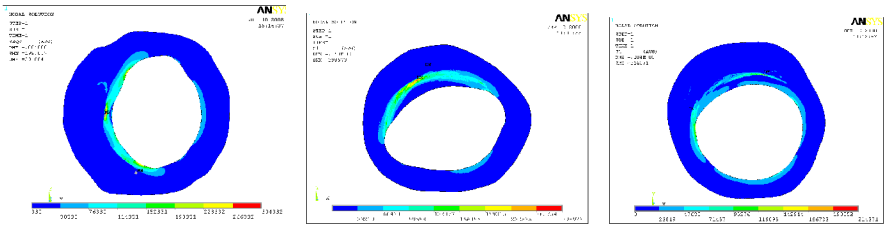

sample 1 sample 2 sample 3

Figure 7.10 FPS distributions for 3 studied plaque samples. Unit: Pa

The maximum First principle stress (FPS) for the three subjects are 304kPa, 299kPa, and 214kPa. In sample 1, three local stress concentrations can be found in the fibrous cap, two in the shoulder regions, and one in the middle, the similar stress distribution can be found in sample 2. In sample 3, because of the two small lipids (L1 and L2), for L1, only one stress concentration can be found near the lumen side, while for L2, the stress concentration is near the lipid region. The comparison with the homogeneous material model also was performed for the three samples, and the difference in the fibrous cap region was summarized as in Figure 7.11 with histogram of stress distributions.

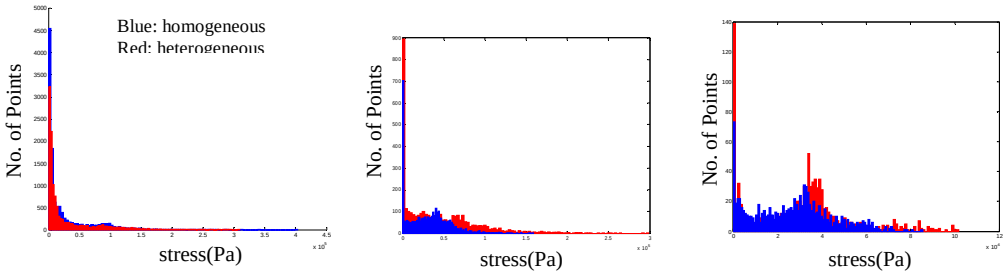

sample 1 sample 2 sample 3

Figure 7.11 FPS difference between homogenous and heterogeneous material model

For sample 1, the stress based on the collagen distribution around the lipid region is similar as the homogeneous analysis, while the stress level is lower, especially for the maximum stress value, 309kPa compared to 400kPa for homogeneous model; for sample 2 and sample 3, the stress level is higher than the homogeneous analysis, and also higher for the maximum stress value. Therefore based on the collagen distribution, the stress distribution can vary greatly compared to the homogeneous cases, and the stress level can be lower or higher.

7.2.5 Strain Distributions

The first principle strain (Pstrain) for the 3 samples is shown in Figure 7.12. Usually in the shoulder of the fibrous cap, there are regions with large strain, also some of high strain regions near the lipid core, which may come from the sudden change of the material properties from arterial wall to the very soft lipid region. The comparison with the corresponding homogenous models was shown also in the Figure 7.12, the second column. Though Pstrain distribution for sample 1 has the similar trend as the homogeneous model, it is slightly lower when coming to high strain regions, similar results can be found in sample 2 and 3. In sample 2, Pstrain in the fibrous cap is much lower than the homogeneous model, which may resulted from the stiff collagen fibres. For the studied 3 plaque samples, stress analysis with homogeneous material model may have the tendency to overestimate the strain level in the fibrous cap.

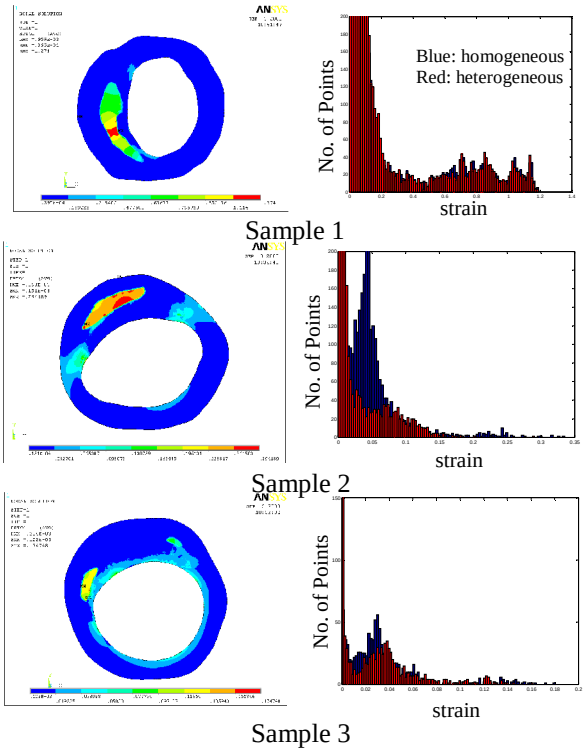

Figure 7.12 First principle strain distribution and comparison with homogenous models

7.2.6 Comparison with the 3 Samples

Usually the critically high stress in the fibrous cap is treated as a possible key factor for the rupture of the thin fibrous cap, however purely based on the stress results maybe misleading for the rupture risk assessment. Because a thin fibrous cap with dense and well structured collagen fibres can sustain a higher stress, and the fibrous cap with degraded collagen fibres may rupture with a low stress. Thus, when coming to the rupture risk assessment, the combination of stress factors with fibrous cap structure would be desirable. In the study, the collagen content in sample 1 is less than the other two samples, and has a thinner fibrous cap, the predicted stress and strain in the sample 1 are also much higher, thus the rupture risk in sample 1 could be higher than sample 2 and sample 3; while for sample 2 and sample 3, though the stress in sample 2 is higher than sample 3, because of the dense collagen fibres, thicker fibrous cap, and with similar level of strain distributions, the rupture risk in sample 2 might be lower than sample 3.

7.3 Discussion

Soft tissue in nature is heterogeneous with varied fiber content, direction, and weaved structure. The local structure could affect the material properties significantly. Research in bone mechanics shows that the variations in trabecular morphology that occur over small length scales 10-100μm can have appreciable effects on the apparent mechanical properties, which impose uncertainty of the stress distribution(Vajjhala et al., 2000). It would be expected that the material variations in the plaque region can affect the mechanical behavior of the plaque stability in a similar way. Dense and well-organized fibers can bear strong stress, while weakened and disorganized fibers are prone to fracture, however it is difficult to incorporate this information into the RB_FEM method. With EB_FEM, the local structure, and fiber content can be included in the stress analysis.

In the study, a stress analysis by EB_FEM using the histological study of the diseased artery was performed. Histology analysis provides a gold standard to characterize the local structure of the arterial plaque with information such as fiber structure, content, etc. With EB_FEM, it becomes applicable to incorporate this structure information into an FEM model to give more detailed mechanical information than with RB_FEM. The stress analysis with proposed material changes in a realistic plaque sample showed that, a well organized fiber region may induce a higher stress value due to its stiffer material property, however the region can still be treated as a safe structure since this type of fibrous cap can bear higher stress. If the fibrous cap is weaker, it has to be treated as an unstable cap even though the stress level is not very high. Therefore with the local structure information, combining with corresponding stress levels in the fibrous cap, the rupture risk assessment may be more reliable and meaningful.

Recently, inflammation and immune response contributing to the atherogenesis have garnered increased interest (Libby et al., 2002). Two processes related to inflammation may participate in disrupting the fibrous cap. Firstly, the local production of inflammatory mediators or cytolytic can cause the endothelial cell death, secondly the expression and activation of matrix metalloproteinases (MMPs) specialized in degrading components of the sub-endothelial basement membrane will be unregulated greatly by

the inflammatory mediators and oxidized lipoproteins. The up-regulated MMP play the major role in the degradation of collagen and other extracellular matrix components, which will weaken the fibrous cap. Huang et al (Huang et al., 2001) once mentioned that 'although macrophage infiltration is important in determining plaque material properties, there are currently no reliable methods of incorporating the effects of inflammation into finite element models'. While with EB_FEM, if the inflammation in that element, and its influence to the local material property could be qualified, it would be feasible to include the inflammation in FEM models. At present, Magnetic Resonance Imaging (Trivedi et al., 2006) is able to image the inflammation in the plaque region. With more information available for the plaque stress analysis, it is desirable to use this information to obtain a more realistic mechanical prediction.

7.4 Summary

In this chapter, the element based material model under the framework of finite element method was developed, which can incorporate the local structure characteristics to provide more detailed mechanical predictions. In the first part, EB_FEM was validated with certain examples and compared with the conventional FEM, including geometry sensitivity test, boundary condition variations, element type, mesh independence test, based on idealized and a realistic model from histology analysis of a human plaque specimen. Both EB_FEM and RB_FEM can produce the identical stress analysis results if the same conditions were used. Then EB_FEM was applied to the stress analysis in 3 human atherosclerotic plaque samples with assumed material property changes in the fibrous cap, representing different clinical scenarios. The stress level and absolute value were affected by the material property change in the fibrous cap, and a local high stress may not always predict the high rupture risk due to the different fibrous cap structure integrates. Therefore the stress analysis with the local material property variation would give more insight into the stability of the plaque. EB_FEM has the potential to incorporate local material property changes, fiber structure, and inflammation response, which will advance the stress analysis in atherosclerotic disease.

Chapter 8 Discussion and Conclusion

8.1 Discussion

Atherosclerotic plaque has been considered to be one of the leading causes of death all over the world, caused by the plaque rupture and subsequent thrombus formation. Until now the exact mechanism of plaque rupture is not clear. From biomechanical aspect, the rupture can be considered to be a mechanical failure event. Therefore it is essential to numerically predict plaque stress with high accuracy; results from those models will be helpful in understanding how and why plaque ruptures.

Numerical modeling has been developed for a long time since it has the advantages of interrogation of the consequence arising from controlled variation of the simulated equations, validating, testing and predicting of analytical theories (Landman 2005). The question is do we believe the nature is written in numbers? A similar theme could be found in Stoppard's play *Arcadia* (Stoppard Tom 1993). In the occasion during a conversation about Newton's laws of motion, Thomasina states: "if you could stop every atom in its position and direction, and if your mind could comprehend all of the actions thus suspended, then if you were really good at algebra you could write the formula for all of the future; and although nobody can be so clever as to do it, the formulas must exist just as if one could". However the applications of these formulas lead to the equations too complex to be solved. Until now, there is no analytical solution for Navier-Stokes equation, the problem of its existence and smoothness has been named one of the seven most important open problems in mathematics (Clay Mathematics Institute). From last century, computer simulation has come to the stage and served as an indispensable powerful tool of discovery, supplementing and complementing experiments and analytical theories. The dramatically development in computer hardware architecture, noval algorithms(for example, finite volume method, finite element method), and new computational platforms(for example, parallel and grid computing) in the last several decades has opened the door for numerical study of systems with forbidding complexity (Landman 2005), for example fluid flow simulation in 3D context. Those advances have resulted in substantial progress and a number of discoveries, in which there lies atherosclerotic plaque stress prediction.

Plaque stress has been studied for several decades from 2D structure only to fully coupled 3D plaque stress in both structure dynamics and hemodynamics. The extremely high stress locations in plaque region have been considered to be main factors responsible for plaque rupture. The biggest challenge lies in how to predict plaque stress with patient specific simulations and high accuracy. For example: realistic geometry reconstruction, patient specific boundary conditions and material models. Studies have demonstrated that 2D plaque models are prone to overestimate the stress levels because of simplifications. 3D plaque stress analysis with coupled fluid structure interaction emerges to advance the accuracy of analysis, not just the stress in the plaque structure, but also the flow pattern around the plaque. In this project, several aspects regarding plaque stress analysis were tackled and discussed: (1) FSI procedure for plaque stress analysis (Chapter 3); (2) 3D plaque geometry reconstruction from *in-vivo* MRI (Chapter 4); (3) patient specific plaque stress analysis (Chapter 5 and 6); (4) multi-scale study of plaque stress combining with histological analysis (Chapter 7).

The development of medical imaging provides the possibility of realistic 3D plaque geometry reconstruction with a high resolution. However the resolution of MR images is not high enough for tiny plaque component reconstruction at present. Furthermore the contrast is not high, which imposes certain uncertainties on plaque stress analysis based on *in-vivo* MRI. The study on plaque components' effects to plaque stress distribution in Chapter 3 showed that plaque stress level is significantly affected by the thickness of fibrous cap compared to lipid size, therefore efforts in increasing the accuracy of fibrous cap reconstruction from *in-vivo* MRI need to be paid in the near future. The improved resolution/quality in plaque imaging with newly-developed MRI protocols would generate more realistic stress predictions.

Due to the complicated structure and irregular geometry of carotid plaques, limitations in *in-vivo* MRI resolution and contrast, the manual segmentation was used in the project, rather than semi-automatic or automatic methods for better segmentation quality especially in lipid region and fibrous cap. The framework for incorporating multi-sequence MR images for plaque reconstruction helps to reduce the segmentation

uncertainties, while the linear registration may still have limitations to fully correct the distortions during MR imaging. The followed plaque geometry reproducibility study showed that the segmentation in lipid region has greatest uncertainties compared to arterial wall segmentation based on *in-vivo* MR images used in the project, and the stress level also significantly depended on the accuracy reconstruction of lipid region because the lipid region segmentation will define the fibrous cap structure in our reconstruction procedure. Therefore the accurate segmentation and reconstruction of plaque components is one of the fundamental issues in the development of medical imaging based computational models.

A proper shrinkage procedure has been applied in 3D plaque reconstruction, which will ensure the plaque geometry will recover *in-vivo* configuration under physiological loadings. During MR scanning, the plaque was supported by the surrounding tissues and pressurized by the blood pressure, therefore the plaque geometry reconstructed from *in-vivo* MRI was under axial stretch and pressurization. Since stress analysis starts at zero loadings, the shrinkage in radial and axial direction was applied before the final 3D reconstruction. The shrinkage in radial direction was based on a trial-error method to define a proper rate from the data provided in CCA. Due to the lack of information regarding axial shrinkage, a 10% was applied based on existed literatures. The discussion on the stress levels caused by different applied axial stretch ratios demonstrated that the axial stretch ratio will greatly affect plaque stress patterns and levels. Therefore how to obtain patient specific axial stretch is also one of the important issues in plaque stress analysis.

The study on plaque geometry reconstruction reproducibility and its effects to plaque stress analysis paved the way for the followed stress analysis on multiple subjects, and built the confidence of the accuracy and reliability of the computational models. A group of 4 subjects was studied first with fully coupled FSI. General stress results were confirmed to the existed research. For example, high stress concentrations can be found in the plaque region, lipid core experiences low stress levels. The studied 4 subjects were experiencing different plaque burden, therefore a comparison in terms of stress levels,

morphological features were made to provide useful information for clinic. It was found plaques with thin fibrous cap and large lipid core may have a much higher stress levels, with stress concentrations in the fibrous cap, and stenosis degree may not be a good predictor for plaque rupture risk. Furthermore, the introduction of wall tensile stress variation may shed lights on plaque fatigue. However due to the small size of the studied group, and lack of information in biological abnormalities, the results needed to be strengthened by a larger group of subjects.

As the further development from the stress analysis on the 4 subjects in Chapter 4, stress analysis was performed on 20 patients in two groups (12 for symptomatic and 8 for asymptomatic) in Chapter 6, the stress level was assessed for each group and compared between them. The stress levels in symptomatic patients are significantly higher than that in asymptomatic, with much thinner fibrous cap and larger lipid core. Therefore the stress level may be used for plaque rupture risk assessment in the future if a critical stress value could be defined. Cheng (Cheng et al., 1993) proposed 300kPa as a critical value for predicting plaque rupture in coronary plaques, and the value has been used in Chapter 3 for plaque rupture risk classification, however the critical value could be different in carotid plaques. From the stress analysis on 20 subjects, the mean stress value for symptomatic patients is around 200kPa. A question could be asked whether 200kPa is the critical value for carotid plaque rupture. From Chapter 6, it has been found that there is a difference in stress levels between vulnerable and stable plaques. From Redgrave's [Redgrave et al., 2008] study, the critical fibrous cap thickness for plaque rupture was considered to be 200μm, much thicker than the critical value in coronary plaques(65 μm), then the critical stress value for carotid plaque rupture might be lower than that in coronary plaques due to the thicker critical fibrous cap thickness. Although the value of 200kPa can not be concluded as the critical stress level for carotid plaque rupture, the study does demonstrate the stress value could be used for plaque rupture prediction if extremely high stress exists.

Based on 20 studied subjects, plaque morphological features also have been studied and correlated with plaque stress in Chapter 6. The results showed that plaques with thinner

fibrous cap, larger lipid core usually experience higher plaque stress, the stenosis degree can not predict the stress levels properly from the fact that stenosis degree between the two groups lies in the same range. The correlation between fibrous cap thickness, lipid core size and stress levels confirmed the definition for a vulnerable plaque, which is characterized by a thin fibrous cap and large lipid pool. Although the statistically significance in fibrous cap thickness and lipid core between symptomatic and asymptomatic group was not reached, partially due to the small size of studied subjects, the results have implied those morphological features are closely related to plaque vulnerability. By investigating local extreme stress concentration locations among those 20 subjects, stress concentration locations occur at plaque shoulder regions, the frequent rupture sites. Furthermore, plaques with a higher stenosis are more likely to have extreme stress conditions upstream, indicating upstream of plaques can be more vulnerable than downstream.

Until now, the direct link between plaque rupture and extreme stress level has not been established. In this research we tried to find the indirect evidence for the hypothesis in Chapter 5: rupture caused by extreme plaque wall stress. 3 TIA patients with ruptured plaques were studied by one-way FSI, the pre-ruptured plaque geometries were reconstructed by rebuilding the fibrous cap structure. Stress analysis shows that the rupture sites do associate a local high wall tensile stress for all subjects. Furthermore, 5 more reconstructions were done for each subject in order to account for the reconstruction uncertainties, still local high stress concentrations can be found in the rupture sites. The coincidence between local high stress concentrations and rupture sites could provide indirect evidence for stress induced plaque rupture hypothesis. It should be mentioned that the hypothesis of rupture caused by extreme plaque wall tensile stress only one of the hypothesis, not the unique one. A comprehensive study on plaque structure dynamics and biology abnormality will be helpful in understanding the mechanism of plaque rupture.

By quadratic surface fitting, the curvedness was investigated for 20 subjects in the fibrous cap surface. Generally, greater curvedness, higher stress level, a positive correlation has

been found for curvedness and stress level. Stress prediction by FSI simulation needs to take long computational time and is hard for convergence. From previous studies, it is well accepted that thin fibrous cap and large lipid pool are associated with vulnerable plaques, and a thinner fibrous cap can cause a very high stress. There may exist relationship between plaque stress and plaque morphological features. The comparison among curvedness, fibrous cap thickness, and wall tensile stress leads to the proposition of wall stress prediction by plaque morphological features. The multi-regression between fibrous cap thickness, curvedness and wall tensile stress was performed, the predicted stress shows similar patterns as the stress distributions from FSI simulation, and the simulation time is greatly reduced, less than one hour if plaque geometry has been reconstructed. It is expected in the future, plaque stress levels and distributions can be quickly obtained by the combination of morphological features, such as fibrous cap thickness, surface irregularities, lipid core features, inflammation activities, collagen distributions, etc.

Another disadvantage of present FSI plaque stress is that the local structure information can not be incorporated into FEM simulation. Histology study on atherosclerosis plaque is considered to be the golden standard of identifying vulnerable plaques, therefore a new procedure for stress analysis was developed to combining conventional FEM and histology study, that is element based FEM in Chapter 7. In this method, the local structure information, mainly collagen content from polarization images of histological sections, was involved in the FEM model by defining different material stiffness according to the collagen distribution. EB_FEM can produce the identical stress results with conventional FEM under same conditions. Stress predictions by EB_FEM show that the stress levels and absolute values are affected by local material properties. The stress analysis with local structure information would give more insights into the stability of plaques. EB_FEM has the potential to incorporate local material property changes, fiber structure, inflammation response, etc., which will advance the stress analysis in the atherosclerotic disease with multi-scale involvement.

8.2 Limitations

The project was focusing on the mechanical behaviors of carotid atherosclerotic plaques in order to seek potential biomechanical factors for plaque rupture risk assessment. Rupture of the fibrous cap is a very complex process. It is not only the mechanical factors that matter, but other abnormalities in tissue and cells, such as elevated inflammatory activity, degraded collagen structures, may also influence the rupture process (Richardson et al., 2002). Comprehensive plaque vulnerability assessment should involve a combination of systemic markers, morphological features, and biomechanical factors. Considering only a few factors may not give a complete picture of plaque rupture risk.

The high-resolution *in-vivo* MRI could nicely capture plaque compositions, and morphology features, and may be adequate for qualitative description, but it is limited for quantitative evaluation for plaque stress analysis. The imaging of a very thin fibrous cap could be beyond the imaging ability of the modern MRI modality. Our study has demonstrated that the plaque components reconstruction based on *in-vivo* MRI has different impacts on stress predictions. Attention needs to be paid when interpreting plaque stress results with patient situation, the uncertainties should be acknowledged.

Although FSI simulation can provide a more realistic stress prediction than 2D/3D structure stress analysis, some major limitations needed to be acknowledged in FSI modeling: (1) The arterial wall model used in the project is crude, the real arterial wall is anisotropic and viscous-elastic; the collagen fibers' orientation and density also influence the mechanical properties of the arterial wall (Holzapfel et al., 2002). (2) Laminar flow assumption may not be valid in the post-stenosis flow due to the flow instability. Non-Newtonian effect also has not been included for fluid simulation. However, their influence to the stress analysis is expected to be insignificant. (3) Patient specific material modeling and patient specific boundary conditions were not applied. Although from previous study, the varied material properties have less effect on stress level, the patient specific material modeling will generate more accurate stress results. The importance of boundaries has been acknowledged in the beginning of plaque stress analysis. Due to the lack of information for all subjects, patient specific boundaries have not been employed.

(4) The residual stress was not fully included, the pre-stretch can help incorporate part of residual stress, however the residual stress characterized by opening angle was not applied since it is hard to obtain those information with *in-vivo* conditions and limited influence on final plaque stress levels from the 2D plaque stress study in Chapter 6.

The limitation of including local structure of plaques in conventional FEM has been discussed in Chapter 7, and a new procedure (EB_FEM) has been suggested. Although EB_FEM can incorporate certain information from histological analysis for plaque stress analysis, it is still under development to reduce some assumptions: (1) collagen content/orientation characterization; (2) material properties modeled by collagen content; (3) the framework from biochemistry to biomechanical study; (4) stress analysis from 2D to 3D, and correlation with biological abnormalities.

The stress prediction by morphological features has been tried in the project, which will greatly reduce the computational time, and make it possible for clinical routine usage. However not all morphological features are considered in the prediction equation, only fibrous cap thickness, and fibrous cap surface irregularities. As discussed before, some other features such as lipid core size, inflammation activities, also will affect the stress results. Therefore a prediction equation with comprehensive parameters from plaque morphological features, and biochemical factors will be desirable.

8.3 Conclusion

In this PhD project, 3D computational plaque stress analysis was performed for multiple patients based on *in-vivo* MRI data by fluid structure interactions. The main results arose from this project are:

- The developed one-way and two-way FSI can generate meaningful stress information regarding plaque rupture. The study on the effects of plaque components to stress distributions confirmed that fibrous cap thickness and lipid core size, the main characteristic features of a vulnerable plaque, are closely related to plaque vulnerability.

- Based on the current MR imaging technology, the 3D plaque geometry reconstruction reproducibility from MRI data was assessed. The current *in-vivo* MRI in the carotid plaque could provide useful and reliable information for plaque morphology. While the accuracy of stress analysis based on plaque geometry is subject to MR image quality, the improved resolution/quality in plaque imaging with newly-developed MRI protocols would generate more realistic stress predictions.
- The study on local extreme stress distributions and their correlation with rupture sites based on 3 transient ischemic patients provided indirect evidence for the hypothesis on plaque rupture caused by stress concentrations at plaque region, and it also strengthens the necessary of stress computation in plaque region for assessing plaque stability.
- Stress analysis on 20 subjects will fill the gap in current literature in 3D FSI plaque stress with different patient groups. The findings in different stress levels between symptomatic and asymptomatic patients will lead to better understanding of plaque rupture and patient management.
- Morphological features analysis and their correlation with plaque stress shed some lights on plaque vulnerability in terms of plaque stress distribution. With sufficient validation, these results may lead to plaque stress prediction by morphological features for clinical routine application, rather than FSI simulation, which require massive computational resource.
- Plaque stress analysis combined with histological analysis can potentially link biomechanical factors with local plaque structure (collagen), inflammation activity (macrophages), etc. The multi-scale study may significantly advance the understanding of biomechanical factors' role in plaque rupture if the relationship between biomechanical environment and biological process can be defined.

The progress in numerical modeling in stress analysis has made fluid-structure-interaction analysis with patient specific plaque models possible. Extreme stress distributions in the plaque region could be predicted, and may be used for plaque rupture risk assessment, these assessments could be helpful in clinical practice. The combination

of plaque MR imaging analysis, computational modeling, and clinical study/validation would advance our understandings of plaque rupture, prediction of possible plaque rupture, and establish new procedures for patient diagnose, management, and treatment.

8.4 Further Development

The study in this research has set up the framework for plaque stress based on modern medical imaging modality for plaque rupture risk assessment. Future investigations and efforts can be made in the followings:

Less-labor and robust plaque geometry reconstruction: In this research, because of the low intensity contrast for plaque components, segmentation and 3D geometry reconstruction were done manually, which will take long time and need skilled researchers. With new developments in MR imaging technology and increased quality of plaque images, it could be possible to develop toolkits for plaque components segmentation and reconstructions, making clinical routing application possible.

Patient specific boundary conditions and material properties modeling: Due to lack of patient specific boundary conditions for each simulation, the flow boundaries used here are not patient specific. Also the residual stress/strain are lack, such as axial pre-stretch, etc. If those data are available, they should be integrated into the mechanical modeling aspects of our approach, and their effects on stress predictions should then be determined. Although the material models may not give significant effects on plaque stress distributions, the patient specific material models are still desired. The effects on stress distributions caused by the varied material properties should be determined and investigated for the current findings on plaque stress.

Combination between biomechanical and biochemistry analysis: Histology analysis of plaque samples has been considered as the golden standard for identifying plaque components and the vulnerability. However the combination of stress analysis and histology study is not so obvious. The developed method for using collagen information in FEM with biomechanical models needs to be improved.

Statistical study on biomechanical factors and plaque rupture risk assessment: More subjects are needed for stress analysis in the future to enhance the findings from this study. The stress level in symptomatic group is significantly higher than asymptomatic group, while a proper stress level value is needed to be determined in the future to classify the severity of patients according to the stress analysis.

Comprehensive study on the relationship between plaque morphological features and plaque stress patterns: stress predictions have been tried by simple equation combing fibrous cap thickness and curvedness. However there are more features which affect stress distributions, therefore with better definition of other plaque features, the predicted stress from plaque morphological features will be much closer to the predicted results from FSI simulation, providing a quicker way to obtain plaque stress distributions. The general equation, accuracy and reliability need to be resolved.

Multi-scale and multi-discipline study on plaque initiation, development, and rupture: The biomechanical factors in plaque initiation, development and rupture need to be studied in a systematical way. Only putting the biomechanical analysis in the whole picture of atherosclerosis plaque, we can better understand how and why plaque rupture, predict and prevent plaque rupture.

References

Ansys documents: http://www.ansys.com/

Arroyo, L.H., Lee, R.T. The unstable atheromatous plaque, Canadian Journal of Cardiology, 14(suppl):11B-13B, 1998

Arroyo, L.H., Lee, R.T. Mechanisms of plaque rupture: mechanical and biological interactions. Cardiovascular research, 41(2):369-375, 1999

Ashwini, S., Soundararajan, D.K., Hunter, W.J., Agrawal, D.K. Comparison of vascular smooth muscle cell apoptosis and fibrous cap morphology in symptomatic and asymptomatic carotid artery disease. Annals of Vascular surgery, 17(1):1-8, 2003

Augst, A.D., Ariff, B., Thom, S.A.G.McG., Xu, X.Y., Hughes, A.D. Analysis of complex flow and the relationship between blood pressure, wall shear stress, and intima-media thickness in the human carotid artery. American Journal of Physiology-heart and circulatory physiology, 293(2): H1031-1037, 2007

Avolio, A., Jones, D., Tafazzoli-Shadpour, M. Quantification of alterations in structure and function of elastin in the arterial media. Hypertension, 32(1): 170-175, 1998

Bank, A.J., Versluis, A., Dodge, S.M., Douglas, W.H. Atherosclerotic plaque rupture: A fatigue process? Medical hypotheses, 55(6):480-484, 2000

Banks, J., Bressloff, N.W. Turbulence modeling in three-dimensional stenosed arterial bifurcations. Journal of Biomechanical Engineering, 129(1): 40-50,2007

Barger, A.C., Beeuwkee, R., Lainey, L.L., Silverman, K.J. Hypothesis: vasa vasorum and neovascularization of coronary arteries. A possible role in the pathophyiology of atherosclerosis. N Engl J Med, 310:175-177, 1984

Barrett, S.R.H., Sutcliffe, M.P.F., Howarth, S., Li, Z.Y., Gillard, J.H. Experimental measurement of the mechanical properties of carotid atherothrombotic plaque fibrous cap. Journal of Biomechanics, 42(11):1650-1655, 2009

Beattie, D., Xu, C., Vito, R., Glagov, S., Whang, M.C. Mechanical analysis of heterogeneous, atherosclerotic human aorta. J Biomech Eng, 120(5): 602-607, 1998

Benjamin, C.B, van der Meulen M.C. Finite element models predict cancellous apparent modulus when tissue modulus is scaled from specimen CT-attenuation, Journal of Biomechanics, 37:613-621, 2004

Bezerra, H.G., Higuchi, M.L., Gutierrez, P.S., Palomino, S.A., Silvestre, J.M., Libby, P., Ramires, J.A. Atheromas that cause fatal thrombosis are usually large and frequently accompanied by vessel enlargement. Cardiovasc Pathol, 10(4):189-196, 2001

Biasucci, L.M., Liuzzo, G., Angiolillo D.J., Sperti G., and Maseri A. Inflammation and acute coronary syndromes. Herz, 25(2): 108-112, 2000

Bluestein, D., Alemu, Y., Avrahami, I., et al. Influence of microcalcifications on vulnerable plaque mechanics using FSI modeling. Journal of Biomechanics, 41(5):1111-1118, 2008

Borges, L.F., Gutierrez, P.S., Marana, H.R.C., Taboga, S.R. Picrosirius-polarization staining method as an efficient histopatological tool for collagenolysis detection in vesical prolapse lesions, Micron, 38:580-583, 2007

Boussel, L., Herigault, G., Sigovan, M., Loffroy, R., Canet-Soulas E., Douek P.C. Modified electrocardiograph-triggered black-blood turbo spin-echo technique to improve T1-weighting in contrast-enhanced MRI of atherosclerotic carotid arteries. Journal of Magnetic Resonance Imaging, 28(2):533-537,2008.

Burke, A.P., Farb, A., Malcom, G.T., Liang Y.H., Smialek, J., Virmani, R. Coronary risk factors and plaque morphology in men with coronary disease who died suddenly. N Engl J Med, 336(18): 1276-1282, 1997

Cai, J., Hatsukami, T.S., Ferguson, M.S., Kerwin, W.S., Saam, T., Chu B., Takaya, N., Polissar, N.L., Yuan, C. In vivo quantitative measurement of intact fibrous cap and lipid-rich necrotic core size in atherosclerotic carotid plaque. Circulation, 29:3437-3444,2005

Caro, C.G., Fitz-Gerald, J.M., Schroter, R.C. Atheroma and arterial wall shear. Observation and proposal of a shear dependent mass transfer mechanism for atherogenesis. Proc. R. Soc. London, Sec. B. 177(1046): 109-159, 1971

Carr, S., Farb, A., Pearce, W.H., Cirmani, R., Yao, J.S.T., Bassiouny, H.S., Gloviczki, P. Atherosclerotic plaque rupture in symptomatic carotid artery stenosis. Journal of vascular surgery, 23(5):755-766,1996

Casscells, W., Naghavi, M., Eillerson, J.T. Vulnerable atherosclerotic plaque: a multifocal disease. Circulation, 107(16): 2072-2075, 2003

CFX documents, version 11.0 : http://www.ansys.com/

Chau, A.H., Chan, R.C., Shishkov, M., MacNeill, B., Iftimia, N., Teraney, G.J., et al. Mechanical analysis of atherosclerotic plaques based on optical coherence tomography. Ann Biomed Eng, 32(11): 1494-1503, 2004

Chen, J., Lu, X.Y. Numerical investigation of the non-Newtonian blood flow in a bifurcation model with a non-planar branch. Journal of Biomechanics, 37(12):1899-1911,2004

Cheng, G.C., Loree, H.M., Kamm, R.D., Fishbein, M.C. and Lee RT. Distribution of circumferential stress in ruptured and stable atherosclerotic lesions. A structure analysis with histopathologicla correlation. Circulation, 87(4):1179-1187, 1993

Cheng, G.C., Briggs, W.H., Gerson, D.S., Libby, P., Grodzinsky, A.J., Gray, M.L., Lee, R.T. Mechanical strain tightly controls fibroblast growth factor-2 release from cultured human vascular smooth muscle cells. Circ. Res. 80:28-36,1997

Chien, S. Effects of disturbed flow on endothelial cells. Ann Biomed Eng, 36(4):554-562, 2008

Chuong, C.J., Fung, Y.C. Three-dimensional stress distribution in arteries. Journal of Biomedical Engineering 105(3):268-274, 1983

Chuong, C.J., Fung, Y.C., J. Biomech. Eng., 108(2):189-192, 1986

Clay Mathematics Institute. The Millennium Prize Problems,
http://www.claymath.org/millennium/

Davies, M.J. A macro and micro view of coronary vascular insult in ischemic heart disease. Circulation, 82(3 suppl): II38-46, 1990

Degroote, J., Bathe, K.J., Vierendeels, J. Performance of a new partitioned procedure versus a monolithic procedure in fluid-structure interaction. Computers and structures 87:793-801, 2009

Devuyst, G., Ruchat, P., Karapanayiotides, T., Jonasson, L., Cuisinaire, O., Lobrinus, J.A., Pusztaszeri, M., Kalanqos, A., Despland, P.A., Thiran, J.P., Boqousslavsky, J. Ultrasound measurement of the fibrous cap in symptomatic and asymptomatic athermanous carotid plaques. Circulation, 111(21): 2776-2782, 2005

Dunmore, B.J., McCarthy, M.J. Ischemic symptoms are linked to immaturity of microvessels within plaques. Journal of Vascular surgery, 45(1):115-159, 2007

Ebenstein, D.M., Coughlin, D., Chapman, J., Li, C., Pruitt, L.A. Nanomechanical properties of calcification, fibrous tissue, and hematoma from atherosclerotic plaques. J Biomed Mater Res A., DOI: 10.1002/jbm.a.32321, 2008

Emmanuel, T., Jean-Francois, T., Joel, C., Emmanuelle, S., Fabrice, B., Pierre, et al. Reproducibility of High-Resolution MRI for the Identification and the quantification of carotid atherosclerotic plaque components. Stroke, 38:1812-1819,2007

Eymard, R., Gallouet, T., Herbin, R. Finite Volume Methods in Handbook of Numerical Analysis. Editor: Ciarlet P.G., Lions J.L. Vol 7, 713:1020,1997

Falk, E., Shah, P.K., and Fuster, V. Coronary plaque disruption, Circulation, 92(3): 657-671, 1995

Farb, A., Burke, A.P., Tang, A.L., Liang, T.Y., Mannan, P., Smialek, J., and Virmani, R. Coronary plaque erosion without rupture into a lipid core. A frequent cause of coronary thrombosis in sudden coronary death. Circulation, 93(7): 1354-1363, 1996

Farhat, C., van der Zee, K.G., Geuzaine, P. Provably second-order time-accurate loosely-coupled solution algorithms for transient nonlinear computational aeroelasticity. Comput. Methods Appl. Mech. Engrg. 195: 1973-2001, 2006

Ferrara, A., Pandolfi. Numerical simulation of arterial plaque ruptures. Int J mater Form, Suppl 1:1095-1098, 2008

Finet, G., Ohayon, J., Rioufol, G. Biomechanical interaction between cap thickness, Lipid Core composition and blood pressure in vulnerable coronary plaque: Impact on stability or instability. Coron Artery Dis, 15(1): 13-20, 2004

Friedman, M.H., Deters, O.J., Mark, F.E., Bargeron, C.B., and Hutchins, G.M. Arterial geometry affects hemodynamics, a potential risk factor for atherosclerosis. Atherosclerosis. 46(2): 225-231, 1983

Fung, Y.C., Biomechanics: Mechanical Properties of Living Tissues, Springer-Verlag, New York, NY, 1993

Fuster, V., Mechanisms leading to myocardial infraction: insights from studies of vascular biology. Circulation, 90(4): 2126-2146, 1994

Gao, H., Long, Q. Effects of varied lipid core volume and fibrous cap thickness on stress distribution in carotid arterial plaques. Journal of Biomechanics, 41 (14):3053-3059, 2008

Gao, H., Long, Q., Howarth, S.P.S., Tang, T.Y., Li, Z.Y., Graves, M.J., Gillard, J.H. The reproducibility study of 3D arterial plaque reconstruction and its effects to the stress analysis based on multiple sequence MRI images. Journal of Magnetic Resonance Imaging, 30(1):85-93, 2009a

Gao, H., Long, Q., Graves, M., Gillard, J.H., Li, Z.Y. Carotid arterial plaque stress analysis using fluid-structure interactive simulation based on in vivo magnetic resonance images of four patients. Journal of Biomechanics, 42(10):1416-1423 , 2009b

Gao, H., Long, Q., Sadat, U., Graves, M., Gillard, J.H., Li, Z.Y. Stress analysis of carotid atheroma in a TIA patient using MRI-based fluid-structure interaction method. British Journal of Radiology, DOI: 10.1259/bjr/20307071

Gasser, T.C., Ogden, R.W., Holzapfel, G.A. Hyperelastic modeling of arterial layers with distributed collagen fiber orientations, J.R. Soc. Interface, 3:15-35, 2006

Gasser, T.C., Holzapfel, G.A. Modeling plaque fissuring and dissection during balloon angioplasty intervention. Annals of biomedical engineering, 35(5):711-723, 2007

Gerbeau, J.F., Vidrascu, M., Frey, P. Fluid-structure interaction in blood flows on geometries based on medical imaging. Computers and structures, 83(2-3):155-165, 2005

Holzapfel, G.A. Determination of material models for arterial walls from uniaxial extension tests and histological structure. Journal of theoretical biology, 238(2):290-302, 2006

Glor, F.P., Ariff, B., Crowe, L.A., Hughes, A.D., Cheong, P.L., Thom, S.A., McG., et al. Carotid geometry reconstruction: a comparison between MRI and ultrasound. Medical physics, 30(12):3251-3261,2003

Giddens, D.P., Tang, T.D., Loth, F. In: Jaffrin MY, Caro C. Fluid mechanics of arterial bifurcations in biological flows. New York: Plenum Press, p51-68, 1995

Gijsen, F.J., van de Vosse, F.N., Janssen, J.D. The influence of the non-Newtonian properties of blood on the flow in large arteries: steady flow in a carotid bifurcation model. J Biomech, 32:601-608, 1999

Giroud, D., Li J.M., Urban, P., Meier, B., Rutishauer, W. Relation of the site of acute myocardial infarction to the most severe coronary arterial stenosis at proper angiography, Am J Cardiol, 69(8): 729-732, 1992

Glagov, S., Weisenberg, E., Zarins, C.K., et al. Compensator enlargement of human atherosclerotic coronary arteries. N Engl J Med. 316(22): 1371-1375, 1987

Goshtasby, A.Ardeshir. 2D and 3D image registration for medical, remote sensing and industrial applications. Wiley Interscience 2005; pp107-140.

Groen, H.C., Gijsen, F.J.H, Van Der Lugt, A., Ferguson, M.S., hatsukami, T.S., Van Der Steen, A.F.W., Yuan, C., Wentzel, J.J. Plaque rupture in the carotid artery is localized at the high shear stress region: A case report. Stroke, 38(8): 2379-2381, 2007

Groen, H.C., Gijsen, F.J.H, Van Der Lugt, A., Ferguson, M.S., hatsukami, T.S., Van Der Steen, A.F.W., Yuan, C., Wentzel, J.J. High shear stress influences plaque vulnerability. Netherlands heart journal, 16(7-8):280-283, 2008

Guo, X., Lu, X., Kassab, G.S. Transmural strain distribution in the blood vessel wall. Am J Physiol Heart Circ Physiol 288: H881-H886, 2005

Hallow, K.M., Taylor, W.R., Rachev, A., Vito, R.P. Markers of inflammation collocate with increased wall stress in human coronary arterial plaque. Biomechanics and modeling in mechanobiology. 1-14, 2009

Hangartner, J.R., Charleston, A.J., Davies, M.J., and Thomas, A.C. Morphological characteristics of clinically significant coronary artery stenosis in stable angina. Br Heart J., 56(6): 501-508, 1986

Hansson, G.K., Libby P., Schonbeck U., Yan, Z.Q. Innate and adaptive immunity in the pathogenesis of atherosclerosis. Circ Res, 91(4): 281-291, 2002

Hatsukami, T.S., Ross, R., Polissar, N.L., et al. Visualization of fibrous cap thickness and rupture in human atherosclerotic carotid plaque in vivo with high-resolution magnetic resonance imaging. Circulation, 102:959-964, 2000

Himburg, H.A., Friedman, M.H. Correspondence of low mean shear and High harmonic content in the porcine iliac arteries. ASME J. Biomech. Eng., 128(6):852-856, 2006

Holzapfel, G.A., Stadler, M., Schulze-Bauer, C.A. A layer-specific three dimensional model for the simulation of balloon angioplasty using magnetic resonance imaging and mechanical testing. Ann Biomed Eng, 30(6): 753-767, 2002

Holzapfel, G.A., Sommer, G., Regitnig, P. Anisotropic mechanical properties of tissue components in human aterosclerotic plaques, J Biomech Eng, 126(5): 657-665, 2004

Hoshino, T., Chow, L.A., Hsu, J.J., Perlowski, A.A., et al. Mechanical stress analysis of a rigid inclusion in distensible material: a model of atherosclerotic calcification and plaque vulnerability. Am J Physiol Heart Circ Physiol, 297:H802-H810,2009

Howarth, S., Li, Z.Y., Trivedi, R.A., U-King-Im, J.M., Graves, M.J., Kirkpatrick, P.J., Gillard, J.H. Correlation of macrophage location and plaque stress distribution using USPIO-enhanced MRI in a patient with symptomatic severe carotid stenosis: a new insight into risk stratification. British journal of Neurosurgery, 21(4):396-398,2007

Huang, H., Virmani, R., Younis, H. Burke, A.P., Kamm, R.D., and Lee, R.T. The impact of calcification on the biomechanical stability of atherosclerotic plaques. Circulation, 103(8): 1051-1056, 2001

Huang, X., Yang, C., Yuan, C., Liu, F., Canton, G., Zheng, J., Woodard, P.K., Sicard, G.A., Tang, D. Patient specific artery shrinkage and 3D zero-stress state in multi-component 3D FSI models for carotid atherosclerotic plaques based on in vivo MRI data, Molecular and Cellular biomechanics, 6(2):121-134,2009

Hubner, B., Seidel U., Scherer T. Fluid-structure interaction with ANSYS and CFX – Investigation of convergence properties of partitioned solutions to hydroelastic systems. 24th CADFEM Users' Meeting (Stuttgart Germany)

Humphrey, J.D. Cardiovascular solid mechanics : Cells, Tissues, and Organs. Springer, New York, 2002.

Humphrey, J.D., Na S. Elastodynamics and arterial wall stress. Annals of Biomedical Engineering 30(4):509-523. 2002

Hyun, S., Kleinstreuer, C., Archie, J.P. Hemodynamics analyses of arterial expansions with implications to thrombosis and restenosis. Med. Eng. Phys. 22(1):13-27, 2000

Imoto, K., Hiro, T., Fujii, T., Murashige A., et al. Longitudinal structural determinants of atherosclerotic plaque vulnerability: A computational analysis of stress distribution using vessels models and three dimensional intravascular ultrasound imaging. Journal of American College of Cardiology, 46(8):1507-1515, 2005

Jahnke, C., Dietric, T., Paetsch, I., Koehler, U., Preetz, K., Schnackenburg, B., Fleck, E., Graf, K., Nagel, E. Experimental evaluation of the detectability of submillimeter atherosclerotic lesions in ex vivo human iliac arteries with ultrahigh-field (7.0T) magnetic resonance imaging. Int J cardiovasc Imaging; 23:519-527,2007.

Jessica, M.M., Davies, M.J. Vulnerable Plaque: Relation of characteristics to degree of stenosis in human coronary arteries, Circulation. 94:928-931, 1996

Jassma, M.J., Bayraktar, H.H., Niebur, G.L., Keaveny, T.M. Biomechanical effects of intraspecimen variations in tissue modulus for trabecualr bone, Journal of biomechanics, 35:237-246, 2002

Kaazempur-Morfrad, M.R., Younis, H.F., Patel, S., Isasi S., Chung C., et al. Cyclic strain in human carotid bifurcation and its potential correlation to atherogenesis: Idealized and anatomically-realistic models. Journal of Engineering mathematics, 47:299-314,2003

Kaazempur-Mofrad, M.R., Isasi, A., G., Younis, H.F., Chan, R.C., Hinton, D., P., Sukhova, G., Lamuraglia, G.M., Lee, R.T., Kamm, R.D. Characterization of the atherosclerotic carotid bifurcation using MRI, Finite element modeling, and histology. Annals of Biomedical engineering, 32(7): 932-946, 2004

Karimi, R., Zhu, T., Bouma, B.E., Kaazempur Mofrad, M.R. Estimation of nonlinear mechanical properties of vascular tissues via elastography. Cardiovasc Eng., 8(4): 191-202, 2008

Kaissis, J.D., Liais, C.D., Sumpio, B.E. Effects of cyclic strain on vascular cells. Endothelium, 11:17-28, 2004

Kerwin, W.S., Han, C., Miler, Z.E., et al. Methods for quantitative analysis of carotid atherosclerotic plaque via MRI[abstract]. Radiology, 225(P):181, 2002

Kock, S.A., Nygaard, J.V., Eldrup, N., Frund, E.T., Klarke, A., Paaske, W.P., Falk, E., Kimi, W.Y. Mechanical stresses in carotid plaques using MRI-based fluid-structure interaction models. Journal of Biomechanics, 41(8):1651-1658, 2008

Koenderink, J.J., Van Doorn, A.J. Surface shape and curvature scales, Image Vision Comput 10:557-565,1992

Ku, D.N., Giddens, D.P., Zarins, C.K., and Glagov S. Pulsatile flow and atherosclerosis in the human carotid bifurcation. Positive correlation between plaque location and low oscillating shear stress. Arteriosclerosis. 5(3): 293-302, 1985

Ku, D.N., Giddens, D.P. Laser Doppler anemometer measurements of pulsatile flow in model carotid bifurcation. J Biomech, 20:407-21, 1987

Kumar, R.K., Balakrishnan, K.R. Influence of lumen shape and vessel geometry on plaque stresses: possible role in the increased vulnerability to a remodeled vessel and the shoulder of a plaque. Heart. 91(11):1459-1465,2005

La Tallec, P., Mouro, J. Fluid structure interaction with large structural displacements. Comput Meth Appl Mech Engng 190:3039-3067,2001

Ladak, H,M., Thomas, J.B., Mitchell, J.R., et al. A semi-automatic technique for measurement of arterial wall from black blood MRI. Med Phys, 28:1098-1107, 2001

Landman Uzi. Materials by numbers: Computations as tools of discovery. PNAS, 102(19):6671-6678, 2005

Ledru, F., Theroux, P., Lesperance, J., et al. Geometric features of coronary artery lesions favoring acute occlusion and myocardial infarction: a quantitative angiographic study. J AM Coll Cardiol, 33:1353-1361,1999

Lee, R.T., Grodzinsky, A.J., Frank, E.H., Kamm, R.D., Schoen, F.J. Structure-dependent dynamic mechanical behavior of fibrous caps from human atherosclerotic plaques. Circulation, 83(5): 1764-1770, 1991

Lee, R.T., Loree, H.M., Cheng, G.C., Lieberman, E.H., Jaramillo, N., Schoen, F.J. Computational structure analysis based on intravascular ultrasound imaging before in vitro angioplasty: prediction of plaque fracture locations. J AM Coll Cardiol, 21(3):777-782, 1993

Lee, R.T., Schoen, F.J., Loree, H.M., Lark, M.W., Libby, P. Circumferential stress and matrix methalloproteinase 1 in human coronary atherosclerosis. Implications for plaque rupture. Arterioscler Thromb Vasc Biol, 16(8): 1070-1073, 1996

Lee, R.T. Plaque stabilization: the role of lipid lowering. Int J Cardiol, 74, Suppl 1, S11-15, 2000

Lee, Sang-Wook, Steinman, D.A. On the relative importance of Rheology for image-based CFD models of the carotid bifurcation. Journal of biomedical engineering. 129(2):273-278, 2007

Lee, Sang-Wook, Antiga, L., Steinman, D.A. Correlations among indicators of disturbed flow at the normal carotid bifurcation. Journal of Biomechanical engineering, 131: 161013-1:7, 2009

Lee, Seung E., Lee Sang-Wook, Fischer, P.F., Hisham S., Loth, B.F. Direct numerical simulation of transitional flow in a stenosed carotid bifurcation. Journal of Biomechanics, 41:2551-2561,2008

Lendon, C.L., Davies, M.J., Born, G.V., Richardson, P.D. Atherosclerotic plaque caps are locally weakened when macrophages density is increased. Atherosclerosis, 87(1):87-90, 1991

Li, G., Mills I., Sumpio, B. Cyclic strain stimulates endothelial cell proliferation: characterization of strain requirements. Endothelium : 177-181, 1994

Li, M.X., Beech-Brandt, J.J., John, L.R., Hoskins, P.R., Easson, W.J. Numerical analysis of pulsatile blood flow and vessel wall mechanics in different degrees of stenosis. Journal of Biomechanics, 40(16):3715-3724, 2007

Li, Z.Y., Howarth, S., Trivedi, R.A., U-King-Im, J.M., Graves, M.J., Brown, A., Wang, L., Gillard, J.H. Stress analysis of carotid plaque rupture based on in vivo high resolution MRI. Journal of Biomechanics, 39(14):2611-2622,2006

Li, Z.Y., Howarth, Simon, P.S., Tang T.J., Gillard, J.H. How critical is fibrous cap thickness to carotid plaque stability? a flow-plaque interaction model. Stroke, 37:1195-1199, 2006b

Li, Z.Y., Howarth, S.P.S., Tang, T., Graves, M.J., U-King-Im, J., Trivedi, R.A., Kirkpatrick, P.J., Gillard, J.H. Structure analysis and magnetic resonance imaging predict plaque vulnerability: a study comparing symptomatic and asymptomatic individuals. Journal of vascular surgery, 45(4):768-775, 2007

Li, Z.Y., Tang, T., U-King-Im, J., Graves, M., Sutcliffe, M., Gillard, J.H. Assessment of carotid plaque vulnerability using structure and geometrical determinants. Circulation Journal, 72(7):1092-1099,2008

Libby, P. Molecular bases of the acute coronary syndromes. Circulation, 91(1):2844-2850, 1995

Libby, P., Geng, Y.J., Aikawa, M., Schoenbeck, U., Mach, F., Cliton, S.K., Sukhova, G.K., Lee, R.T. Macrophages and atherosclerotic plaque stability. Current opinion in Lipidology, 7(5):330-335, 1996

Libby, P. Atherosclerosis: The New View, Sci Am, 286(5): 46-55, 2002

Long, Q., Xu, X.Y., Collins, M.W., Griffith, T.M., Bourne, M. Fluid dynamics of the aortic bifurcation using magnetic resonance imaging and computational fluid dynamics. Internal medicine (Clinical and Laboratory), 5:35-42, 1997

Long, Q., Xu, X.Y., Ariff, B., Thom, S.A., Hughes, A.D., Stanton, A.V. Reconstruction of blood flow patterns in a human carotid bifurcation: A combined CFD and MRI study. J Magnetic Resonance Imaging, 11: 299-311, 2000

Long, Q., Ariff, B., Zhao, S.Z., Thom, S.A., Hughes, A.D., Xu, X.Y. Reproducibility study of 3D geometrical reconstruction of the human carotid bifurcation from magnetic resonance images. Magnetic resonance in medicine, 49(4):665-674,2003

Loree H.M., Kamm R.D., Atkinson C.M., Lee R.T. Turbulent pressure fluctuations on surface of model vascular stenosis. Am. J. Physiol. Heart Circ. Physiol., 261:H644-H650,1991

Loree, H.M., Kamm, R.D., Stringfellow, R.G., Lee, R.T. Effects of fibrous cap thickness on peak circumferential stress in model atherosclerotic vessels. Circ Res, 71(4): 850-858, 1992

Loree, H.M., Grodzinsky, A.J., Park, S.Y., Gibson, L.J., Lee, R.T. Static circumferential tangential modulus of human atherosclerotic tissue. J Biomech, 27(2): 195-204, 1994a

Loree, H.M., Tobias, B.J., Gibson, L.J., Kamm, R.D., Small, D.M., Lee, R.T. Mechanical properties of model atherosclerotic lesion lipid pools. Arterioscler Thromb, 14(2):230-234, 1994b

Lovett, J.K., Rothwell P.M. Site of carotid plaque ulceration in relation to direction of blood flow: An angiographic and pathological study, Cerebrovasc Dis, 16:369-375, 2003.

Lowder, M.L., Li, S., Carnell, P.H., Vito, R.P. Correction of distortion of histologic sections of arteries, J Biomech, 40(2): 445-450, 2007

Ma, P., Li, X., Ku, D.N. Convective mass transfer in carotid bifurcation. J Biomech, 30:365-371, 1997

Maehara, A., Mintz, G.S., Bui, A.B., Wlater, O.R., Castaqna, M.T., Canos, D., Pichard, A.D., et al. Morphologic and angiographic features of coronary plaque rupture detected by intravascular ultrasound. Journal of the American college cardiology. 40(5):904-810,2002

Marshall, I., Zhao, S., Papathansopoulou, P., Hoskins, P., Xu, X.Y. MRI and CFD studies of pulsatile flow in healthy and stenosed carotid bifurcation models. Journal of Biomechanics, 37(5):679-687,2004

Masson, I., Boutouyrie, P., Laurent, S., Humphrey, J.D., Zidi, M. Characterization of

arterial wall mechanical behaviro and stresses from human clinical data. Journal of Biomechanics, 41(12):2618-2627,2008

Mcivor, A.M., Valkenburg, R.J. A comparison of local surface geometry estimation methods. Machine vision and applications, 10:17-26, 1997

Moore, J.A., Steinman D.A., Holdworth, D.W., Ethier, C.R. Accuracy of computational hemodynamics in complex arterial geometries reconstructed from magnetic resonance imaging. Journal of Biomedical engineering, 27(1):32-41,1999

Moreno, P.R., Flak, E., Palacios, I.F., Newell, J.B., Fuster, V., Fallon, J.T. Macrophage infiltration in acute coronary syndromes: Implication for plaque rupture. Circulation, 90(2): 775-778,1994

Morton, S.A., Melville, R.B., Visbal, M.R. Accuracy and coupling issues of aeroelastic Navier-stokes solutions of deforming meshes, in: 38th AIAA structures, structural dynamics and materials conference, Kissimmee, Florida, 7-10 April 1997, AIAA Paper 97-1085

Moyle, K.R., Antiga, L., Steinman, D.A. Inlet conditions for image-based CFD models of the carotid bifurcation: it is reasonable to assume fully developed flow? Journal of Biomechanical engineering, 128(3): 371-379, 2006

Naghavi, M., Libby, P., et al. From vulnerable plaque to vulnerable patient: a call for new definition and risk assessment strategies: Part I. Circulation 108: 1664-1672, 2003

Newby, A.C., Zaltsman, A.B. Fibrous cap formation or destruction—the critical importance of vascular smooth muscle cell proliferation, migration and matrix formation. Cardiovasc Res, 41(2): 345-360, 1999

Niebur, G.L., yuen, J.C., Hsia, A.C., Keaveny, T.M. Convergence behavior of high-resolution finite element models of trabecular bone, Journal of Biomechanical engineering, 121(6):629-635, 1999

Niebur, G.L., Feldstein, M.J., Yuen, J.C., Chen, T.J., Keaveny, T.M. High-resolution finite element models with tissue strength asymmetry accurately predict failure of trabecular bone, Journal of Biomechanics, 33:1575-1583, 2000

Nighoghossian, N., Derex, L., Douek, P. The Vulnerable Carotid Artery Plaque: Current Imaging Methods and New Perspectives , Stroke, 36:2764-2772, 2005.

Nquyen, K.T., Clark, C.D., Chancellor, T.J., Papavassiliou, D.V. Carotid geometry effects on blood flow and on risk for vascular disease. Journal of Biomechanics, 41(1):11-19,2008

Ohayon, J., Teppaz, P., Finet, G., Rioufol, G. In-vivo prediction of human coronary plaque rupture locations using intravascular ultrasound and the finite element method. Coron

Artery Dis., 12(8):655-653, 2001

Ohayon, J., Finet, G., Treyve, F., Rioufol, G., Dubreuil, O. A three dimensional finite element analysis of stress distribution in a coronary atherosclerotic plaque: in vivo prediction of plaque rupture location. Biomechanics applied to computer assisted surgery, 37:225-241, 2005

Ohayon, J., Dubreuil, O., Tracqui, P., Le Floch, S., Rioufol, G., Chalabreysse, L., Thivolet, F., Pettiqrew, R.I., Finet, G. Influence of residual stress/strain on the biomechanical stability of vulnerable coronary plaques: Potential impact for evaluating the risk of plaque rupture. American journal of physiology-heart and circulatory physiology, 293(3):H1987-H1996,2007

Ohayon, J., Finet, G., Gharib, A.M., Heerzka, D.A., et al. Necrotic core thickness and positive arterial remodeling index: Emergent biomechanical factors for evaluating the risk of plaque rupture, American Journal of Physiology-Heart and Circulatory physiology, 295(2):H717-H727, 2008

Phan, B.P., Chu, B., Kerwin, W.S., Xu, D., Yuan, C., Hatsukami, T., Zhao, X. Effect of constrast enhancement on the measurement of carotid arterial lumen and wall volume using MRI. Journal of Magnetic Resonance Imaging, 23(4):481-485,2006.

Piet, A.M., Paul, S., Jan, J., Sizma, R.M.H. Fluid shear as a possible mechanism for platelet diffusivity in flowing blood, Journal of Biomechanics, 19(10):799-805, 1986

Pocaterra, M., Gao, H., Das, S., Pinelli, M., Long, Q. Circumferential residual stress distribution and its influence in a diseased carotid artery. Proceedings of 2009 ASME summer bioengineering conference, Lake Tahoe, CA, June 17-21,2009

Richardson, P.D. Davies, M.J., and Born G.V. Influence of plaque configuration and stress distribution on fissuring of coronary atherosclerotic plaques. Lancet 2(8669): 941-944, 1989

Richardson, P.D. Biomechanics of plaque rupture: progress, problems, and new frontiers. Ann Biomed Eng, 30(4): 524-536, 2002

Redgrave, J.N., Gallaqher, P., Lovett, J.K., Rothwell, P.M. Critical cap thickness and rupture in symptomatic carotid plaques: The oxford plaque study. Stroke, 39(6):1722-1729, 2008

Rogers, W.J., Prichard, J.W., Hu, Yong-Lin, Olson, P.R., Benckart, D.H., et al. Shcarcterization of signal properties in atherosclerotic plaque components by intravascular MRI. Arterioscler Thromb Vasc Biol, 20:1824-1830, 2000

Rosamond, W., Flegal, K., Friday, G., Furie, K., Go, A., Greenlund, K. Heart Disease and stroke statistics—2007 Update: A report from the American Heart association

statistics committee and stroke statistics subcommittee. Circulation, 115(5): e69-171, 2007

Saam, T., Ferguson, M., Yarnykh V.L., Takaya, N., Xu, D., Polissar, N.L., Hatsilao, T.S., Yuan, C. Quantitative evaluation of carotid plaque composition by in vivo MRI. Arterioscler Thromb Vasc Biol, 25:234-239, 2005.

Schroeder, A.P., Falk, E. Vulnerable and dangerous coronary plaque. Atherosclerosis 1995; 118 Suppl: S141-149

Schoenhagen, P., Ziada, K.M., Kapadia, S.R., et al. Extent and direction of arterial remodeling in stable versus unstable coronary syndromes: an intravascular ultrasound study. Circulation, 101(6): 598-603, 2000

Shah, P.K., Falk, E., Badimon, J.J., Fernandez-Ortiz, A., Mailhac, A., Villareal-Levy, G., Fallon, J.T., Regnstrom, J., Fuster, V. Human monocyte-derived macrophages induce collagen breakdown in fibrous caps of atherosclerotic plaques: Potential role of matrix degrading metalloproteinases and implications for plaque rupture. Circulation, 92(6):1565-1569, 1995

Shah, P.K. Mechanisms of plaque vulnerability and rupture, Journal of the American college of cardiology, 41(4), suppl S:15-22, 2003.

Shojima, M., Oshima, M., Takagi, K., et al. Magnitude and role of wall shear stress on cerebral aneurysms: computational fluid dynamic study of 20 middle cerebral aneurysms. Stroke, 35:2500-2505, 2004

Stary, H.C., Chandler, A.B., Dinsmore, R.E., et al. A definition of advanced Types of atherosclerotic lesions and a histological classification of atherosclerosis. A report from the committee on vascular lesions of the council on arteriosclerosis. American Heart Association. Arterioscler Thromb Vasc Biol, 15(9): 1512-1531, 1995a

Stary, H.C., Chandler, A.B., Dinsmore, R.E., Fuster, V., Glagov, C., Insull, W., et al. A definition of advanced types of atherosclerotic lesions and a histological classification of atherosclerosis. A report from the committee on vascular Lesions of the council on Arteriosclerosis, American Heart Association. Circulation, 92:1355-74, 1995b

Stary, H.C. Natural history and histological classification of atherosclerotic lesions: an update. Arteriscler Thromb Vasc Biol, 20(5):1177-8, 2000

Stefano, D., Felice, R., F., Balbarini, A. Angiogenesis as risk factor for plaque vulnerability. Current Pharmaceutical design, 15(10):1095-1106,2009

Steinman, D.A. Image-based computational fluid dynamics modeling in realistic arterial geometries, Ann Biomed Eng., 30(4): 483-97, 2002a

Stenman, D.A., Thomas, J.B., Ladak, H.M., Milner, J.S., Rutt, B.K., Spence, J.D. Reconstruction of carotid bifurcation hemodynamic and wall thickness using computational fluid dynamics and MRI. Magn Reson Med, 47(1): 149-59, 2002b

Steinman, D.A., Milner, J.S., Norley, C.J., Stephen, P.L., Holdsworth, D.W. Image based computational simulation of flow dynamics in a giant intracranial aneurysm. AJNR Am J Neuroradiol, 24:559-566, 2003

Steinman, D.A. Image-based computational fluid dynamics: a new paradigm for monitoring hemodynamics and atherosclerosis. Curr Drug Targets cardiovasc haematol Disord, 4(2): 183-197, 2004

Stoppard Tom, Arcadia (Faber and Faber, London), 1993

Tan, F.P.P., Soloperto, G., Bashford, S., Wood, N.B., THom, S., Hughes, A., Xu, X.Y. Analysis of flow disturbance in a stenosed carotid artery bifurcation using two-equation transitional and turbulence models. Journal of Biomechanical engineering, 130(6): 061008-1:12, 2008

Tang, D., Yang, C., Zheng, J., Woodard, P.K., Sicard, G.A., Saffitz, J.E., Yuan, C. 3D mri-based multicomponent fsi models for atherosclerotic plaques. Ann Biomed Eng, 32(7), 947-960, 2004a

Tang, D., Yang, C., Zheng, J., Woodard, P.K., Sicard, G.A., Saffitz, J.E., et al. 3D computational mechanical analysis for human atherosclerotic plaques using MRI-based models with fluid-structure interactions. Lecture notes in computer science, 3217(1):328-336, 2004b

Tang, D., Yang, C., Kobayashi, S., Ku, D.N. Effect of a lipid pool on stress/strain distributions in stenotic arteries: 3-D fluid structure interactions(FSI) models. Journal of Biomechanical Engineering, 126(3):363-370, 2004c

Tang, D., Yang, C., Zheng, J., Woodard, P.K., Saffitz, J.E., Sicard, G.A., Pilgram, T.K., Yuan, C. Quantifying effects of plaque structure and material properties on stress distributions in human atherosclerotic plaques using 3D FSI models. Journal of Biomedical Engineering, 127(7): 1185-1194,2005a

Tang, D., Yang, C., Zheng J., Woodard, P.K., Saffitz, J.E., Peteruccelli, J.D., Sicard, G.A., Yuan C. Local maximal stress hypothesis and computational plaque vulnerability index for atherosclerotic plaque assessment. Annals of biomedical engineering. 33(12 spec iss):1789-1801, 2005b

Tang, D., Yang, C., Mondal, S., Liu, F., Canton, G., Hatsukami, T.S., Yuan, C. A negative correlation between human carotid atherosclerotic plaque progression and plaque wall stress: in vivo MRI-based 2D/3D FSI models, Journal of Biomechanics, 41(4):727-736,2008

Tang, D., Teng, Z., Canton, G., Hatsukami, T.S., Dong, L., Huang, X., Yuan, C. Local critical stress correlates better than global maximum stress with plaque morphological features linked to atherosclerotic plaque vulnerability: An in vivo multi-patient study. Biomedical engineering online, 8(15),2009

Toussaint, J., Southern, J.F., Fuster, V., et al. T2-Weighted contrast for NMR charaxterization of human atherosclerosis. Aeterioscler Thromb Vasc Biol, 15:1533-1542, 1995.

Topoleski, L.D., Salunke, N.V., Humphrey, J.D., Mergner, W.J. Composition and history dependent radial compressive behavior of human atherosclerotic plaque. J Biomed Mater Res, 35(1): 117-127, 1997

Topoleski, L.D., Salunke, N.V. Mechanical behavior of calcified plaques: A summary of compression ad stress relaxation experiments. Z Kardiol, 89 Suppl 2: 85-91, 2000

Trivedi, R.A., U-king-Im, J.M., Graves, M.J., Horsley, J., Goddard, M., Kirkpatrick, P.J., Gillard, J.H. MRI-derived measurements of fibrous-cap and lipid-core thickness: the potential for identifying vulnerable carotid plaques in vivo, Neuroradiology, 46:738-743, 2004

Trivedi, R.A., Mallawarachi, C., U-king-Im, J.M., et al. Identifying Inflamed carotid plaques using in Vivo USPIO-enhanced MR imaging to label plaque macrophages. Arterioscler Thromb Vasc Biol, 26:1601-1606,2006.

Trivedi, R.A., Li, Z.Y., U-King-Im, J., Graves, M.J., Kirkpatrick, P.J., Gillard, J.H. Identifying vulnerable carotid plaques in vivo using high resolution magnetic resonance imaging-based finite element analysis. Journal of Neurosurgery, 107(3):536-542, 2007

Tuzcu, E.M., Hobbs, R.E., Rincon, G., Bott-Silverman, C., et al. Occult and frequent transmission of atherosclerotic coronary disease with cardiac transplantation. Insights from intravascular ultrasound, Circulation, 91(6): 1706-1713, 1995

Underhill, H., Kerwin, W.S., Hatsukami, T.S., Yuan, C. Automated measurement of mean wall thickness in the common carotid artery by MRI: a comparison to intima-media thickness by B-mode ultrasound, J Magn Reson Imaging, 21:809-817,2005

Vajjhala, S., Kraynik, A.M., Gibson, L.J. A cellular solid model for modulus reduction due to resorption of trabeculae in bone, Journal of Biomechanical engineering, 122:511-515, 2000

Varnava, A.M., Mills, P.G., Davies, M.J. Relationship between coronary artery remodeling and plaque vulnerability, Circulation, 105(8): 939-943, 2002

Vengrenyuk, Y., Carlier, S., Xanthos, S., Cardoso, L., Ganatos, P., Virmnani, R., Einav, S.,

Gilchrist, L., Weinbaum, S. A hypothesis for vulnerable plaque rupture due to stress-induced debonding around cellular microcalcificaitons in thin fibrous cap. Proceedings of the national academy of sciences of the united states of America. 103(40): 14678-14683,2006

Veress, A.I., Vince, D.G., Anderson, P.M., Cornhill, J.F., et al. Vascular mechanics of the coronary artery. Z Kardiol, 89 Suppl 2: 92-100,2000

Versluis, A., Bank, A.J., Douglas, W.H. Fatigue and plaque rupture in myocardial infarction, Journal of Biomechanics, 39(2):339-347,2006

Veshkina, N., Obidowski, D., Swiniarski, J., Zbicinski, I. Verification of fluid structure interaction model of pulsating flow in a silicone pipe. Proceeding of Modeling, identification and control, 675-032, 2010.

Vierendeels, J., Lanoye, L., Degroote, J., Verdonck, P. Implicit coupling of partitioned fluid-structure interaction problems with reduced order models. Computers and structures 2007, 85(11-14):970-976

Virmani, R., Kolodgie, F.D., Burke, A.P., Farb, A., Schwartz, S.M. Lessons from sudden coronary death: a comprehensive morphological classification scheme for atherosclerotic lesions. Arterioscler thromb basc boil. 20(5): 1262-1275, 2000

Virmani, R., Burke, A.P., Kolodgie, F.D., Farb, A. Pathology of the thin-cap fibrouatheroma: a type of vulnerable plaque. Journal of interventional cardiology, 16(3):267-272,2003

Virmani, R., Kolodgie, F.D., Burke, AP, Finn, A.V., Gold, H.K., Tulenko, T., Wrenn, S.P., and Narula, J. Atherosclerotic plaque progression and vulnerability to rupture: angiogenesis as a source of intraplaque hemorrhage, Arterioscler Thromb Vasc Biol, 25(10): 2054-2061, 2005

Vito, R.P., Dixon, S.A. Blood vessel constitutive models,-1995-2002. Annu Rev Biomed Eng, 5: 413-439, 2003

Von Ingersleben, G., Scbmiedl, U.P., Hatsukami, T.S., Nelson, J.A., Subramaniam, D.S., Ferguson, M.S., Yuan, C. Characterization of atherosclerotic plaques at the carotid bifurcation: Correlation of High-Resolution MR Imaging with Histologic Analysis—Preliminary study. RadioGraphics , 17:1417-1423,1997

Vonesh, M.J., Cho, C.H., Pinto, J.V., Jr., Kane, B.J., Lee, D.S., et al. Regional vascular mechanical properties by 3D intravascular ultrasound with finite element analysis. Am J Physiol, 272(1): H425-437,1997

Wilcox, J.N. Analysis of local gene expression in human atherosclerotic plaques. J Vasc Surg, 15(5): 913-916, 1992

Williamson, S.D., Lam, Y., Younis, H.F., Huang, H., Patel, S., Kaazempur-Mofrad, M.R., Kamm, R.D. On the sensitivity of wall stresses in diseased arteries to variable material properties, J Biomech Eng, 125(1): 147-155, 2003

Wu, Hsien-Chih, Chen S.Y. J., Shroff, Sanjeev G., Carroll, J.D. Stress analysis using anatomically realistic coronary tree. Med. Phys. 30(11):2927-2936, 2003

Yang, C., Tang, D., Yuan, C., Hatsukami, T.S., Zheng, J., Woodard, P.K. In vivo/ex vivo MRI-based 3D non-Newtonian FSI models for human atherosclerotic plaques compared with fluid/wall-only models. Computer modeling in engineering and sciences. 19(3):233-245,2007

Yarnykl, V.L., Terashima, M., Hayes, C.E., Shimakawa, A., Takaya, N., Nguyen, P.K., et al. Multi-contrast black blood MRI of carotid arteries: comparison between 1.5 and 3 Tesla magnetic field strengths. J Magn Reson Imaging, 23:691-698,2006

Younis, H.F., Kaazempur-Mofrad, M.R., Chan, R.C., Isasi, A.G., Hinton, D.P., Hinton, D.P., et al. Hemodynamics and wall mechanics in human carotid bifurcation and its consequences for atherogenesis: investigation of inter-individual variation. Biomech Model Mechanobiol., 3(1):17-32, 2004

Yuan, C., Kirk, B.W., Smith, L.H., Hatsukami, T.S. Measurement of atherosclerotic carotid plaque size in vivo using high resolution magnetic resonance imaging. Circulation ,98:2666-2671,1998.

Yuan, C., Mitsumori, L.M., Ferguson, M.S., Polissar, N.L., Echelard, D., Ortiz, G., Small, R., Davies, J.W., Kerwin, W.S., Hatsukami, T.S. In vivo accuracy of multispectral magnetic resonance imaging for identifying lipid-rich necrotic cores and intraplaque hemorrhage in advanced human carotid plaques. Circulation ,104:2051-2056, 2001.

Yuan, C., Kerwin, W.S., Ferguson, M.S., Polissar, N., Zhang, S., Cai, J., et al. Contrast-enhanced high resolution MRI for atherosclerotic carotid artery tissue characterization. J Magn Reson Imaging, 15:62-67,2002a

Yuan, C., Zhang, S., Polissar, N.L., Echelard, D., et al. Identification of fibrous cap rupture with magnetic resonance imaging is highly associated with recent transient ischemic attack or stroke. Circulation,105:181-185, 2002b

Zhao, S.Z., Xu, X.Y., Hughes, A.D., Thom, S.A., Stanton, A.V., Ariff, B., Long, Q. Blood flow and vessel mechanics in a physiologically realistic model of a human carotid arterial bifurcation. J. Biomechanics 33: 975-984, 2000.

Zhao, S.Z., Ariff, B., Long, Q., Thom, S.A., Hughes, A.D., Xu, X.Y. Inter-individual variations in wall shear stress and mechanical stress distribution at the carotid artery bifurcation of healthy humans. J. Biomechanics, 35:1367-1377, 2002

Zheng, J., EI Naga, I., Rowold, F.E., Pilgram, T.K., Woodard, P.K., Saffitz, J.E., Tang, D. Magnetic resonance in medicine, 54(6):1360-1368,2005

Publication List

Journal Papers/Book Chapter during PhD

1) **Hao Gao**, Quan Long. Stress analysis on carotid atherosclerotic plaques in the coming book "Atherosclerosis Disease Management", edited by Dr Jasjit Suri, Springer.(submitted)
2) **Hao Gao**, Quan Long, Umar Sadat, Martin Graves, Jonathan H Gillard, Zhiyong Li. Stress analysis of carotid atheroma in a TIA patient using MRI-based fluid-structure interaction method. British Journal of Radiology, DOI: 10.1259/bjr/20307071
3) **Hao Gao**, Quan Long, SPS Howarth, TY Tang, ZY Li, MJ Graves, JH Gillard. The reproducibility study of 3D arterial plaque reconstruction and its effects to the stress analysis based on multiple sequence MRI images. Journal of Magnetic Resonance Imaging, 2009, 30(1):85-93.
4) **Hao Gao**, Quan Long, Martin Graves, Jonathan H Gillard, Zhi-Yong Li. Carotid arterial plaque stress analysis using fluid-structure interactive simulation based on in vivo magnetic resonance images of four patients. Journal of Biomechanics, 2009, 42(10):1416-1423
5) **Hao Gao**, Quan Long. Effects of varied lipid core volume and fibrous cap thickness on stress distribution in carotid arterial plaques. Journal of Biomechanics, 2008, 41 (14):3053-3059

Drafts in Preparation

6) **Hao Gao**, Quan Long, Martin Graves, Jonathan H Gillard, Zhi-Yong Li. Stress analysis between symptomatic and asymptomatic patients with carotid plaques and clinical implication.(in preparation for Stroke)
7) **Hao Gao**, Quan Long, Martin Graves, Jonathan H Gillard, Zhi-Yong Li. Stress analysis of carotid atheroma in transient ischemic attack patients, evidence for stress induced rupture.(in preparation for Stroke)
8) Michael Luppi, **Hao Gao**, Ahsan Choudhury, Warren Hopkins, Saroj Das, Michele Pinelli, Quan Long. Assessment of structure distortion of paraffin wax histology section of human carotid atherosclerotic plaque specimen.(in preparation for Journal of Biomechanics)
9) **Hao Gao**, Quan Long, Martin Graves, Jonathan H Gillard, Zhi-Yong Li. Plaque surface irregularities and correlation to plaque stress distribution.(in preparation for Journal of Biomechanics)

Peer Reviewed Conference Papers&Talks

1) **Hao Gao**, Quan Long, et al., Curvedness study on atherosclerosis plaques and its implication to plaque stress, Accepted for oral presentation by 6th World Congress on Biomechanics, Singapore, 2010.
2) **Hao Gao**, Quan Long, et al., Effects of plaque geometry features on plaque stress distribution and rupture risk of carotid plaques. Accepted for oral presentation by 6th World Congress on Biomechanics, Singapore, 2010.
3) Xiao Liu, **Hao Gao**, Quan Long, Analysis of blood flow in ten reconstructed 'Healthy' carotid bifurcations from stenotic carotid arteries based on MR images.

Accepted for oral presentation by 6th World Congress on Biomechanics, Singapore, 2010.

4) Stefano Raimondi, **Hao Gao** et al., Quantitative analysis of left ventricle geometry and motion for a patient after myocardial infarction. Accepted for oral presentation by 6th World Congress on Biomechanics, Singapore, 2010.
5) **Hao Gao**, Quan Long, et al., Stress analysis on carotid plaques between symptomatic and asymptomatic patients. BAS Spring Meeting 2009, Oxford.
6) **Hao Gao**, Quan long, Martin Graves, Jonathan H. Gillard, Zhiyong Li. Stress Analysis On Human Arterial Plaques By Fluid Structure Interactions—Multi-case Study. Proceeding 2009 Summer Bioengineering Conference, ASME, June, 2009, Lake Tahoe, CA, USA
7) **Hao Gao**, Quan long, Martin Graves, Jonathan H. Gillard, Zhiyong Li. stress analysis of carotid atheroma in transient ischemic attack patients. Proceeding 2009 Summer Bioengineering Conference, ASME, June, 2009, Lake Tahoe, CA, USA
8) Ahsan R. Choudhury, Michael Luppi, Warren Hopkins, **Hao Gao**, Saroj Das, Ian Kill, Michele Pinelli, Quan Long. High resolution 3D reconstruction of an atherosclerotic plaque by a combination of histology and 3D ultrasound. Proceeding 2009 Summer Bioengineering Conference, ASME, June, 2009, Lake Tahoe, CA, USA
9) Massimo Pocaterra, **Hao Gao**, Sajoj Das, Michele Pinelli, Quan Long. Circumferential residual stress distribution and its influence in a diseased carotid artery. Proceeding 2009 Summer Bioengineering Conference, ASME, June, 2009, Lake Tahoe, CA, USA
10) Michael Luppi, **Hao Gao**, Ahsan Choudhury, Warren Hopkins, Saroj Das, Michele Pinelli, Quan Long. Assessment of structure distortion of paraffin wax histology section of human carotid atherosclerotic plaque specimen. Proceeding 2009 Summer Bioengineering Conference, ASME, June, 2009, Lake Tahoe, CA, USA
11) **Hao Gao**, Quan Long, et al. (1)Stress analysis on carotid plaques between symptomatic and asymptomatic patients; (2) Development of an element based material property model and its applications on arterial plaque stress analysis. The 16th Finite Element Workshop 2009 on Wednesday, July 15th and Thursday, July 16th in Ulm, Germany Finite Element Workshop 2009, Ulm Germany.
12) **Hao Gao**, Quan Long, et al. Fluid-Structure Interaction Study on Human Arterial Plaque With Patient Specific Geometry and Boundary Conditions. Proceeding 2008 Summer Bioengineering Conference, ASME, June, 2008, Marco Island, FL, USA
13) Jie Wu, Quan Long, Shixiong Xu, **Hao Gao**, et al. Numerical Study of Tumour Blood Perfusion Based on 3D Tumour Angiogenic Microvasculatures. Proceeding 2008 Summer Bioengineering Conference, ASME, June, 2008, Marco Island, FL, USA
14) **Hao Gao**, Quan Long, et al., Development of an element based material property model and its applications on arterial plaque stress analysis. ICCES, Mar, 2008, Honolulu, Hawaii, USA
15) **Hao Gao**, Quan Long, et al., Finite element stress analysis with element based material property model and its applications on arterial plaque rupture study. The 3rd international symposium on biomechanics in vascular biology and cardiovascular disease, Rotterdam, The Netherlands, April 24-25, 2008.
16) Giulia Fabbri, Quan Long, **Hao Gao**, et al. Stress Analysis of Carotid Arterial Stenosis with 3-D Fluid-Structure Interaction Simulations, Proceedings of the 2007 Summer Bioengineering Conference, ASME, Keystone, CO, USA June, 2007
17) **Hao Gao**, Quan Long., et al. Fluid structure interaction analysis in stenotic carotid artery with lipid core. European Society of Biomechanics Workshop 2007, Trinity College Dublin, Ireland, Aug 26-27, 2007